i

This report contains information of proprietary nature, and its contents
may not be published or reproduced in any form without prior consent of
the research worker(s) involved in USDA and NASA.

SPECTRAL SURVEY OF

IRRIGATED REGION CROPS AND SOILS

1971 ANNUAL REPORT   WESLACO, TEXAS

UNITED STATES

DEPARTMENT OF AGRICULTURE

October 1, 1970 - September 30, 1971

71-02

Table of Contents

Chapter VII.   EQUIPMENT CALIBRATION AND DEVELOPMENT

P E R S O N N E L

ARS-SWC personnel assigned to the remote sensing investigations research program at Weslaco during this reporting period were:

Craig L. Wiegand, Ph.D.	Supervisory Soil Scientist and Director
Ross W. Leamer, Ph.D.	Soil Scientist
Harold W. Gausman, Ph.D.	Plant Physiologist
William A. Allen	Research Physicist
Ruben Cardenas	Plant Physiologist
Arthur J. Richardson	Physicist
Helen B. Osborne	Secretary
Evelyn N. Crawford	Clerk-Stenographer
Audrey J. Ryan	Clerk-Typist
Ronald L. Bowen	Photographer
Jose A. Cuellar	Biological Technician
David E. Escobar	Biological Laboratory Technician
Alvin H. Gerbermann	Agricultural Research Technician
Juan R. Noriega	Physical Science Aid
Romeo R. Rodriguez	Soil Research Technician
Robert J. Torline	Computer Programmer

ARS-SWC summer and part-time employees assigned to the remote sensing program include:

Guadalupe Cardona	Student Aid
Victor A. Flores, Jr.	Biological Laboratory Technician
Nellie Mae Garcia	Student Aid
David L. Nelson	Photographer
Daniel A. Weber	Physical Science Technician

Participation in the Work Study and Neighborhood Youth Corps (NYC) program by the Weslaco Center has been successful and beneficial to the Remote Sensing Program and to the college and high school participants. Work Study participants were: Edward Argueta, Armando Berumen, Guadalupe Cardona, Javier Cavazos, San Juanita Gonzalez, Randy Schwab, Jose Avila, Mary Sanchez, Pete Garza, Humberto Cano, and Gary Brandt. NYC participants were: Guadalupe Cardona, Enrique Curiel, and Dora Paz.

ACKNOWLEDGEMENTS/COOPERATORS

SUMMARY

Chapter I--APPLICATIONS [1]

<u>OPTICAL MECHANICAL SCANNER</u>

<u>Canopy temperature as an indicator of plant water stress</u>

The difference between crop canopy surface temperature and air temperature 40 cm above the crop was predicted theoretically and then measured under field conditions as plant water stress increased during drying cycles for cotton. The energy balance equation was rearranged to yield surface temperature as a function of environmental, radiation, and plant water stress conditions. Calculated temperature differences (surface minus air temperature) of 1 to 6C were found with typical plant water stress conditions. Thermocouples placed in contact with the lower leaf surfaces in the top 1/3 of a full canopy measured temperature differences of about 6C during peak radiation loads and plant water stress of -20 bars. A 1 mr field of view, airplane-mounted RS-14 thermal scanner measuring in the 8 to 14 μm band, with two internal calibration sources was used during July 1970 to determine emittance from cotton crops under stress conditions. Analysis of the data indicates emittance differences of several degrees between well-watered cotton and cotton under moderate to high plant water stress. The results suggest scheduling irrigations of cotton by measuring canopy temperatures with an aerial scanner.

<u>Temperature of soils and of crop canopies differing in water conditions</u>

An airplane-mounted thermal scanner was used to measure irradiance in the 8- to 14-μm wavelength interval over an extensively instrumented agricultural area. The area included soils differing in water and tillage condition, and replicated cotton plots with a wide range of plant water stress. The scanner data were recorded on analog magnetic tape and on 70-mm film. The film densities of the various soil and cotton treatments and film calibration information were determined with a microdensitometer. The observed irradiances corresponded to cotton plant canopy temperature differences up to 6C between the most and least water-stressed plots. The irradiance data from soils showed large differences as a function of time after tillage and irrigation. It is concluded that thermal imagery offers potential as a useful aid for delineating water-stressed and nonstressed fields of crops, evaluating uniformity of irrigation, and evaluating surface soil water conditions.

---

[1] For further information please refer to Chapter I in text.

PHOTOGRAPHIC

Sensing of boron and chloride toxicities of citrus trees

Photography and corresponding film density measurements were used to discriminate between healthy Red Blush grapefruit trees and trees whose foliage exhibited boron (B) and chloride (Cl⁻) toxicity symptoms.

Photographs were taken from an aircraft (3,000 ft altitude) and "Cherry picker" (8 ft above trees) with a Hasselblad camera equipped with a 50-mm focal length lens, and loaded with 70-mm Kodak Ektachrome Infrared Aero 8443 film (EIR). Light reflectance from B- and Cl⁻-affected trees produced pinkish images on photographs compared with red images for healthy trees.

Affected leaves compared with healthy green citrus leaves had less chlorophyll, a higher water content, were thicker and smaller in area, and had higher B and Cl⁻ contents.

Spectrophotometrically measured total diffuse reflectance of top leaf surfaces showed that B- and Cl⁻-affected leaves, compared with healthy leaves, had decreased reflectance (10%) over the 750- to 1350-nm near-infrared wavelength range, and increased reflectance (13%) at the visible green peak of 550 nm.

Optical count densities were determined on transparencies using a Joyce, Loebl automatic recording microdensitometer. For photographs at 3,000 ft altitude, best discrimination among healthy and affected trees using optical density measurements was obtained with a blue bandpass filter; a red bandpass filter gave best discrimination for photographs taken at a height of 8 ft above the trees.

Pre-visual detection of watermelon mosaic virus in cucumber

Watermelon mosaic virus-2 (WMV-2) was pre-visually detected on cucumber leaves (Cucumis sativis L.) 5 days after cotyledonary swabbing by taking daily photographs with Kodak Aerochrome Infrared 2443 film (AIR)--symptoms were photographically detected 2 days earlier than visual detection on leaves whose cotyledons were swabbed with abrasive and WMV-2 inoculum. Photographic transparencies revealed that virus-infected leaves had areas of darker red color saturation than uninfected leaves.

Pre-visual detection of virus diseases of plants photographically would facilitate early diagnosis and roguing of diseased plants in breeding and seed increase programs. Early treatment of plant diseases could help prevent extensive crop loss. For example, AIR photographs could be taken of a crop and the film processed and evaluated within 4 hours. Pre-visual detection of virus diseases may be also useful for crop production estimates.

Detection and monitoring of soil erosion by wind

Evaluation of microdensitometer readings from aerial photographs (RB-57 platform) of eroding and noneroding soils reveals that the film density is less for eroding than for noneroding soils. Land features such as blow-outs in rangeland, turnrows at the edge of a field, and bare creek beds are readily detectable from the RB-57 photos with the microdensitometer. The RB-57 photos have been used to locate several sites for the ERTS-A study of wind erosion on sandy soils.

Efforts will continue to mathematically express color signatures of soils. Microdensitometer tracings will be studied to relate soil color characteristics to the erodible state of the soil. Evidently, the average size soil particle on the eroding surface is greater than on the non-eroding surface, but the surface roughness is greater on the noneroding surface. To verify this observation, the reflectance from sandy soils as influenced by soil roughness needs to be evaluated.

Movement and feeding activity of the Eastern white-winged dove

The food resources available to white-winged doves are being inventoried, and the feeding patterns of the birds are being studied in a project begun in June 1971, and expected to continue through October 1972.

Through the use of NASA-USDA photographs (Mission 158, RB-57) and visual observations in the field, the available food supplies were charted. Records of whitewing feeding activity and patterns were made. The photographs were very useful to locate fields selected for observation and to determine the location and extent of native brush used as cover and nesting by the birds in relation to feeding areas. The investigator saved appreciable time by having access to the photographs.

Participation in 1971 corn blight Watch

Mr. A. H. Gerbermann of Weslaco spent 4 1/2 months during 1971 at LARS (Laboratory for Applications of Remote Sensing) Purdue University. He participated in photo-interpretation aspects of the corn blight Watch experiment. Some of his observations follow.

His experience indicates that Southern Corn Leaf Blight (SCLB) in-fected corn plants can be detected from healthy plants with color infrared film when 3% of the upper leaves (above 7th node) are infected. Fields larger than 10 acres should be used when photographs are taken at a scale of 1:120,000.

Ground observation will always be needed when a large geographical area is surveyed for SCLB. Specific conclusions have not been made because the data are presently being statistically analyzed by LARS.

Estimating citrus fruit numbers and yield

The use of ground survey teams to count fruit for yield estimations is tedious, time consuming, and costly. Photography may be a useful tool to improve fruit counting techniques. Hence, the Statistical Reporting Service (SRS) has conducted cooperative experiments with the Rio Grande Valley Soil and Water Research Center to study the use of photography for estimating fruit production.

It was found that citrus fruit counts made from 35 mm slides (ground level photographs) are generally highly and positively correlated with estimates of fruit per tree. Fruit counts and canopy area measurements from aerial photographs have not shown much promise. The need and the potential of an automated fruit counting technique is great.

MICROWAVE

Convair-990 Mission

The NASA/GSFC CV-990 aircraft, equipped with a number of microwave radiometer systems, overflew a flight line on March 1, 1971. Ground moisture content (by weight) samples were taken by Texas A&M University and SWC (Soil Water Conservation) personnel from the 2 to 4 cm and from the 14 to 16 cm soil depth intervals. The GSFC (Goddard Space Flight Center) provided tabulated values of antenna temperature as a function of elapsed flight time.

An error in navigation resulted in a direct correspondence between antenna beam pattern and soil samples in only 8 large fields. The radiometer data from the 1.42, 2.69, and 10.69 GHz systems showed a definite dependence on the shallower-sampled soil moisture content. (The range in moisture content among samples at the 15 cm depth was narrow). The decrease in antenna temperature with an increase in soil moisture content was linear for the 1.42 GHz frequency but curvilinear for the 2.69 and 10.69 GHz frequencies, and it amounted to a decrease of about 1°K in antenna temperature for each 1% increase in water content.

The data suggest that possibly soil moisture contents can be measured to the accuracy of the microwave antenna temperatures with standard deviations ranging from 3.3 to 6.1°K. However, the airborne measurements were taken over fields of similar soil and surface properties, and the response of the 0.69 and 10.69 GHz radiometers was insensitive at water contents below 20%. Estimates of moisture contents to an accuracy of 5 to 6% are probable under rather uniform conditions and to perhaps 10% under most conditions.

PROSPECTUS

<u>Remote sensing for conservation and environmental planning</u>

There is critical need for new ideas and techniques to provide more accurate and timely information for planning conservation measures and managing our crop, range, and forest resources. Remote sensing tools and techniques can record and examine land use patterns and the agricultural environment on scales and at wavelengths in the energy spectrum that have been heretofore unavailable.

Resource inventory and soil mapping can be used to illustrate key points including: (1) resources can be wisely managed only if their extent, value, and character are known; (2) information needs must be clearly defined to prevent gathering useless information; (3) remote sensing is especially useful for parametric land evaluation; (4) operational remote sensing systems are complicated and costly, but cost effective; (5) at the present stage of development, remote sensing should not be considered a threat to, but rather a supplement to, traditional techniques of information gathering; and (6) small scale photography (on the order 1:1,000,000), such as that acquired from space, has been found consistently more useful than the ground resolution would suggest.

SUMMARY

Chapter II.--SPACECRAFT PROJECTS [1]

ERTS-A Proposal: Reflectance of vegetation, soil, and water

The work statements of Weslaco's ERTS-A proposal submitted to NASA are to be negotiated. The primary objectives of Weslaco's proposal are: (1) to compare experimental results from ERTS-A data with predictions of analytical models for interaction of light with vegetation for leaf area index (LAI) determinations; (2) to determine whether or not differences in chlorophyll concentrations of plants can be detected from an orbiting satellite; (3) to determine the seasonal changes of the various crops and soils in Hidalgo County, Texas; to discriminate among them; and, in some cases, to estimate acreages by means of reflectance measured from ERTS-A; and (4) to develop an operational systems of satellite data analysis tailored to the needs of the U. S. Department of Agriculture.

EREP Proposal: Irrigation scheduling, freeze warning, and salinity detecting

The work statements of Weslaco's EREP proposal submitted to NASA are to be negotiated. The primary objectives of Weslaco's proposal are: (1) to utilize Skylab's multispectral scanner (MSS) data to assess temperatures of plant canopies in relation to midday insolation, ambient air temperature, and plant water stress conditions, low temperatures (near-freeze conditions) in the winter, and geographical distribution of plant canopy and earth surface temperatures from the Gulf of Mexico inland; (2) to use MSS data to detect, survey, and map saline soil areas; (3) to use the six-band Multispectral Photographic Facility (MPF) to identify, survey, and map saline and nonsaline soil areas; and (4) to correlate EREP's MSS results with results of MPF, ERTS-A and B Return Beam Vidicon, ERTS-A and B Multispectral Scanners, Aircraft observations, and ground observations.

The ultimate objective is to use space observations internationally for determining the need for crop irrigations and for freeze warnings in subtropical and semitropical areas.

---

[1] For further information please refer to Chapter II in text.

Effective use of ERTS multisensor data in the Great Plains Corridor

The subject ERTS-A proposal has been negotiated with NASA, and the scope of the study has been reduced to a smaller geographic area than originally proposed. The title and the north and south end test sites of the corridor remain. The corridor was proposed originally to increase the probability that cloud conditions would permit acceptable imagery to be obtained of the earth surface over at least some test sites each satellite pass and to emphasize the temporal aspects of crop growth and maturity in the analyses.

The main objectives of the negotiated proposal are to study changes in the quantity, quality, and distribution of resources in the test areas; to investigate procedures for predicting land, soil, and crop patterns; and to produce maps using ERTS-A imagery to delineate the resources.

Great Plains coordinated project on evapotranspiration

It is feasible that the agricultural production and the economy of the vast Great Plains area can be greatly enhanced by using satellite data for incorporation of evaporation information into evapotranspiration models, for predicting incident radiation at any position on the Great Plains for use in physical models describing evaporation and photosynthesis, and for mapping evaporative demand contours on the Great Plains.

The Coordinated Project on evapotranspiration provides an opportunity to use satellite capabilities to study energy and mass (water) balances on the scale of the Great Plains. Such capability has not been previously available. The subcommittee on remote sensing expects to prepare one or more proposals for ERTS-B experimentation.

SUMMARY

Chapter III. SPECTRUM MATCHING AND PATTERN RECOGNITION [1]

Bendix 9-channel scanner studies

Quantitative reflectance data from aircraft-borne multispectral scanners are used in remote sensing investigations by the U. S. Department of Agriculture at Weslaco, Texas. Long range objectives are: identification of yield-limiting crop and soil conditions, prediction of yields, and automatic recognition of crop and soil types. Reflectance data in the 380 to 1000 nm wavelength interval (WLI) were collected in the spring and summer of 1969 using the 9-channel Bendix scanner provided by a NASA Houston contract. Weslaco's personnel made ground observations during the overflights. Statistical analysis of scanner data in relation to ground truth was carried out at Bendix and Weslaco. Principal axis factor analysis, elliptical boundary-condition pattern recognition algorithm, and multiple linear regression analysis comprised the statistical investigations at Weslaco. Principal axis factor analysis determined that the optimum scanner channels needed to relate reflectance with ground observation data could be accounted for by two principal factors corresponding to the visible and infrared WLI. These two principal factors accounted for over 90% of the total variance for every flight date. The elliptical pattern recognition algorithm indicated that it is possible to discriminate among water, bare soil, and vegetation (overall recognition was 73.3 to 100%). Finer division of the vegetation categories could be accomplished only when unique field conditions existed such as maturity differences, harvesting, and water stress. Regression analysis indicated that reflectance data were related to percent ground cover and plant height (r = .621** to .875**). In the visible WLI, vegetation is lower reflecting than bare soil, producing a negative relation between reflectance and ground cover. In the infrared WLI, vegetation is higher reflecting than bare soil, producing a positive relation between reflectance and ground cover. These results indicate that good progress is being made in relating quantitative reflectance scanner data to ground truth information such as percent cover, plant height, and crop and soil conditions.

---

[1] For further information please refer to Chapter III in text.

MISSION 32M STUDIES

Preliminary science report

Plans for continuing analysis

Mission 32M (Univ. of Mich. C-47 aircraft) was conducted Feb. 27 to Mar. 4, 1971. A duplicate analog tape of the Feb. 27 flight needs to be acquired so that the Data Systems Analysis Division of the Agricultural Research Service can use it on their analog to digital facility presently on order. Digital magnetic tapes of at least selected channels of data are also desired to develop and test data handling procedures for ERTS-A data.

There is a high priority on digitizing the training sample sites of flight line 4 (Eastern Willacy County) so that the data can be evaluated for effects of salinity and soil type on spectral signatures. In addition, thermal imagery taken at dawn needs to be examined for evidence of water tables and caliche layers in the soil profile, and sandy surface soils.

We will continue to make vegetation pattern recognition tests. The Mission 32M data are among the first we have had with results in the near-infrared wavelength region where laboratory data indicate there is powerful information for discrimination.

Mission 32M data sets will be made available to cooperating organizations such as the Statistical Reporting Service, Remote Sensing Center of Texas A&M University, and Data Systems Analysis Division, for specific analyses and for development of their data handling capabilities.

Effects on Future Missions

Utilization of Mission 32M data is helping to prepare us for participation in ERTS-A and EREP programs.

The data may also offer a comparison of the behavior of spectrally similar channels in the Bendix scanner and the University of Michigan scanner. The Bendix scanner overflights were made in 1969, and we received the data this spring in a useable format. Although there is a difference in time of the flights, some flight lines were common to both missions, and a number of fields were in similar conditions on both missions. Thus, it may be possible to compare the responses of the Bendix and the University of Michigan multi-channel scanners in common wavelength intervals.

Conducting missions concurrently, as was done for Mission 32M and RB-57 Mission 158, is commendable because ground observation requirements are reduced, and the sets of data tend to be complementary. For example, thermal scanner and microwave data are both responsive to soil moisture conditions. Such data enable investigators to verify conditions that existed in the fields by comparing results of the thermal scanner and microwave sets of data.

Spectra of swatches from the University of Michigan's standard reflectance panels

The Weslaco area was overflown at an altitude of 2,000 ft by the University of Michigan's aircraft (Mission 32M) on February 27, 1971. Imagery was obtained with an optical mechanical scanner.

Cloth reflectance standards of different colors (reference reflectance panels) were laid on the ground (within flight line 2) at flight time to provide surfaces of known reflectance in the recorded signals. The reflectance of all objects under the variable outdoor conditions are then made relative to the known standards. Swatches were removed from each standard, and their reflectance was measured in the laboratory with a Beckman DK-2A reflectometer at 10-nm intervals over the 500- to 2500-nm wavelength interval (WLI).

Differences in reflectance among the swatches occurred over the entire 500- to 2500-nm WLI, but the most noticeable effect was in the 500- to 750-nm visible WLI. The green reflectance standard had a light reflectance of about 34% compared with 4% for red cloth panel at the 500-nm WL. The gray materials reflected less light as their darkness increased at all WL. They were designed to have nominal reflectances of 4, 8, 16, 32, and 64%, respectively, from darkest to lightest gray.

These data give the reflectance of a set of widely used reflectance standards; adoption of universal standards would facilitate data comparisons and interpretations among researchers.

Soil spectra

Average digitized analog signals were compared over various wavelength intervals (WLI) for two soils within a series (Delmita loamy fine sand and Delmita fine sandy loam) and a soil of another soil series (Comitas loamy fine sand). Two soil types within the Delmita series appear to differ more spectrally than the soils of two different series (Delmita vs. Comitas). Results indicate that the Delmita soils could be mapped successfully by automatic means with the average digitized analog signal for several WLI. There is a possibility that the Delmita soil can be distinguished from the Comitas soil with average digitized analog signals of channels 1 (400 to 430 nm), 2 (440 to 470 nm), 3 (480 to 510 nm) and 4 (490 to 530 nm).

A preliminary mapping of soils considered here as companion soils along two flight line segments has been done by the University of Michigan. For this purpose, the optimum channels of the short wavelength scanner, in the order of lowest misclassification probability, were channels 9, 6, 4, 1, 7, and 10. Work will be continued on the spectra of the modal training sites and on computerized mapping.

SUMMARY

Chapter IV--PHOTOGRAPHIC PROCEDURES AND INTERPRETATION [1]

The use of Kodak Aerochrome infrared color film, type 2443, as a remote
sensing tool

A new infrared color film, Eastman Kodak Aerochrome 2443, has replaced
Eastman Kodak Ektachrome Infrared Aero 8443 film, providing a new horizon
and challenge for remote sensing applications with aerial photography.

A panel of research workers selected "the print" they would prefer to
use from positive and negative transparencies of the 2443 and 8443 films.
Eighty-six percent of the panel preferred "the print" made from negative
processing of the 2443 film.

A comparison of the 8443 with the 2443 film indicated that the 2443
film had lower contrast and some loss of vivid coloration, but it was
superior in yielding details among shadows of plant canopies either as
a positive or negative "print".

The quality control of taking and processing 2443 photographs was
investigated. An EG and G Mark VI sensitometer was used to expose the
film, and a Joyce, Loebl microdensitometer with white, blue, red, and
green filters was used to obtain steps of the step wedges printed on the
2443 film. An analysis of variance was conducted on transformed densi-
tometric data to determine the significance among wedges, steps among
wedges, among filters, and their various interactions. The interaction
of wedges with steps was not statistically significant indicating that
results were repeatable regardless of the steps or wedges used. Repeat-
able densitometric readings can be obtained on sensitometric strips
exposed on an EG and G Mark VI sensitometer.

Film storage conditions for 2443 film are more critical than they
were for 8443 film. The 2443 film should be kept refrigerated for all
storage time other than loading, exposing, and processing.

Comparison of Infrared color 2443 and 8443 films for discriminating among
five citrus tree classifications

A pattern recognition technique (EBC - Elliptical Boundary Criterion)
was used in an attempt to discriminate among 5 citrus tree classifications:
boron (B)- and chloride (Cl⁻)-affected (excess) grapefruit, foot-rot affected
orange, healthy grapefruit, Iron (Fe)-deficient grapefruit and healthy orange
trees. For the 5 classifications, EIR compared with AIR film gave the best
results. Average recognitions were 65.0 and 55.7% for EIR and AIR films, res-
pectively. Within the EIR results, B- and Cl⁻-affected grapefruit and foot-
rot affected orange trees were easiest to identify (81.7 and 83.3% correct
identifications, respectively).

---

[1] For further information please refer to Chapter IV in text.

When fewer than 5 categories were used, best discrimination was obtained with AIR compared with EIR film. Correct recognition was 76.1% for discriminating among B- and Cl^--affected grapefruit, foot-rot affected orange, and grapefruit, and 94.2% for identifying B- and Cl^--affected grapefruit from Fe-deficient grapefruit trees.

Hints on the care, exposure, and processing of Kodak Ektachrome film and paper

The recommendations of the photographic laboratory staff at Weslaco are summarized for the care, exposure, and processing of Ektachrome film and paper. The use of proper filters, recommended chemical solutions and temperatures, immersion times, and safety procedures is emphasized.

Correlation of ground cover estimated from aerial photos with ground observations

A study was conducted to obtain correlations of percent crop cover of various crops obtained from ground observations with percent crop cover estimated from aerial photographs. Coefficients for the correlations of ground observations with film observations (all highly significant, $p = .01$) were: cantaloupe, .96; citrus, .94; corn, .95; cotton, .98; onion, .81; forage, .96; and grain sorghum, .94.

The results indicate that photo estimates of percent cover can be used to predict reliable estimates of percent ground cover. It seems feasible, therefore, that photo estimates of ground cover can be used to replace the tedious and time consuming observations made by ground data survey teams. To this end, regression equations will be developed for predicting percent ground cover from photo estimates of percent cover.

SUMMARY

Chapter V--INTERACTION OF LIGHT WITH PLANTS [1]

Calibration of field spectroradiometers

The USDA Rio Grande Soil and Water Research Center contracted with the Willow Run Laboratories of the Institute of Science and Technology at the University of Michigan to calibrate the Exotech Model 20 spectroradiometers owned by the USDA.

The values given by this initial calibration make possible the conversion of voltage signals from the spectroradiometers into meaningful units of energy.

Field operation of the instruments result in a wider range of levels of measurement so that electronic gain settings are used that were not used in the initial calibration. These variations and the complex nature of the spectro-radiometers suggest that calibration checks under well-controlled conditions should be made periodically.

A leaf cross section treated as an optical system

The Willstätter-Stoll (W-S) theory of light reflectance from a leaf has been verified by extensive ray tracing. The cellular structure of a typical leaf (maple leaf, Acer negundo L.) has been simulated in two dimensions by a chain of intersecting circular arcs that represent the interfaces be-tween plant cells and air. The simulated leaf is treated as a periodic structure of infinite lateral extent based on a fundamental pattern of 100 arcs. The model is characterized by two indices of refraction, typ-ically $n_1=1.4$ and $n_2=1.0$ corresponding, respectively, to medium and air. An incident ray of a specified state of polarization divides into a re-flected and a refracted component at each interface unless the ray is emerg-ing from the higher index medium at an incident angle in excess of the criti-cal value. In this case reflection is total and there is no refracted ray. The energy of each ray is allocated to its resultant components at each inter-face by means of the Fresnel relations. Energy is attenuated in the medium by absorption expressed by Lambert's law. The process is continued for a given incident ray until all resultant rays have been absorbed or have emer-ged as reflectance or transmittance. The problem is tractable in a computer of moderate memory provided that bookkeeping is discontinued for each ray when its energy falls below a prescribed threshold. The calculation results in predicted values of reflectance, transmittance, absorptance, and polari-zation for each assumed leaf cross section configuration. The technique can be modified to provide predictions based on the assumption that every inter-face is perfectly diffusive. The results for the perfectly specular and perfectly diffusive cases bracket the experimental values obtained from a real leaf.

---

[1] For further information please refer to Chapter V in text.

Discrimination among different kinds of plant leaves by spectral reflectance in the near infrared

Spectral reflectance measurements centered at 1.25, 1.65, and 2.20 µm were investigated for discriminating among 24 different kinds of leaves. These three channels are located at the peaks of atmospheric windows III, IV, and V. In accordance with a flat plate model, a leaf can be regarded as a pile of N identical elementary compact layers separated by air spaces. The reflectance R_∞ of an infinite thickness of such leaves is a function of the calculated thickness D/N for a typical assumed elementary compact layer. The quantity D is the thickness of water with average absorptance, over the spectral range 1.4 to 2.5 µm equivalent to that of the leaf.

Infinite reflectance R_∞ is displayed at the 1.65 µm wavelength as a function of N and D. The assumed functional relationship is specified by

$$R_\infty = 1 + \Sigma\, a_i (D/N)^i \quad,$$

where the coefficients a_i, (i=1, 2, ..., 5), are determined constants. The parameter N is the calculated number of identical elementary compact layers in the leaf and D is the thickness of water with absorptance equivalent to the leaf (equivalent water thickness). The resulting curved surface is bounded by the planes R_∞ = 5-, R_∞ = 20, N = 1.0, N = 2.5, and D = 600 µm. There are straight lines on the curved surface that pass through the reflectance axis and they are reflectance contours; the curved surface is developable. The reflectance surface can be visualized as a portion of a spiral ramp of increasing pitch centered around the reflectance axis. Such a surface exists for each wavelength. Reflectance diminished as D increases when N is held constant. This limiting value of reflectance with increasing D is the component produced by the upper epicuticular surface of the leaf. Reflectances for virtually all 24 kinds of leaves discussed fall within plotting error on the curved surface. Reflectance has meaning neither for N < 1 (VAI < 0), nor for D < 0. Reflectance for D = 0 is taken conventionally as unity.

The standard error of estimate is about 1% at 1.65 µm between observations and computed values. Similar values at 1.25 and 2.20 µm are not as promising; the standard errors of estimate are about 4% at these wavelengths. The quantities R_∞ and D can be regarded as observables. The parameter N, a measure of the intercellular air spaces in the leaf, is more difficult to determine experimentally. Leaf reflectance R_∞ over the range 1.0 to 2.5 µm is a function of leaf water content and intercellular air space.

A surprisingly high reflectance was obtained for leaves around 1.00 µm but has no special value for the purpose of discriminating among different kinds of leaves. At 1.00 µm, many different kinds of leaves appear equally reflective. This ambiguity of information is a result of the high transparency of water in the 1.00 µm region of the spectrum. At 1.65 µm, however, water has appreciable absorption but the reflectance signal is still sufficiently high to be useful. Reflectance at 2.20 µm is characterized by relatively high liquid water absorption.

SUMMARY

Chapter VI--PLANT PHYSIOLOGICAL AND HISTOLOGICAL FACTORS [1]

The leaf mesophylls of twenty crops, their light spectra, and optical and geometrical parameters

The purpose of the research was to relate the mesophyll structure of 20 important agricultural plants with their light spectra, and optical and geometrical parameters.

Thick, succulent lettuce leaves had the highest H_2O content (97.0%), and dorsiventral avocado, orange, and peach, and compact sugarcane leaves had the lowest H_2O contents (60.6 to 72.4%).

Soybean, peach, pumpkin, and pigweed leaves were thinnest (.140 to .170 mm) and sunflower, lettuce, and onion leaves were thickest (.407 to .978 mm).

The mean reflectances of most crops at 550 nm fell within the 13.3 ± 2.8% (standard deviation) range except avocado and orange (8.9 and 10.2%, respectively), and corn, pepper, sorghum, bean, and sugarcane leaves (16.2 to 18.6%). The spectral transmittance curves were similar to their spectral reflectance curves, but slightly lower in magnitude. Leaves with high absorptance had well-differentiated dorsiventral mesophylls with many chloroplasts in their palisade cells. Leaves with low absorptance had poorly differentiated mesophylls.

At the 1000-nm wavelength, pigweed, corn, sugarcane (compact mesophylls), and soybean leaves had the lowest reflectances (45.1 to 46.0%) and dorsiventral bean, orange, and pepper leaves with very porous mesophylls had the highest reflectances (51.0 to 56.2%). Relative to absorptance, values for soybean and bean leaves (1.8%) and sugarcane, tomato, and onion leaves (6.7 to 7.5%) fell outside of the 4.0% (mean) ± 1.7% (standard deviation) range.

Effective optical constants were calculated. The dispersion curves of most of the crop leaves were similar. Sixteen crops were analyzed to obtain geometrical parameters that specify the amount of H_2O and air in the leaf. Statistically, there was no highly significant difference between H_2O obtained experimentally and water determined theoretically.

---

[1] For further information please refer to Chapter VI in text.

Effects of leaf age for four growth stages of cotton and corn plants on leaf
reflectance, structure, thickness, water and chlorophyll concentrations and
selection of wavelengths for crop discrimination

The effects of leaf age within four growth stages of cotton (Gossypium
hirsutum L.) and corn (Zea mays L.) on parameters indicated in the title were
studied. The parameter's influence on the selection of optimum spectral
channels for the discrimination of vegetation was determined.

Extensive data are presented on the influence of cotton and corn leaf
maturation within growth stages on leaf thickness and leaf water content.
Complex interactions are presented.

Corn leaf maturation within growth stages had little influence on near-
infrared light (750- to 1350-nm wavelength interval) reflectance because leaf
mesophylls remained relatively compact. Cotton leaf mesophylls, however,
developed many air spaces (became "spongy") with maturation, and mature leaves
had higher near-infrared light reflectance than young leaves.

The correlation of reflectance with chlorophyll (CHL) concentration for
the four growth stages of corn was highly significant ($r = -0.75$, $p = 0.01$)
at the 550-nm wavelength (WL); the correlation of reflectance with CHL for
the four growth stages of cotton was significant ($r = -0.50$, $p = 0.05$) at the
650-nm WL.

The largest differences among reflectances of corn leaves of different
ages within growth stages occurred when tassels were appearing in the leaf
whorls. This may be the best time to discriminate corn from other vegetation
with remote sensors--reflectance differences among cotton leaves within the
four growth stages were similar.

A correlation analysis showed that channels at the 680-, 850-, 1650-,
and 2200-nm WL are optimum channels for the discrimination of vegetation.

Light reflectance, chlorophyll assays, and photographic film densities of
isogenic barley lines

The correlations were studied among light reflectance measurements,
chlorophyll (CHL) assays and photographic film optical density readings made
on isogenic barley lines. CHL concentrations of the isogenic lines were
negatively correlated with spectrophotometrically measured reflectances.
Golden Liberty and Betzes, however, had a decreased concentration of CHL b
relative to CHL a compared with the other isogenic lines (Liberty, Compana,
Pale Green Betzes, Golden Compana). Optical count readings made on conven-
tional color (CC) and Eastman Kodak Aerochrome infrared 2443 (AIR) films
with a densitometer were negatively correlated with CHL concentrations.
Discrimination among the isogenic lines appears best with AIR compared with
CC film.

Light reflectance, transmittance, and absorptance of nutrient-sufficient and -deficient squash leaves

Nutrient deficiencies, with the exception of -P (phosphorus), increased the visible light reflectance of Mexican squash leaves as much as 20% at the 550-nm wavelength compared with leaves of nutrient-sufficient plants. Near-infrared light reflectance was affected to a much lesser extent. In the visible region, -Mg (magnesium) leaves had the highest and -P leaves had the lowest reflectance. In the near-infrared region, -N (nitrogen) leaves had the highest and -Fe (iron) leaves had the lowest reflectance. Effects of nutrient levels on transmittance and absorptance are discussed.

Photomicrographic record of light reflected at 850 nanometers by cellular constituents of Zebrina pendula leaf epidermis

Light reflected at the 850-nm wavelength from living zebrina pendula Schnizl. specimens was recorded on Kodak high speed black-and-white infrared (IR) film. Cellular membranes reflected IR light more strongly than the surrounding protoplasm. This was also evident for the membranes of the cytoplasm (plasmalemma), nucleus (nuclear membrane), and chloroplasts (chloroplast envelope). The middle lamella also reflected IR light more strongly than the cell walls.

Differential reflectance among cellular constituents is caused by refractive index discontinuities. Thus, refractive index discontinuities other than air-cell interfaces are responsible for a small part of near-IR (750 to 1350 nm) reflectance by leaves.

The effects of citrus blackfly feeding-injury on leaf structure and its influence on the reflectance characteristics of citrus foliage

Studies were conducted to determine effects of blackfly feeding-injury on leaf structure and reflectance characteristics of citrus foliage. Blackfly damaged leaves had more visible light reflectance and transmittance (1 to 2% range) at the 550-nm wavelength than unaffected leaves. It made little difference if measurements were made on the bottom or the top of leaf.

SUMMARY

Chapter VII--EQUIPMENT CALIBRATION AND DEVELOPMENT [1]

Calibration of a laboratory spectrophotometer for specular light by means of stacked glass plates

Stacked glass plates have been used to calibrate a laboratory spectro-photometer, over the spectral range 0.5 to 2.5 μm, for specular light. The uncalibrated instrument was characterized by systematic errors when used to measure the reflectance and transmittance of stacked glass plates. Calibration included: first, a determination of the reflectance of a standard composed of $BaSO_4$ (barium sulfate) paint deposited on an aluminum plate; second, the approximation of the reflectance and transmittance residuals be-tween observed and computed values by means of cubic equations; and finally, the removal of the systematic errors by a computer. The instrument, after calibration, was accurate to 1% when used to measure the reflectance and transmittance of stacked glass plates.

A spectroradiometer for field use

The configuration and operation of a field spectroradiometer (Exotech Model 20 Spectroradiometer) is described that measures the intensity of incident and reflected radiation from .37 to 2.52 μm and emitted radiation from 2.76 to 13.88 μm. The instrument was built by Exotech Incorporated from specifications and plans furnished by the USDA. Exotech contributed many engineering concepts based on knowledge of the theory involved.

The instrument consists of two systems with each system made up of an optical unit and a control unit. One system covers the spectral range 0.37 to 2.52 μm; the other system covers the spectral range of 2.76 to 13.88 μm. The optical units of the two systems mount side by side on a tiltable base mounted on an aerial lift truck. Separation between the objective lenses is less than 12 inches to minimize parallax.

The control units are mounted in a camper-type equipment van, and they are connected to the optical units through 200 feet of cable. Preamplifiers and auxiliary electronics in the optical units are designed to operate with-out picking up interferences over this length of cable. The entire system is designed to operate over the range of temperatures encountered outdoors.

Computer facilities at Weslaco

In December 1970, an IBM 1800 Processor Controller (32K core storage) was acquired through intra-government transfer. Many peripherals have been added. To process analog data, the IBM 1800 has been interfaced with a mini-computer (Hewlett-Packard 2114B, 8K core storage). The two interfaced computers, capable of operating independently, allow researchers at Weslaco to perform most data handling and processing requirements necessary in agri-cultural research.

---

[1] For further information please refer to Chapter VII in text.

Proposed additions to the system include increased memory, another magnetic tape drive, and an image display device. The latter two additions will allow researchers to display magnetic tape produced from data generated by multispectral scanners mounted in aircraft or spacecraft.

A visual display to aid analysis of digital data

With the volume of multispectral data available, a CRT (cathode ray tube) image display system would provide a powerful tool for use in solving many agricultural, environmental, and sociological problems. The use of a CRT display on multispectral scanner data, from such sources as the NASA 24-channel and University of Michigan 19-channel scanners, as well as digitized data from ERTS-A (Earth Resources Technology Satellite) and Skylab's EREP (Earth Resources Experimental Package) would allow Weslaco's researchers to develop a better understanding of the interaction of electromagnetic energy with the agricultural environment.

Field spectroradiometer digital logger

The Model 20 Exotech spectroradiometer owned by the USDA is designed to measure the spectral radiometric properties of agricultural cover, natural terrain, and soils from either ground based platforms or from aircraft. The spectroradiometer rotates circular variable filters (CVF) through the optical path in front of detectors to obtain the spectral distribution information. Four filter wheels, each with its own detector, are used to cover the .37- to 13.88-μm spectral range. Spectra are scanned at six possible speeds from two scans/sec to two scans/min.

An analog voltage signal proportional to the radiometric energy passing through the filter is generated by each detector. A 1000 pulse per revolution (rev) signal indicates the wavelength of the energy passing through the CVF. Four radiometric signals and two pulse train signals are produced simultaneously. All these are analog (A) voltage signals that must be converted to digital (D) values.

Ten bit digital words are required to record the maximum accuracy of the spectroradiometer. At the maximum scan rate, the intensity measurements alone produce 8000 ten-bit words/sec (4 CVF x 2 rev/sec x 1000 samples/rev). The wavelength dependent signal gives forth 4000 words/sec (2 pulse trains x 1000 pulses per rev x 2 rev/sec).

Thus, a data logger suitable for this spectroradiometer would have to make 12,000 A to D conversions/sec and record all D values. The fact that all signals are being generated simultaneously adds to the complexity of the data logging problem.

The spectroradiometer has a number of controls that affect the conversion of output signals to radiometric values. Besides the scanning speed control (6 positions), each detector has a separate electronic amplifier with a gain control (7 positions); the reference blackbody for the long wavelength detectors has an adjustable temperature control (10-turn pot); and the short wavelength detectors have a scanning mode control (3 positions):

one, incident; two, reflected; or three, alternate incident and reflected. All these controls produce A signals related to their settings that must be recorded along with the radiometric data. The recording of other housekeeping information such as date, time, target identification, temperature, humidity, etc., is necessary for adequate interpretation of radiometric data.

Initial steps have been taken to get a data logging system for the Exotech spectroradiometer. A two-step procedure is being used: first, formal proposals are being requested (REP) from several companies to whom the logging requirements for the spectroradiometer are being sent; and second, the proposals resulting from these requests will be evaluated, balanced against available funds, and final specifications of a data logger will be written.

Mini-maxi computer interface

Disregarding current input and output (I/O) problems, it is generally believed that the HP (Hewlett-Packard 2114B mini-computer)--IBM (International Business Machines) 1800 computer (maxi-computer) interface made at Weslaco has given a tremendous gain in computing power, and the mini-maxi computer interface has greatly extended I/O capabilities. Transfer rates of paper tape characters read on the HP-OPTR (optical paper tape reader) and sent to the IBM 1800 range from 138.9 to 541.9 characters/sec, while the transfer rate of 16-bit computer words from memory to memory is greater than 7000 words/sec.

Current uses of the interface include the processing of paper tape data collected from various instruments, the processing of neutron probe readings (used to determine soil moisture in field experiments) that are recorded in the field on marked sense cards and read by the optical mark card reader on the HP, and the processing of single channel analog (A) tape.

Additional uses involve the processing of A tape generated from such devices as hot wire anemometers, the Barnes Model T5 infrared camera, and many varied optical mechanical scanners. Another planned use of the interface is the loading of core image programs from the IBM 1800 disk into HP memory. This feature alone will give a tremendous amount of flexibility allowing HP core image programs currently stored on paper tape to be loaded into HP memory from the 1800 disk as required. The loading time of core image programs would be greatly reduced for large programs.

The mini-maxi computer interface has made current data processing at USDA faster and more efficient. This interface will provide new applications to problem solving as future experiments are conducted.

CANOPY TEMPERATURE AS AN INDICATOR OF PLANT WATER STRESS

J. F. Bartholic and L. N. Namken

The following information is from a
manuscript prepared for publication in
Agricultural Meteorology. These re-
sults were produced under Research
Outline 72, "Influence of Plant Water
Stress on Growth and Evapotranspiration."

INTRODUCTION

From energy transfer theory, it can be shown that as plant water stress in-
creases and transpiration decreases, leaf temperature rises to increase heat trans-
fer to the air and thermal radiation to the sky (Bartholic et al., 1970). However,
the degree to which leaf temperature increases with increasing water stress is not
clearly understood. A number of authors have proposed theories for heat transfer
from a leaf. Raschke (1960) reviewed work on energy transfer between a plant and
its environment. A leaf temperature and transpiration model has been discussed by
Gates (1964). His leaf model predicts that, under certain wind and radiation con-
ditions, leaf temperature could be 10 to 15C higher than ambient air temperature.
Linacre (1964, 1967) also considered energy transfer from a leaf. In a recent
article (Drake et al., 1970), leaf temperatures and transpiration were discussed
in connection with boundary and leaf layer resistances. Differences as great as
12C were obtained between leaf and air temperature.

A few models that include leaf and air temperature have been proposed for the
complete crop canopy. These models layer the canopy and develop sets of equations
to yield the energy fluxes to and from each canopy layer. These models are proving
useful for understanding energy transfer, provided sufficient information about
leaf area index (LAI), leaf resistance, radiation distribution, and air movement
within the canopy are available (Waggoner et al., 1969; Stewart and Lemon, 1969).

The models are of little value without field measurements. A review of leaf
and air temperatures has been made by Linacre (1964, 1967). Tanner (1963) dis-
cussed plant temperatures measured with a radiation thermometer. Frequently,
daytime leaf temperatures were 5 to 10C higher than air temperatures. Ehrler and
Van Bavel (1967) reported that sorghum leaf temperatures, prior to irrigation,
could be 4 or 5C warmer than air temperature in Arizona. The measurements were
made with thermocouples placed in the midrib of fully exposed flag leaves. Some-
what different results were reported later by Van Bavel and Ehrler (1968) when they
showed leaf temperatures several degrees lower than air temperature. It should be
noted, however, that these leaf temperatures were an average of thermocouple
measurements in the midrib of leaves in the top half of a well-watered sorghum
canopy. Wiegand and Namken (1966) investigated the influences of plant moisture
stress, solar radiation, and air temperature on cotton leaves during three growing
seasons. They found that, under a dry soil moisture regime with full solar radia-
tion, leaf temperatures could be as much as 10C warmer than the air. Generally,
the difference between leaf and air temperature for stressed plants was 4 to 8C.
Baker (1966) reported similar results.

To facilitate stress studies, Namken et al. (1969, 1971) related stem radial contraction of cotton plants to water stress.

Detailed plant and soil thermal regime has been obtained for agricultural areas with an aircraft mounted thermal scanner (Wiegand et al., 1968, 1970). The ability of an aerial scanner to provide extensive thermal information relative to crop and soil conditions was demonstrated. Myers et al. (1970) suggested obtaining plant canopy temperatures with thermal scanner techniques and presented thermograms depicting emittance from cotton crops under varying stress conditions.

SUMMARY

The difference between crop canopy surface temperature (T_s) and air temperature (T_a) 40 cm above the crop was predicted theoretically and then measured under field conditions as plant water stress increased during drying cycles for cotton. The energy balance equation was rearranged to yield surface temperature as a function of environmental, radiation, and plant water stress conditions. Calculated temperature differences (T_s-T_a) of 1 to 6C were found with typical plant water stress conditions (Fig. 1). Thermocouples placed in contact with the lower leaf surfaces in the top 1/3 of a full canopy, measured temperature differences of about 6C during peak radiation loads and plant water stress of -20 bars. An airplane mounted RS-14 thermal scanner with a 1 mr field of view measuring in the 8 to 14 µm band with two internal calibration sources was used during July of 1970 to determine emittance from cotton crops under various stress conditions. Analysis of the data indicates emittance differences representing several degrees between well-watered cotton and cotton under moderate to high plant water stress. The results suggest the possibility of scheduling irrigations of cotton on the basis of aerial scanner measured canopy temperature.

LITERATURE CITED

Baker, D. N. 1966. Microclimate in the field. Trans. of the ASAE, X:77-84.

Bartholic, J. F., L. N. Namken, and C. L. Wiegand. 1970. Combination equations used to calculate evaporation and potential evaporation. ARS 41-170, Agricultural Research Service, USDA, Nov. 1970.

Drake, G. B., K. Raschke, and F. B. Salisbury. 1970. Temperatures and transpiration resistances of Xanthium leaves as affected by air temperature, humidity, and wind speed. Plant Physiol. 46:324-330.

Ehrler, W. L., and C. H. M. Van Bavel. 1967. Sorghum foliar responses to changes in soil water content. Agron. J. 59:243-246.

Gates, David M. 1964. Leaf temperature and transpiration. Agron. J. 56:273-277.

Linacre, E. T. 1964. A note on a feature of leaf and air temperatures. Agr. Meteor. 1:66-72.

Linacre, E. T. 1964. Calculations of the transpiration rate and temperature of a leaf. Archiv für Meteorologie, Geophysik und Bioklimatologie, Ser. B: 13:391-399. Springer Verlag, New York.

Linacre, E. T. 1967. Further notes on a feature of leaf and air temperatures. Archiv für Meteorologie, Geophysik und Bioklimatologie, Ser. B. Allgemeime und Biologiche Klimatologie 15:422-436.

Linacre, E. T. 1967. Further studies of the heat transfer from a leaf. Plant Physiol. 42:651-658.

Myers, V. I., M. D. Heilman, R. J. P. Lyon, L. N. Namken, D. Simonett, J. R. Thomas, C. L. Wiegand, and J. T. Woolley. 1970. Soil, water, and plant relations. Remote Sensing with Special Reference to Agriculture and Forestry. National Academy of Sciences, Washington, D. C. p. 253-297.

Namken, L. N., J. F. Bartholic, and J. R. Runkles. 1969. Monitoring cotton plant stem radius as an indication of water stress. Agron. J. 61:891-893.

Namken, L. N., J. F. Bartholic, and J. R. Runkles. 1971. Water stress and stem radial contraction of cotton plants (Gossypium hirsutum L.) under field conditions. Agron. J. 63:623-627.

Raschke, K. 1960. Heat transfer between the plant and the environment. Ann. Rev. Plant Physiol. 11:111-126.

Stewart, D. W., and E. R. Lemon. 1969. The energy budget at the earth's surface: A simulation of net photosynthesis of corn. Microclimate Investigations Interim Report 69-3, Northeast Branch, SWC, ARS, USDA and N. Y. State College of Agriculture, Cornell University, Ithaca, N. Y. U. S. Army Electronics Command Technical Report ECOM 2-68 1-6.

Tanner, C. B. 1963. Plant temperatures. Agron. J. 55:210-211.

Van Bavel, C. H. M., and W. L. Ehrler. 1968. Water loss from a sorghum field and stomatal control. Agron. J. 60:84-86.

Waggoner, P. E., G. M. Furnival, and W. E. Reifsnyder. 1969. Simulation of the microclimate in a forest. Forest Science 15:37-45.

Wiegand, C. L., and L. N. Namken. 1966. Influences of plant moisture stress, solar radiation, and air temperature on cotton leaf temperature. Agron. J. 58:582-586.

Wiegand, C. L., M. D. Heilman, and A. H. Gerbermann. 1968. Detailed plant and soil thermal regime in agronomy. Proc. 5th Symp. of Remote Sensing of Environ., Univ. of Mich., Ann Arbor, April 16-18, 1968. p. 325-342.

Wiegand, Craig L., and Jon F. Bartholic. 1970. Remote sensing in evapotranspiration research on the great plains. IN: Evapotranspiration on the Great Plains. Research Committee Great Plains Agricultural Council. Publ. No. 50, Kansas State University, Manhattan, Agricultural Experiment Station, Mar. 1970, p. 137-180.
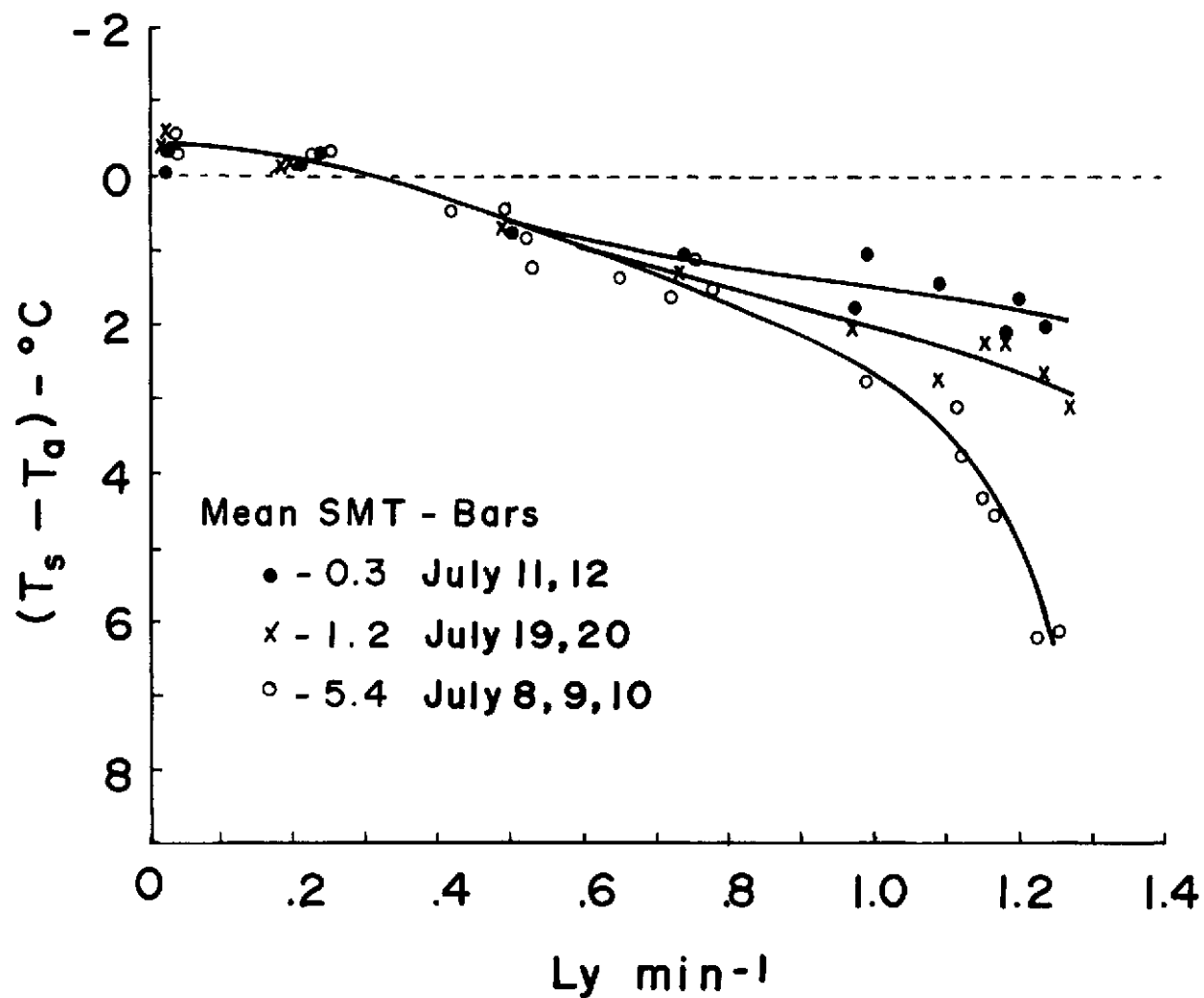
Fig. 1.--Relation between cotton canopy surface temperature minus air temperature at 40 cm above canopy (T_s-T_a) for different mean soil moisture tensions (SMT) of the top 90 cm of the soil profiles.

TEMPERATURE OF SOILS AND OF CROP CANOPIES

DIFFERING IN WATER CONDITIONS

J. F. Bartholic, L. N. Namken, and C. L. Wiegand

INTRODUCTION

Surface temperatures of agricultural fields are of great importance. Soil temperatures too hot or too cold inhibit seed germination. During summer months, if the soil surface layer is dry, temperatures may reach 50 to 60C (Wiegand et al., 1968) and destroy emerging plants. Irrigating to cool the soil enhances seed germination in summer seedbeds. Practices such as tillage that roughen the surface affect turbulent transfer at the soil surface and thus modify surface tempera-tures. During the winter and spring months, soil surface temperature information can be used to help decide when to initiate freeze protection practices (Bartholic et al., 1970).

Evaporation from a wet surface (soil or plant leaves) is strongly affected by surface temperature since the vapor pressure at the surface is a function of sur-face temperature. However, crop canopy and soil surfaces become progressively drier as soil water becomes more limiting, resulting in decreased evaporation, and a corresponding higher temperature at thermal equilibrium.

Considerable work has been reviewed on how plant temperatures increase with decreasing available soil water (Linacre, 1967). Other workers have indicated that canopy temperature could provide an indication of the relative water stress of a crop as soil water is depleted, and that temperature differences between well-watered and stressed crops should indicate a relative need for irrigation (Bar-tholic and Namken, 1971; David, 1969; Horton et al., 1970; Myers et al., 1970; Wiegand and Namken, 1966; Wiegand, 1971). Within large irrigation projects, it should be possible to identify fields needing irrigation from crop canopy tempera-ture information. Within individual fields, plants in areas not irrigated ade-quately should stress sooner and have a warmer canopy temperature than the non-stressed plants in well-watered surrounding areas.

Unfortunately, it is difficult to obtain surface temperatures (T_S) from ground-based sensors. Thermocouples or other point temperature measurements need to be replicated many times so this method for determining T_S becomes cumbersome to monitor many fields. Considerable work has been done with radiation thermome-ters to determine crop temperature. Although this is an improvement compared with the use of thermocouples, ground monitoring nonetheless permits integration of only a relatively small area of a field.

Consideration is given to an alternate approach (Wiegand et al., 1968; Myers et al., 1970; Bartholic and Namken, 1971) to obtain surface temperatures and to delineate water-stressed and well-watered fields of crops in large irrigated areas. An airplane-mounted RS-14 thermal scanner was used to measure thermal irradiance, mainly a function of surface temperature.

SUMMARY

An airplane-mounted thermal scanner was used to measure irradiance in the 8- to 14-μm wavelength interval over an extensively instrumented agricultural area. The area included soils differing in water and tillage condition, and replicated cotton plots with a wide range of plant water stress. The scanner data were recorded on analog magnetic tape and on 70-mm film. The film densities of the various soil and cotton treatments and film calibration information were determined with a microdensitometer. The observed irradiances corresponded to cotton plant canopy temperature differences up to 6C between the most and least water-stressed plots. The irradiance data from soils showed large differences as a function of time after tillage and irrigation. It is concluded that thermal imagery offers potential as a useful aid for delineating water-stressed and nonstressed fields of crops, evaluating uniformity of irrigation, and evaluating surface soil water conditions.

LITERATURE CITED

Bartholic, J. F., C. L. Wiegand, R. W. amer, L. N. Namken. 1970. Thermal scanner data for studying freeze conditions and for aiding irrigation scheduling. Third Annual Earth Resources Program Review, Vol. II, p. 27-1 to 27-23.

Bartholic, J. F., and L. N. Namken. 1971. Canopy temperature as an indicator of plant water stress. Agricultural Meteorology. (In Press).

David, W. P. 1969. Remote sensing of crop water deficits and its potential applications, an annotated bibliography. Tech. Rpt. No. RSC-06, Texas A&M Univ. Remote Sensing Center. 49 p.

Horton, M. L., L. N. Namken, and J. T. Ritchie. 1970. Role of plant canopies in evapotranspiration. IN: Evapotranspiration on the Great Plains. Publication No. 50, K. S. U., Agric. Expt. Sta. p. 301-338.

Linacre, E. T. 1967. Further notes on a feature of leaf and air temperatures. Archiv für Meteorologie, Geophysik und Bioklimatologie. Serie B: Algemeime und Biologiche Klimatologie, 15:422-436.

Myers, V. I., M. D. Heilman, R. J. P. Lyon, L. N. Namken, D. Simonett, J. R. Thomas, C. L. Wiegand, and J. T. Woolley. 1970. Soil, water, and plant relations. IN: Remote Sensing with Special Reference to Agriculture and Forestry. National Academy of Science, Washington, D. C. p. 253-297.

Wiegand, C. L., and L. N. Namken. 1966. Influence of plant moisture stress, solar radiation, and air temperature on cotton leaf temperature. Agron. J. 58: 582-586.

Wiegand, C. L., M. D. Heilman, and A. H. Gerbermann. 1968. Detailed plant and soil thermal regime in agronomy. Proc. 5th Symp. of Remote Sensing of Environ., Univ. of Mich., Ann Arbor. p. 325-342.

Wiegand, C. L. 1971. Agricultural applications and requirements for thermal infra-red scanners. Proc. International Workshop on Earth Resources Survey Systems, Ann Arbor, Mich. Vol. II, p. 66-81.

SENSING OF BORON AND CHLORIDE TOXICITIES OF CITRUS TREES

R. Cardenas, A. Peynado, H. W. Gausman,
A. H. Gerbermann, and R. L. Bowen

INTRODUCTION

The objective of research reported here is to develop the use of aerial photography and corresponding film density measurements to discriminate between healthy trees and unhealthy citrus trees whose foliage exhibit boron (B) and chloride (Cl^-)[1] toxicity symptoms (affected). To interpret photographic images of healthy and affected trees, the relation of the tonal responses of Kodak Ektachrome Infrared Aero 8443 (EIR) film to reflectance of healthy and affected citrus foliage must be understood, and the best method for measuring and comparing film density readings must be determined.

Norman (1965) and Norman and Fritz (1965) obtained encouraging results with EIR film in connection with detecting stressed citrus trees. They obtained distinctive colors on EIR transparencies for foot rot, advanced nematode infestation, very early Tristeza virus reaction, and manifestations of Psorosis, Xyloporosis, and Exocortis viruses. Gausman et al. (1969) showed that foot rot-affected trees appeared as white compared with red images for healthy trees on EIR film. The literature indicates, however, that many variables need to be evaluated before EIR film detection of citrus tree diseases can be accurate and dependable. For example, information is needed on EIR film images of citrus trees with B and Cl^- toxicities and iron (Fe) deficiency to see if these three images can be differentiated from each other and from the foot rot image. Identification of B and Cl^- toxicities and Fe deficiency with aerial photography would be useful to the citrus industry for application of corrective measures before fruit production is curtailed. The detection of severely foot rot-affected trees could be used to tell growers what trees needed to be replaced.

MATERIALS AND METHODS

Results were obtained in 1970 from a split-plot experimental design with two irrigation treatments (plots) within each of four blocks. Irrigation treatments have been applied every summer since 1963 and consist of irrigating with (a) canal water from the Rio Grande River (control treatment) and (b) canal water with the addition of 4,000 ppm of salts containing NaCl (sodium chloride), $CaCl_2$ (calcium chloride), and 6 ppm B (salt treatment). Each of the two irrigation plots within each block has eight Red Blush grapefruit trees (Citrus paradisi, Macf.), each on a different rootstock. Only the Red Blush grapefruit trees with the Troyer citrange rootstock were considered because they were more sensitive to B and Cl^-.

---

[1] The ion of chlorine (Cl^-) will be used since its usage is more common in the literature than the element (Cl).

Thirty-five leaves (approximately 6 months old) of the late-summer flush were sampled from branch apices of Red Blush grapefruit trees with the Troyer citrange rootstock within each control and salt treatment plot of the four blocks. Leaves were wrapped immediately in Saran and placed on ice to limit dehydration.

In the laboratory, leaf samples were randomly separated into three groups for (a) B and Cl⁻ assays, (b) total chlorophyll determination, and (c) spectral, leaf thickness, leaf area, and water content measurements. A Beckman Model DK-2A spectrophotometer equipped with a reflectance attachment was used to obtain diffuse reflectance and transmittance measurements on upper (adaxial) surfaces of one leaf from each of the eight trees. The spectral measurements were recorded at discrete 50-nm increments over the 500- to 2500-nm wavelength interval. Data were corrected for a decrease in reflectance of the MgO reference, caused by deterioration during aging to give absolute radiometric data (Sanders and Middleton, 1953). Thickness measurements were made at three locations on each leaf used for spectral measurements with a linear displacement transducer and digital voltmeter (Heilman et al., 1968). Leaf area was measured with a planimeter. Percent water content was determined on an oven-dry weight basis (68 C for 72 hrs).

Leaves sampled for B and Cl⁻ assays were washed in water and detergent, rinsed with tap water, rinsed four times with distilled water, and then freeze-dried. Methods of Hatcher and Wilcox (1950) and Cotlove et al. (1958) were used for the B and Cl⁻ analyses, respectively.

Total chlorophyll (chlorophyll a + chlorophyll b) was determined using procedures of Hall and Hacskaylo (1963) and Horwitz (1965). Total chlorophyll in mg/l was calculated as:

$$7.12 \log_{10} \frac{I_o}{I} \quad \text{(at 660 nm)}$$

$$+ 16.8 \log_{10} \frac{I_o}{I} \quad \text{(at 642.5 nm)},$$

where I_o and I are transmittance values for the petroleum ether solvent and unknown solutions, respectively.

Photographs were taken from an aircraft and from the bucket of a Truco aerial lift ("cherry picker") with a Hasselblad camera, 50-mm focal length lens using 70-mm EIR film and a Kodak Wratten 15 filter with an approximate 100% absorption edge at 500 nm. Photographs were taken from the Truco at a height of 8 ft above each tree; overflight photographs were taken at an altitude of 3,000 ft. The scale of aerial photography was 1:18,000.

Optical count readings were made on EIR transparencies with a Joyce, Loebl recording microdensitometer using no filter (white light) and red (Wratten 92), green (Wratten 93), and blue (Wratten 94) bandpass filters in the densitometer's light beam. The microdensitometer output is in optical counts that are punched onto paper tape. The paper tape microdensitometer output consists of a base line count corresponding to the standard optical densities of the first step of the calibrated step wedge in use, plus added counts that depend on the particular step on the wedge that balances the light transmission by the film being analyzed in the second light beam. The distance the uniformly graduated step wedge travels to balance the transmission by the film determines the count registered by the encoder. The optical count is related to the optical density (O.D.) by the relation:

$$O.D. = [(Optical\ counts - base\ reading)(wedge\ factor)]$$

$$+ (step\ wedge\ density).$$

An area of 2 x 2 sq cm on each tree was selected for eight photographic transparencies taken from the Truco's bucket. Eight scan lines (2 mm distance between any pair of lines) were run for each tree of each transparency for each of the four filters. Twenty-five readings (data bits) were taken on each scan line representing a transparency area of 0.0798 sq mm.

One transparency was selected from the aerial photographs, and one scan line was run for each of eight trees and for each of the four filters. Scans were run in the central area of the tree canopies. Twenty-five readings were taken on each scan line representing a transparency area of 0.0062 sq mm.

Spectrophotometric data were analyzed for variance (Steel and Torrie, 1960). Duncan's multiple range test was used to test differences among means when F ratios were statistically significant (Duncan, 1955).

RESULTS AND DISCUSSION

Affected citrus leaves had leaf symptoms typical of B and Cl^- toxicities with scattered yellow spots on upper (adaxial) surfaces, brownish, resinous gummy spots on lower (abaxial) surfaces, and edge of tip burn compared with green healthy leaves (Peynado and Young, 1969). Chemical analyses showed that B and Cl^- contents were 285.5 ± 23.6 (standard error) ppm B and 0.24 ± 0.10% Cl^- for healthy leaves, and 832.5 ± 75.2 ppm B and 0.33 ± 0.12% Cl^- for affected leaves (Table 1). Affected leaves also had less chlorophyll than healthy--11.7 ± 0.6 mg/liter for affected leaves as compared with 15.2 ± 1.6 mg/liter for healthy leaves (Table 1).

Statistically significant differences (p = 0.01) existed among means of leaf surface area. Average areas per leaf were 40.4 ± 1.5 cm^2 and 28.9 ± 1.9 cm^2 for healthy and affected leaves, respectively. There were no statistically significant differences (p = 0.05) between affected and healthy leaves in leaf thickness. Average leaf thicknesses were 0.32 ± 0.02 mm and 0.31 ± 0.01 mm for affected and healthy leaves, respectively (Table 1). The percent leaf water content of affected leaves (57.1 ± 3.5) was not significantly different from healthy leaves (55.2 ± 4.1)(Table 1).

Relative to spectral measurements, statistically significant differences (p = 0.01) existed among means of all wavelengths for healthy and affected leaves for reflectance, transmittance, and absorptance (calculated as absorptance = 100 - percent reflectance + percent transmittance) measurements. Spectrophoto-metrically measured reflectance of top leaf surfaces showed that B- and Cl⁻-affected leaves had about 1 to 4% less reflectance than healthy leaves over the 750- to 2500-nm wavelength range (Fig. 1) except near the 1450- and 1950-nm water absorption bands where reflectance was approximately the same. In the visible range (500 to 750 nm), affected leaves had 13% more reflectance than healthy leaves at the 550-nm green wavelength peak (Fig. 1).

Affected leaves had 2.0 to 3.0% more absorptance than healthy leaves (Fig. 2) over the 750- to 1350-nm near-infrared wavelength range. The absorptance of healthy and affected leaves was essentially the same over the 1350- to 2500-nm wavelength interval. The greatest effect on absorptance was at the 550-nm wavelength where the absorptance of affected leaves was 18% lower than the absorptance of healthy leaves.

For EIR photographs taken from both the Truco's bucket and the aircraft, reflectance of light from B- and Cl⁻-affected trees produced light-red (pinkish) images, compared with dark-red images for healthy trees.

Optical density readings were made on the tree images of EIR transparencies with white light and red-, blue-, and green-filtered light. Means and ranges of optical density readings are shown in Table 2 for photographs taken at an alti-tude of 3,000 ft from the aircraft and in Table 3 for photographs taken 8 ft above the trees from the Truco's bucket. For photographs taken from the aircraft, best discrimination between healthy and affected citrus trees was obtained with a blue bandpass filter. Density values (Table 2) were 1.177 ± 0.012 and 1.029 ± 0.014 for healthy and affected trees, respectively. For photographs taken at a height of 8 ft above the trees from the Truco's bucket, best discrimi-nation was obtained with a red bandpass filter. Density values (Table 3) were 1.158 ± 0.017 and 0.953 ± 0.027 for healthy and affected trees, respectively. Although more density readings were made on tree images of the photographic transparencies obtained from the Truco's bucket than from the aircraft, results indicate that a red bandpass filter is best for photographs taken at a low alti-tude, and a blue bandpass filter is best for photographs taken at a high altitude. These results agree with the findings of Albert (1970) who reported that the camera by altitude interaction was often statistically significant. The different results obtained with the blue and red bandpass filters were apparently caused by the attenuation of light reflected from the citrus tree foliage at the 3,000 ft altitude.

Further work is planned for comparing film images of B- and Cl⁻- toxicities, iron (Fe) deficiency, and foot rot of citrus trees (Gausman et al., 1969). The new Kodak Aerochrome Infrared 2443 (AIR) film will be used in future research.

If visual interpretation among images of foot rot and the nutritional maladies proves impractical, computer discrimination procedures will be applied to densi-tometer readings on AIR film transparencies (Richardson et al., 1970).

LITERATURE CITED

Albert, W. G. 1970. Statistical analysis in multispectral remote sensing. M.S. Thesis, Texas A&M University Institute of Statistics, College Station, Texas. 58 p.

Cotlove, E., H. V. Trantham, and R. L. Bowman. 1958. An instrument for and method for automatic, rapid, accurate, and sensitive titration of chloride in biological samples. J. Lab. & Clin. Med. 50:358-371.

Duncan, D. B. 1955. Multiple range and multiple F tests. Biometrics 11:1-42.

Gausman, H. W., W. A. Allen, R. Cardenas, and Marcia Schupp. 1969. The influence of Cycocel treatment of cotton plants and foot rot disease of grapefruit trees on leaf spectra in relation to aerial photographs with infrared color film. Proc. 1969 Workshop on Aerial Color Photography in the Plant Sciences, Gainesville, Fla., Mar. 5-7, 1969. p. 16-24.

Hall, W. C., and J. Hacskaylo. 1963. Methods and procedures for plant biochemical and physiological research. The Exchange Store, College Station, Texas. 68 p.

Hatcher, J. T., and L. V. Wilcox. 1950. The colorimetric determination of boron with carmine. Anal. Chem. 22:567-569.

Heilman, M. D., C. L. Gonzalez, W. A. Swanson, and W. J. Rippert. 1968. Adaptation of a linear transducer for measuring leaf thickness. Agron. J. 60:578-579.

Horwitz, W. 1965. Official methods of analysis. 3rd edition. Assoc. of Official Agric. Chemists, Washington, D. C. p.115.

Norman, G. G. 1965. Infra-red proves useful in disease detection project. Citrus World 2:10.

Norman, G. G., and N. J. Fritz. 1965. Infrared photography as an indicator of disease and decline in citrus trees. Proc. Florida State Hort. Soc. 78:59-63.

Peynado, A., and R. Young. 1969. Relation of salt tolerance to cold hardiness of red blush grapefruit and Valencia orange trees on various rootstocks. Proc. First Inter. Citrus Symp. 1:1793-1801.

Richardson, A. J., R. J. Torline, D. A. Weber, R. W. Leamer, and C. L. Wiegand. 1970. Computer discrimination procedure comparisons using film optical densities. SWC Research Rept. 422. 87 p.

Sanders, C. L., and E. E. K. Middleton. 1953. The absolute spectral diffuse reflectance of magnesium oxide in the near infrared. J. Opt. Soc. Am. 43:58.

Steel, R. G. D., and J. H. Torrie. 1960. Principles and procedures of statistics. McGraw-Hill Book Co., New York. 481 p.

Table 1.--Effects of control and salt irrigation treatments on chemical (total chlorophyll, B, Cl⁻, percent water content) and physical (area, thickness) characteristics of Red Blush grapefruit leaves.

Irrigation treatment	Chemical characteristics[1]				Physical characteristics[2]	
	Total chlorophyll	B	Cl⁻	Water content	Leaf thickness	Area per leaf
	mg/l	ppm	%	%	mm	cm²
Control	15.2 ± 1.6[3]	285.5 ± 23.6	0.24 ± 0.10	55.2 ± 4.1	0.31 ± 0.01	40.4 ± 1.5
Salt	11.7 ± 0.6	832.5 ± 75.2	0.33 ± 0.12	57.1 ± 3.5	0.32 ± 0.02	28.9 ± 1.9

[1] Average of four determinations.

[2] Average of four measurements.

[3] Standard error.

Table 2.--Means and ranges of optical density readings for white light and red-, blue-, and green-filtered light of EIR transparencies obtained at an altitude of 3,000 ft above healthy (control) and B- and Cl⁻-affected Red Blush grapefruit trees.[1]

Light	Healthy trees			B- and Cl⁻-affected trees		
	Lowest reading	Highest reading	Mean of readings	Lowest reading	Highest reading	Mean of readings
White	0.982[2]	1.148	1.049 ± 0.016[3]	0.834	1.129	0.943 ± 0.014
Red	0.054	0.848	0.628 ± 0.020	0.424	0.860	0.567 ± 0.016
Blue	1.090	1.273	1.177 ± 0.012	0.884	1.206	1.029 ± 0.014
Green	1.074	1.184	1.126 ± 0.010	0.940	1.176	1.048 ± 0.010

[1] For each of the white light and red-, blue-, and green-filtered light densitometer set-ups, one transparency with four healthy and four affected tree images was scanned with one scan line per tree and 25 readings per scan.

[2] Optical density = [(optical count - base reading)(wedge factor)] + (step wedge density)

$$= [(O.C. - 40)(.011)] + (.71)$$

[3] Standard error.

Table 3.--Means and ranges of optical density readings for white light and red-, blue-, and green-
filtered light of EIR transparencies obtained at a height of 8 ft above healthy (control)
and B- and Cl⁻-affected Red Blush grapefruit trees.[1]

Light	Healthy trees			B- and Cl⁻-affected trees		
	Lowest reading	Highest reading	Mean of readings	Lowest reading	Highest reading	Mean of readings
White	1.102[2]	1.352	1.239 ± 0.010[3]	0.942	1.205	1.077 ± 0.014
Red	0.980	1.302	1.158 ± 0.017	0.795	1.079	0.953 ± 0.027
Blue	1.129	1.314	1.189 ± 0.010	0.975	1.209	1.102 ± 0.013
Green	1.082	1.234	1.166 ± 0.006	0.952	1.139	1.057 ± 0.010

[1] For each of the white light and red-, blue-, and green-filtered light densitometer set-ups, eight
transparencies were scanned with eight scan lines per tree and 25 readings per scan.

[2] Optical density = [(optical counts - base reading)(wedge factor)] + (step wedge density)

$$= [(O.C. - 40)(.011)] + (1.01).$$

[3] Standard error.
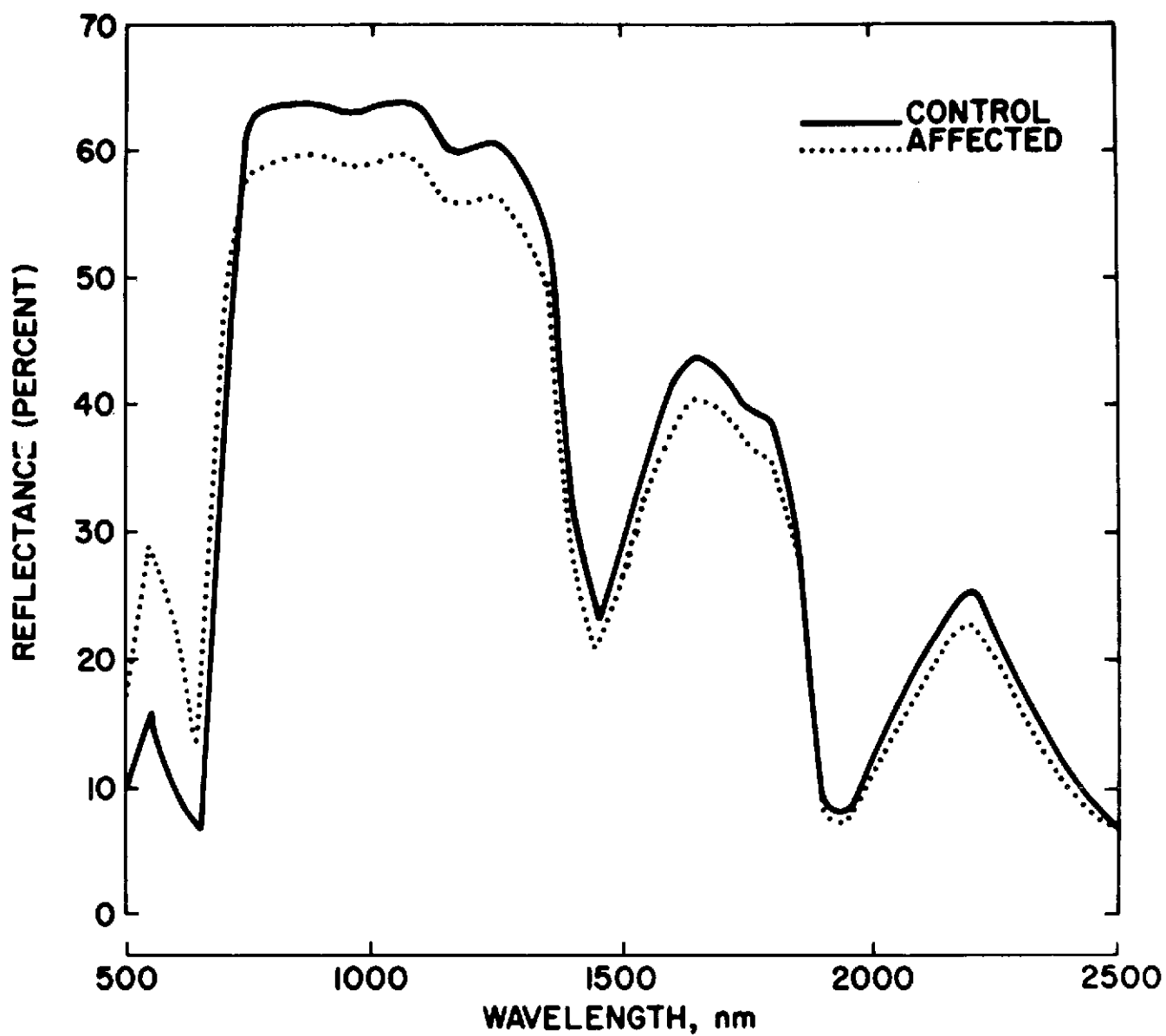
Fig. 1.--Total diffuse light reflectance of upper surfaces of control
(healthy) and affected Red Blush grapefruit leaves. Each spectrum is
an average of four leaves.
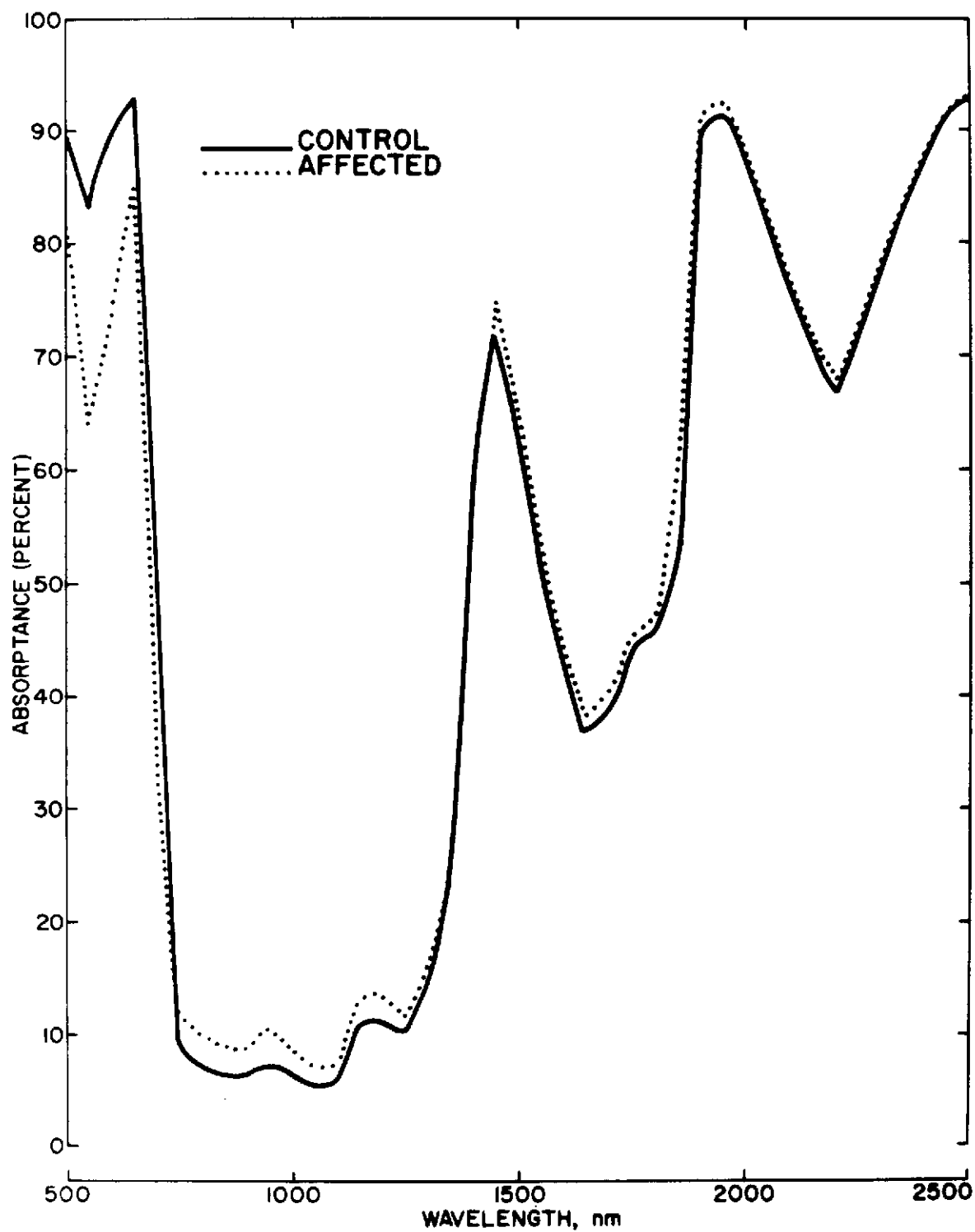
Fig. 2.--Total light absorptance of control (healthy) and affected Red Blush grapefruit leaves. Each spectrum is an average of four leaves.

PRE-VISUAL DETECTION OF WATERMELON MOSAIC VIRUS IN CUCUMBER

R. Cardenas, C. E. Thomas, and H. W. Gausman

The following manuscript has been prepared
for publication in Phytopathology.

INTRODUCTION

This paper presents results of research that was conducted to ascertain if
watermelon mosaic virus-1 (WMV-1) and watermelon mosaic virus-2 (WMV-2) could be
pre-visually detected by photographing cucumber plants with Kodak Aerochrome
Infrared 2443 (AIR) film. However, pre-visual detection of plant diseases has
had variable success. Manzer and Cooper (1967) found that late blight of pota-
toes could be detected by aerial infrared photography 1 to 3 days before visual
symptoms became apparent. A 1971 oral communique with Dr. G. R. Cooper indicated
that pre-visual detection has been increased to 5 days. However, tobacco ring-
spot virus could be detected only about 1 day before visual symptoms were evident
(Burns et al., 1969). In contrast, Heller (1968) found that beetle damage could
not be predetected, and Meyer (1967) reported that variability interfered with
pre-visual detection of tree diseases.

Cellular discoloration affects reflectance of light over the 700- to
1350-nanometer (nm) wavelength interval. This response is useful in detecting
nonvisual symptoms of plant leaf stress (Cardenas et al., 1970).

MATERIALS AND METHODS

Cucumber plants (cultivar National Pickling) were grown in the greenhouse
in sandy clay loam soil contained in 4.6-liter clay crocks. A 10-20-5 fertilizer
was added to the soil at a rate of 27.3 kg/ha of nitrogen. All plants were
watered daily with 200 ml of rainwater. Plants were thinned to eight per crock
3 days after their emergence.

A randomized complete block experimental design was used with five replica-
tions (crocks) of three treatments: (1) control--cotyledons swabbed with
abrasive and sterile distilled water, (2) cotyledons swabbed with abrasive and
WMV-1 inoculum, and (3) cotyledons swabbed with abrasive and WMV-2 inoculum.
This paper considers results obtained with WMV-2 because a complete photographic
sequence was not obtained for plants inoculated with WMV-1. Each cotyledon was
inoculated 5 days after emergence, 2 days after the first true leaf was macro-
scopically visible. Plants were very uniform--their first true leaves appeared
and unfolded at the same time.

A series of photographs of all plants were taken beginning 2 days after inoculation and continuing at 24-hr intervals for 7 days until visual symptoms of WMV-2 appeared on leaves of inoculated plants. Photographs were taken with artificial light (Honeywell Electronic, Auto/Strobonar flash) with a Hasselblad camera, 80-mm lens, Tiffen yellow filter and 70-mm AIR film. Five days after inoculation of cotyledons and 2 days prior to the appearance of visual symptoms, WMV-2 symptoms were detected on the first true leaves in AIR photographs. Pre-visual WMV-2 symptoms produced a darker red saturation of leaf areas on AIR film prints and transparencies compared with the lighter and uniform red saturation of leaves from control plants. Two days after the pre-visual detection of WMV-2 photographically, the virus showed visually with a characteristic yellow and green mottling pattern and leaf curling.

SUMMARY

Watermelon mosaic virus-2 (WMV-2) was pre-visually detected on cucumber leaves (Cucumis sativis L.) 5 days after cotyledonary swabbing by taking daily photographs with Kodak Aerochrome Infrared 2443 film (AIR)--symptoms were detected 2 days earlier on leaves whose cotyledons were swabbed with abrasive and WMV-2 inoculum than on plants swabbed with abrasive and sterile distilled water. Photographic transparencies revealed that virus-infected leaves had areas of darker red color saturation than uninfected leaves.

Pre-visual detection of virus diseases of plants photographically would facilitate early diagnosis and roguing of diseased plants in breeding and seed increase programs. Early treatment of plant diseases could help prevent extensive crop loss. For example, AIR photographs could be taken of a crop and the film processed and evaluated within 4 hours. Pre-visual detection of virus diseases may be also useful for crop production estimates.

LITERATURE CITED

Burns, E. E., M. J. Starzyk, and D. L. Lynch. 1969. Detection of plant virus symptoms with infrared photography. Trans. Illinois State Acad. Sci. 62(1).

Cardenas, R., H. W. Gausman, W. A. Allen, and Marcia Schupp. 1969-1970. The influence of ammonia-induced cellular discoloration within cotton leaves (Gossypium hirsutum L.) on light reflectance, transmittance, and absorptance. Remote Sens. Environ. 1:199-202.

Heller, R. C. 1968. Previsual detection of Ponderosa Pine trees dying from bark beetle attack. Proc. 5th Symp. Remote Sens. Environ., Univ. of Michigan, Ann Arbor. p 387-434.

Manzer, F. E., and G. R. Cooper. 1967. Aerial photographic methods of potato disease detection. Maine Agric. Exp. Sta. Bull. 646. 14 p.

Meyer, M. P. 1967. No title. Proc. Workshop Infrared Color Photography in the Plant Sciences, Winter Haven, Florida, 5:5-7.

DETECTION AND MONITORING OF SOIL EROSION BY WIND

D. W. Fryrear

INTRODUCTION

Soil erosion by wind is a problem in the Southern Great Plains. The problem intensifies during drought conditions. Evaluating the spread and extend of wind erosion is a slow time-consuming process. High altitude aerial photography offers a rapid method of periodically inspecting the vast landscape of the Southern Great Plains to check the current status of wind erosion conditions on a scale that has not been possible before. Objectives in using photography for this purpose are: (1) to attempt to relate soil color characteristics to the wind erodibility of the soil, (2) to identify evidence of past wind erosion, and (3) to relate the spectral information with erosiveness so that deteriorating soil conditions can be detected in time to institute ameliorative procedures.

MATERIALS AND METHODS

High altitude photography (RB57F aircraft) will be examined to determine soil reflectance characteristics associated with wind erosion. The photos will also form a base map for comparison with ERTS-A (Earth Resources Technology Satellite) imagery. Flights will be requested to coincide with the critical wind erosion period, and a summer flight will be used for contrast in soil reflectance.

A standing order will be placed for ERTS-A data from the MSS channels 2 and 4, and for color positives and negatives from each satellite pass over the area of interest, latitude 31° to 34° and longitude 100° to 104°. If detailed analyses are merited, composite prints and computer compatible tapes of MSS digital data will be requested.

Ground truth data on soil surface condition (texture and roughness), surface residue (type, amount, and orientation), surface soil moisture, and crops (type, spacing, surface cover, and height) will be taken from sites selected from the RB57F flight imagery. Frequency of sampling will coincide with alternate satellite passes.

RESULTS AND DISCUSSION

Surface soil samples from eroding sites have been taken and analyzed for particle size distribution and Munsell soil color (Table 1). Microdensitometer readings have been obtained for the color (Kodak Ektachrome) and color IR (Kodak Aerochrome 2443) films from the sites for both flights.

Several large sites, 600 acres or larger, have been located from the RB57F flights for use in the ERTS-A program. Although insufficient data and analytical procedures are available, the microdensitometer results in Table 1 suggest that the light reflectance is higher from fields that have recently eroded than from fields that have not eroded. Bowers (1965) reported an exponential increase in reflectance for incident radiation of 1,000 mμ wavelength as kaolinite soil particle size decreased.

A visual evaluation of the photos and microdensitometer readings suggests that the aerial photo technique may be a valuable method of determining the potential erodibility of a field or area. If a standard exposure point is available on each frame, the microdensitometer reading may be correlated with erodibility. Without the standard exposure point, each frame must be checked for noneroding sites and the signature from these sites must be used as a comparison with the eroding or potential eroding sites.

Land features such as turnrows at the edge of a field, blown-in-fence-rows, bare creek beds, and sand dunes in rangelands are readily visible on the film and on the microdensitometer tracing. The color IR is generally more sensitive than conventional color film to the features of interest particularly on the lighter soil (Gerbermann et al., 1971). For example, where the color microdensitometer readings on color film have an amplitude of ±0.02, the reading on the color IR film will have an amplitude of ±0.05. The color IR photos from the July flight contain more data on the status of the soil-plant situation than the color photos.

The color signature from shallow eroding soils around Big Spring was markedly different between the January and July flights. In preparing a seedbed after the January flight, subsurface soil was brought to the surface and the July microdensitometer readings were considerably higher than the January readings (see Drake soil, Table 1). The cotton in July was not tall enough to appreciably reduce the reflectance because on other areas within the field the July microdensitometer readings were 0.87 and 0.67 for the color and color IR films, respectively. There was little difference in the microdensitometer readings for the entire field with the Drake soil in January.

SUMMARY

Evaluation of the microdensitometer readings from aerial photographs (RB57F platform) of eroding and noneroding soils reveals that the film density is less for the eroding soils than for the noneroding soils. Land features such as blow-outs in rangeland, turnrows at the edge of a field, and bare creek beds are readily detectable from the RB57F photos with the microdensitometer.

It is very difficult to plan a flight 6 to 12 months in advance because the flight may precede a severe wind erosion storm, or the soil may not be in a condition that will allow it to blow. With the ERTS-A, we may have minimal erosion during its one-year life. The RB57F photos have been used to locate several sites for the ERTS-A study on wind erosion on sandy soils.

We plan to continue our efforts to mathematically express the color signature from soils. The microdensitometer tracings will be studied to relate soil color characteristics to the erodible state of the soil. Evidently the average size soil particle on the eroding surface is greater than on the noneroding surface, but the surface roughness is greater on the noneroding surface. To verify the observation, the reflectance from sandy soils as influenced by soil roughness needs to be evaluated.

LITERATURE CITED

Bowers, S. A., and R. J. Hanks. 1965. Reflection of radiant energy from soils. Soil Sci. 100:2, 130-138.

Gerbermann, A. H., H. W. Gausman, and C. L. Wiegand. 1971. Color and color-IR films for soil identification. Photogram. Eng. XXXVII:359-364.

Table 1. Soils on various sample sites around Big Spring, Texas, with Munsell soil color number and microdensitometer white light readings from the color and color IR transparencies for the Jan. 15 and Jul. 9, 1971, RB57F flights. The sites were eroding on Jan. 15, 1971. Noneroding readings were taken from the same soils as eroding readings but from a noneroding area within each site.

| | | Microdensitometer reading | | | | |
| | | Color | | Color IR | | |
Soil	Munsell Color No.	Jan. 15	Jul. 9	Jan. 15	Jul. 9	
Portales sand	7.5YR 6/2	.38	.74	.38	.78	
		.53	.73	.48	.71	Noneroding
Reaves	10YR 6/2	.42	.75	.38	.75	
Tivoli sand	7.5YR 6/4	.44	1.02	.43	.83	
		.60	1.14	.62	1.28	Noneroding
Drake	10YR 7/2	.37	.96	.41	1.00	
Amarillo loamy fine sand	7.5YR 5/6	.46	.82	.50	.87	
		.56	.81	.62	.95	Noneroding
Amarillo loamy fine sand	5YR 4/8	.50	.84	.48	.90	
			.71		.52	Bare turnrow

MOVEMENT AND FEEDING ACTIVITY OF THE

EASTERN WHITE-WINGED DOVE

D. D. Dolton

Mr. D. D. Dolton is a Research Assistant,
Department of Wildlife and Fisheries
Sciences, Texas A&M University

INTRODUCTION

The eastern white-winged dove (Zenaida asiatica) is a migratory game bird prized by sportsmen for many years. It breeds in concentrated nesting colonies in the Lower Rio Grande Valley of Texas and Northeastern Mexico.

Dove populations are decreasing in Texas for two main reasons: First, native brush, the traditional nesting habitat for whitewings, has been cleared for farming in Texas, and there is a marked increase in brush clearing in and around the nesting areas in Mexico; and second, the food available to whitewings before and during the early September hunting season in Texas declines rapidly in July because of the harvesting of grain sorghum, a major source of food in Texas. Some bird resistant varieties of grain are grown, too, but their influence on the dove population has not been determined. In Mexico, corn is available for whitewings during the hunting season, and it entices many birds away from Texas.

If we are to enjoy future whitewing shooting, the factors that attract and hold birds in Texas need to be improved. Hence, a study is being conducted to inventory food resources for white-winged doves in the Lower Rio Grande Valley of Texas and Mexico, and to determine the motivational factors directing the feeding patterns of whitewings.

MATERIALS AND METHODS

Field work was begun in June, 1971. Activity was directed toward becoming familiar with the Rio Grande Valley of Texas and Mexico, noting bird distributions, and developing census taking of birds and sampling techniques of available food.

Through the use of NASA photographs and visual observations in the field, the available food supplies (natural and cultivated) were charted in the study area. Records were made of whitewing feeding activities and patterns. Crop samples were collected from doves to verify visual observations of feeding activity. Selected grain fields were sampled weekly and analyzed to relate the moisture content and nutritional stage of the grain to feeding habits of the birds.

Aerial photographs (NASA RB-57, Mission 158), provided by the Rio Grande Soil and Water Research Center, were of invaluable assistance. Scales of 1:120,000 (RC-8 camera), 1:60,000 (Zeiss camera), and 1:20,000 (local 70 mm Hasselblad cameras) were used. Black and white photos with a scale of 1:120,000 provided the greatest coverage into Mexico (the plane did not fly over Mexico, but photographic coverage extended into Mexico). A 10-power hand lens was used to enlarge features such as small roads and brush tracts. Since no detailed maps of Mexico were available, these photos saved an estimated two to three weeks of time in traveling and mapping areas of interest.

Conventional color photographs (scale 1:60,000) were used in Texas for mapping fields and brush tracts.

A mosaic of infrared photographs (scale 1:20,000), prepared by the Rio Grande Soil and Water Research Center, was used for detailed mapping of the area containing the largest nesting colony of whitewing doves in Texas.

RESULTS AND DISCUSSION

Over 12 times as many acres were planted to grain sorghum as to corn in Texas. Visual observations in Mexico indicated that many more acres of corn were planted than grain sorghum, and corn was harvested at a slower rate than sorghum. This proved to be important for providing a food source for Texas whitewings in September. By late August, thousands of acres of Croton L. became available in the ranch country north of the Rio Grande Valley in Texas.

Preliminary results of grain sorghum sampling indicate that whitewings show no preference to the percentage of moisture in the grain when it is nearly ripe.

Whitewing flights were observed throughout the Rio Grande Valley. Crops collected from whitewings indicated that grain sorghum is the main food eaten in early and mid-summer; whereas corn is the principal food by late summer.

The available food supply motivates the flights of white-winged doves. This becomes very apparent as the food supply diminishes because of grain harvesting in the weeks preceding the hunting season. Hence, most whitewings move from their nesting sites and concentrate in various brush tracts along the river to roost and be near a food source. By hunting season, most feeding is done in Mexico since corn is available there in late summer.

Where several corn or grain sorghum fields were partly harvested, whitewings fed in Texas until they migrated south. The most striking example was a 1500-acre grain sorghum field west of La Joya that was partly harvested. Over 21,000 birds fed in this field. It was leased for hunting and provided some of the best shooting in the Rio Grande Valley.

A factor being studied is the whitewings' preference for one grain field compared with others that apparently received the same management.

SUMMARY

The purposes of the project reported on here are to inventory the food resources available to white-winged doves and to study the feeding patterns of the birds. The project was begun in June, 1971, and it will continue through October, 1972.

Through the use of NASA-USDA photographs and visual observations in the field, the available food supplies were charted. Records of whitewing feeding activity and patterns were made. Selected grain fields were sampled and analyzed, but no definite conclusions have been reached about preferences by doves for a certain field.

For increased whitewing populations in Texas during the hunting season, more food and shelter must be made available to the birds.

PARTICIPATION IN 1971 CORN BLIGHT WATCH EXPERIMENT

A. H. Gerbermann

Mr. Gerbermann spent 4 1/2 months at
LARS during the experiment and parti-
cipated in the photo-interpretation
program.

INTRODUCTION

In the summer and fall of 1970, Purdue University, in cooperation with the
National Aeronautics and Space Administration (NASA) and the Indiana Agricultural
Experiment Station and Extension Service explored new methods of detecting and
monitoring southern corn leaf blight (SCLB) in a 7-state study area, an intensive
study area was designated in Western Indiana. This disease erupted suddenly and
assumed economic importance because it reduced corn yields 15 to 20% in 1970.
The reduced corn production resulted in higher prices for all feed grains.

In 1970, cameras loaded with Kodak Ektachrome Infrared Aero 8443 film
and sophisticated sensors (scanners) were used in a pilot project to study
their usefulness in detecting corn blight. This work demonstrated that SCLB
could successfully be detected at altitudes up to 60,000 ft.

The 1971 Corn Blight Watch Experiment, conducted from April 15 to October
15, was a continuation of the 1970 work on a larger scale. State universities,
NASA, and the USDA cooperated in a program to monitor a large area of the corn
belt, about 200 counties in a seven state area (Nebraska, Minnesota, Ohio,
Indiana, Missouri, Illinois, Iowa), for the outbreak and spread of SCLB.
The specific agencies involved were: the Statistical Reporting Service
(SRS/USDA), the Agricultural Stabilization and Conservation Service (ASCS/USDA),
the Extension Service (ES/USDA), the Cooperative State Research Service
(CSRS/USDA), the Agricultural Research Service (ARS/USDA), the Cooperative
Extension Service (CES), the State Agricultural Experiment Stations (SAES),
NASA, Purdue University and its Laboratory for Applications of Remote Sensing
(LARS), and the Institute for Science and Technology (IST) at the University of
Michigan.

The primary objectives of the experiment (LARS, 1971) were: (1) to detect
an outbreak of SCLB within the corn belt region if it occurred; (2) to monitor
any spread of SCLB across the corn belt region; (3) to assess various levels
of infection within the corn belt; (4) to apply remote sensing technology to
amplify information gathered from ground visits; and (5) to develop technology
and procedures to be available for similar situations occurring in the future.

Resources (aircraft, personnel, etc.) were contributed by the cooperators.
NASA provided an RB-57F aircraft for the period of the Watch. In addition, NASA
sponsored the University of Michigan's C-47 aircraft for data collection over
the intensive study area. LARS devoted all of its resources to the Corn Blight
Watch Program for the duration of the Watch.

The program was organized and directed by a committee comprised of members of the cooperating organizations. Areas of responsibility and their organizational assignments were: Public Information Release - SRS, NASA, USDA Cooperative Information Center; Statistical Sampling Design - SRS; Ground Data Acquisition - SRS, LARS, ASCS, CES, SAES; Airborne Data Acquisition - NASA, IST, LARS; Photo-Interpretation - LARS, ASCS, SAES; Preparation of Survey Materials - SRS, LARS; Aerial Photography Processing - NASA; and Machine Analysis - LARS, IST.

MATERIALS AND METHODS

Design and Ground Observations

SRS was responsible for the experimental design of the program, and SRS selected 30 flight lines 100 miles long by 8 miles wide across the 7-state study area. These lines were photographed (1:120,000 scale) with black-and-white film. These photographs were enlarged to a 1:20,000 scale for base maps. Later SRS, using the base maps, selected 230, 1 by 8 mile segments for enumeration. 200 segments were located along the 30 flight lines, and the remaining 30 segments were located in the intensive study area in Western Indiana. The 1 by 8 mile segments were mapped on the 1:20,000 scale base maps, and these were sent to the county ASCS offices in the 7-state study area.

The ASCS personnel, after training, visited with each farm operator and gathered data pertaining to: (1) location of fields each operator farmed, (2) variety of crops planted in each field, (3) field boundaries, (4) number of acres per field, and (5) specifics for corn fields--planting date, type of cytoplasm in seed planted, irrigation management, plant population, variety planted, row direction, and crop rotation. The county ASCS offices classified all fields operated by one operator as tracts, and they were given a letter designation.

During May 25 to June 10 the information collected by ASCS personnel was put on punch cards by the state ASCS offices and sent to SRS in Washington, D.C. SRS used this information to select 8 to 10 corn fields (visited biweekly) located in each of the 1 by 8 mile segments.

On the first biweekly visit, the enumerator located two sampling units in each of the fields selected for biweekly visits according to instructions in Field Observation Manual (1971). The observer tagged the first 5 plants in each unit. The following observations were made on these plants: number of plants with tassels; number of plants with blight lesions on stalks; number of plants with stalk rot; number of plants with ears or silked ear shoots; number of ears or silked ear shoots; number of ears with blight lesions; number of ears with kernel formation; number of ears with ear rot; plant height; length of the leaf at the 7th node; width of the mid-point of the leaf at the 7th node; estimate of the degree of blight infestation; representation of the field by the sample unit; ear maturity; other stresses--drought, weeds, lodging, etc.; total number of leaves (normal and infested) above and below the 7th node; and percent of the leaf area above and below the 7th node with lesions.

When lesions were first observed, the observer sent a leaf sample to the State Pathology Laboratory for positive identification of SCLB.

Overflights

From June 14 to September 30, all segments were overflown at 60,000 ft (Scale 1:120,000) biweekly with an RB-57F aircraft mounted RC 8 camera (Wild Herrburg), 9 x 9 inch format, 6-inch focal length lens, and Kodak Aerochrome 2443 film. Every Friday for the duration of the watch period (June 14 to September 30), a small jet aircraft flew the exposed film from Topeka, Kansas, staging site of RB-57F, to NASA Houston for processing and inventory. The results were sent by air freight to LARS. Also, during each two-week period the University of Michigan's IST C-47 aircraft overflew the 30 segments at an altitude of 10,000 ft or lower in the intensive study area. Electromagnetic energy reflected by crops in various wavelength bands was measured. It was hoped that the energy level in some or all wavelength bands would differ enough for the various levels of blight infection to distinguish them by computer methods.

Photo-Interpretation

At LARS, the photography frame numbers of enumerated segments were merged with the ground observations, and computer printouts of frame numbers and ground observations were given to a team of two photo-interpreters. The photo-interpreter used a Variscan (an instrument with the capability of illuminating film transparencies and enlarging them to various scales) to enlarge the 1:120,000 scale image to a 1:20,000 scale.

The photo-interpreters trained themselves by selecting fields that had various levels of blight infection and no infection from the ground observation data and then observed these fields on the film. Later, photo-interpreters observed fields on the film and rated them according to the magnitude of blight infestation. The accuracy was determined by checking against the ground observation data. Then the photo-interpreters rated other corn fields in the segment that had not been checked for SCLB. The photo-interpreters were asked to rate each field for: (1) normal or abnormal appearance; (2) presence or absence of SCLB; (3) uniformity of infection (one or more levels of infection in a field); (4) percent of field infected by each level of blight; (5) other causes for abnormal appearance (drought, nutrient deficiencies, weeds, etc.).

At the end of each two week period the photo-interpreter's ratings were put on punch cards, and the acreage at each blight level was determined.

RESULTS AND DISCUSSION

The author participated in the photo-interpretation aspect of the program, and therefore, the following discussion will deal with photography. It was his observation, however, that information from photographs was more useful to detect SCLB that scanner information.

Generally, there was no difference in the appearance of noninfested corn fields and those fields that had plants with only the lower leaves infected. This is logical because the upper leaves on the corn plant culm would have the dominating influence on the reflected energy levels. Infection could be detected when 3 to 5 percent of the upper leaf area was infected; ease of detectability increased as the percentage of infection increased.

However, the ease of detection decreased with plant maturation. At plant senescence, normal corn ready for harvest could not be distinguished from SCLB-infected corn. This is also logical, because normal and infected plants have both lost their chlorophyll at senescence.

When corn and soybean plants were both immature, discrimination between the two crops was difficult. At the scales used (1:120,000) in this study, small fields (under 10 acres) were very difficult to find and to interpret.

Any condition such as a nutrient deficiency or toxicity can cause corn leaves to yellow and affected plants are easily detected because a bright pink color is produced on color infrared film instead of the normal red color.

Different geographic areas register the same condition differently on color infrared film. For example, normal corn in Missouri has the same light red to pink color film images that nutrient deficient corn has in Illinois.

SUMMARY

A large coordinated experiment was conducted out of the Laboratory of Applications of Remote Sensing (LARS), Purdue University, from April 15 to October 15, 1971, to test remote sensing procedures for detecting the outbreak, monitoring the spread, and assessing the levels of Southern Corn Leaf Blight (SCLB). State and Federal agencies and Universities cooperated in the effort which encompassed 7 states. The author participated in the photo-interpretation aspects of the experiment. His experience indicates that SCLB infected corn plants can be detected from normal plants with color infrared film when 3% of the leaf area of the upper leaves (above 7th node) are infected. Fields larger than 10 acres should be used when photographs are taken at a 1:120,000 scale.

Ground observation will always be needed when a large geographical area is surveyed for SCLB. Specific conclusions have not been made because the data are presently being statistically analyzed by LARS.

LITERATURE CITED

Field Observation Manual. 1971. Corn blight watch experiment. USDA publication. 40 p.

LARS Staff. 1971. A summary of the 1971 corn blight watch experiment. Purdue University, Lafayette, Indiana. p. 1-8.

ESTIMATING CITRUS FRUIT NUMBERS AND YIELD

D. H. Von Steen and R. W. Leamer

This research was produced under Research
Outline 71, "Use of Photography in Estimating
Citrus Fruit Numbers and Yield."

INTRODUCTION

The development of new methods of estimating crop yields generally begins with investigations based on small samples to explore alternative techniques and characteristics to be measured. The use of photography to estimate citrus fruit numbers and yield was such an investigation.

Objective sampling techniques, or making fruit counts on a sample of limbs, has been done on several tree crops (Allen and Von Steen, 1968; Allen, 1969); mainly oranges, peaches, cherries, apples, almonds, pecans, walnuts, filberts, grapefruits, and lemons. It has been found that the number of fruit per tree contributes more yield variability per tree than size or weight per fruit. Unless auxiliary data on yield potential are available, it is necessary to make limb counts on a large sample of trees to obtain an estimate of tree production. Accurate fruit counts on sample limbs are costly and difficult to achieve in large scale surveys.

This paper reports on an investigation that was conducted to evaluate the potential of photography as auxiliary information on fruit set per tree. That is, can this photographic information be used with counts of fruit made by field crews in the sense of double sampling or as a useful variable in ratio estimation?

MATERIALS AND METHODS

In earlier work (Huddleston, 1971; Raj, 1968), each side of the tree was divided into quarters by using vertical and horizontal aluminum poles to form a "plus" sign. Eight 35 mm slides (transparencies) were obtained per tree. Four slides were obtained from each of two sides of the tree 180° apart. But the analysis of this earlier work showed no statistical differences among counts from photography of different sides of trees. In either method used, one slide covered each quarter of a side with some overlap with the adjoining quarter to insure complete coverage.

Photographs were taken with either a Miranda or Minolta single lens reflex camera with a light meter behind the lens. High speed Ektachrome film was used for most photographs with Kodachrome II used for the remaining photos.

The photo interpretation was done by projecting the slide on a grided screen. The number of fruit counted in each square of the grid was recorded.

An automated method of counting the fruit is also being investigated--
each slide is scanned with a microdensitometer to obtain film optical densities.
The optical densities can be used to discriminate fruit shape and size from
other objects. Work on this type of pattern recognition is underway, but
results are not available at this time.

RESULTS AND DISCUSSION

Three years of data (1968 to 1970) have been analyzed (Table 1). There
is some variation among percents counted and correlations among years. This
variation could have been caused by several things. First, the 1968 results
were based on a small nonrandom sample, but the results are actual or complete
counts. However, in 1969 and 1970 results were based on a random selection
of blocks using estimated fruit per tree from a sample of limbs. The 1969
and 1970 correlation coefficients in Table 1 have not been corrected for samp-
ling errors. Another possible reason for the variation is that different
counters were used each year. Thus, it would be desirable to develop an auto-
mated fruit counting method that would be consistent from slide to slide and year
to year.

The positive correlations of fruit counts from photographs with estimated
total fruit per tree are encouraging. But in order to benefit from using an
auxiliary variable in a regression or unbiased ratio estimates, the correlation

coefficient (r) must be greater than 1/2 $\left(\dfrac{S_{\bar{x}} \, \bar{y}}{\bar{X} \, S_{\bar{y}}} \right)$. For grapefruit this restric-

tion was met, but it was not met for a specific age group of oranges.

Other auxiliary variables using color aerial photography have been inves-
tigated, such as measurements of canopy area and fruit counts. Number of fruit
counted from aerial photographs has been so small that it shows little promise.
Canopy area has been difficult to measure, and the measuring instrument used
lacked precision.

SUMMARY

The use of auxiliary variables may provide a means of obtaining a more pre-
cise estimate of tree fruit for a given cost. Citrus fruit counts made from
35 mm slides are generally highly and positively correlated with estimates of
fruit per tree. Fruit counts and canopy area measurements from aerial photo-
graphs have not shown much promise. The need and the potential of an automated
fruit counting technique is great.

LITERATURE CITED

Allen, R. D., and D. H. Von Steen. 1968. Use of photography and other objective yield procedures for citrus fruit. Texas Research, Statistical Reporting Service Research Report, Washington, D. C.

Allen, R. D. 1969. Use of photography and other objective yield procedures for citrus. Texas Research. Statistical Reporting Service Research Report, Washington, D. C.

Huddleston, H. F. 1971. Use of photography in sampling for number of fruit per tree. Agricultural Economics Research, Vol. 23, No. 3.

Raj, D. 1968. Sampling theory. McGraw Hill, Inc., New York.

Table 1.--Percents of fruit counted and coefficients for correlations of
estimated fruit counts from photographs with estimated total fruit
per tree for 1968, 1969, and 1970.

Type of fruit	Year	Percent counted	Correlation coefficient
Early oranges	1968	30.9	.798**
	1969	25.4	.684** [1]
	1970	17.4	.757** [1]
Valencias	1968	31.0	.546
	1969	29.1	.751** [1]
	1970	24.5	.533* [1]
Grapefruit	1968	32.4	.915**
	1969	19.3	.617** [1]
	1970	15.5	.376 [1]

*   Correlation coefficient greater than zero, p = .95
**   Correlation coefficient greater than zero, p = .99
[1]   Biased downward due to errors in number of fruit per tree from sampling

CONVAIR-990 MISSION

B. R. Jean[1], J. W. Rouse, Jr.[2], and C. L. Wiegand

> This information was taken from referenced
> reports by B. R. Jean et al. of the Remote
> Sensing Center, Texas A&M University.
> Weslaco participated in mission planning
> and ground "truthing", but not in data
> analysis.

INTRODUCTION

Microwave wavelength, roughly 1 mm to 100 cm, sensors are responsive to
the electromagnetic emissions of natural surfaces. The emissions are a
function of the dielectric properties of the medium (Paris, 1969). The
water content of soil dominates its dielectric properties. Because the
water content of the surface soil mantle is of great concern in plant water
relations, hydrology, and the energy balance of the earth, operational
passive microwave sensors would be of considerable value to agriculture and
the geosciences.

The development of microwave systems is still in the early stages;
analytical models are not available to handle surface roughness and non-
homogeneous moisture content distributions encountered in field applications.
Good quality field data are, in themselves, scarce.

Researchers at the Remote Sensing Center, Texas A&M University (TAMU),
have considered both analytical models of microwave emission and results under
controlled experimental conditions (Jean, 1971; Jean et al., 1972; Paris, 1969).
This report deals only with the aspects of that program involving a compari-
son of the ground measurements of water content along a flight line with
airborne microwave radiometer responses.

MATERIALS AND METHODS

The flight line selected for the radiometer mission was along U.S. High-
way 281 from coordinates 26°03.6'N 97°59.5'W to 26°06.0'N 98°14.2'W. Most of
the fields along the flight line are rectangular. The dimensions of a typical
field are roughly 400 by 500 m with the soil along the line being quite uniform.
The soil is primarily a heavy clay with a relatively high water holding capacity.

Soil samples were taken along the flight line from very near the surface
(upper 3 cm) and from a depth of about 14 to 16 cm. The near the surface sample
was obtained by scraping away the top cm of crust and collecting the sample from
the next 2 cm. The crust was not included in the sample because the top layer
of soil was usually very dry, regardless of the moisture content of the soil
beneath it.

---

[1] Presently with the Bendix Research Laboratory, Southfield, Michigan.

[2] Director, Remote Sensing Center, Texas A&M University.

The NASA/GSFC (Goddard Space Flight Center) Convair (CV)-990 aircraft, equipped with microwave radiometer systems at frequencies 1.42, 2.69, 4.99 and 10.69 GHz, made overflights of the flight line on the afternoon of March 1 (between 22:50:00 and 23:16:00 Greenwich time). The 1.42 and 4.99 GHz radiometers operated in both the horizontal and vertical polarization modes. The aircraft flew at an altitude of about 915 m with an average ground speed of about 140 m/sec. Tabulated values of antenna temperatures as a function of elapsed flight time were provided by the NASA GSFC.

RESULTS AND DISCUSSION

From a projection of the antenna beam of the actual flight path on an aerial photomosaic of the flight line it was determined that there were 8 fields that could be used for correlating the apparent temperature with the sampled moisture content. The data from these 8 fields were studied as a function of the average values of the surface moisture content. These averages were not computed for an entire field, but for the area corresponding roughly to the viewing cell length of the radiometer systems. Since the subsurface moisture content was essentially constant over the selected test fields, only surface moisture content was considered in the analysis.

The objectives in the analysis of the data were to determine the degree of correlation of radiometer data with soil moisture content, and to determine the dependence of apparent temperature on soil moisture content.

The radiometer data from the 1.42, 2.69, and 10.69 GHz systems showed a definite dependence on soil moisture content. The coefficients for the correlation of antenna temperature with soil moisture content were: 1.42 GHz (vertical), -.616; 1.42 GHz (horizontal), -.648; 2.69 GHz, -.696; and, 10.69 GHz, -.619.

A least squares straight line was fit to the 1.42 GHz data for both the vertical and horizontal channels with resulting slopes of -1.36°K/percent moisture content for the vertical channel, and -1.16°K/percent moisture for the horizontal channel. A non-linear relation of apparent temperature with percent moisture content for the 2.69 GHz and 10.69 GHz data was evident. The average variation of apparent temperature with moisture content determined from the high moisture ends of the curves was -1.12°K/percent moisture content (2.69 GHz) and -0.99°K/percent moisture content (10.69 GHz). Considering the relatively small variation of the dielectric properties of soils with frequency, the decreasing sensitivity of airborne measurements seems related to the greater effective surface roughness as the measurement frequency increases.

The average apparent radiometric temperature and the average moisture content of each of the 8 fields along with their standard deviation is given in Table 1 for each of the microwave frequencies that were responsive to soil moisture content.

The average variation of apparent temperature with moisture content for the airborne measurements ranged from -1.36°K/percent moisture content to -0.99°K/percent moisture content.

Considering the change in apparent temperature to be 1°K for each 1% change in moisture content, then to determine the average moisture content of a single data cell to within 1.75° (the average observed standard deviation in moisture content across the sampled fields was 1.75%) requires a temperature sensitivity of 1.75°K. From the average standard deviations of apparent temperature of the systems listed in Table 1, it appears that moisture content variations can be determined to an accuracy of 3.3 to 6.1%, depending on the system used. However, the 2.69 and 10.69 GHz data are not linearly related to moisture content, and for the lower ranges of moisture contents, they are insensitive to moisture variations. Therefore, considering the entire range of moisture content, the accuracy in determining moisture contents under nearly ideal conditions is 5 to 6% moisture content. However, it must be emphasized that the results from the airborne measurements were obtained by comparing measurements from fields with similar soils and surface properties. All of the fields considered were bare or had only small plant seedlings. For the situation of measuring the apparent temperature of very dissimilar fields, especially when ground cover becomes a variable, the variations caused by these additional parameters may mask the effects of soil moisture on the apparent antenna temperature. A more realistic estimate of the accuracy that could be achieved in actual practice is 10 to 15% moisture content.

SUMMARY

The NASA/GSFC CV-990 aircraft, equipped with a number of microwave radiometer systems, overflew a flight line on March 1, 1971. Ground moisture content (by weight) samples were taken by TAMU and SWC (Soil and Water Conservation) personnel from the 2 to 4 cm and from the 14 to 16 cm depth intervals. The GSFC provided tabulated values of antenna temperature as a function of elapsed flight time.

An error in navigation resulted in a direct correspondence between antenna beam pattern and soil samples in only 8 large fields. The radiometer data from the 1.42, 2.69, and 10.69 GHz systems showed a definite dependence on the shallower-sampled soil moisture content. (The range in moisture content among samples at the 15 cm depth was narrow). The decrease in antenna temperature with an increase in soil moisture content was linear for the 1.42 GHz frequency but curvilinear for the 2.69 and 10.69 GHz frequencies, and it amounted to a decrease of about 1°K in antenna temperature for each 1% increase in water content.

The data suggest that possibly soil moisture contents can be measured to the accuracy of the microwave antenna temperatures with standard deviations ranging from 3.3 to 6.1°K. However, the airborne measurements were all taken over fields of similar soil and surface properties, and the response of the 2.69 and 10.69 GHz radiometers was insensitive at water contents below 20%. The authors conclude that estimates of moisture contents to an accuracy of 5 to 6% is probable under rather uniform conditions and to perhaps 10% under most conditions.

LITERATURE CITED

Paris, J. 1969. Microwave radiometry and its application to marine meteorology and oceanography. Ref. No. 69-1T, Dept. Ocean., Tex. A&M Univ.

Jean, B. 1971. Selected applications of microwave radiometric techniques. Tech. Rept. No. RSC-30, Remote Sensing Center, Tex. A&M Univ.

Jean, B. R., J. A. Richerson, J. W. Rouse, Jr., and M. L. Wiebe. [1972] Microwave radiometer measurements of soil moisture. (Publication vehicle uncertain; IEEE or Remote Sens. of Environ.).

Table 1. The average apparent radiometric temperature and the average moisture content of the surface 2 cm to 7 cm depth along with their standard deviation for each microwave frequency on the NASA/GSFC CV-990 for which ground data were available.

Field No.	Frequency, GHz				Moisture content
	1.42 (Vert.)	1.42 (Hori.)	2.69	10.69	%
	Temperature, °K ± Standard Deviation				
104	290.0 ± 5.4	282.2 ± 4.9	284.4 ± 2.3	287.7 ± 2.7	6.67 ± 2.03
105	268.9 ± 4.9	267.9 ± 6.5	276.9 ± 1.3	283.7 ± 1.3	22.27 ± 1.95
107	283.7 ± 3.1	275.0 ± 7.8	280.5 ± 6.1	286.9 ± 3.1	14.14 ± 2.69
111	288.5 ± 3.2	282.4 ± 6.0	284.9 ± 6.8	283.3 ± 8.5	8.46 ± 0.86
113	292.4 ± 8.4	282.3 ± 8.5	286.0 ± 2.1	288.6 ± 4.0	10.11 ± 1.99
116	296.3 ± 6.0	291.6 ± 6.5	284.3 ± 1.5	288.3 ± 1.2	15.96 ± 1.89
120	253.1 ± 4.4	250.9 ± 2.6	252.7 ± 3.0	259.6 ± 4.6	34.98 --
122	270.1 --	270.1 --	262.2 --	262.5 --	13.50 ± 0.84
Avg. Stnd. Dev.	5.1	6.1	3.3	3.6	1.75

REMOTE SENSING FOR CONSERVATION AND ENVIRONMENTAL PLANNING

C. L. Wiegand and L. J. Bartelli

This information was taken from a paper
presented at the Soil Conservation Society
of America National Meeting at Columbus,
Ohio, Aug. 15-18, 1971, that is to be pub-
lished in the Proceedings. These results
were produced under Research Outline 58,
"Identification of crops on Kodak Ektachrome
Infrared Aero film (type 8443) using differ-
ences among white, red, green, and blue
light film optical densities."

INTRODUCTION

We are all aware that farmed, grazed, and forest lands occupy the bulk of
the landscape. Soil surveys and ecological characterization are lagging, how-
ever. Park (1970) stated that at the current rate of soil surveying the U.S.
would not be completely surveyed until the year 1998.

Is it too much to wonder then how one can wisely plan the utilization of
and conservatively manage those resources whose extent, value, and character
are unknown?

Before going further let me show you an example of difference in utiliza-
tion of a resource. The illustration (Fig. 1) is the photograph, taken
March 12, 1969, by the crew of Apollo 9, of the agricultural development
that has occurred on either side of the New Mexico-Texas state line. The
original photograph was taken from 137 miles up and covered close to 10,000
square miles. The square or rectangular patches are characteristic of culti-
vated fields while those portions of the photograph devoid of such a pattern
are primarily grazing land. It is obvious that the cultivated fields are more
numerous in the right half (Texas) of the photograph than in the left half
(New Mexico) and that the pattern changes at the state line. Why? The primary
reason seems to be the difference in groundwater basin management in the two
states. In Texas the landowner is also the owner of the groundwater, whereas
the State is the owner of the groundwater in New Mexico.

Who is to say which State is making the wiser use of the waters of the
Ogallala aquifer? Perhaps a similar photograph taken 50 years hence will show
a reversal in the agricultural scene, with the Texans reverting from row crop
to grassland farming because of depletion of the aquifer while the New Mexicans
still have some groundwater.

Remote Sensing Concepts

Any device that obtains information about objects without making contact
with them is a remote sensor. Thus devices used on the ground or mounted in
aircraft and satellites for observing the earth are remote sensors. There are
many such sensors (Nat'l. Acad. Sci., 1970; Wiegand and Bartholic, 1970).
Their development and application has been greatly aided by support from the
National Aeronautics and Space Administration.

The use of sensors in high altitude aircraft and spacecraft yields a broad perspective while retaining relatively detailed information. Large areas can be covered. In 1970, the high altitude plane (50,000 to 60,000 feet) utilized in the Earth Observations Program of the Manned Spacecraft Center, Houston, covered 10% of the U.S. in it's scheduled missions (MSC, 1971). It photographed 3 entire counties on a mission for us in less than 2 hours.

Spacecraft have world-wide coverage capability. The Earth Resources Technology Satellite-A scheduled for launch in the spring of 1972 has the capacity to observe the entire surface of the earth each 18 days (Park, 1969).

There are many wavelengths of energy in the electromagnetic spectrum that can be used for observations that neither the human eye nor photographic film is sensitive to. Such sensors include radar microwave radiometers, and optical mechanical scanners (Nat'l. Acad. Sci., 1970; Johnson, 1969).

Remote sensing now encompasses data and information processing methodology, communications capability, sensor systems deployment in aircraft and spacecraft, and resource classification systems for large scale survey and inventory of the earth's surface (Luney and Dill, 1970; Johannsen and Baumgardner, 1968).

A popular concept in remote sensing is the "multispectral" approach (Carneggie, 1970; Malila, 1967; Myers and Allen, 1968; Johannsen and Baumgardner, 1968). This idea is based on the fact that interaction of specific wavelengths of electromagnetic energy with matter results in a characteristic response for each particular kind of matter and that simultaneous measurements in several wavelengths will permit improved discrimination among significant objects of interest.

Resource Information Needs

Colwell (1969) summarizes the vegetation resource data needed for crops, timber, rangeland forage, and brushland. His summary is presented in Table 1. Belcher et al. (1967), listed 117 potential applications of remote sensing in agriculture, 71 in forestry, and 72 in rangeland. They listed the following as having benefits of outstanding significance: resource evaluation, soil classification and mapping, disaster applications, rural transportation development, and world food budget.

Types of Surveys

First stage surveys provide sufficient information to allow the identification of development requirements or possibilities. The National Cooperative Soil Survey is an example. The natural soil is classified, its distribution is mapped and potential and behavior patterns are determined for each map delineation.

Second stage surveys seek enough information to determine whether or not proposed projects or uses are feasible from both the physical and cost/benefit aspects. The land capability classification of the Soil Conservation Service is an example. It is based on the permanent qualities of the land that can not be easily changed. For example, the presence of brush or trees, low soil fertility, etc., are not considered permanent attributes. The classes are a measure of the degree of hazard or limitation but not of the kind of management necessary.

Third stage surveys concentrate on the details of what is to be produced, the necessary management practices, the cost of carrying out the development, and likely yields. The Bureau of Reclamation has developed a system that is in world-wide use in assessment of irrigation projects. It yields an estimate of the repayment capacity of the land.

Geographers are concerned about land use. Thematic maps have scales of 1:100,000 to 1:2,000,000 and are usually pieced together from sources that vary in quality, quantity, and date of collection (Simonett, 1968). Thus they are interested in the possibility of using spacecraft-acquired measurements. Anderson (1971) concluded that it is often difficult to fit interpretations of land use from remote sensing measurements into existing land use classifications. He recommended the identification of land uses on an activity basis to serve a variety of purposes.

On the other hand, land evaluation is usually done at scales of 1:15,000 to 1:50,000 (Stewart, 1968). In the past, black-and-white aerial photos on panchromatic film have been almost exclusively used. Color, black-and-white infrared, and color infrared are rapidly being adopted, however, (Heller, 1970) as are such advanced techniques as image compositing, color recombining, and density slicing.

Gerbermann et al. (1971) used 12 soils differing widely in color and other properties to compare color and color infrared films for soil identification. They found that soils of low chroma (gray or neutral in color) are best distinguished with color infrared film; in contrast, colorful soils are best distinguished on conventional color film. Rib and Miles (1969) sought an optimum combination of sensors for delineating and mapping soils. They used aerial films, radar, a thermal infrared scanner, and an optical mechanical scanner (ultraviolet to far infrared), and they concluded that the optimum system was the optical mechanical scanner flown simultaneously with conventional color photography. Kristof (1971) mapped six different soil surface categories by computer. He concluded that mapping of soil associations by computer is entirely feasible.

The U.S. Geological Survey has a program to assess the usefulness of space photography for national resource mapping. They have produced a 1:3,000,000 scale soils map of the Southwestern U.S. and Mexico from Gemini IV and V photography (Morrison, 1968), a land use map of the same area at the scale 1:1,000,000 (Thrower, 1970), and photomaps from rectified Apollo 6 photography of the Pacific Ocean to Northern Louisiana belt at the scale 1:500,000 (Dept. of Interior, 1970).

Operational Systems

Operational systems for acquiring, processing, and disseminating remotely sensed information on a large scale are complicated and costly. A typical configuration requires a central data and ground control center that controls and communicates with the satellite bearing the sensors. The data center receives the telemetered data, digitizes it, processes it to standard formats, and provides quality control. Supplemental but time synchronous local and global meteorological data, airborne data, and ground observations are also fed to the data center (Holter, 1970).

Data catalogs must be prepared and archiving and retrieval must be pro-
vided for the casual user. Users who are interested in near real time
analyses must have their own computers communicating directly with
those of the data center. The Department of the Interior is proceeding
currently with construction of such a Center at Sioux Falls, South
Dakota. Gurk et al. (1968) provided conceptual inputs that are being
incorporated.

In the agricultural field, the Laboratory of Applications of Remote
Sensing at Purdue University has been particularly concerned with the
definition of computerized handling and analysis of very large quanti-
ties of data (Laboratory for Agricultural Remote Sensing, 1967;
Landgrebe and Phillips, 1967; Fu et al., 1969).

Muir (1970) has been concerned with earth resources information
systems that use satellite-based remote sensors. He has evaluated
their costs and benefits when applied operationally. His diverse
studies have dealt with the world rice crop, U.S. wheat rust control,
U.S. hydroelectric power, Pacific Ocean tuna fishing, and malaria
control, but in the article cited he restricted himself to water
management in the Columbia River Basin of the Pacific Northwest. He
concluded that the cost-benefit ratio is very favorable and satellite
systems are superior to airplane systems if the area covered exceeds
1 million square miles.

The most extensive application of remote sensing in agriculture
to date is the monitoring of corn blight in the summer of 1971. State
universities, NASA, and the USDA cooperated in biweekly overflights of
portions of 7 Corn Belt states. The objectives were to detect outbreaks
if they occur, to monitor any spread of the disease, to assess levels
of infection, and to supplement information gathered from ground visits
with remotely sensed information. It will provide valuable experience
to all the organizations involved on how to organize and conduct efforts
in similar future situations.

In any operational system, features must be classified into mean-
ingful and consistently identifiable categories (Colwell, 1968). Multi-
stage sampling techniques that utilize space, aerial, and ground
sampling have proven especially efficient and powerful (Colwell, 1969;
Aldrich, 1971 a, 1971 b). Ground measurements or observations on repre-
sentative members of the classification categories at the time of
sensor overflights have been found essential for techniques development
(calibrating sensors; judging the correctness of remote sensor derived
identifications, hence the value of remote sensing for specific appli-
cations)(Pettinger, 1971). Ground "truth" is also required in opera-
tional systems to verify category placement of features and to train
the computer with feature characteristics required to assign unknown
sites into categories. In soil mapping, for example, if the soils of an
area are already known in general, sites of modal soils can be used to
train the computer or to judge the tonal and color characteristics of
surrounding soil. The photography or computer printouts can be used
to locate soil boundaries and to select sites for additional borings
within the identified area. A new area will require similar ground "truth"
studies.

SUMMARY

There is critical need for new ideas and techniques to provide more accurate and timely information for planning conservation measures and managing our crop, range, and forest resources. Remote sensing tools and techniques can record and examine land use patterns and the agricultural environment on scales and at wavelengths in the energy spectrum that have been heretofore unavailable.

Resource inventory and soil mapping are used to illustrate key points including: (1) resources can be wisely managed only if their extent, value, and character are known; (2) information needs must be clearly defined to prevent gathering useless information; (3) remote sensing is especially useful for parametric land evaluation; (4) operational remote sensing systems are complicated and costly, but cost effective; (5) at the present stage of development remote sensing should not be considered a threat to, but rather a supplement to, traditional techniques of information gathering; and (6) small scale photography (on the order 1:1,000,000), such as that acquired from space, has been found consistently more useful than the ground resolution would suggest. We assume here that much of the resource information available in the near future will be acquired by satellites such as the Earth Resources Technology Satellite-A scheduled for launch in the spring of 1972.

LITERATURE CITED

Aldrich, R. C. 1971 a. Space photos for land use and forestry. Photogram. Eng. 37:389-401.

Aldrich, R. C. 1971 b. Forest and range inventory and mapping. Proc. Intl. Workshop, Earth Resources Survey Systems, Univ. of Mich., Ann Arbor, May 3-14. Vol. II, p. 82-106.

Anderson, J. R. 1971. Land-use classification schemes. Photogram. Eng. 37:379-387.

Belcher, D. J., E. E. Hardy, R. L. Shelton, and E. L. Schepis. 1967. Potential benefits to be derived from applications of remote sensing of agricultural, forest, and range resources. Center for Aerial Photographic Studies, Cornell Univ., Ithaca, N.Y. Pub. No. 3, 150 p.

Carneggi, D. M. 1970. Remote Sensing: Review of principles and research in range and wildlife management. In Range and Wildlife Habitat Evaluations, A Research Symposium. USDA For. Ser. Misc. Pub. No. 1147, p. 165-178.

Colwell, R. N. 1968. Determining the usefulness of space photography for natural resource inventory. Proc. Fifth Symp. Remote Sens. of Environ., Univ. of Mich., Ann Arbor, p. 249-289.

Colwell, R. N. 1969. The inventory of vegetation resources--User requirements vs remote sensing capabilities. Proc. Second Ann. Earth Resources Aircraft Program Review, NASA-MSC, Houston, Tex., Sept. 16-18, Vol. II, p. 18:1-71.

Department of the Interior. 1970. Apollo 6 photomaps of the West-East corridor from the Pacific to Northern Louisiana. U. S. Geological Survey, Washington, D.C.

Fu, K. S., D. A. Landgrebe, and T. L. Phillips. 1969. Information processing of remotely sensed agricultural data. Proc. Inst. Electr. and Electr. Engs. 57:639-653.

Gerbermann, A. H., H. W. Gausman, and C. L. Wiegand. 1971. Color and color-IR films for soil identification. Photogram. Eng. 37:359-364.

Gurk, H., P. Wood, and C. Smith. 1968. Ground data-handling system study
    for the Earth Resources Observation Satellite, Phase 1. Radio Corp. of Amer.,
    Final Rept. No. AED R-3408.
Heller, R. C. 1970. Imaging with photographic sensors. In Remote Sensing
    with Special Reference to Agriculture and Forestry. National Academy of
    Sciences, Washington, D.C., p. 35-72.
Holter, M. R., H. W. Courtney, and T. Limperis. 1970. Research needs: The
    influence of discrimination, data processing, and system design. In Remote
    Sensing with Special Reference to Agriculture and Forestry. National
    Academy of Sciences, Washington, D.C., p. 354-421.
Johannsen, C. J., and M. F. Baumgardner. 1968. Remote sensing for planning
    resource conservation. Proc. Ann. Meeting Soil Conserv. Soc. Amer.,
    p. 149-155.
Johnson, P. L. (Ed.). 1969. Remote sensing in ecology. Univ. of Ga. Press,
    Athens, 244 p.
Kristof, S. J. 1971. Preliminary multispectral studies of soils. J. Soil and
    Water Conserv. 26:15-20.
Laboratory for Agricultural Remote Sensing. 1967. Remote multispectral
    sensing in agriculture. LARS Ann. Rept., Vol. 2, Agr. Expt. Sta. Res. Bul.
    832, Purdue Univ., Lafayette, Ind.
Landgrebe, D. A., and T. L. Phillips. 1967. A multi-channel image data
    handling system for agricultural remote sensing. Proc. S.P.I.E. Computerized
    Imaging Techniques Seminar, Washington, D.C.
Luney, P. R., and H. W. Dill, Jr. 1970. Uses, potentialities, and needs in
    agriculture and forestry. In Remote Sensing with Special Reference to
    Agriculture and Forestry. National Academy of Sciences, Washington, D.C.
    p. 1-34.
Malila, W. A. 1967. Multispectral techniques approach for contrast, enhance-
    ment, and discrimination. Presented at the Joint Meetings of ASP and ACME,
    St. Louis, Mo.
Manned Spacecraft Center. 1971. Earth Observations Aircraft Program, Fiscal
    Year 1970. NASA-MSC, Houston, Tex., 86 p.
Morrison, R. B. 1968. Preliminary soil classification map of Southwestern
    U.S. and Mexico from space photography. NASA-MSC Tech. Ltr. NASA-111, 13 p.
Muir, A. H. 1970. A water management model using Earth Resources Satellites.
    In Proc. Princeton Univ. Conf. on Aerospace Methods for Revealing and Eval-
    uating Earth's Resources (J. P. Layton, Ed.), P. 19:1-15.
Myers, V. I., and W. A. Allen. 1968. Electrooptical remote sensing methods as
    nondestructive testing and measuring techniques in agriculture. Appl. Opt.
    7:1819-1838.
National Academy of Sciences. 1970. Remote Sensing with Special Reference to
    Agriculture and Forestry. Washington, D.C., 424 p.
Park, A. B. 1969. Remote sensing of time dependent phenomena. Proc. Sixth
    Symp. Remote Sens. of Environ., Univ. of Mich., Ann Arbor, Vol. II, p. 1227-
    1236.
Park, A. B. 1970. User needs in agriculture and forestry. In Proc. Princeton
    Univ. Conf. on Aerospace Methods for Revealing and Evaluating Earth's
    Resources (J. P. Layton, Ed.), p. 13:1-26.
Pettinger, L. R. 1971. Field data collection--an essential element in remote
    sensing application. Proc. Intl. Workshop, Earth Resources Survey Systems,
    Univ. of Mich., Ann Arbor, May 3-14, Vol. II, p. 49-66.
Rib, H. T., and R. D. Miles. 1969. Multisensor analysis for soils mapping.
    Engineering Reprints, Civil Engineering, CE 266, Purdue Univ., Lafayette,
    Ind., p. 22-37 (Reprinted from Special Report 102, Highway Research Board,
    Washington, D.C.).

Simonett, D. S. 1968. Thematic land-use mapping with spacecraft photography and radar. Proc. Ann. Earth Resources Aircraft Program Review, NASA-MSC, Houston, Tex., Sept. 16-18, Vol. I, p. 8:1-20.

Stewart, G. A. 1968. Land Evaluation. In Land Evaluation (G. A. Stewart, Ed.), St. Martin's Press, N.Y., p. 1-10.

Thrower, N. J. W. 1970. Annals map supplement number twelve: Land use in the southwestern United States--From Gemini and Apollo Imagery. Annals of the Assoc. of Amer. Geographers, Vol. 60, No. 1, p. 208-209.

Wiegand, C. L., and J. F. Bartholic. 1970. Remote sensing in evapotranspiration research on the Great Plains. In Proc. Seminar Evapotranspiration in the Great Plains. Kansas St. Univ., Manhattan, Agric. Expt. Sta. Pub. 50, p. 137-180.

Table 1.--Type of vegetation resource data needed for crops, timber, rangeland forage, and brushland vegetation (After Colwell, 1969).

Agricultural Crops	Timber Stands	Rangeland Forage	Brushland Vegetation (mainly shrubs)
Crop Type (Species and variety)	Timber Type (Species composition)	Forage Type (Species composition)	Vegetation Type (Species composition)
Present crop vigor and state of maturity	Present tree and stand vigor by species and size class	Present "Range Readiness" (for grazing by domestic or wild animals)	Vegetation density
Prevalence of crop-damaging agents by type	Prevalence of tree-damaging agents by type	Prevalence of forage-damaging agents (weeds, rodents, diseases, etc.) by type	Other types of information desired will depend upon primary importance of the vegetation (whether for watershed protection, game habitat, aesthetics, etc.)
Prediction of time of maturity and eventual crop yield per acre by crop type and vigor class	Present volume and prediction of probable future volume per acre by species and size class in each stand	Present animal-carrying capacity and probable future capacity per acre by species and range condition class in each forage type	
Total acreage within each crop type and vigor class	Total acreage within each stand type and vigor class	Total acreage within each forage type and condition class	Same as above
Total present yield by crop type	Total present and probable future yield by species and size class	Total present and probable future animal carrying capacity	Same as above
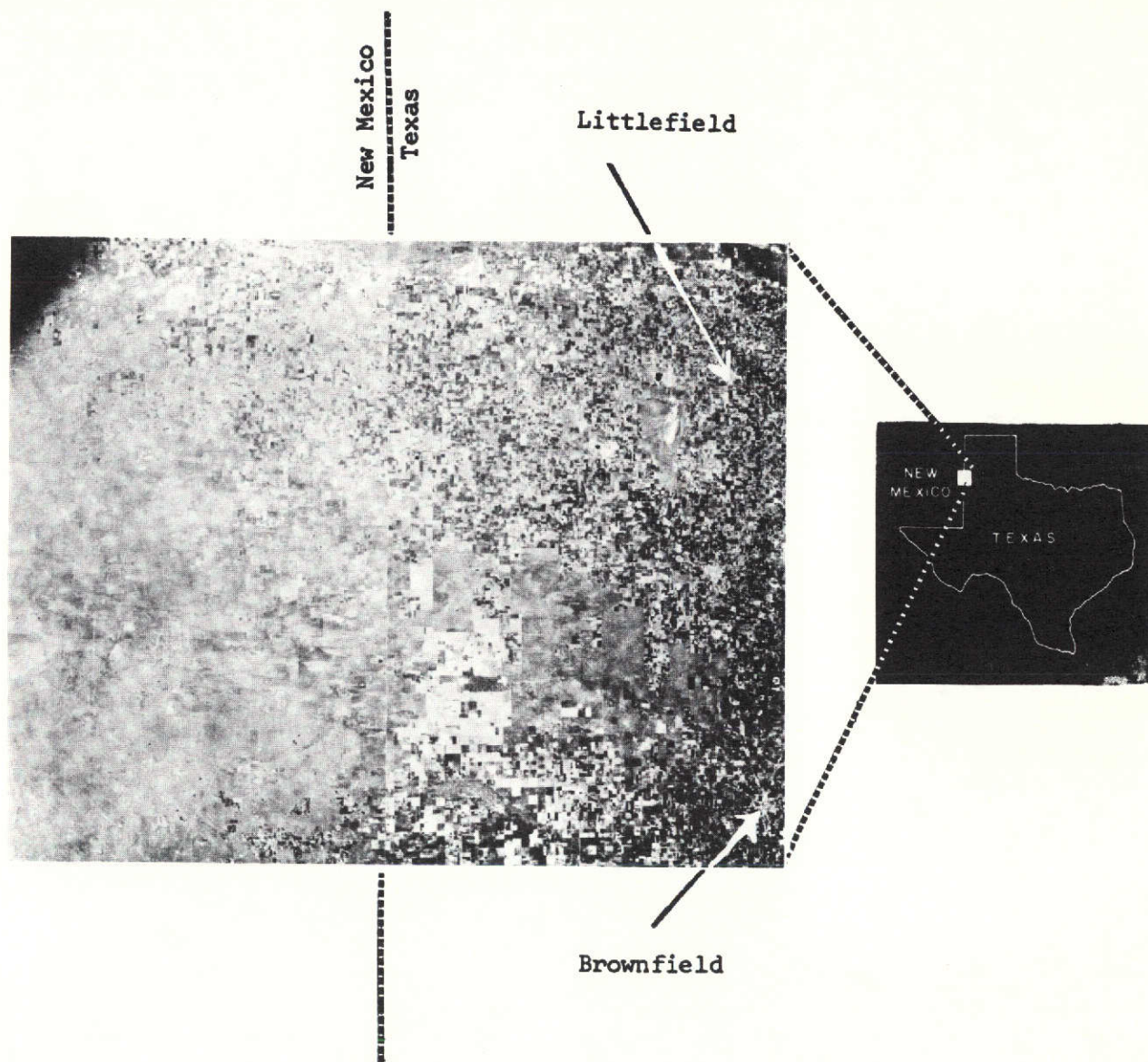
Fig. 1.--Difference in agricultural development in New Mexico
(left half of photograph) and Texas (right half of photograph)
as recorded photographically from the Apollo 9 satellite. A
difference in policy on ground water utilization in the two
states accounts for more extensive crop farming in Texas.
Scale of photograph is 1:1,300,000.

ERTS-A PROPOSAL: REFLECTANCE OF VEGETATION, SOIL, AND WATER

C. L. Wiegand, Principal Investigator
W. A. Allen and H. W. Gausman, Co-Investigators
R. H. Miller, Agency Coordinator

This information was taken from the proposal
for participation in ERTS-A (Earth Resources
Technology Satellite) Space Flight Investigations
(Park, 1971) and the 90-Day Preliminary Science
Report for Mission 158, Site 32.

INTRODUCTION

The objective of earth resources research at Weslaco, Texas is to determine the characteristics of reflectance and emission signatures of various crop genera and soil conditions to permit their multispectral observation and identification from remote sensors at ground, aircraft, or spacecraft altitudes. To accomplish this objective, it is necessary to determine the most suitable wavelengths for surveying land resources and crop conditions from space, to determine the systems required to obtain the data, and to develop procedures for analyzing and disseminating telemetered data.

Mission 158 was flown March 4, 1971, by the NASA RB-57 airplane to obtain high altitude imagery with wavelengths similar to those that will be used on ERTS-A (Earth Resources Technology Satellite-A) and skylab's EREP (Earth Resources Experimental Package) spacecraft. Mission 158 objectives were:

1. To gain experience using data similar in scale and spectral interval to space data prior to launch of ERTS and EREP vehicles.

2. To prepare base maps of Cameron, Willacy, and Hidalgo counties for use in selecting test sites and documenting space investigations.

3. To study the imagery to reveal features such as distribution and occurrence of saline soil, soil color variation, number and extent of water bodies, wind erosion damage to soils, and crop and soil conditions affecting production.

4. To examine the general thermal patterns observed over the entire Lower Rio Grande Valley with RS-7 thermal imagery.

The purpose of the ERTS-A proposal is to develop an operational system of ERTS data analysis for the needs of the U. S. Department of Agriculture. Seasonal changes in reflectance of various soils and of various crops grown in the Rio Grande Valley will be studied using satellite, ground, and aircraft spectral data. Comparisons will be made between ERTS data and predictions from analytical models describing the interaction of light with plant canopies (Allen et al., 1970); discrimination of specific crop and soil conditions of interest will be attempted; chlorophyll (CHL) concentration of plant leaves will be correlated with reflectance in the visible part of the spectrum; and discrimination capability of film optical densities will be compared with optical mechanical scanner data discrimination capability (Richardson et al., 1970). The investigation is an extension of scientific work already accomplished and activities in progress.

SUMMARY

Objectives

The objectives of Weslaco's ERTS-A proposal submitted to NASA are:[1]

1. To compare experimental results from ERTS-A data with predictions of analytical models for interaction of light with vegetation for leaf area index (LAI) determinations.

2. To determine whether or not differences in CHL concentrations of plants can be detected from an orbiting satellite.

   (Objectives 1 and 2 are preparatory to ultimately estimating crop yield potential and vigor from satellite-measured estimates of LAI and CHL concentration)

3. To determine the seasonal changes of the various crops and soils in Hidalgo County, Texas; to discriminate among them; and, in some cases, to estimate acreages by means of reflectance measured from ERTS-A.

4. To develop an operational system of satellite data analysis tailored to the needs of the U. S. Department of Agriculture.

Orbiting satellites can be depended on to stay on schedule and yield repetitive observations of the whole globe. Providing resolution is adequate and the areas to be sensed are not cloudy, satellites are the ideal vehicles for agricultural resource sensing. Thus, the usefulness of satellite observations needs to be investigated. Experience with the Apollo 9 SO-65 experiment (Wiegand et al., 1971) indicates that the resolutions obtainable by the ERTS-A RBV (Return Beam Vidicon) and MSS (Multispectral Scanner) systems will be adequate for the proposed investigation.

The substudies implied by the above objectives can be logically grouped into the following categories:

1. Crop vigor and potential crop yield

   a. Leaf area index, LAI

---

[1] The work statements are to be negotiated.

      b.   Iron deficiency detection (lack of CHL)

      c.   Crop vigor categories within crops and their relation to yield

      d.   Rangeland condition

2.   Crop discrimination

      a.   Cotton versus sorghum

      b.   Among vegetables

      c.   Optimum time of the year to discriminate citrus from other crops

      d.   Among dominant rangeland plants

3.   Soil discrimination

      a.   Bare versus cropped land

      b.   Among major soil types

      c.   Spectral contrast between freshly irrigated and nonirrigated soil

      d.   Spectrum of saline soil, compared with nonsaline soil, and salt-affected soil's distribution

QUESTIONS

A question that needs answering very early in the use of ERTS-A data is: What sizes of fields can be identified for acreage estimates with what respective probabilities. (The distribution of field sizes in the Rio Grande Valley has implications in the size of farm equipment required, for example, and would in itself be worthy of study.)

In addition to testing LAI and CHL concentration versus reflectance, the ERTS-A data will be studied to answer:

    a.   Can the reflectance measured from space for a given crop be divided into poor, average, and excellent categories of crop vigor that relate to probable yield per unit area?

    b.   Can cotton and grain sorghum be distinguished from other crops? If so, how do the acreage estimates determined from ERTS-A data agree with acreage of these crops as determined by the Agricultural Stabilization and Conservation Service (ASCS) that administers the acreage controls?

    c.   Can the vegetable crops onion, cabbage, and carrots be distinguished? If so, how do the acreages estimated from ERTS-A agree with industry or the Crops Reporting Service acreage estimates?

d. Can citrus be distinguished from other crops, and what time of the year can citrus be best distinguished from other crops?

e. How does the reflectance spectrum of rangeland vary seasonally? Can the distribution of dominant rangeland species be determined from the data?

f. Can bare soil be recognized? What is its signature? On each passage of the satellite, what percentage of the cultivated land is bare?

g. Do major soil types differ enough spectrally to permit distinguishing them in the ERTS-A data?

h. How much does soil still wet from irrigation differ spectrally from adjacent nonirrigated soil of the same type?

i. Can saline soil areas be distinguished from nonsaline soils? Can the extent of saline soil be estimated from ERTS-A data?

j. Can a temporal multivariate signature be developed to answer questions "a" through "i" above, that improves discrimination on a date-by-date basis?

An additional area of investigation is:

4. MSS digitized data versus optical density (OD) of composite transparencies for discrimination.

A typical question to ask here is, for one set of data (approximately 200 fields and perhaps 8 classification categories) how do the MSS digitized data and the OD of color composites compare for percent correct identification of the categories used?

Answers to the above questions will help to develop an operational system of ERTS-A data analysis.

LITERATURE CITED

Allen, W. A., H. W. Gausman, and A. J. Richardson. 1970. Mean effective optical constants of cotton leaves. J. Opt. Soc. Amer. 60:542-547.

Park, A. B. Feb. 2, 1971. Preparation of proposals for investigations using data from earth resources technology satellite (ERTS-A) and skylab (EREP). Earth Observations Program Office, NASA, Washington, 13 p., Appendices A-G.

Richardson, A. J., R. J. Torline, D. A. Weber, R. W. Leamer, and C. L. Wiegand. 1970. Computer discrimination procedure comparisons using film optical densities. SWC Research Report 422 (multilithed locally). Dec. 1970. 82 p.

Wiegand, C. L., R. W. Leamer, D. A. Weber, and A. H. Gerbermann. 1971. Multibase and multiemulsion space photos for crops and soils. Photogram. Eng. XXXVII: 147-156.

EREP PROPOSAL: IRRIGATION SCHEDULING, FREEZE WARNING,

AND SALINITY DETECTING

C. L. Wiegand, Principal Investigator
W. A. Allen, H. W. Gausman, R. W. Leamer, L. N. Namken,
and J. R. Thomas, other investigators
R. H. Miller, Agency Coordinator

This information was taken from the
proposal for participation in Skylab's
EREP (Earth Resources Experimental
Package) Space Flight Investigations
(Naugle, 1970).

INTRODUCTION

EREP objectives are to extend use of sensors beyond capabilities of
automated spacecraft, to use men to observe, discriminate and select appro-
priate areas for study; and to provide an early source of unique research data
for analyses (Technical Photography, 1971). Some data acquired will be used
in evaluating agricultural applications of space observations. These include
identifying crops and other vegetation, measuring growth rates of plants,
assessing crop vigor, detecting disease infestations, determining land struc-
ture and surface composition, mapping snow cover, and assessing water runoff
characteristics.

This spacecraft is scheduled for launch in 1972. Teams of three astro-
nauts will journey to the orbiting laboratory (Skylab) and work in its "shirt
sleeve" environment. The third crew to occupy the Skylab will concentrate on
earth resources experiments; the mission is scheduled to last 56 days.

In addition to Skylab's EREP objectives stated above, remote sensing
researchers at Weslaco, Texas plan to use Skylab's capabilities to map saline
soil areas and to determine radiometric temperatures of plant canopies during
near freezing temperature conditions in winter or in response to different
soil moisture stresses in summer.[1/] (If Skylab orbits in winter, one experi-
ment will be conducted; if it orbits in summer, the other will be conducted.)

[1/] The work statements are to be negotiated.

SUMMARY

The objectives of the proposed study are:

1. To utilize Skylab's multispectral scanner (MSS) data to assess temperatures of plant canopies in relation to:

    a. midday insolation, ambient air temperature, and plant water stress conditions,

    b. low temperatures (near-freeze conditions) in the winter, depending on satellite launch time and orbit and the probability of near-freeze temperatures occurring; and

    c. geographical distribution of plant canopy and earth surface temperatures from the Gulf of Mexico inland.

2. To use MSS data to detect, survey, and map saline soil areas.

3. To use the six-band Multispectral Photographic Facility (MPF) to identify, survey, and map saline and nonsaline soil areas.

4. To correlate EREP's MSS results with results of:

    a. MPF

    b. ERTS-A and B Return Beam Vidicons

    c. ERTS-A and B Multispectral Scanners

    d. aircraft observations

    e. ground truth

The ultimate objective is to use space observations internationally for determining the need for crop irrigations and for freeze warnings in subtropical and semitropical areas.

LITERATURE CITED:

Naugle, J. E. Dec. 22, 1970. Opportunities for participation in space flight investigations. Memo Change 33, NASA Handbook (NHB)8030.1A, Washington, D.C., p. 1-9.

Technical photography. 1971. NASA seeks experimenters. 3:1, 24.

EFFECTIVE USE OF ERTS MULTISENSOR DATA

IN THE GREAT PLAINS CORRIDOR

V. I. Myers and C. L. Wiegand

This information was taken from the ERTS-A
proposal of the same title, and from phone
and letter exchanges between the authors.
V. I. Myers is Director, Remote Sensing
Institute, South Dakota State University,
and Principal Investigator for the study.

SUMMARY

The subject ERTS-A proposal has been negotiated with NASA by the Principal
Investigator, and the scope of the study has been reduced to a smaller geographic
area than originally proposed. The title and the north and south end test sites
of the corridor remain. The corridor was proposed originally to increase the
probability that cloud conditions would permit acceptable imagery to be obtained
of the earth surface over at least some test sites each satellite pass and to
emphasize the temporal aspects of crop growth and maturity in the analyses.

The main objectives of the negotiated proposal are to study changes in the
quantity, quality, and distribution of resources in the test areas; to investi-
gate procedures for predicting land, soil, and crop patterns; and to produce
maps using ERTS-A imagery to delineate the resources.

The role of Weslaco USDA personnel in the study will be to emphasize the
identification and prediction of vegetation categories. The scope of the effort
will not be defined, however, until a negotiation session has been held with NASA
representatives.

GREAT PLAINS COORDINATED PROJECT ON EVAPOTRANSPIRATION

C. L. Wiegand

Research on evapotranspiration will be
continued under Research Outline 80,
"Efficacious Utilization of Radiant
Energy in the Soil-Crop-Atmosphere
System"

INTRODUCTION

Researchers at this Center have been working with the Research Committee of
the Great Plains Agricultural Research Council [1] and its Subcommittee on Remote
Sensing to examine the possibilities of using satellite capabilities in studies
of evapotranspiration. This report records some of the effort that has been
expended and indicates the current status of the project.

BACKGROUND

The Great Plains of the United States--a region bounded roughly by longi-
tudes 95° and 105°W and by latitudes 30° and 48°N--constitutes one of the most
extensive, uniform, and important agricultural regions in the world. Its climate,
physiography, and land use patterns are similar to other important agricultural
regions in Europe, Asia, Australia, and South America.

Evaporation from free water surfaces in this region exceeds annual rainfall
by amounts that increase from east to west. Adequate moisture is normally unavail-
able to permit maximal crop production--although for short times water excesses
may occur following intense or extended rainfall. Because of these basic clima-
tological facts, plant growth and hence agricultural production and the economy
of this vast region is particularly dependent on evaporative demand and the
water balance.

---

[1]
The Great Plains Agricultural Council consists of 32 public agencies; namely,
the Agricultural Experiment Stations from the 10 Great Plains states, the
Agricultural Extension Service from each of the 10 Great Plains states, and
the following 12 USDA agencies: The Agricultural Research Service, the
Economic Research Service, the Forest Service, the Federal Extension Service,
the Soil Conservation Service, the Agricultural Stabilization and Conservation
Service, Farmers Home Administration, Federal Crop Insurance Corporation,
Marketing and Consumer Service, Statistical Reporting Service, Cooperative
State Research Service, and Rural Electrification Service. Some purposes of
the Council are: to analyze problems of Plains' Agriculture, to promote a
coordinated attack on agricultural problems of the region, and to develop
possible solutions to selected problems.

This dependency is evident in the effort expended by research agencies represented in the Great Plains Agricultural Council to measure, control and predict evapotranspiration (ET). It is also evidenced by the large number of research installations throughout the region devoted to the study of plant responses to water availability, to the use of soil management to optimize water use efficiency, and to the prediction of water demand and allocation of water resources for irrigation.

Typical models used to describe the energy of water mass balances involved in ET are based on point measurements. If satellite data could be incorporated into ET models, spatially integrated information on an area as large as the Great Plains would be obtainable. Realizing this possibility the Research Committee of the Great Plains Agricultural Council appointed a committee of scientists to investigate the utilization of ERTS, ITOS, NIMBUS, and SKYLAB satellite capabilities in ET studies.

This action was taken after the Research Committee of the Council sponsored a seminar entitled "Evapotranspiration in the Great Plains" (Research Committee, 1970). Members of the Remote Sensing Subcommittee were: Dr. Ed Kanemasu, Kansas; Dr. Jack Stone, Oklahoma; Dr. Jack Runkles, Texas; Dr. William Marlatt, Colorado; Drs. Joe Ritchie and Craig Wiegand, ARS, Texas; and Dr. Maurice Horton, South Dakota. Dr. Norman Rosenberg, Nebraska, served as chairman. This group met at Oklahoma City on Nov. 19 and 20, 1970 with Dr. John Rouse, Texas A&M Remote Sensing Center; Dr. Fred Godshall, NOAA, Silver Spring, Md., and Dr. B. E. Dethier of Cornell, Chairman NE-69, who acted as advisers. The purpose of the meeting was to decide on aspects of ET that could utilize satellite data and to specifically formulate a proposal (s) for ERTS-A.

Utilizing the ideas generated at Oklahoma City, a rough draft of four proposals (subtasks) was produced. The common objective of the proposals was to determine the operational feasibility of utilizing satellite data in conjunction with data collected by ground platforms, weighing lysimeters, and specific ground experiments to obtain information for better management of the soil and water resources of the Great Plains.

The four subtasks were entitled:

Ground Platform Network for the Great Plains
Atmospheric Water Balance of the Great Plains
Mapping Solar Radiation Flux Density for the Great Plains
Definition of a Satellite Evapotranspiration Model (SETM) and a
    Sensor Package for an Evapotranspiration Vehicle (ETV)

On Feb. 8 and 9, 1971, the Subcommittee met at the Goddard Spaceflight Center. Dr. V. V. Salomonson hosted the group. Each of the subtasks was discussed. It was decided that the atmospheric water balance study could not be carried out at this time because the instruments for making the measurements do not sufficiently scan the Great Plains, and reduction of the raw data for this purpose would be extremely difficult. (It had been proposed to use the infrared interferometer spectrometer (IRIS) and satellite infrared spectrometer (SIRS) data from Nimbus IV and the similar instruments on Nimbus V for this purpose. One or both of these will be in orbit simultaneously with ERTS-A).

Moreover, the satellite ET model and sensor package is not truly responsive to currently planned satellites. The proposal is more appropriate for the Advanced Applications Flight Experiment (AAFE) Program, and plans are to explore this route. The package needs to be ready for use on the Space Station.

Two proposals were produced for ERTS-A funding consideration. One was entitled "Mapping Solar Radiation Flux Density for the Great Plains" (Dr. Joe T. Ritchie, Principal Investigator) and dealt with relating the response of the return beam Vidicon (RBV), as an indicator of cloudiness, to measurements of the solar radiant flux density reaching the ground. By determining the relation between cloudiness and incident solar radiation, it might be possible to predict incident radiation at any position on the Great Plains from satellite cloudiness information. This capability would be very valuable because incident solar radiation is the most important variable in physical models describing the evaporation and photosynthesis processes. Incident solar radiation can be only obtained now by direct measurement. The proposal will not be funded under the ERTS-A program. The proposal is more closely related to interests of the National Oceanographic and Atmospheric Administration (NOAA), and coordination should continue with them to improve the experiment.

The other proposal was titled "Applicability of ERTS Data Collection and Dissemination Systems for a Ground-based Great Plains Network of Bowen Ratio Evapotranspiration Measurements" (Dr. Norman Rosenberg, Principal Investigator), and it dealt with interrogating ground data platforms instrumented to solve the Bowen ratio (Bowen, 1926) at six sites on the Great Plains and with comparing the Bowen ratio results with ET determined by weighing lysimeters at the same sites. The proposal is aimed at eventually developing enough satellite-interrogated sites to periodically map evaporative demand contours on the Great Plains. The proposal will not be funded, however, under the ERTS-A invitation for proposals.

SUMMARY

It is feasible that the agricultural production and the economy of the vast Great Plains area can be greatly enhanced by using satellite data for incorporation of evaporation information into ET models, for predicting incident radiation at any position on the Great Plains for use in physical models describing evaporation and photosynthesis, and for mapping evaporative demand contours on the Great Plains.

The Coordinated Project on ET provides an opportunity to utilize satellite capabilities to study energy and mass (water) balances on the scale of the Great Plains. Such capability has not been previously available. The subcommittee on remote sensing expects to propose one or more proposals for ERTS-B experimentation. Participation in the AAFE program may be necessary to produce the sensor packages required for the studies that need to be conducted on ET.

LITERATURE CITED

Research Committee, Great Plains Agricultural Council. 1970. Proceedings Seminar, Evapotranspiration in the Great Plains, held Mar. 23-25, at Bushland, Texas. Public. No. 50, Agric. Expt. Sta., Kansas State Univ., Manhattan, 401 p.

Bowen, I. S. 1926. The ratio of heat losses by conduction and by evaporation from any water surface. Phys. Rev. 27:779-787.

BENDIX 9-CHANNEL SCANNER DATA STUDIES

A. J. Richardson, C. L. Wiegand, R. W. Leamer,

A. H. Gerbermann, and R. J. Torline

These results were produced under Research
Outline 53, "Crop Identification Through
Spectrum Matching Techniques -- Sub title --
Bendix 9-Channel Scanner Data Studies".

INTRODUCTION

Quantitative reflectance data from aircraft-borne multispectral scanners
were used in remote sensing investigations of the U. S. Department of Agriculture
at Weslaco, Texas. These data were used to test crop discrimination procedures
and to explain sensor response variations in terms of ground truth. Long range
objectives are identification of yield-limiting crop and soil conditions, pre-
diction of yields, and automatic recognition of crop and soil types.

In the spring and summer of 1969, NASA Houston made overflights with the
9-channel Bendix scanner providing quantitative scanner data in the 380- to
1000-nm wavelength interval (WLI). The overflights were made on April 13, May 8
and 9, June 6, and July 9. These data gave seasonal coverage from time signals
that represent mainly the soil background, caused by very young row crop plants,
up to full canopy development where signals are almost entirely caused by the
crop. The NASA contract with Bendix Aerospace Systems Division (Ann Arbor,
Michigan) provided the scanner data, and Weslaco provided the ground truth col-
lection during the flights. Signature processing studies relating scanner data
to ground truth were carried out at Ann Arbor and Weslaco. This report summarizes
Weslaco's investigations.

MATERIALS AND METHODS

Five flight lines, listed in Table 1 by number, length, location, and soil
type, were selected for study prior to the 4 Bendix overflights. Table 2 lists
the fields contained in these 5 flight lines. The fields represent a range in
soil types from heavy clay to sandy loam. Five crop categories, citrus, corn,
cotton, sorghum, and bare soil, make up the bulk of the fields in Table 2. Matu-
ration, harvest, and tillage of crops occurred in a number of fields in some cate-
gories during the April, May, June, and July flight dates.

Two ground truth reports were prepared. One report entitled, "Ground Truth
Summary, April-July, 1969, Site 32, Weslaco, Texas" (Rpt. 69-03, dated 12/1/69)
was prepared in 35 copies and distributed to NASA, Bendix, USDA, and other cooper-
ators interested in using the scanner data. The other report, "Detailed Ground
Truth, April-July, 1969, Site 32, Weslaco, Texas" (Rpt. 70-01, dated 3/2/70) con-
sists primarily of photocopies of the seasonal ground truth data sheets for each
individual field on each flight line.

Ground truth information was punched on IBM computer cards. The Weslaco IBM 1800 computer was used to sort ground truth according to flight date, crop category, and field condition. Sorting according to ground truth grouped all fields into similar categories so that training fields could be randomly selected to represent each crop and soil category.

Digital scanner data were obtained from Bendix. Reflectance data for each field listed in Table 2 were recorded on digital magnetic tape. One scan was sampled for each field for 8 channels of the Bendix 9-channel scanner.

Principal axis factor analysis was applied to the reflectance data of training fields (Veldman, 1967). This analysis yielded statistics for pattern recognition algorithms. The analysis transforms the original reflectance data into principal axis factor scores. Factor scores have the property that crop and soil differences are maximized using a minimum number of factor scores. In other words, crop and soil variations in the 8 original scanner channels are represented by a reduced number of principal axis factor scores.

Pattern recognition algorithms based on probability error ellipses were computed for each crop category (Richardson, et al., 1971). Error ellipses were based on factor scores, rather than on the original scanner reflectance data, to take advantage of the variable reduction. The pattern recognition procedure determines the ellipse a candidate set of transformed reflectance measurements falls in from a particular field. The ellipse the measurements fall in identifies that measurement. If the set of measurements does not fall inside any ellipse, then the field is placed in a threshold category as not belonging to any crop as soil category tested. The error ellipse threshold was set at the 5% probability level for this study.

Regression analysis was used to test the effect of percent ground cover and plant height on reflectance measurements. The regression equations resulting from this analysis are useful for prediction of percent ground cover and plant height.

RESULTS AND DISCUSSION

The mean factor scores $(\overline{F}_i)$ and error ellipse coefficients (C_{ij}) used as standard signatures for pattern recognition studies for the April, May, June, and July flights are listed in Tables 3 and 4, respectively. The indices i and j = 1, 2, ···, NF are the number of factor scores extracted from the factor analysis. These results are based on randomly selected training fields from each crop and soil category. Categories tested are ranked according to the $\overline{F}_1$ means for all flights, since factor 1 accounts for most of the total variance and therefore is the most important factor.

Ranking $\overline{F}_1$ means in descending order of magnitude reveals the general structure among the categories for each flight. The category structure for April and May is similar (Table 3). The water and bare soil categories are ranked 1 and 2, respectively, in both flights. Vegetative categories follow these two categories. In April, cotton and sorghum follow bare soil. This is reasonable because according to ground truth both fields were mostly bare soil. For the recognition results shown in Tables 5 and 6, the bare soil category for April was considered to be a combination of bare soil, cotton, and sorghum fields. For the other three flights, the bare soil category was fields with bare soil.

The June and July flights are similar in category structure as revealed in Table 4 using the $\bar{F}_1$ means. The vegetative categories are ranked first with bare soil category ranked next. Water samples were ranked last in June. There were no water samples taken in July. In both June and July, the cotton category ranked first within the vegetative categories. In July, cotton had become so distinctive that it was possible to distinguish cotton fields very accurately.

The recognition results in Table 5 and 6 indicate that it is possible to distinguish bare soil, vegetation, and water reliably. As was expected, higher recognition results were obtained using randomly selected training fields in each category. Recognition results on a per field basis were higher than on a per sample basis. These results show that automatic recognition procedures are feasible for general land use applications involving soil, vegetation, and water.

Requirements for more detail of specific vegetation categories will be more difficult to meet. It was not possible to distinguish any specific vegetative category in April or May with any degree of accuracy. In June and July, it was possible to distinguish citrus and cotton.

Figures 1 and 2 are factor score scatter diagrams for April and May. In general, soil and crop categories have the same arrangement of point clusters. In both diagrams, the cluster of points in the upper right corner, identified with G's, is the water category distribution. Proceeding downward and to the left are the points identifying the bare soil distributions. The vegetative distributions are about midway down and to the left in each diagram. These distributions indicate the difficulty of identifying individual vegetative categories. None of the vegetative categories have distinctive clusters of points like the water and bare soil categories.

The diagrams in Figs. 3 and 4 are the factor score scatter diagrams for the June and July flight dates. In June, citrus (D's), water (F's) and bare soil (A's) had fairly well-defined clusters of points, respectively. Vegetative categories distributions other than citrus were confused in June. In July the cotton distribution (A's) had very good separation. These two developments gave 91.0% recognition for citrus in June and 86.4% recognition for cotton in July. In both cases "false alarm" errors were low.

Table 7 lists coefficients for the correlations of percent ground cover and plant height with Bendix 9-channel reflectance measurements. All fields were used to calculate the correlation coefficients except citrus and water samples. Citrus fields were deleted from the analysis because it seemed unreasonable to consider trees and row crops in the same regression analysis. Water samples were deleted for similar reasons.

The coefficients (Table 7) in column A correlate ground cover with reflectance measurements at each WLI for each flight. Similarly, column B correlates plant height with reflectance measurements for each flight. In general, there is a better correlation of ground cover with reflectance measurements than of plant height with reflectance measurements. The linear correlation coefficients for individual WLI were usually statistically significant, but they are not strong enough ($r^2 = .725$) to insure accurate predictions of ground cover or plant height. The multiple correlations for the linear and nonlinear case are high enough (highest $r^2 = .875$) to possibly insure accurate predictions. For ground cover and plant height predictions, April is the worst date. Most fields are bare soil so correlations were low. The last three dates in May, June, and July have more vegetative fields so correlations were stronger.

The reflectance spectra for cotton, sorghum, soil, and water for the April, May, June, and July flights in Figs. 5 and 6 help to explain the correlation results in the visible and infrared WLI. For all 4 flight dates, the reflectance spectra in the visible WLI for cotton and sorghum are lower than the soil spectra. In the infrared WLI, the cotton and sorghum reflectance spectra cross over the soil spectra and become higher. This means that as the vegetative cover increases, the overall reflectance in the visible WLI produced by soil and vegetation decreases because vegetation reflects less light than soil in the visible range. In the infrared WLI, the overall reflectance increases as vegetative cover increases because vegetation reflects more light than soil in the infrared range.

From these spectral curves it can be seen that each flight was a different experiment. The spectral curve for bare soil and water are different for all four flight dates. It was expected that these two categories would have invariate spectras for all flight dates. The spectras for cotton and sorghum change from one flight date to another. Some of this variation is to be expected since their ground cover and general field conditions are changing. There is some variation in these two categories that is not expected. It can be seen in April that cotton and bare soil have similar spectras since cotton was really very immature at this time. Sorghum in April is slightly different as it was a little more mature than cotton.

SUMMARY

Standard signatures were developed for each crop genera and bare soil condition, and they are listed in Tables 3 and 4. The factor scores and error ellipse coefficients in these tables statistically describe crop, bare soil, and water categories for pattern recognition studies. The F_1 means are the most important factor score for signature development. These means when ranked in descending order of magnitude show the relative structure among crop, bare soil, and water categories. It was found that April and May, and June and July had similar category structure, respectively.

Pattern recognition studies using these signatures were conducted and results are listed in Tables 5 and 6. These results indicate that it is possible to distinguish bare soil, vegetative, and water categories accurately. Accuracy declined when attempts were made to achieve finer discrimination of the vegetative categories such as cotton, sorghum, and corn. In most cases background vegetative categories could not be adequately separated from a vegetative category of interest. For example, in May it was not possible to distinguish citrus from everything else because there was a high number of "false alarm" error because of background categories of sorghum, cantaloupe, and cotton that degraded results. In other words, it was possible to identify citrus with some degree of accuracy (71.50%), but fields of sorghum, cantaloupe, and cotton were also identified as citrus. High number of "false alarm" errors caused by background categories cannot be tolerated in any successful discrimination procedure.

In June, it was possible to distinguish citrus with an acceptable degree of accuracy 91.0% with a low number of "false alarm" errors. One reason for this development is that, considering overall field conditions, citrus in June was not growing as vigorously as the other vegetative categories. The same development occurred in July for cotton. The cotton category can be distinguished from everything else with an accuracy of 86.4% with very few errors because of "false alarms".

In general, it appears that bare soil, vegetation, and water can always be distinguished accurately. In some instances, as with citrus in June and cotton in July, field conditions will be such that the possibility exists that a particular vegetative category of interest will be recognized accurately.

As shown in Table 7, there is an indication that ground cover and plant height can be predicted using Bendix 9-channel scanner reflectance measurements. For all 4 flights it was possible to predict ground cover more accurately than plant height. For all 4 flights, the visible and infrared WLI have opposite responses to ground cover and plant height. In the visible WLI, as ground cover and plant height increased, reflectance decreased. In the infrared WLI, the opposite response occurred. Apparently in the visible WLI, the relatively low reflecting vegetation is covering the relatively high reflecting soil causing the overall reflectance to decrease with increasing vegetative cover. An opposite situation prevails in the infrared WLI where soil is less reflective than vegetation. The relative reflectance of soil and vegetation in the visible and infrared can be seen from Figs. 5 and 6.

LITERATURE CITED

Veldman, D. J. 1967. Fortran programming for the behavioral sciences, Holt, Rinehart, and Winston, Inc., New York. 466 p.

Richardson, A. J., R. J. Torline, and W. A. Allen. 1971. Computer identification of ground patterns from aerial photographs. Proceedings of the Seventh International Symposium on Remote Sensing of Environment, University of Michigan, Ann Arbor. May 17-21. p. 1357-1376.

Table 1. — Flight line numbers, locations, soil types, and length of each flight line over which Bendix 9-channel scanner data were obtained in 1969.

Flight line	Location	Soil types present	Line length
No.			Miles
1	Research Farm Highway 88 (Mi 5 W & 12 N)	Sandy clay loam	1
3	FM Rd 1015 (Mi 3 W from Mi 12 N to Floodway)	Clay Clay loam Fine sandy loam Sandy clay loam Silty clay	7
11	"I" Rd (between Pharr and San Juan) from Exp 83 N for 5 mi.	Clay loam Sandy clay loam Fine sandy loam	5
12	FM 1426 (E of San Juan) from Rio Grande to Exp 83	Clay Silty clay loam Silty clay	7.5
13	Highway 281 (Military Highway) from Hidalgo to S of Donna then cross country to Int'l Bridge at Nuevo Progreso	Clay Silty clay Silty clay loam	17

Table 2. -- Crop genera, weeds, bare soil, and water, and number of
fields of each by flight date.

	Flight date			
Crop	4/13	5/8-9	6/6	7/9
Cotton	73	69	42	73
Corn	19	21	8	9
Cantaloupe	7	8	4	1
Citrus	26	25	11	26
Sorghum	39	46	26	42
Pepper	1	1		1
Cabbage	1	2		
Tomato	3	3	2	
Native vegetation	2	2	2	2
Coastal Bermuda grass	2	2	2	2
Oats	3			
Onion	11	1		
Bare soil	31	41	33	49
Weeds	6			2
Carrot	5	3		
Alfalfa	1	1		1
Red cabbage	1	1		
Flax	2			
Water	9	3	6	
TOTAL	242	229	136	208

Table 3 -- Mean values and error ellipse coefficients for principal axis factor scores 1 and 2 used for pattern recognition tests. Crop categories for the April and May flights are ranked in descending order according to $\overline{F}_1$.

April Categories	Factor score means $(\overline{F}_i) \times 10^3$		Error ellipse coefficients $(C_{ij}) \times 10^{-5}$		
	$\overline{F}_1$	$\overline{F}_2$	C_{11}	C_{12}	C_{22}
Water	1.521	.119	.116	-.150	1.586
Bare Soil	1.196	.611	.725	-.840	3.725
Cotton	1.192	.618	1.096	.065	3.717
Sorghum	.503	.555	.183	-.183	3.605
Corn	.371	.545	.309	.389	5.427
Citrus	.087	.517	.169	.278	4.265
Carrot	-1.209	.550	.232	.220	2.925

May Categories	Factor score means $(\overline{F}_i) \times 10^3$		Error ellipse coefficients $(C_{ij}) \times 10^{-5}$		
	$\overline{F}_1$	$\overline{F}_2$	C_{11}	C_{12}	C_{22}
Water	1.830	-.307	.163	.331	2.616
Bare Soil	1.788	.321	.118	-.078	2.206
Cotton	.769	.346	.269	-.069	2.255
Cantaloupe	.355	.290	.343	.038	3.791
Citrus	-.235	.367	.078	.029	2.028
Corn	-.671	.187	.182	.139	3.339
Sorghum	-.784	.242	.123	.001	3.009

Table 4. -- Mean values and error ellipse coefficients for principal axis factor scores 1 and 2 used for pattern recognition tests. Crop categories for the June and July flights are ranked in descending order according to $\overline{F}_1$.

June	Factor score means $(\overline{F}_i) \times 10^3$		Error ellipse coefficients $(C_{ij}) \times 10^{-5}$		
Categories	$\overline{F}_1$	$\overline{F}_2$	C_{11}	C_{12}	C_{22}
Cotton	1.404	-.476	.439	.026	.246
Sorghum	1.219	-1.017	1.269	-.147	.150
Corn	1.187	-.428	.642	.144	.198
Citrus	.272	-1.116	.207	-.033	.215
Bare Soil	-.676	-.671	1.044	.039	.090
Water	-1.266	.099	1.119	-.918	.925

July	Factor score means $(\overline{F}_i) \times 10^3$		Error ellipse coefficients $(C_{ij}) \times 10^{-5}$		
Categories	$\overline{F}_1$	$\overline{F}_2$	C_{11}	C_{12}	C_{22}
Cotton	2.861	1.706	.428	-.687	3.073
Corn	.503	1.075	.378	-.293	1.519
Citrus	.393	1.478	.139	.057	.622
Sorghum	.367	1.273	.427	.086	.321
Bare Soil	-.787	1.968	1.047	.044	.475

III.9

Table 5. -- Recognition results for the April, May, June, and July flights. Results are given for training fields and all fields considering bare soil, vegetation, and water categories on a per sample basis.

Categories	Training samples					All samples			
	April	May	June	July		April	May	June	July
	%	%	%	%		%	%	%	%
Bare Soil	81.9	88.9	94.6	92.4		78.7	80.7	81.7	87.4
Vegetation	85.6	86.7	92.4	96.3		58.4	57.3	96.0	56.4
Water	97.5	95.3	90.4	-		95.1	93.1	89.7	-

Table 6. -- Recognition results for the April, May, June, and July flights. Results are given for training fields and all fields considering bare soil, vegetation, and water categories on a per field basis.

Categories	Training fields					All fields			
	April	May	June	July		April	May	June	July
	%	%	%	%		%	%	%	%
Bare Soil	87.4	100.0	100.0	100.0		89.5	100.0	94.0	90.6
Vegetation	100.0	96.8	100.0	100.0		73.3	88.0	98.9	99.1
Water	100.0	100.0	100.0	-		100.0	100.0	100.0	-

Table 7. — Coefficients in correlations of percent ground cover (A) and plant height (B) with Bendix 9-Channel reflectance measurements over the 380- to 1000-nm WLI for April, May, June, and July flights. Water and citrus fields were not used.

| Wavelength in nm | Linear correlation coefficients | | | | | | | |
| | April | | May | | June | | July | |
	A	B	A	B	A	B	A	B
380-440	-.579**	-.429*	-.626**	-.626**	-.677**	-.616**	-.525**	-.449*
440-500	-.549**	-.417*	-.620**	-.539**	-.725**	-.649**	-.485**	-.421*
500-560	-.494**	-.389*	-.605**	-.534**	-.675**	-.611**	-.451*	-.390
560-620	-.448**	-.361	-.544**	-.461**	-.636**	-.599**	-.341	-.302
620-680	-.505**	-.392*	-.649**	-.554**	-.699**	-.626**	-.474**	-.401*
680-740	-.410*	-.336	-.624**	-.569**	-.627**	-.597**	-.302	-.268
740-860	.467**	.234	.583**	.485	.653**	.421	.590**	.477**
860-1000	.477**	.242	.589**	.559**	.708**	.526**	.651**	.531*
Linear Multiple Correlation Coefficients	.721**	.475	.801**	.707**	.841**	.749**	.835**	.697**
Non-linear Multiple Correlation Coefficients	.752**	.621**	.819**	.740**	.860**	.788**	.875**	.751**

* Significant at the 5 percent probability level.

** Significant at the 1 percent probability level.
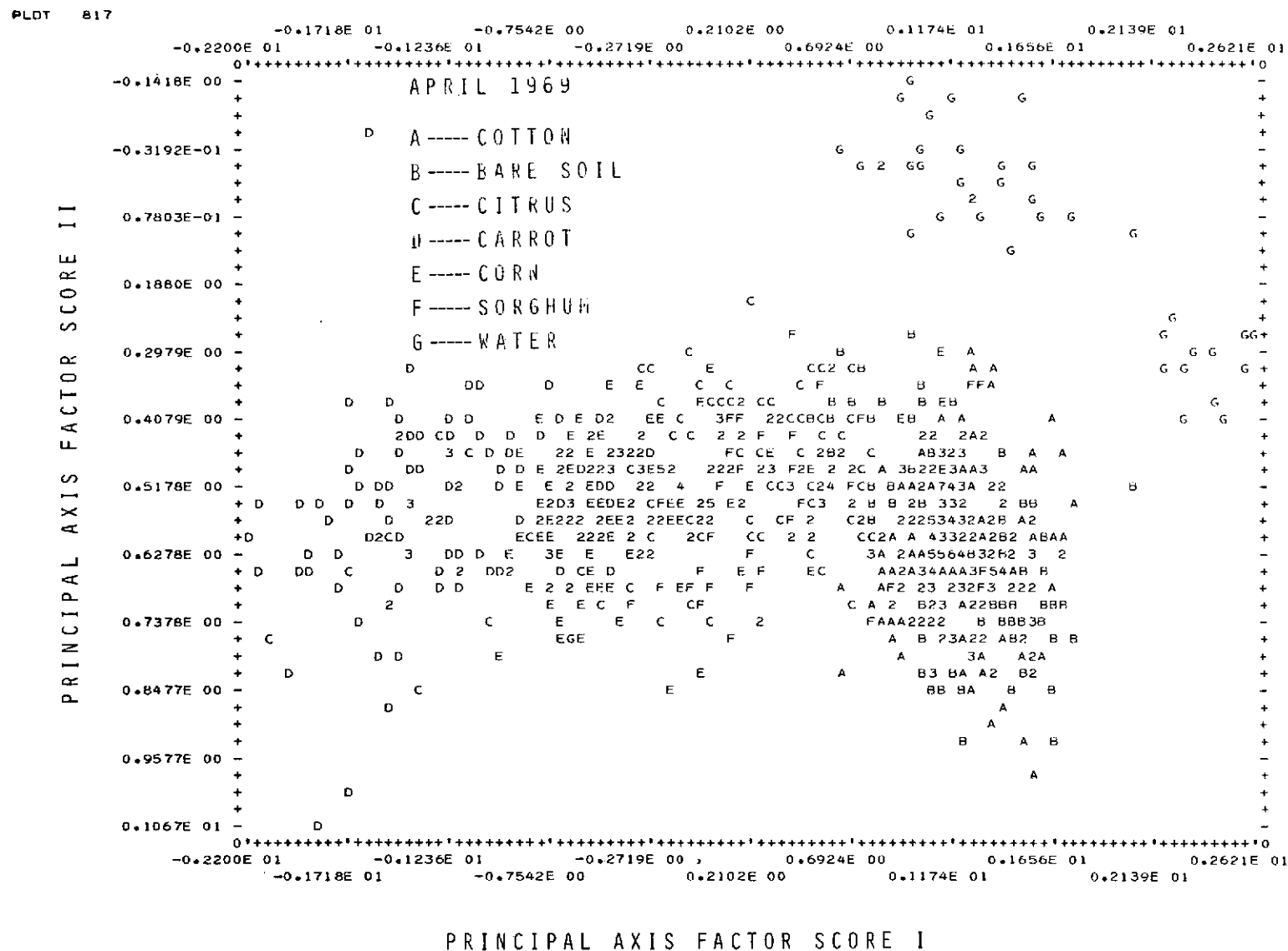
Fig. 1.--Scatter diagram of principal axis factor scores 1 and 2 for cotton (A), bare soil (B), citrus (C), carrot (D), corn (E), sorghum (F), and water (G) categories during the April 1969 flight date.

```
              -0.1646E 01        -0.4764E 00        0.6934E 00        0.1863E 01        0.3033E 01
       -0.2231E 01        -0.1061E 01        0.1084E 00        0.1278E 01        0.2448E 01        0.3618E 01
```

MAY 1969

A —— BARE SOIL

B ——— COTTON

C ——— CORN

D ——— CANTALOUPE

E ——— CITRUS

F ——— SORGHUM

G ——— WATER

PRINCIPAL AXIS FACTOR SCORE II

PRINCIPAL AXIS FACTOR SCORE I
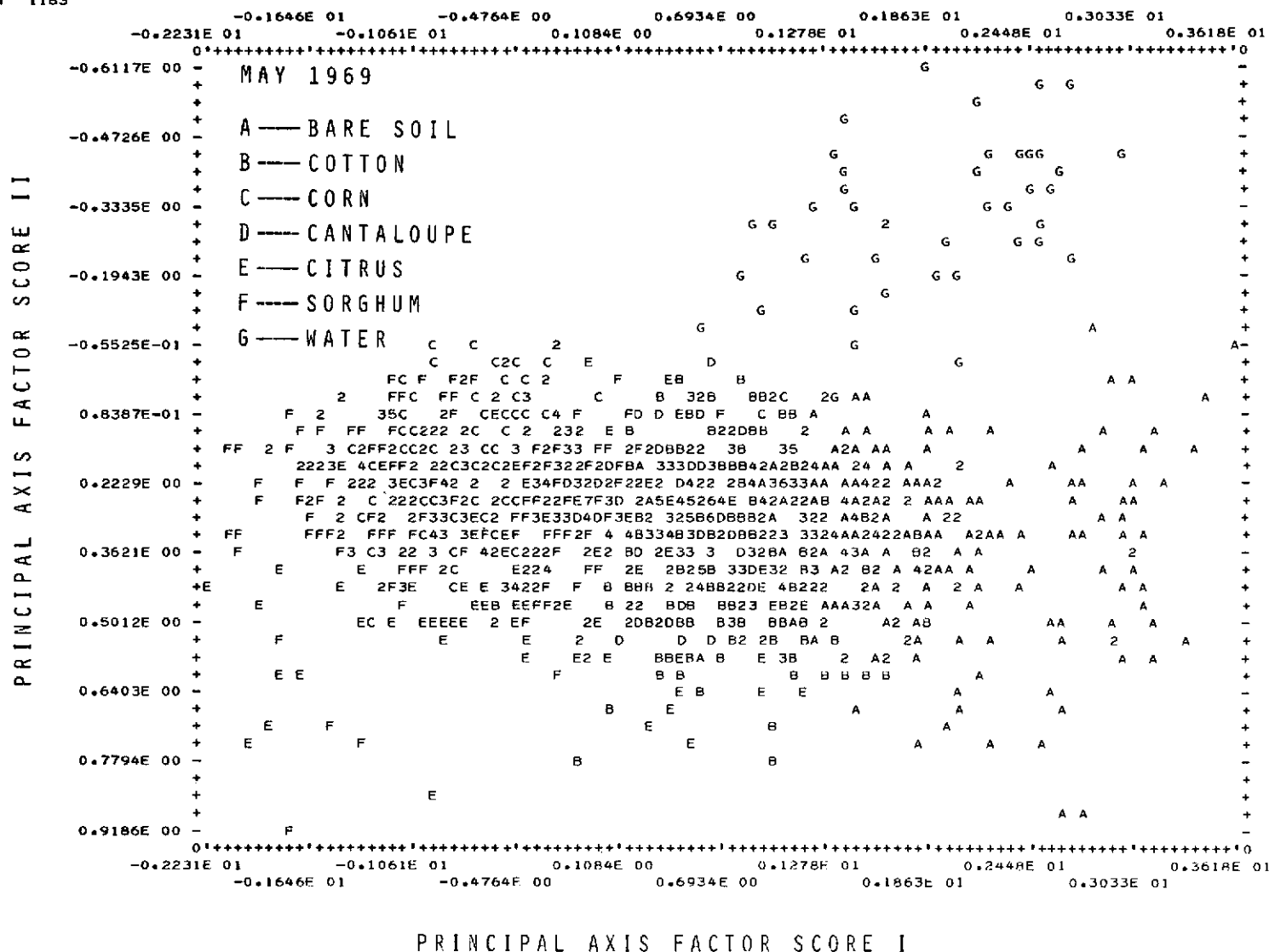
Fig. 2.--Scatter diagram of principal axis factor scores 1 and 2 for bare soil (A), cotton (B), corn (C), cantaloupe (D), citrus (E), sorghum (F), and water (G) categories during the May 1969 flight date.
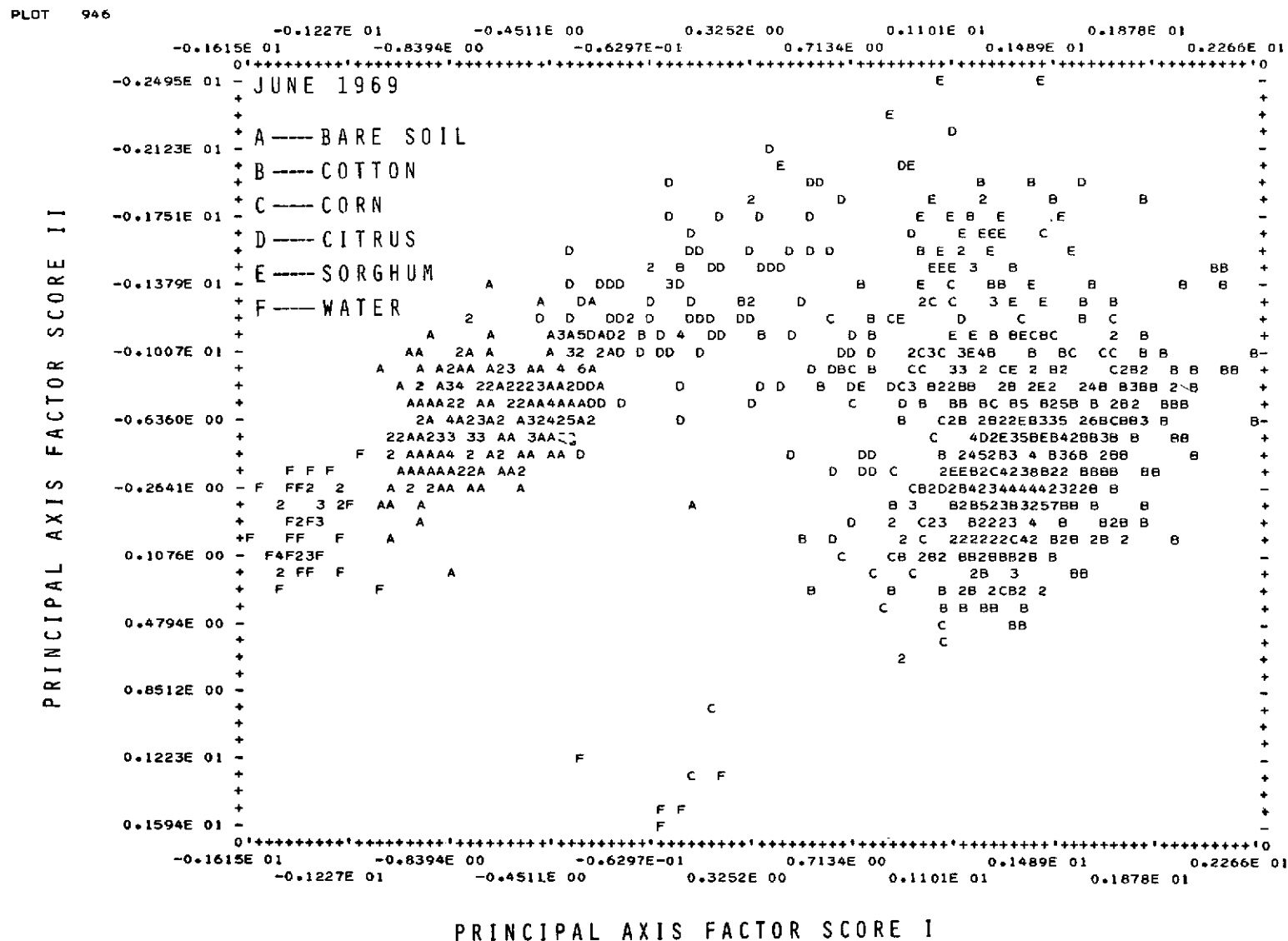
Fig. 3.--Scatter diagram of principal axis factor scores 1 and 2 for bare soil (A), cotton (B), corn (C), citrus (D), sorghum (E), and water (F) categories during the June 1969 flight date.

```
                    -0.7521E 00          0.3474E 00          0.1446E 01          0.2546E 01          0.3646E 01
          -0.1301E 01          -0.2023E 00          0.8972E 00          0.1996E 01          0.3096E 01          0.4195E 01
          0'++++++++++'+++++++++'+++++++++'+*++++++++'+++++++++'!+++++++++'+++++++++'++++++++++'+++++++++'+++++++++'+++++++++'0
0.2962E 00 -                                            D                                                                    -
          +                                                                                                                  +
          +                                                                                                                  +
          +                                                                                                                  +
0.6997E 00 -                        BD BB D     D                                                                            -
          +                       BB    2 3 264D B3DB                                                                        +
          +                       B2B22D62732472223 D22B B                                                                   +
          +                       22B D 236564432283525B4B2   C    2                                                         +
0.1103E 01 -                       D 2 3D25%5323736C3234D2B 4B D    B                                                        -
          +                         23243653252X 4 24D232C B B                                                               +
          +          C2 DE      32D3D2DD324633D224DD D22B  3CB      C           A2  AA                                       +
          +          EE 2  2    DD CC 2D 3 2253D4D2 3B C2 2  D  C    B        A   A                                          +
0.1506E 01 -     E   CE2CEECC       2DCBCC DDD 3D22DD42C C2 D 2C      AA   A 3  AA2A2 33A A2 32 A                             -
          +      E2E   E22C C C DDCDD  B   D DD22 D D 2      C C      A      3A  4AAAAA2736 AA  A  A                          +
          +  EE E273E32E4  E     C    D C    B   2C  C                 A  A 2 323AAAA3A5%42AA3A3A22                          +
          +  E  2EE22E 5E42   2ED   2D  C                              A       AAAA32 3AA2245AAAAA A A A                     +
0.1910E 01 -2 EEE3 E45 2 3CCED C C 2  D2 D DD    C D                          AA 2  2 A AA3A  A    A A                       -
          + E  3 E2 E  422  E2 D D   D C 23D     C                             A 2  2    A  A                                +
          + E  E  EEE2EE  2E      C   OD       C   D                                      A  A                               +
          +  2 EE  33 EE     2  D    DD                                            A                              A+
0.2313E 01 -     E2EE  23 E E               D       C                                                                        -
          +      E2  EEE                                                                                                     +
          +       E 2E2      E                                                                                               +
          +       EE E 2                                                                                                     +
0.2717E 01 -    E       EE                                                                                                   -
          +        E                       JULY 1969                                                                        +
          +                                                                                                                  +
          +                                                                                                                  +
0.3120E 01 -                               A ---- COTTON                                                                     -
          +                                                                                                                  +
          +                               B ---- CORN                                                                       +
0.3524E 01 -                                                                                                                 -
          +                               C ---- CITRUS                                                                     +
          +                                                                                                                  +
          +                               D ---- SORGHUM                                                                    +
0.3927E 01 -                                                                                                                 -
          +                               E ---- BARE SOIL                                                                  +
          +                                                                                                                  +
          +                                                                                                                  +
0.4331E 01 -                                                                                                                 -
          +                                                                                                                  +
          +                                                                                                                  +
          +                                                                                                                  +
0.4734E 01 -    D                                                                                                            -
          0'++++++++++'+++++++++'+++++++++'+++++++++'+++++++++'+++++++++'+++++++++'+++++++++'+++++++++'+++++++++'+++++++++'0
          -0.1301E 01          -0.2023E 00          0.8972E 00          0.1996E 01          0.3096E 01          0.4195E 01
                    -0.7521E 00          0.3474E 00          0.8972E 00          0.2546E 01          0.3646E 01
```

PRINCIPAL AXIS FACTOR SCORE II

PRINCIPAL AXIS FACTOR SCORE I

Fig. 4.--Scatter diagram of principal axis factor scores 1 and 2 for cotton (A), corn (B), citrus (C), sorghum (D), and bare soil (E) categories during the July 1969 flight date.
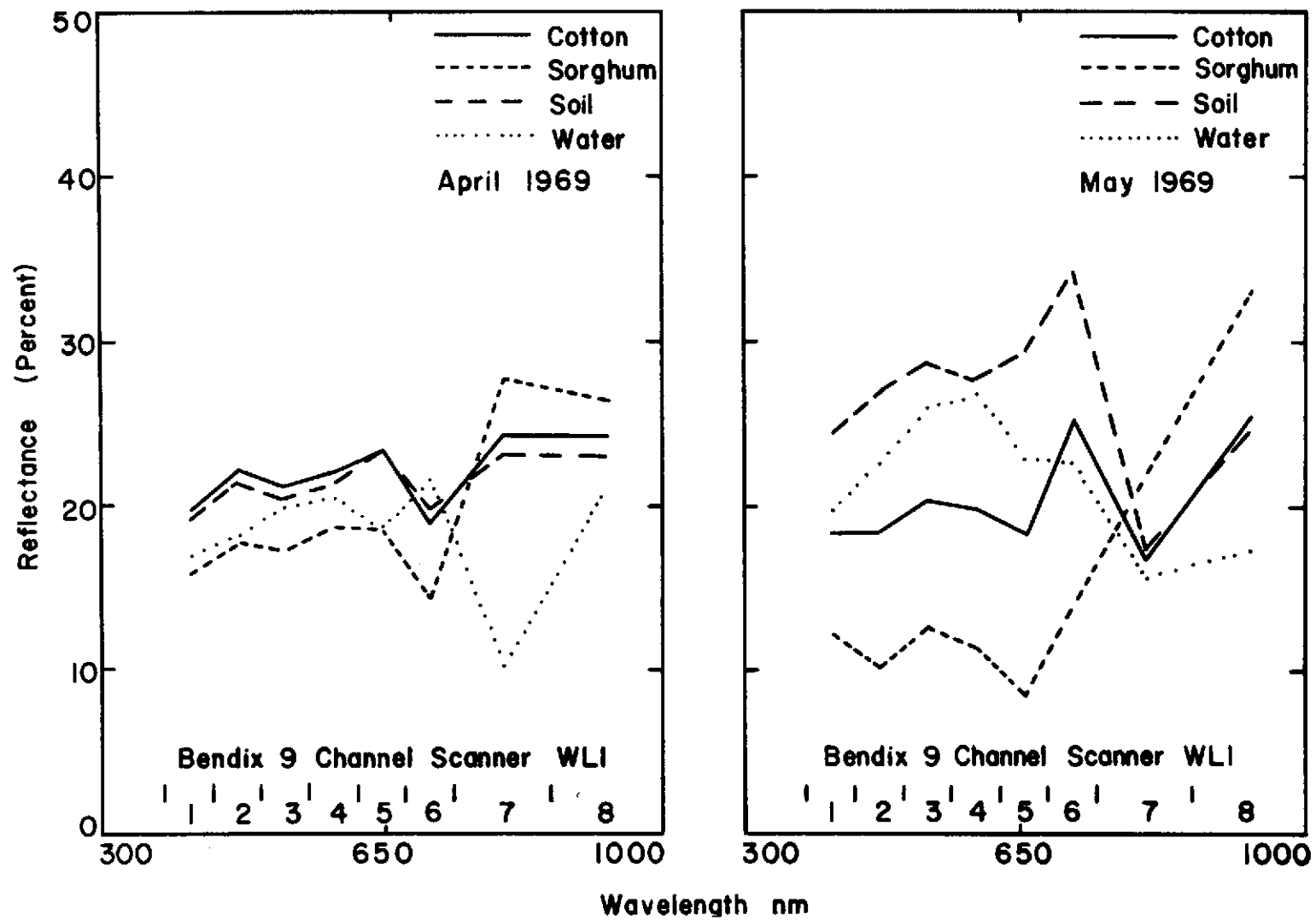
Fig. 5.--Reflectance spectra of cotton, sorghum, bare soil, and water using the Bendix 9-channel scanner during April and May 1969.
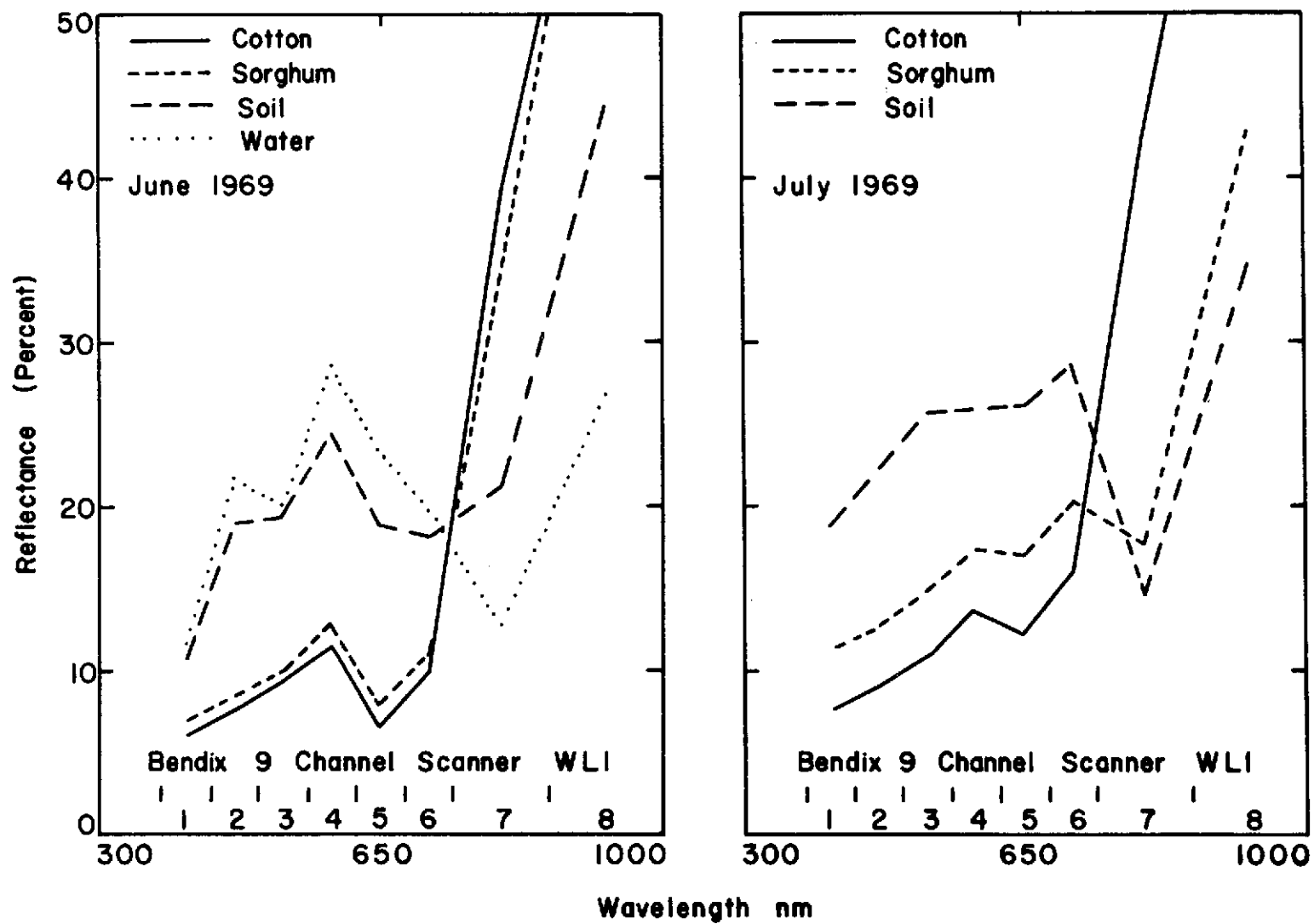
Fig. 6.—Reflectance spectra of cotton, sorghum, bare soil, and water using the Bendix 9-channel scanner during June and July 1969.

MISSION 32M: PRELIMINARY SCIENCE REPORT

C. L. Wiegand

INTRODUCTION

The objective of earth resources research at Weslaco, Texas is to determine characteristics of reflectance and emission signatures of various general crop and soil conditions to permit their multispectral observation and identification from remote sensors at ground, aircraft, or spacecraft altitudes.

The general objectives of Mission 32M were: (1) to advance knowledge on the interaction of electromagnetic radiation with plants and soils, and (2) to perform pattern recognition analyses using the spectral signatures from the optical-mechanical scanner aboard the Michigan C-47 aircraft.

The specific objectives of Mission 32M were: (1) to obtain multispectral data from late winter vegetable crops and from uncropped soil or soils newly planted to the warm season crops of cotton, grain sorghum and corn; (2) to carefully examine data of several wavelengths within the 1.2- to 2.2-μm spectral range for crop discrimination; (3) to look for evidence to evaluate water table depths and to note the occurrence of caliche layers from thermal imagery taken at dawn; and (4) to determine the spectral signature of salt-affected soil.

MATERIALS AND METHODS

The Mission Plan (see Literature Cited) called for one daytime flight using all available wavelengths for about 75 miles of flight line and one flight in the early morning (dawn) over selected flight lines using only the thermal channels. The flight lines were:

Line 1
Location: Northwest of Edinburg
Length: 17 miles
Purpose: Soil mapping in row-cropped and rangeland areas
Comments: Bare soil sites and those with range vegetation should differ spectrally even if the soil type is the same. Insufficient crop fields for vegetation discrimination. Interested in effects of sandy surface and profile caliche layers on thermal imagery.

Lien 2
Location: North of Weslaco, including Research Farm
Length: 5 miles
Purpose: Crop and soil discrimination
Comment: Soil types not very diverse

Line 3
Location: E-W line along Highway 281 near the Rio Grande
Length: 18 miles
Purpose: Crop discrimination and soil mapping
Comments: Includes flood plain and low terrace soils; soils not very colorful. An appreciable fraction of the fields were wet from irrigation.

Line 4   Location: East of Raymondville
              Length: 8 miles
              Purpose: Mapping saline soil.
                          Thermal patterns especially as affected by water table
                          depth.

The C-47 Michigan aircraft and field crew arrived at Harlingen, Texas on Feb. 26, 1971. Discussions were held with Mr. Phil Hasell about conducting the mission. About noon on Feb. 27, the weather began clearing and the aircraft was airborne at 1340 CST. Eighteen scanner data channels and four film filter combinations for the aerial camera were recorded over approximately 50 miles of flight line. Because of overcast conditions, the dawn mission could not be flown on Feb. 28, Mar. 1, and Mar. 2. It was conducted on the morning of Mar. 3, under clear, very windy conditions. Because of the high winds, there was very low thermal contrast in the terrain, and the mission was repeated with NASA's permission the morning of Mar. 4, under calm radiational cooling conditions. Four thermal wavelength data channels were used.

The ground truth obtained in conjunction with Mission 32M was valuable for two other missions that were flown during this same time interval. On Mar. 4, the RB-57F aircraft overflew three counties during the conduct of Mission 158. The Ames Research Center's Convair-990 overflew two of the lines with microwave radiometers on Mar. 1 and 2. These data have been studied by Remote Sensing Center, Texas A&M University, personnel. (See "Convair-990 Mission" under Microwave section, Chapter I.)

RESULTS AND DISCUSSION

Analyses Conducted to Date

Emphasis has been given to automated soil mapping in cooperation with the University of Michigan under NASA Contract NAS 9-9784. The 0.66- to 0.76-µm wavelength interval scanner imagery from the mission (film roll 227015) has been used to prepare flight line maps. On these maps bare soil training sample sites have been located on modal soils selected by the Soil Conservation Service (CSC) cooperating soil scientists, Mr. Jerry Jacobs and Mr. DeWayne Williams. Crop training samples have also been selected consisting of cabbage, onion, carrot, oat, pasture (usually Bermudagrass) and citrus crops.

Because of emphasis on the corn blight watch under the NASA 9-9784 contract, it was necessary to restrict the analysis to two short segments of line 1. On these segments, Mr. Fred Thomson of the University of Michigan has provided recognition maps of three different analyses: (1) the optimal six channels from the 12-channel scanner, (2) the three near-infrared channels, and (3) the response as simulated for black-and-white film type 3400. The University of Michigan has also provided computer listings for each training sample consisting of means, standard deviations, a correlation matrix, a set of Eigen values, and a set of Eigen vector coefficients. A set of punch cards has been provided with means, standard deviations, and the correlation matrix. Documentation of the optimal channel selection program listing has also been provided.

About Aug. 1, computer line printer displays or maps were received -- one for each of the three different analyses. Ground mapping of the same areas by SCS personnel has been completed. Preliminary examination showed that the type 3400 film simulation, compared with the other two analyses, corresponded most closely to photographic imagery of the flight lines. The University of Michigan personnel have emphasized that preliminary maps have been provided to date and that they probably can be greatly improved with simple changes. In completing the ground surveys, the SCS personnel found more soil types than the number of training samples provided the Univ. of Michigan. Also, some training samples provided as bare soil were later found to include vegetation. Arrangements are being made to rerun these line segments.

SUMMARY

Plans for Continuing Analysis

Good progress has been made on analyzing the Mission 32M data. A number of additional uses are planned for the data, including acquisition of a duplicate analog tape so that the Data Systems Analysis Division of the Agricultural Research Service can use it on their A to D facility presently on order. We also wish to obtain digital magnetic tapes of at least selected channels of data to develop and test data handling procedures for ERTS-A data.

Apparently, USGS is the only other group that is studying the spectral signatures of saline soils. There is a high priority on digitizing the training sample sites of flight line 4 so that the data can be evaluated for effects of salinity and soil type on spectral signatures. These data will be used for studying signatures from saline soil areas under EREP (Earth Resources Experimental Package), if our proposal is funded.[a] In addition, thermal imagery taken at dawn needs to be examined for evidence of water tables and caliche layers in the soil profile, and sandy surface soils.

We will continue to make vegetation pattern recognition tests. The Mission 32M data are among the first we have had with results in the near-infrared wavelength region where laboratory data indicates there is powerful information for discrimination.

We will continue to make Mission 32M data sets available to cooperating organizations such as the Statistical Reporting Service, Remote Sensing Center of Texas A&M University, and Data Systems Analysis Division, for specific analyses and for development of their data handling capabilities.

Effects on Future Missions

Utilization of Mission 32M data is helping to prepare us for participation in ERTS-A and EREP programs.

The data may also offer a comparison of the behavior of spectrally similar channels in the Bendix scanner and the University of Michigan scanner. The Bendix scanner overflights were made in 1969, and we received the data this spring in a useable format. Although there is a difference in time of the flights, some

a/ A letter has been received from NASA indicating a willingness to negotiate.

flight lines were common to both missions, and a number of fields were in similar conditions on both missions. Thus, it may be possible to compare relatively the response in the various wavelengths between the Bendix and the University of Michigan multi-channel scanners in future missions.

Conducting missions concurrently, as was done for Mission 32M and RB-57F Mission 158, is commendable because ground truthing requirements are reduced, and the sets of data tend to be complementary. For example, thermal scanner and micro-wave data are both responsive to soil moisture conditions. Such data enable investigators to verify conditions that existed in the fields by comparing results of the thermal scanner and microwave sets of data.

LITERATURE CITED

Mission Plan, Mission 32M, Earth Resources Aircraft Program, Manned Spacecraft Center, NASA, Houston, MSC-03735, Feb. 1971.

MISSION 32M:

SPECTRA OF SWATCHES FROM THE UNIVERSITY OF

MICHIGAN'S STANDARD REFLECTANCE PANELS

H. W. Gausman and C. L. Wiegand

INTRODUCTION

Four flight lines in the Weslaco area (NASA Site 32) were overflown at an altitude of 2,000 ft and one at 500 ft by the University of Michigan's aircraft (Mission 32 M) on February 27, 1971. Imagery was obtained with an optical mechanical scanner.

Cloth reflectance standards of different colors (reference reflectance panels) were on the ground, within flight line 2, at flight time to provide surfaces of known reflectance in the recorded signals. The reflectance of other objects along the flight lines can be expressed relative to the standards.

Swatches were removed from each standard, and their reflectance was measured in the laboratory with a Beckman DK-2A ratio-recording spectroreflectometer at 10-nm intervals over the 500- to 2500-nm wavelength interval (WLI). A $BaSO_4$ standard was used on the instrument. Data were converted to absolute radiometric values using a N.B.S. Vitrolite plate as the absolute reflectance standard.

SUMMARY

Figure 1 depicts the results of reflectance measurements made with the spectrophotometer. Differences in reflectance among the swatches occurred over the entire 500- to 2500-nm WLI, but the most noticeable effect was in the 500- to 750-nm WLI.

The human eye is sensitive to light within the 400- to 700-nm WLI, but it "sees" best at the 550-nm (green peak) wavelength (WL). The color a person sees for a material depends on the visible wavelength of light it reflects most strongly. Thus, green cloth (Lot No. 2043) had a light reflectance of about 34% compared with 4% for red cloth (Lot No. 2042) at the 500-nm WL (Fig. 1). The gray materials reflected less light as their darkness increased at all WL. They were designed to have nominal reflectances of 4, 8, 16, 32 and 64%, respectively, from darkest to lightest gray. Nevertheless, many WL outside the visible range are useful for characterizing materials and for making measurements for each of the channels of the optical mechanical scanner.

The adoption of universal standards would facilitate data comparisons and interpretations among researchers.
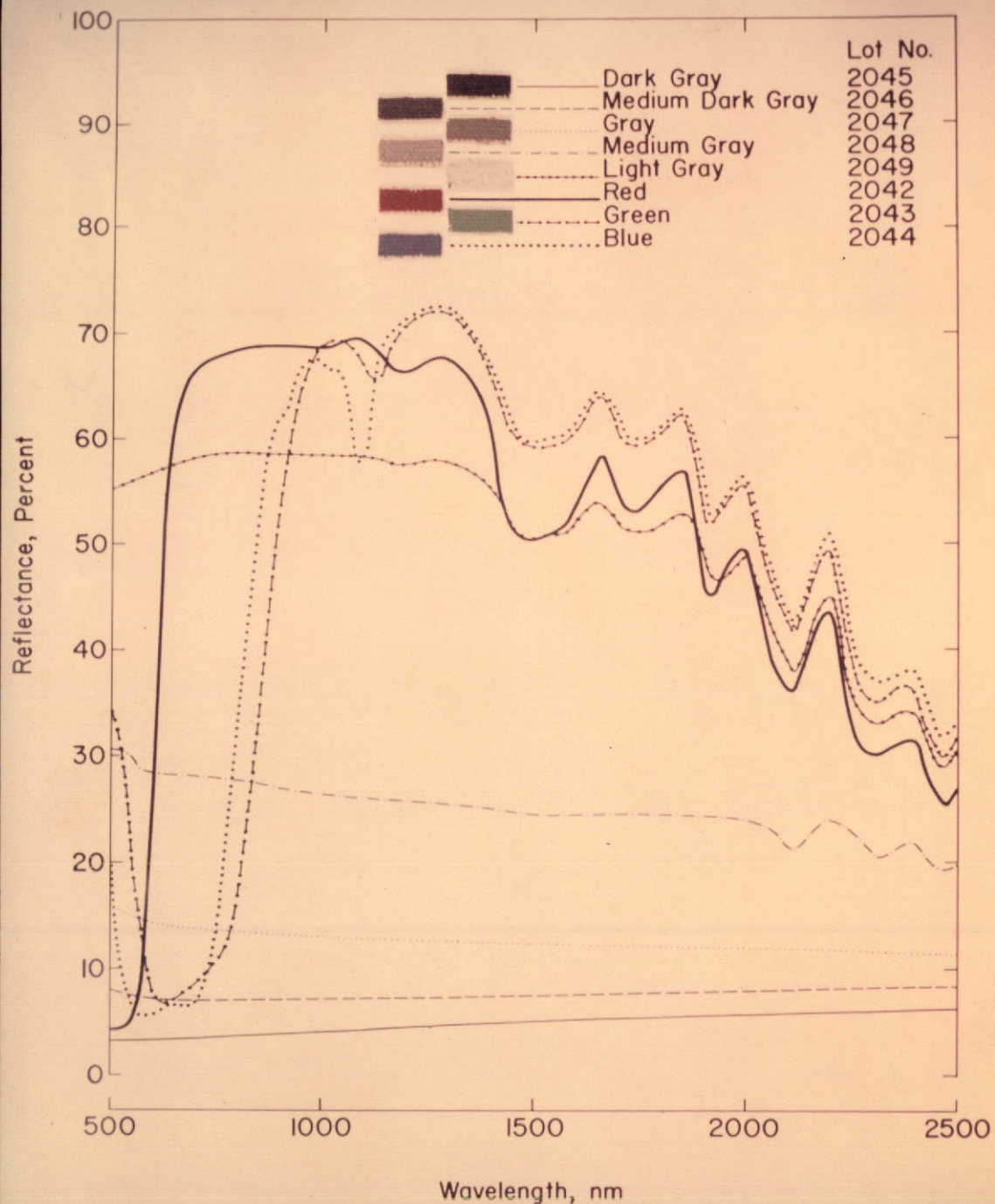
Fig. 1.--Spectrophotometrically measured reflectances over the 500- to 2500-nm wavelength interval of swatches from Univ. of Mich. color cloth standards (standard reflectance panels). Optical scanner imagery of the panels was obtained at altitudes of 500 and 2,000 ft.

MISSION 32M: SOIL SPECTRA

A. H. Gerbermann

INTRODUCTION

The general objectives of Mission 32M are presented under "Mission 32M: Preliminary Science Report." This paper compares the multispectral signatures of 3 uncropped soils from a segment of one flight line.

MATERIALS AND METHODS

The mission was conducted February 27, using the University of Michigan's C-47 aircraft. A 12-channel optical mechanical scanner responsive to electro-magnetic radiation over the 400- to 920-nm wavelength interval (WLI), and a 3-channel near-infrared scanner responsive to 1000 to 1400, 1500 to 1800, and 2000 to 2600 nm WLI were used.

Ground observations taken for this mission consisted of the percentage and type of soil cover, and the identification of all soils on selected segments of the flight line. Modal sites for the different soil types were also identified in each flight line area. These modal soil sites were outlined on a black and white photograph of the flight line and sent to the University of Michigan for use as training samples in an automatic classification system developed by the University. The modal site information is used to develop a training signature for each soil type.

The University of Michigan provided us with the average response (digitized analog signal) for each channel and the standard deviation among the response values for each training sample within each scanner channel.

Characteristics of the A horizon for the soils of this report are:
    Comitas--Textures range from heavy loamy fine sand to fine sand. Colors range from dark grayish brown to brown. In the dry condition, values (Munsell system) are 4 to 5, chromas 2 to 4, and hues 7.5YR to 10YR.
    Delmita--Textures range from fine sandy loam to loamy fine sandy. Colors range from reddish brown to light red or light brown in the dry condition, values (Munsell system) are 4.5 to 6, chromas 3 to 6, and hues 2.5YR to 7.5YR.

RESULTS AND DISCUSSION

The results presented in Fig. 1, 2, and 3 are those obtained from 10 channels (channels 1, 3, 5, 6, 7, 8, 9, 10, 11, 12) of the 12-channel optical mechanical scanner and the 3 channels of the near-infrared scanner. For this report, the channels of the 12-channel scanner are referred to as channels 1 through 10; and the channels of the near-infrared scanner are referred to as channels 11, 12, and 13. The response values shown represent each channel from 2, 3, or 4 training

samples (modal soil sites). The length of the horizontal bars corresponds to the WLI of the particular channel represented, and the vertical width of the bar corresponds to the standard deviation among the sample elements within a particular channel.

Figure 1 presents the response (the digitized analog signal is shown on the ordinate) for a Delmita loamy fine sand (l. f. s.) for various WLI. The standard deviations were largest for channels 5, 6, 7, 10, and 12 compared with the other channels.

Figure 2 depicts the analog signal of a Delmita fine sandy loam (f. s. l.) [1] for various WLI. The soil in Fig. 2 is from the same series as Fig. 1, but it is from a different soil type. [2] Again, channels 5, 6, 7, and 10 have large standard deviations compared with the other channels.

A comparison of Fig. 1 (Delmita l. f. s.) and 2 (Delmita f. s. l.) shows that the average analog signals for all channels in Fig. 2 are substantially lower than those in Fig. 1. The range of the data in Fig. 2 is also lower than the data of Fig. 1. In Fig. 1 the average analog signal for channel 1 (400 to 440 nm) is lower than for channel 2 (430 to 470 nm), but in Fig. 2 the average analog signal is lower for channel 2 than channel 1.

The analog signals at different WLI for a Comitas loamy fine sand (l. f. s.) soil are shown in Fig. 3. Channels 5, 6, 7, and 10 again show a large standard deviation compared with the other channels.

When Fig. 2 (Delmita f. s. l.) and 3 (Comitas l. f. s.) are compared, it will be noted that their response levels for all channels are very similar. They differ only in that the response levels in channels 1, 2, 3, and 4 are higher for the Comitas l. f. s. (Fig. 3) than for the Delmita f. s. l. (Fig. 2).

On comparing Comitas l. f. s. (Fig. 3) with Delmita l. f. s. (Fig. 1) it will be observed that Comitas l. f. s. has a lower average level of response than the Delmita f. s. l., and that channels 1 and 2 have a higher average response level in Fig. 3 than in Fig. 1.

When Fig. 1, 2, and 3 are compared, it is evident that there is more difference between soils within the same series (Delmita l. f. s. vs. Delmita f. s. l.) than there is between soils of different series (Delmita soils vs. Comitas soils). Apparently, soil types within a series can differ more spectrally than soils of different series. This has been also reported by Kristof et al. (1971).

---

[1] Soil Series--a group of soils alike in all differentiating characteristics except the texture of the A horizon.

[2] Soil Type--soils alike in characteristics including the texture of the A horizon.

SUMMARY

Average digitized analog signals were compared over various WLI for two soils within a series (Delmita loamy fine sand and Delmita fine sandy loam) and a soil of another soil series (Comitas loamy fine sand). Two soil types within the Delmita series appear to differ more spectrally than the soils of two different series (Delmita vs. Comitas). Results indicate that the Delmita soils could be mapped successfully by automatic means with the average digitized analog signal for several WLI. There is a possibility that the Delmita soil can be distinguished from the Comitas soil with average digitized analog signals of channels 1 (400 to 430 nm), 2 (440 to 470 nm), 3 (430 to 510 nm) and 4 (490 to 530 nm).

A preliminary mapping of soils considered here and companion soils along two flight line segments has been done by the University of Michigan. For this purpose, the optimum channels of the short wavelength scanner, in the order of lowest misclassification probability were channels 9, 6, 4, 1, 7, and 10. Work will be continued on the spectra of the modal training sites and on computerized mapping.

LITERATURE CITED

Kristof, S. J. and A. L. Zachary. 1971. Mapping soil types from multispectral scanner data. Proc. of the Seventh International Symposium on Remote Sensing of the Environment. Vol. III, p. 2095-2099.
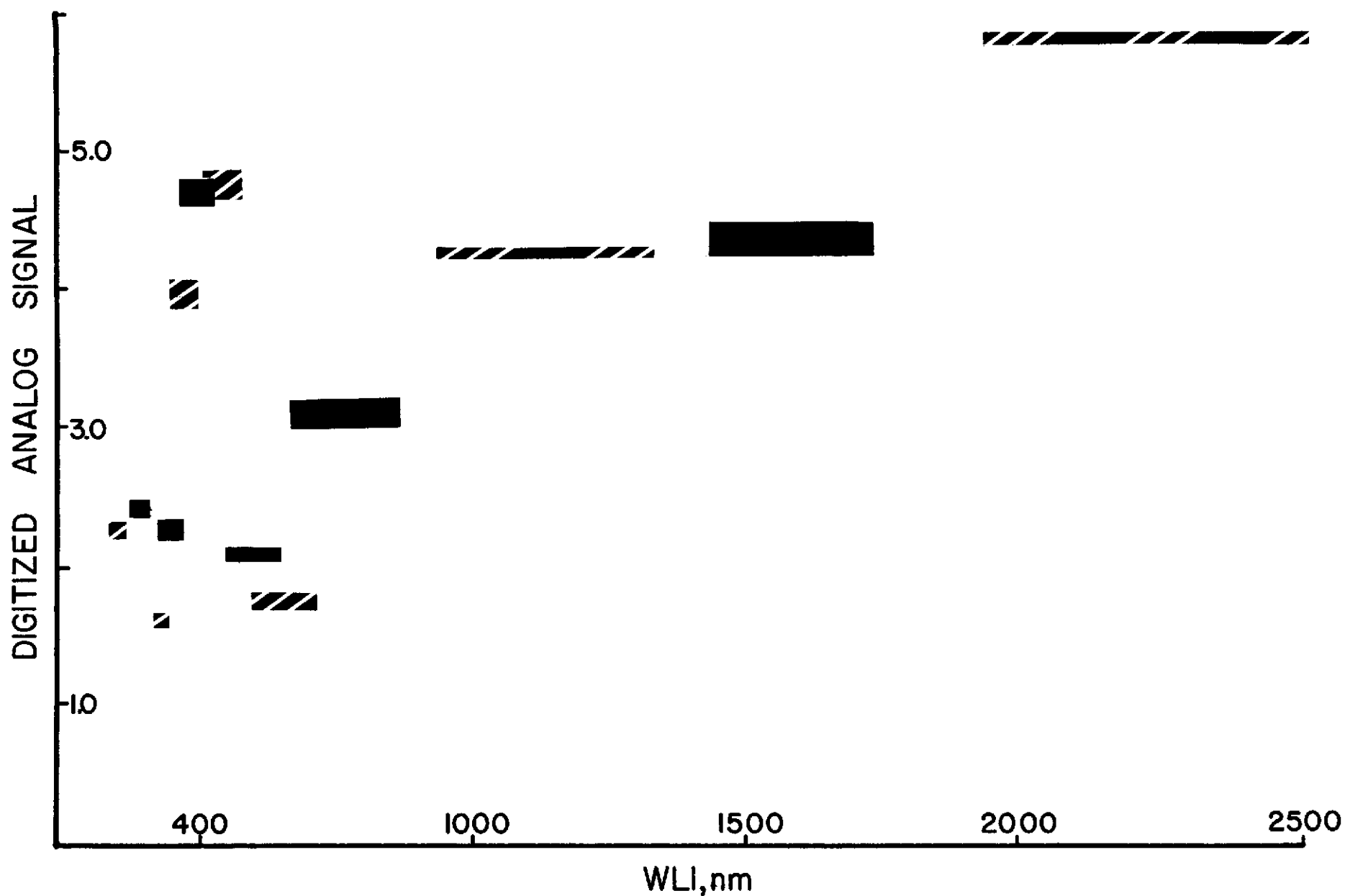
Fig. 1.--The average digitized analog signals for Delmita loamy fine sand soil at various WLI (scanner channels). The length of the horizontal bars indicates the WLI of the various channels and the width displays the standard deviation among resolution elements within a particular channel.
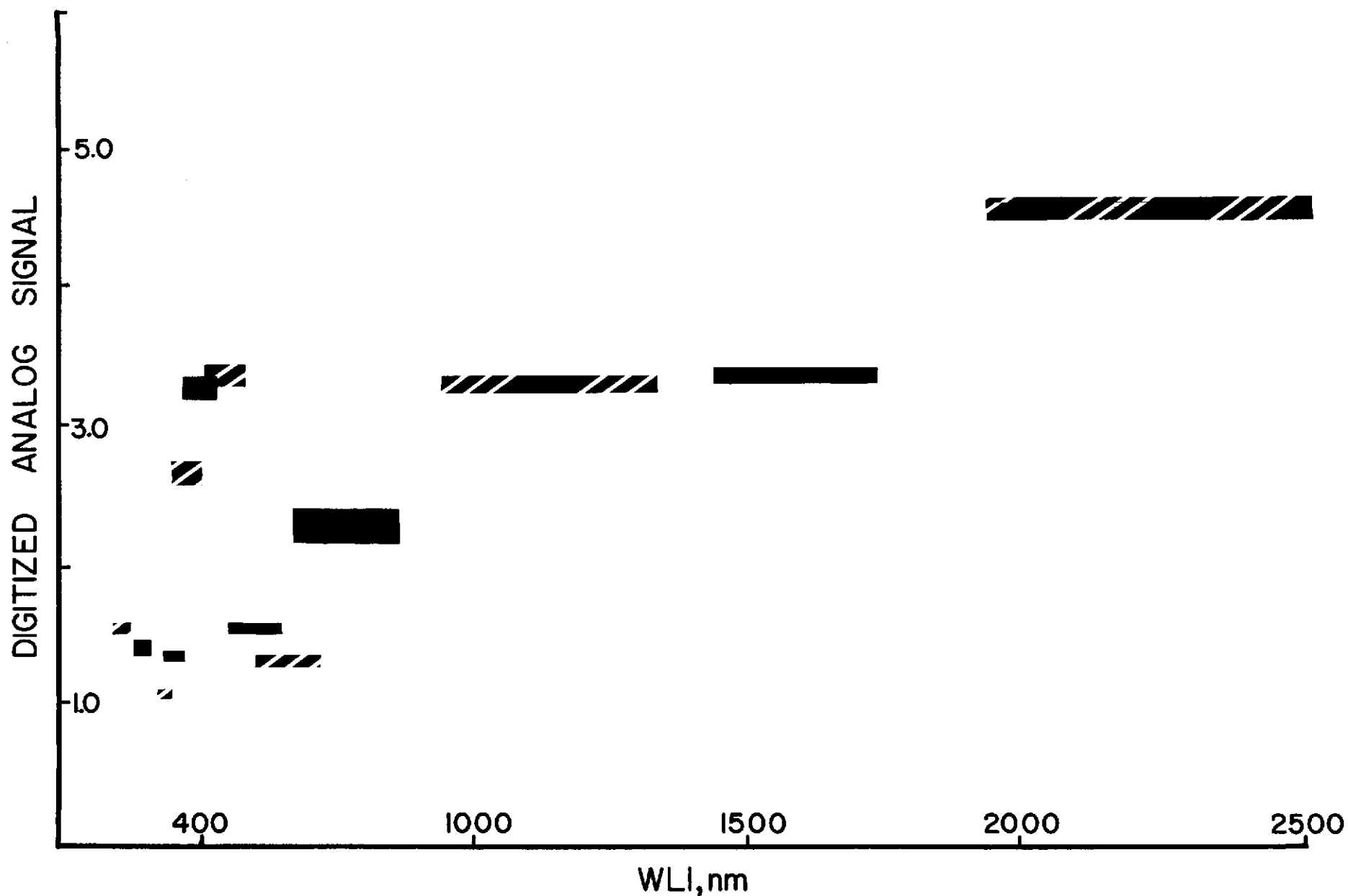
Fig. 2.--The average digitized analog signals for the Delmita fine sandy loam soil at various WLI (scanner channels). The length of the horizontal bars indicates the WLI of various channels and the width displays the standard deviation among resolution elements within a particular channel.
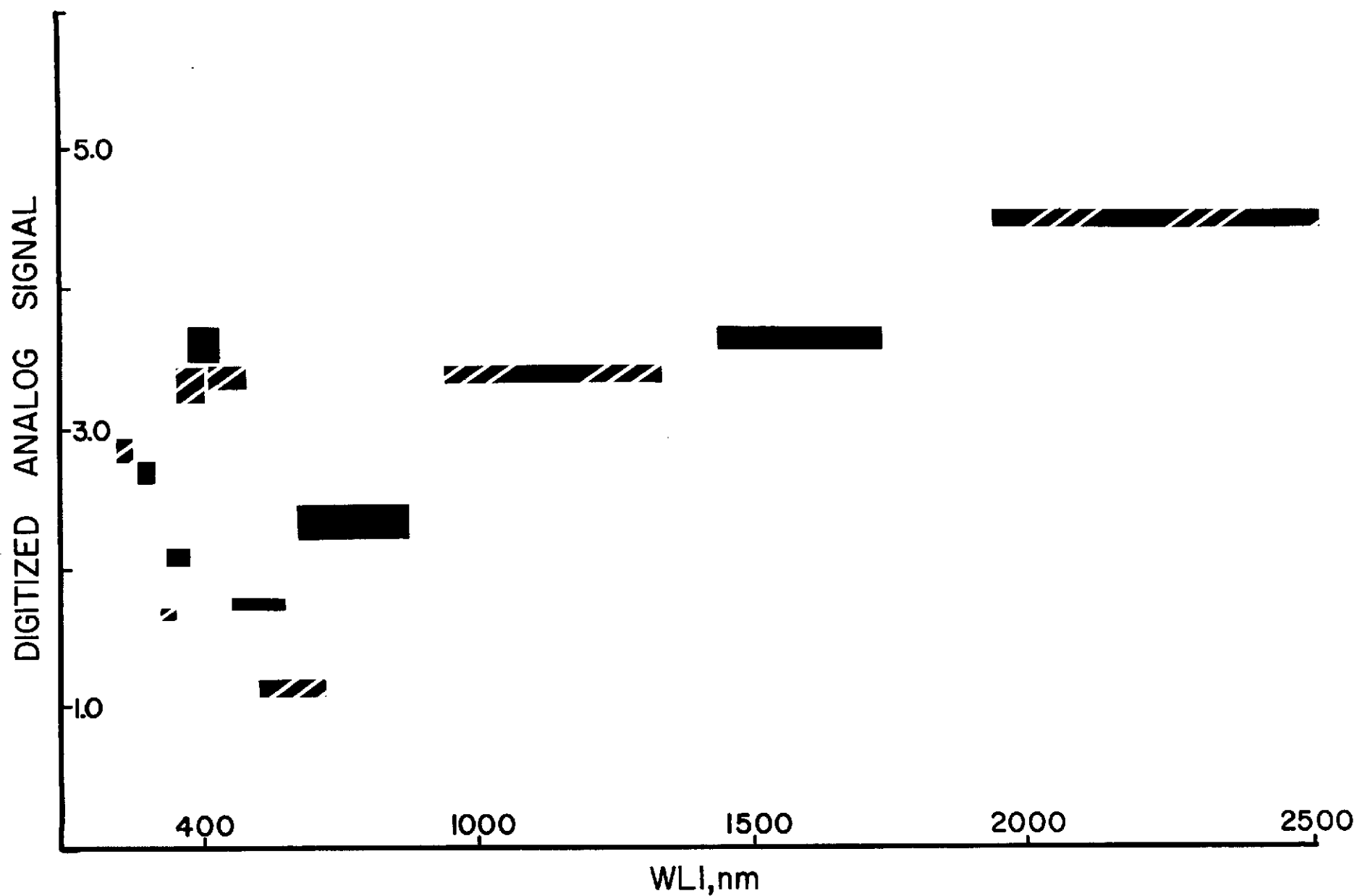
Fig. 3.—The average digitized analog signals for the Comitas loamy fine sand soil at various WLI (scanner channels). The length of the horizontal bars indicates the WLI of the various channels and the width displays the standard deviation among resolution elements within a particular channel.

THE USE OF KODAK AEROCHROME INFRARED COLOR FILM,

TYPE 2443, AS A REMOTE SENSING TOOL

G. R. Cooper, R. L. Bowen, and H. W. Gausman

INTRODUCTION

The use of black and white infrared light sensitive film in "remote sensing" of natural resources is a relatively recent development. It was followed closely with the use of Eastman Kodak's false color infrared film for camouflage detection (Applied Infrared Photography, 1968; Fritz, 1967). The film is well known as Kodak Ektachrome Infrared Aero, type 8443. It was made available to interested researchers "over the counter." A new infrared color film, Kodak Aerochrome, type 2443, has replaced the 8443 film (Data Release, 1971; Earth Observations Division Technical Bulletin, 1970), providing a new horizon and challenge for remote sensing applications with aerial photography. The 2443 had lower contrast than the 8443 film (Data Release, 1971; Earth Observations Division Technical Bulletin, 1970), and allowed the researcher to "probe" deeper into areas that would have appeared as solid black shadows on the 8443 film. The cyan (infrared sensitive) layer of 2443 is approximately 1 1/2 stops slower, at a density of 1.4, than the yellow and magenta emulsion layers.

MATERIALS AND METHODS

Test procedures applied to the 35 mm Ektachrome infrared color film and compared with results for the 70 mm infrared color film indicated that Eastman Kodak may be marketing two different films. When each was processed to a negative, the 35 mm film produced a blue base color; whereas the 70 mm film base color ranged from essentially neutral to a slight magenta cast. The data reported here are on the 70 mm film unless otherwise indicated.

Comparison of 8443 and 2443 Films

Because infrared color prints are needed for publication and as a tool for field crews doing "ground truth" work, the development of the new type 2443 Aerochrome Infrared Film to a negative was investigated (Pease, 1969-1970). A panel of research workers was asked to select "the print" they would prefer to use from both positive and negative transparencies of the 8443 and 2443 films. Eighty-six percent of the panel indicated a preference for "the print" made from the negative processing of the 2443 film. A reproduction of the test given the panel is portrayed in Fig. 1.

A general comparison of the old 8443 with the new 2443 infrared color film indicated that the 2443 film had a lower contrast and some loss of the vivid coloration that characterized the 8443 film. However, the 2443 film was superior in yielding details among shadows of plant canopies whether processed to a positive or negative. The negative processing, in particular, reveals much more detail in plant canopies than does the old 8443. This is apparent in the examples portrayed in Fig. 1.

Quality Control and Analysis of Variance of Density Readings of Sensitometric Strips Exposed on an EG and G Mark VI Sensitometer

The quality control of taking and processing photographs was investigated. An EG and G Mark VI sensitometer was used for exposing the film. A Joyce, Loebl microdensitometer was used to obtain optical density readings of the step wedges printed on the 2443 film. Readings were logged on paper tape for IBM-1800 computer input and subsequent statistical analyses. The negative processing of 70 mm film allowed 21 steps of the step wedge to be accurately measured for all three colors; whereas the positive transparency processing would yield only 19 steps for all colors.

The analysis of variance shown in Table 1 was conducted on transformed densitometric data (log base 10). Considering main effects, wedges, steps, and filters had highly significant variance (p = 0.01). Significant differences among steps and filters were expected, but differences among wedges seem undesirable until consideration is given to their means and the interaction of wedges with steps. The density means for wedges 1, 2, and 3 were 27.2, 27.7, and 27.0, respectively. The interaction of wedges with steps was not statistically significant indicating that results were repeatable regardless of the steps or wedges used.

The statistical significance (p = 0.01) of the interaction of wedges with filters was mainly caused by the response of wedge 3 with white light. Readings that were lower with this combination are believed to be in error. The statistical significance (p = 0.01) of the interaction of filters with steps was expected.

Results, therefore, indicate that repeatable densitometric readings can be obtained on sensitometric strips exposed on an EG and G Mark VI sensitometer.

Processing of Kodak Aerochrome, Type 2443, 70 mm Film to a Negative

This processing requires essentially no modification of the normal C-22 processing to a positive. The film is exposed as it would be for a positive with no apparent gain or loss of film speed. Two modifications are: (a) the developer pH is adjusted to pH of 10.6, and (b) developer time is reduced from 14 to 12 minutes. The result is a clean, unmasked, color negative that is easy to print.

The film base responds to aging at room temperature to produce a magenta tint that becomes more intense with increased storage time at room temperature. Frozen film taken from a freezer, thawed at room temperature, loaded, exposed, and developed immediately shows an almost neutral base coloration with only a 0.10 density. Successive development of individual sensitometric strips, developed individually in a Nikor tank and reel, showed the procedure to be reliably reproducible if temperature, timing, and pH were carefully controlled. Individual printing equipment varies too much to allow recommendations for initial filter packs, but a white light print (no filtration, halogen lamp) will give results that allow an easy assessment of the need for further filtration.

Processing Kodak Aerochrome Infrared, Type 2443, 70 mm Film to a Positive in Kodak Ektachrome E-4 Chemistry

This was done according to Eastman Kodak recommendations. However, pH of the solutions made up from the 1 gallon and 3 1/2 gallon size packages varied rather widely among lots. Accordingly, the solutions were adjusted to uniform pH values obtained from the photographic section of NASA at Houston, Texas. The effects of these variations are still being investigated, and no specific recommendations will be made at this time.

Other Aspects of Processing Kodak Aerochrome, 2443

The effect of agitation on the E-4 process as applied to 2443 film appears to be more critical than with SO-397 normal color film in the same process and should therefore be carefully standardized and watched for signs of improper agitation.

Research on the storage of 2443 film indicates that film storage conditions are more critical for 2443 than they were for 8443 film. Thus, it is necessary to keep the 2443 film refrigerated or actually frozen for all storage time other than loading, exposing, and processing.

LITERATURE CITED

Applied Infrared Photography. 1968. Kodak Publication No. M-28. Eastman Kodak Company, Rochester, New York. 96 p..

Data Release. 1971. Eastman Kodak Company, Rochester, New York. 5 p.

Earth Observations Division Technical Bulletin. 1970. TF6/TB1, NASA, Manned Spacecraft Center, Houston. 2 p., 4 Fig.

Fritz, N. L. 1967. Optimum methods for using infrared-sensitive color films. Photogram. Eng. 33:1128-1138.

Pease, R. W. 1969-1970. Color infrared film as negative material. Remote Sens. Environ. 1:195-198.

Table 1. Summary table for the analysis of variance for transformed (log base 10) density readings of sensitometric strips exposed on an EG and G Mark VI sensitometer.

Source of variation	DF	MS
Among runs (R)	1	0.0062
Among wedges (W)	2	0.01140**
Steps among wedges (S)	18	3.42589**
Among filters (F)	3	2.27717**
W x F	6	0.00090**
W x S	36	0.00032
F x S	54	0.06694**
W x F x S	108	0.00025
Error 1/	227	0.00025

** Denotes statistical significance, p = 0.01

1/ Interactions comprising error.

Source of variation	DF	MS
W x R	2	0.00005
F x R	3	0.00086
W x F x R	6	0.00144
S x R	18	0.00014
W x S x R	36	0.00024
F x S x R	54	0.00035
W x F x S x R	108	0.00014

Figure 1. Representative prints obtained by processing Kodak Ektachrome Infrared Aero, Type 8443, and Kodak Aerochrome, Type 2443, films to both positives and negatives. Print A is from a positive transparency of 8443, print B is from a negative transparency of 8443, print C is from a positive transparency of 2443, and print D is from a negative transparency of 2443 film.

COMPARISON OF INFRARED COLOR 2443 AND 8443 FILMS

FOR DISCRIMINATING AMONG FIVE CITRUS TREE CLASSIFICATIONS

R. Cardenas, A. J. Richardson, and H. W. Gausman

This research was produced under Research Outline
74, "Photographic Sensing of Boron and Chloride
Toxicities and Iron Deficiency of Citrus Trees."

INTRODUCTION

Citrus tree foliage affected by too much boron (B) and chloride (Cl^-) pro-
duced light-red images on Kodak Ektachrome Infrared Aero 8443 (EIR) transpar-
encies compared with dark-red images for healthy trees (Cardenas et al., 1970).

This paper compares photographic results of the discontinued EIR film with
its replacement, Kodak Aerochrome Infrared 2443 (AIR), for discriminating among
5 classifications of citrus: healthy orange, healthy grapefruit, B- and Cl^- -
affected (excess) grapefruit, foot-rot affected orange, and iron (Fe)-deficient
grapefruit trees. The Elliptical Boundary Criterion (EBC) pattern recognition
technique was used (Richardson et al., 1970).

MATERIALS AND METHODS

The EIR and AIR photographs, 70 mm film, were taken using two Hasselblad
camera bodies each equipped with a 50 mm lens. A Tiffen orange filter was used
over the lens of each camera. An exposure of 1/250 at f/10 was used. The cameras
were mounted over a port in the bottom of the aircraft's fuselage to take photo-
graphs directly over the test areas. Photographs of two areas were taken be-
tween 1045 and 1120 hr CST at an altitude of 2,000 ft.

One area consisted of healthy orange, healthy grapefruit, B- and Cl^- affected
grapefruit, and foot-rot affected orange trees. The other area consisted of Fe-
deficient grapefruit trees. Both areas were photographed at approximately the
same time.

Four trees of each of the 5 citrus tree classifications were selected from
EIR and AIR transparencies for optical density measurements with a Joyce, Loebl
automatic recording microdensitometer using tungsten light ("white filter"),
and red (Wratten 92), green (Wratten 93), and blue (Wratten 94) bandpass filters.
One scan line was obtained at the center of each tree, and 15 density readings
of the microdensitometer were recorded automatically for each filter on punched
paper tape with a Datex automatic data recording instrument.

The Datex automatic data recording instrumentation has an encoder that divides the range of the microdensitometer into 156 equal segments. The densities recorded on the punched paper tape are "optical counts" that range between 0 and 156. The microdensitometer is adjusted so that film density of each ground pattern area falls within this range of "optical counts" by adjusting to one of several steps of a calibrated gray density scale. Optical densities can be calculated by comparing the "optical counts" of the ground pattern area to the "optical counts" of the appropriate step of the calibrated gray scale. In this paper, "optical counts" were used; they were not converted to optical densities.

RESULTS AND DISCUSSION

The EBC pattern recognition method (Richardson et al., 1970) gave better total discrimination with EIR compared with AIR transparencies among healthy orange, healthy grapefruit, B- and Cl⁻-affected grapefruit, orange foot-rot affected and Fe deficient grapefruit trees. The EIR film gave an average of 65% recognition compared with 55.7% for AIR film, Table 1. The third column in Table 1 shows the percent correct recognition (R) and the remaining columns show the number of readings correctly recognized for each classification or not recognized. For example, EIR film had 50 readings recognized correctly as B- and Cl⁻- and 10 incorrect readings: 6 as foot-rot, 3 as grapefruit, and 1 as orange. Correct recognitions were highest (83.3%) for B and Cl⁻ and lowest (46.7%) for Fe compared with the remaining 3 categories--foot rot, grapefruit, and orange. Grapefruit and orange had 60.0 and 53.3% correct recognition, respectively. Fourteen grapefruit readings were called orange and 12 orange readings were called grapefruit.

With AIR film, B and Cl⁻ had the lowest recognition (30.0%), grapefruit had the second lowest recognition (38.3%), and orange had the highest recognition (83.3%).

When only 3 categories (B and Cl⁻, foot-rot, and grapefruit) were tested (data not shown) for pattern recognition, best discrimination was obtained with AIR (76.1%) compared with EIR (72.8%) film. When only 2 categories (B and Cl⁻, and Fe) were tested (data not shown), best discrimination was obtained with AIR (94.2%) compared with EIR (76.7%) film.

The primary difference in the sensitometry between EIR and AIR film is that AIR has lower minimum densities and the sensitometric curve bends to form the toe of the curve more quickly (Fritz, 1971). This characteristic has little effect on appearance of the photography, but it decreases the exposure latitude of AIR film thereby making the exposure selection more critical.

SUMMARY

A pattern recognition technique (EBC - Elliptical Boundary Criterion) was used in an attempt to discriminate among 5 citrus tree classifications: B- and Cl⁻-affected (excess) grapefruit, foot-rot affected orange, healthy grapefruit, Fe-deficient grapefruit and healthy orange trees. For the 5 classifications, EIR compared with AIR film gave the best results. Average recognitions were 65.0 and 55.7% for EIR and AIR films, respectively. Within the EIR results, B- and Cl⁻-affected grapefruit and foot-rot affected orange trees were easiest to identify (81.7 and 83.3% correct identifications, respectively).

When fewer than 5 categories were used, best discrimination was obtained with AIR compared with EIR film. Correct recognition was 76.1% for discriminating among B- and Cl$^-$-affected grapefruit, foot-rot affected orange, and grapefruit, and 94.2% for identifying B- and Cl$^-$-affected grapefruit from Fe-deficient grapefruit trees.

LITERATURE CITED

Cardenas, R., H. W. Gausman, A. Peynado. 1971. Detection of boron and chloride toxicities by aerial photography, Third Biennial Workshop on Aerial Color Photography in the Plant Sciences. Gainesville, Florida. p. 267-288.

Fritz, N. L. 1971. New color films for aerial photography, Third Biennial Workshop on Aerial Color Photography in the Plant Sciences. Gainesville, Florida. p. 44-68.

Richardson, A. J., R. T. Torline, D. A. Weber, R. W. Leamer, and C. L. Wiegand. 1970. Computer discrimination procedure comparisons using film optical densities. Weslaco SWC Research Report 422 (Multilithed locally) 85 p.

Table 1. Comparison of AIR (lower table) and EIR (upper table) photography for discriminating among 5 classifications of citrus. The EBC pattern recognition (R) technique was used on densitometer measurements ("optical counts") made on the film transparencies. Data are the total of 4 filters ("white", red, blue, green), 15 readings for each filter.

| Classifi-cation | Total readings | Correct R | R in each classification | | | | | No R |
			B & Cl⁻	Foot-rot	Grape-fruit	Fe	Orange	
	No.	%	No.	No.	No.	No.	No.	No.
EIR FILM								
B & Cl⁻	60	83.3	50	6	3	0	1	0
Foot-rot	60	81.7	9	49	0	0	1	1
Grapefruit	60	60.0	5	4	36	0	14	1
Fe	60	46.7	25	5	2	28	0	0
Orange	60	53.3	2	7	12	7	32	0
Mean		65.0						
AIR FILM								
B & Cl⁻	60	30.0	18	13	6	0	23	0
Foot-rot	60	63.3	2	38	2	9	9	0
Grapefruit	60	38.3	3	5	23	2	27	0
Fe	60	63.3	1	13	0	38	8	0
Orange	60	83.3	0	1	5	3	50	1
Mean		55.7						

HINTS ON THE CARE, EXPOSURE, AND

PROCESSING OF KODAK EKTACHROME FILM AND PAPER

R. L. Bowen and D. L. Nelson

This note summarizes the recommendations of the photographic laboratory staff at Weslaco on the care, exposure, and processing of Ektachrome film and paper.

A. Care of film and paper.

1. Care of Ektachrome film and Ektachrome paper is a very important part of a quality photograph. The film and paper must be stored either at a temperature lower than 40F, or in a frozen condition until time of use. The film and paper should be allowed at least five hours to come to room temperature before it is used.

2. Ektachrome film and Ektachrome paper must be loaded in cameras and easels, respectively, in total darkness. Any light will fog the film or paper.

B. Exposure of film and paper.

1. The two types of Ektachrome film considered here are: Ektachrome EF Aerographic, SO-397; and Aerochrome Infrared 2443.

a. The Ektachrome EF Aerographic film SO-397 is high speed (aerial index of 12). We have had good results taking photographs on the ground with camera settings determined with the light meter set for an ASA speed of 120. On a very bright day, f 11 at 1/250 sec has given very good results without a filter.

b. The Aerochrome Infrared film 2443 is high speed aerial film (aerial index of 10), and it has an ASA speed of approximately 100 for ground photography. On bright days with a Tiffen orange filter, we get good results using f 13 at 1/125 sec.

2. Ektachrome paper must be exposed in total darkness. Over-exposed Ektachrome paper will turn white, not black. Under-exposed paper will turn black. Black borders are normal. To expose your first Ektachrome print use no filter and print with white light. Guess at the time and the f stop. Not knowing what kind of equipment you have, the authors recommend a short time of about 0.5 sec and an f stop of 8 to start. If the print is black, or dark, you need more time or more light. If the print is white, or light, you need less time or less light. When exposure (density) is right, add a

color filter to make a color-balanced print. You will find
you can make a sharp, color-balanced print of high quality
in this manner. A few words of caution: never place color
filters between the positive transparency and the paper!
Always place the filters between the light source and the
transparency so you will have no light diffusion, and thus
your enlargement and contact print will be "razor sharp".
Also, you should always add the color you need to balance
the print. For instance, if you need red color, add a red
filter; if you need green color, add a green filter.

C. Processing of film and paper.

1. Ektachrome EF Aerographic SO-397 or Aerochrome Infrared 2443
    can be processed in the same chemicals at the same time.
    Follow the Kodak E-4 process step by step. Make no changes
    in recommended chemical solutions or in temperature and times
    of immersion in the chemical solutions and water baths.

    Since there is a difference in whether processing is done
    with spiral reels or rewind systems, we will give you the
    time and temperature recommendation for processing E-4. The
    temperature should be kept at 85F. Time in E-4 chemicals
    given below is very critical.

    Time in solutions for spiral reels are: Prehardener for
    3 minutes. Neutralizer for 1 minute. First developer for
    7 minutes. First stop for 2 minutes. These steps must be
    done in total darkness. Remaining steps can be done in
    normal room light. Wash for 4 minutes. Color developer for
    15 minutes. Second stop for 3 minutes. Wash for 3 minutes.
    Bleach for 5 minutes. Fixer for 4 minutes. Wash for 6
    minutes. Stabilizer for 1 minute. Dry below 110F.

2. The E-4 processing sequence for a rewind system at 85F has
    some changes in chemicals and times. The E-4 Neutralizer
    is replaced with Kodak Neutralizer MX 875 and Kodak Neutral-
    izer Additive MX 870. The time for each step is given below:

    Prehardener for 5 minutes. Neutralizer for 1 minute. First
    developer for 9 minutes. First stop for 2 minutes. These
    steps must be done in total darkness. Remaining steps can
    be done in normal room light. Wash for 4 minutes. Color
    developer for 15 minutes. Second stop for 3 minutes. Wash
    for 3 minutes. Bleach for 10 minutes. Fixer for 10 minutes.
    Wash for 8 minutes. Stabilizer for 1 minute. Dry below
    140F.

3. Tray processing of Ektachrome RC paper is quite simple if
    the instructions are carried out as indicated on containers
    of Kodak Ektaprint R chemicals. To have a color print in
    24 1/2 minutes, carefully do the following steps: Keep the
    temperature at 85F. Do the first two steps in total darkness.
    First developer for 4 minutes. First stop for 1 minute.
    Remaining steps can be done in normal room light. First

wash for 4 minutes. Reversal exposure for 15 sec. Color
developer for 4 minutes. Hardener stop for 2 minutes.
Bleach for 2 minutes. Second wash for 1 minute. Formalin
fixer for 2 minutes. Final wash for 3 minutes. Stabilizer
for 1 minute. Rinse for 1/2 minute. In order to get a
very good gloss on the paper, all excess moisture must be
squeegeed from the print. Then let the print air dry; do
not heat, ferrotype, or drum dry it. If you have controlled
the time and temperature, you will have an excellent color
print.

BE CAREFUL NOT TO INHALE CHEMICAL FUMES OR GET THE CHEMICALS
ON YOU OR IN YOUR EYES! GOOD VENTILATION IS IMPORTANT.

The Ektachrome color and Ektachrome IR prints used in all reports and
papers at this location have been produced according to the above procedures.

CORRELATION OF GROUND COVER ESTIMATED FROM

AERIAL PHOTOS WITH GROUND OBSERVATIONS

J. A. Cuellar

INTRODUCTION

Field survey teams have been used for collecting ground observation data for remote sensing programs. This is ideal for studies dealing with small acreages. However, in the future when aerial assessments have to be made of farm crops on national and global scales, the use of ground data gathering crews will become impractical and obsolete. Therefore, the method of acquiring ground data information must be rapid but still reliable. The plant canopy (geometry, maturation, and pigment content) has an important influence on electromagnetic radiation reflectance and emittance patterns of crops and their yield. Thus, a study was conducted to obtain correlations of percent crop cover obtained from ground observations with percent crop cover estimated from aerial photographs.

MATERIALS AND METHODS

Local aerial flights were made once a month over 6 flight lines, a total of approximately 40 miles, during April, May, June, and July, 1969 in connection with Bendix scanner studies (see Chapter III). The 6 flight lines were photographed with a Zeiss camera containing Kodak Ektachrome Infrared Aero 8443 film, 9 1/2-in format. The flights were:

| | Date and altitude | | | |
Flight line	April 13	May 13	June 6	July 9
1	2100 ft.	1600 ft.	2000 ft.	4000 ft.
3	2100	1600	2500	4000
10	2100	2100	----	4000
11	2100	1600	2500	4000
12	2100	1600	2500	4000
13	2100	----	3500	4000

Ground observations were made on fields adjacent to paved roads as close as possible to the flight dates. The ground observation data consisted of: kind of plant, percent crop cover, percent weed cover, plant height, stage of maturity, row spacing, row orientation, type of tillage, soil moisture condition (wet or dry), and such parameters as nutrient deficiencies and diseases that might affect the response of airborne sensors.

Corn, cotton, cantaloupe, citrus, forage, onion, and grain sorghum crops were available during the four month study period.

Ground Observations

In determining the percent of the soil surface covered by the vegetal canopy from ground observations, two categories were used:

1. Solid canopy (bare soil exposed only on furrows). The "bare soil width" and the "row width" were measured. The bare soil width is the amount of bare soil showing between the canopies of two adjacent rows. The row width is the distance from the center of a bed to the center of an adjacent bed, normally 100 cm (39.4 in).

    The percent crop cover was calculated as:

    $$\left(\frac{RW - BW}{RW} \right) 100 = \% \text{ cover}$$

    RW = row width, cm
    BW = bare soil width, cm

2. Open canopy (bare soil exposed through canopy and furrow). The open canopy was considered as being "solid", and the formula above was used to determine the percent cover. A subjective estimate was made of the open spaces in the leaf canopy, and this amount was subtracted from the assumed cover to obtain the actual cover.

A representative area was selected from within a field to make the measurements. In fields with nonuniform cover, a few areas were sampled to obtain field representation. The sample areas were normally 225 square feet in size, but they varied in size for small fields.

Film Observations

The same general areas used for ground observations were used on the transparencies to make the measurements for estimating percent crop cover. Measurements were made by means of a Bausch and Lomb micrometer with the aid of a Bausch and Lomb zoom 70 stereoscope mounted on a Richards' light table with .7 to 3.0 magnifications. Using the measurements obtained, the percent cover was then determined by the "solid canopy" method. All film estimates used in the correlation analyses were made by a single observer; however, some fields were selected at random and observed by another individual. The comparison of both observers' estimates was excellent. The fields that varied had a deviation among estimated covers of only ± 3%. Both observers made the film estimates independently without any reference to the ground observation data.

RESULTS AND DISCUSSION

Since the aerial flights covered mostly the cotton and grain sorghum season, greater emphasis was placed on the analyses of these two crops, but some information was also obtained for corn, citrus, cantaloupe, onion, and forage crops.

Coefficients for the correlations of ground observations with film observations were highly significant (p = 0.01) for all crops. Correlation coefficients were: cantaloupe, .957; citrus, .939, corn, .950; cotton (Fig. 2), .982; onion, .807; forage, .956; and grain sorghum (Fig. 1), .945. Regression analyses indicated that the data for all crops could be fit best to a linear line (first degree polynomial).

The number of paired observations was 167 and 182 for Fig. 1 and 2, respectively. Points that fell on top of each other are displayed only once in the figures.

It can be noticed in Fig. 1 that 9 of the plotted points show the photo estimates of ground cover to be much higher than the ground observer estimates. There is a tendency to overestimate ground cover on aerial photographs because the magenta color appears solid on the film when there are actually openings in the plant canopy. The difficulty in estimating ground cover of row crops increases as the altitude of the flights increases because of film resolution restrictions or need for higher magnification of the image to distinguish interrow bare areas from the vegetation of the crop rows. The flights of this study were made at altitudes of 1600, 2100, 2500, and 4000 ft. Use of the micrometer and the magnification of the stereoscope enabled ground cover estimates from all photographic altitudes.

For the cotton data (Fig. 2) the y intercept is 1.91. However, at the upper end the photo estimate is 94% ground cover when the ground estimate is 100%. This tendency to overestimate ground observation cover is attributed to the ground observer's difficulty to accurately estimate cover as ground cover approaches 100%. This is especially true of tall vegetation such as mature corn where the ground observer can not look down on the crop. In such cases the estimates from aerial photographs are probably more accurate than ground observations.

SUMMARY

The results indicate that photo estimates of percent cover can be used to predict reliable estimates of percent ground cover. It seems feasible, therefore, that photo estimates of ground cover can be used to replace the tedious and time consuming observations made by ground data survey teams. To this end, regression equations will be developed for predicting percent ground cover from photo estimates of percent cover. (Note: The regression analysis considered in this report used the photo estimates as the dependent variable. In actual practice, it may be desired to use photo estimates as the independent variable to predict ground cover).
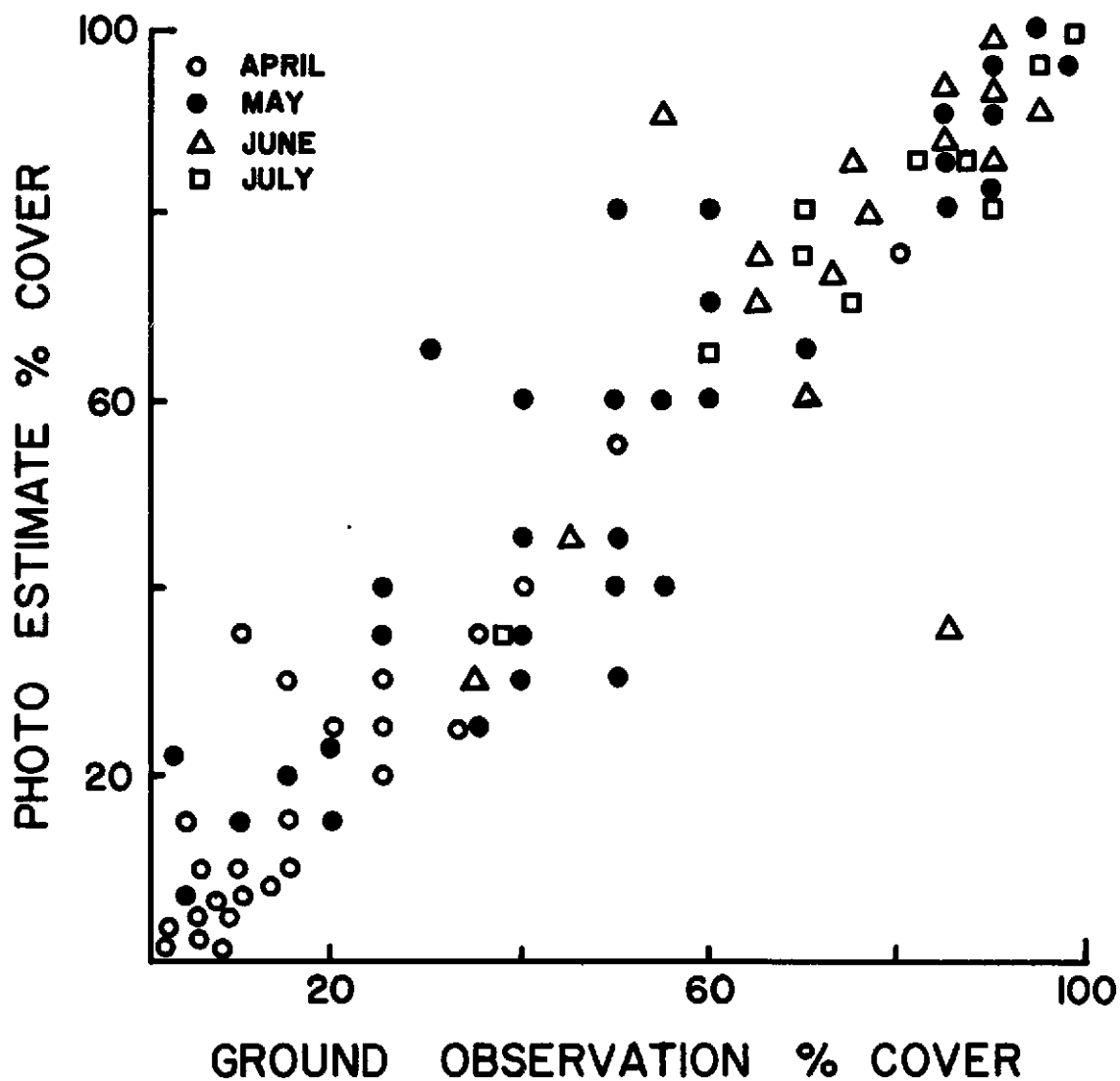
Fig. 1.--The correlation (r = .95) of percent grain sorghum crop cover from ground observations with estimates of percent crop cover from aerial photographs on four sampling dates. The number of observations was 167.
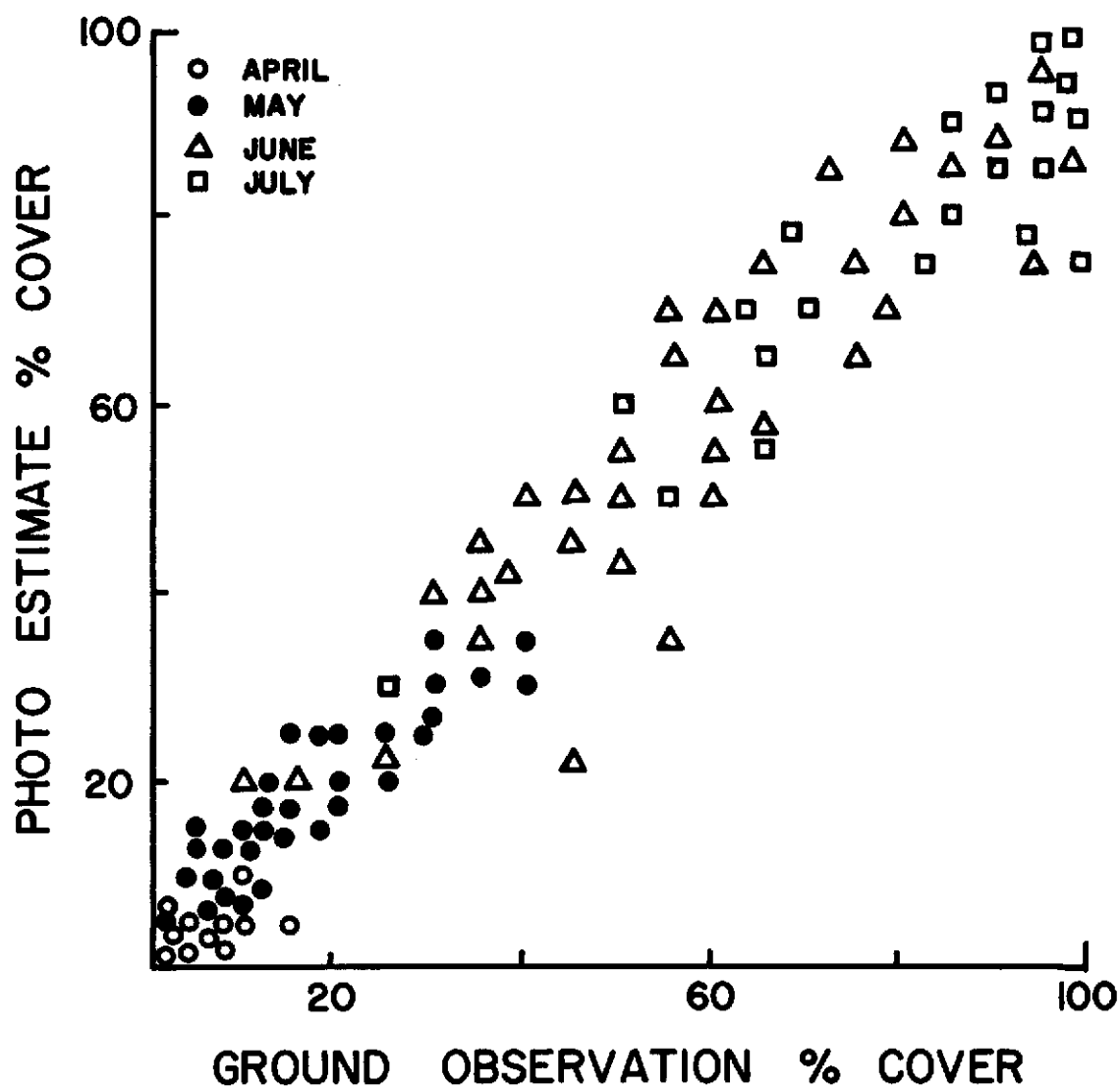
Fig. 2.--The correlation (r = .98) of percent cotton crop cover from ground observations with estimates of percent crop cover from aerial photographs for four sampling dates. The number of observations was 182.

CALIBRATION OF FIELD SPECTRORADIOMETERS

R. W. Leamer

INTRODUCTION

The Exotech Model 20 spectroradiometers measure intensity of incident and reflected radiation from .37 to 2.52 µm and emitted radiation from 2.76 to 13.88 µm. Spectral scans are made by rotating circular variable filters (CVF) through the optical path in front of detectors. The detectors produce an electrical signal that is proportional to the amount of energy passing through the CVF and falling on the detector. The rotation of the CVF allows energy of successively differing wavelengths (WLs) to fall on the detectors.

To calculate a spectrum of energy from a target, it is necessary to have two basic items of information: (1) the wavelength (WL) of the energy falling on the detector, and (2) the proportionality constant of the detector-amplifier system at that WL.

MATERIALS AND METHODS

Calibration

The USDA Rio Grande Soil and Water Research Center contracted with the Willow Run Laboratories of the Institute of Science and Technology at the University of Michigan to calibrate the spectroradiometers owned by USDA.

These spectroradiometers use four CVFs and four detectors with two of each in two separate instruments. The instruments can be operated separately or concurrently. The instrument referred to as the short WL unit contains a silica (Si) detector and a lead sulfide (PbS) detector. Wavelengths from .37 to 2.52 µm are measured by this instrument. The long WL unit contains an indium antimonide (InSb) and an HgCdTe (trimetal) detector to measure WLs from 2.76 to 13.88 µm. Each instrument produces three primary electrical signals: an analog output (amplified) from each detector, and a 1,000 step analog staircase ramp related to CVF position (WL). Other electrical signals relating to housekeeping details such as gain settings, scanning speed, blackbody temperature, etc., are also produced, but they will not be discussed.

In each unit, one CVF and the shaft angle encoder are coupled directly to the same shaft; the second CVF is driven by a sprocket belt from the reference shaft. Thus, the second CVF can be, either intentionally or unintentionally, displaced in relation to the WL ramp signal. Any displacement is easily detected by the operator, and adjustments can be made or the displacement accounted for in the data reduction procedure.

Wavelength (WL)

The Willow Run Laboratories' procedure for relating center WL passed by the CVF and the position of the filter wheel as measured by the ramp voltage was to illuminate the aperture with energy containing spectral lines at known WLs. A high pressure mercury (Hg) lamp (General Electric H100-A4) with the outer glass shell broken away to allow greater emission on either side of the visible range, was used to calibrate the short WL unit.

Figure 1 is a plot of the WL positions of the 11 lines present in the light from a Hg lamp as a function of percent of the peak ramp voltage. The curve is plotted with the short WL end of the CVF beginning at the start of the voltage ramp. The CVF in front of the Si detector passes WLs from .37 to .76 μm in one-half revolutions. The other half of the CVF wheel is blank; consequently, there is no detector signal in the second half of the voltage ramp.

Only the filter in front of the PbS detector has an active filter in the second half of the CVF wheel. The two filters in the PbS channel cover .72 to 1.32 μm and 1.27 to 2.52 μm. The center WL range transmitted by the CVF in the PbS channel is plotted in Fig. 2 as a function of the percent of the peak of the voltage ramp. The overlap of ranges of the two filters is shown as a discontinuity. At the time of the Willow Run Laboratory calibration, there was a slight discrepancy between the shortest WL of the CVF and the start of the voltage ramp. Because this discrepancy can be controlled by adjustment of the sprocket belt, the data have been plotted as if there were perfect correspondence between shortest WL and start of the voltage ramp.

In the long WL unit, the CVF in the InSb channel is the belt-driven filter. This was also found to be displaced so that the start of the ramp did not coincide with the shortest WL. The data in Fig. 3 are plotted as if the voltage ramp began with the start of the filter disk. Figure 4 is a plot of WL as a function of the percent of the peak voltage ramp for the HgCdTe channel. The beginning of the ramp signal and the beginning of the detector signal output were in agreement for this channel.

Two methods were used to produce lines of known WL in the long WL unit. The easiest method was to insert a sheet of polystyrene between the instrument aperture and a 2,000C blackbody. Polystyrene has known strong absorption bands in the infrared. Other points in the infrared were also established by irradiating the slits of a Zeiss monochromator with a calibrated WL drum.

Selected WLs from the exit slit of the Zeiss instrument were used to irradiate the aperture of the Exotech spectroradiometer. Carbon dioxide (CO_2) in the atmosphere has a strong absorption band at 4.25 μm; this point is also shown in Fig. 3.

Field of View

These spectroradiometers have two possible fields of view, 1° and 15°. The optical system was designed to give a 15° field of view (FOV) through the aperture; the 1° FOV is obtained by inserting a lens outside the aperture. The field of view of an instrument is usually determined by observing the detector signal as a small area source is moved across the field. In an instrument with a sharply defined field stop as those have, the FOV is usually sharply defined. There is often some fuzzing along the edges, but the usual response curve is flat as a point source of light is moved across the FOV. These spectroradiometers did not give the usual type of curve. Figure 5 shows the types of signal response curves from the Si detector as a point source light was moved across the FOV of the short WL instrument.

The optical system can be considered to be made up of a detector with a chopper blade in front of it. The chopper acts as a gate and alternately exposes the detector to radiation and blocks it from radiation. A sync signal is generated electronically from different positions of the chopper blade. The sync signal thus has the same period and frequency as the detector signal. With good lenses in the optical system where the full FOV illuminates the entire surface of the detector, a point source will illuminate a point on the detector. The sync signal is fixed by system parameters; however, the phase of the detector signal varies depending on where the point image falls on the detector surface.

As a function of the phase relation, ϕ, between the detector and sync signals, the expression governing the demodulated signal is

$$\cos \phi \, (\cos 2 \omega t - 1) + \sin \omega t \cdot \sin \phi$$

where $\omega = 2 \Pi f$ where f is the frequency of the chopped signal.

The periodic (ωt) terms are eliminated in the electronics so the resultant signal varies as the $\cos \phi$ which varies from zero to one, depending on the value of ϕ. The phase relation, ϕ, and thus the signal, is affected by the location the image falls on the detector. Moving the image across the detector surface in the direction of chopper blade movement (horizontally in this case) should result in more effect on the demodulated signal than moving the image perpendicular (vertically) to the chopper blade movement. Figures 5 b and 5 d show that this happens in this instrument.

Oscilloscope patterns of the unfiltered, demodulated signal taken at the time of calibration, showed that the dissymmetry became pronounced as a point source was moved off-center of the FOV in that the negative swings became nearly as great as the positive so that the average became nearly zero when the point source approached the edge of the FOV. By electronically adjusting the sync pulse out of phase with the signal obtained from a large area source, it was possible to obtain a negative signal from a point source near the edge of the FOV.

The 15° FOV gives a more normal type of curve as shown in Figs. 5 a and 5 c. The distortion of the peak is barely noticeable as a point source is moved across the FOV. Vignetting causes some reduction in the irradiation of the detector as the light beam passes through the edges of the transfer optics.

Spectral Radiance

To eliminate the variability caused by an uneven intensity with the FOV, the calibration of spectral response was restricted to observation of sources uniform within the FOV.

The signals from the detectors are related to the variation as the detector is exposed alternately to the target (T) and a reference blackbody (R). The signal S (volts) is proportional to the difference between the two signals, S_T and S_R. Each signal is made up of two components, that from the primary source (target or reference blackbody) and that from the surroundings.

The signals can be represented by:

$$S_T = k_T L_{\lambda T} \Delta\lambda + T$$

and

$$S_R = k_R L_{\lambda R} \Delta\lambda + R$$

where: $k_T = k_T (\lambda, \text{geom})$ is a proportionality factor relating target radiance

L_T $(= L_{\lambda R}\Delta\lambda)$ to the first component of the signal voltage, S_T;

and $k_R = k_R (\lambda, \text{geom})$ is a proportionality factor relating the reference radiance L_R $(= L_{\lambda R} \cdot \Delta\lambda)$ to the first component of the reference voltage, S_R.

T is the voltage due to extraneous radiation when the detector is exposed to the target

R is the voltage due to extraneous radiation when the detector is exposed to the reference source.

The k's are functions of wavelength and geometry. The resultant signal is thus given by:

$$S = S_T - S_R = k_T L_T + T - k_R L_R - R = k_T L_T - k_R L_R + (T - R) \tag{1}$$

The terms $k_R L_R$ and $(T - R)$ can be eliminated by exposing the spectroradiometers to two levels of radiation from a calibration source and taking the difference between the resultant signals. The equation reduces to:

$$\Delta S = S(1) - S(2) = k_T L_T (1) - k_T L_T (2)$$

where 1 and 2 correspond to the two levels of radiation from the calibration source.

Because $L_T = L_{\lambda T}\Delta\lambda$ where $L_{\lambda T}$ is the spectral radiance

$$S_1 - S_2 = \Delta S = k_T \Delta\lambda(L_{\lambda T}(1) - L_{\lambda T}(2)).$$

The ΔS is obtained from the signals from the two radiation levels of the calibration source. The values of $L_{\lambda T}$ can be read from tables (Pivovonsky and Nagel, 1961).

The spectral radiance responsivity can be calculated from:

$$R(\lambda) = k_T \Delta\lambda = \frac{\Delta S}{L_{\lambda T}(1) - L_{\lambda T}(2)} \qquad (2)$$

To determine the radiance (at λ) of an unknown target, the procedure is reversed. $R_{(\lambda)}$ is known and one blackbody level is used as a reference. Then:

$$\Delta S = SU - S_{BB} = R(\lambda)(L_{\lambda U} - L_{BB})$$

where U and BB correspond to signals and radiances from the unknown sources and the reference blackbody, respectively.

$$\text{Then} \quad L_{\lambda U} = \frac{S_U - S_{BB}}{R(\lambda)} + L_{BB} \quad . \qquad (3)$$

Thus the unknown spectral radiance is obtained from Eq. (3). The spectral dependence of R is shown as $R(\lambda)$.

This calculation is based on the use of a calibrated blackbody source as a reference. Field use of such a reference is inconvenient as a standard procedure. An alternate method more easily used in the field, Eq. (1) can be used to plot several readings from several blackbody temperatures. Figure 6 shows two curves plotted from two reference blackbody temperature settings.

All the constraints of the system can be calculated from the information in these curves. The steps are:

1. Calculate $k_T \Delta\lambda = R(\lambda)$ from the slope of either line.

2. Calculate $k_R \Delta\lambda$ from

$$S' \text{ (from graph)} = k_R(L_R(1) - L_R(2))$$

$$= k_R \Delta\lambda(L_{R\lambda}(1) - L_{R\lambda}(2))$$

where 1 and 2 correspond to the two settings of the internal reference blackbody.

3. Calculate (T-R) = K from

$$S'' \text{ (from graph)} = -k_R \Delta\lambda L_{R\lambda}(1) + (T-R)$$

so that

$$(T-R) = K = k_R \Delta\lambda L_{R\lambda}(1) - |S''|$$

4. If K is a constant, any unknown $L_{\lambda T}$ can be calculated from:

$$L_{\lambda T} = \frac{1}{R(\lambda)} [S-K + (k_R\Delta\lambda)L_{\lambda R}] \tag{4}$$

In these instruments k is not always a constant so Eq. (4) cannot be used with assurance of good results unless a check is made on each run. Most of the variation in k occurs in the long WL instrument. A satisfactory check can be made for each run by using the internal reference blackbody to run consistency checks on the instrument. These checks consist of clamping a surface painted with 3M black paint in front of the aperture and recording the signals and the reference temperature as the temperature of the reference blackbody is changed. Knowing the temperature of the 3M black surface, a curve can be plotted for any set of measurements. The slope of the line will be the reverse of Fig. 6. Assuming that k_T and k_R are constant, the value of K can be readily determined.

Calibration Results

Two sources were used to calibrate the long WL instrument. One was an ambient-temperature conical field source consisting of a simple metal cone coated internally with black enamel. This source quickly assumes the ambient air temperature and is not temperature controlled. The second source was a similar cone with a water jacket. Water was circulated through the jacket and a temperature controlled reservoir by a recirculating pump. The ambient temperature source was used to obtain an average value for ambient radiation and to check for consistency. The controllable blackbody was varied from near ambient (in an air-conditioned laboratory) to 55C.

$R(\lambda)$ was calculated for one WL in each channel. The WL for InSb was 5.23 μm, for HgCdTe it was 9.55 μm. Table 1 gives the pertinent values for InSb and HgCdTe for the 1° FOV. Values above the horizontal line in each section of the table are for varying the temperature of the external blackbody with uniform temperature of the internal blackbody. Below the line are values obtained by varying the internal blackbody temperature while maintaining the external black-body nearly constant. Table 2 gives similar observed values for the 15° FOV. The internal blackbody was not varied for the 15° FOV measurements because it was assumed the signal from the internal blackbody is independent of the FOV.

The values of the spectral radiance responsivities ($R(\lambda)$) expressed as volt per watt/cm^2-ster-μm are:

InSb	1° FOV	λ 5.23 μm	$R = 64.3$
	15° FOV	λ 5.23 μm	$R = 87.5$
HgCdTe	1° FOV	λ 9.55 μm	$R = 12.0$
	15° FOV	λ 9.55 μm	$R = 16.2$

$R(\lambda)$ can be determined at any other WL by following the same procedure. However, it is easier to use Eq. (2) and take ratios as follows:

$$\frac{R(\lambda_a)}{R(\lambda_b)} = \frac{\Delta S(a)}{\Delta S(b)} \cdot \frac{\Delta L_\lambda(b)}{\Delta L_\lambda(a)} \tag{5}$$

where: a = measurements for which $R(\lambda)$ has been calculated and

b = measurements for any other WL.

For example

$$\Delta L_\lambda \ (5.26 \ \mu m) = L_{\lambda T}(1) - L_{\lambda T}(2) \ \text{at} \ 5.26 \ \mu m.$$

The calibration of the short WL instrument was limited to two radiance levels at the 1° FOV and one for the 15° FOV. Two measurements were also made to check the calibration of the incident radiation measurement. A quartz iodine lamp (General Electric, type 6.6A/T4Q/1CL-200-watt) that had been calibrated by the National Bureau of Standards was used as the primary source of radiation. Two levels of radiance were obtained by locating the lamp at two distances (43 and 129 cm) from a reflecting surface. A sheet of Fiberfrax large enough to fill the FOV was used as the reflecting surface. The directional reflecting characteristics of Fiberfrax were found to be sufficiently constant over the spectral range of the instrument to be considered independent of WL for the purpose of this calibration.

Calibration measurements were made by setting the optical axis of the spectroradiometer normal to the reflecting surface and placing the lamp on a line at an angle of 45° from the normal to the reflecting surface.

The spectral radiance from the Fiberfrax in the direction of the normal is given by:

$$L_\lambda(\lambda) = \frac{E_\lambda(\lambda)}{\sqrt{2}} \cdot P'(\lambda)$$

where $L\lambda$ is a spectral radiance in watts/cm^2-ster-µm

E_λ is the value of radiance given by NBS

P' is bidirectional reflectance of the Fiberfrax $P'(\lambda) = \dfrac{\sqrt{2}}{\dfrac{A}{D^2}}$

Where A = area of aperture

D = distance between aperture and detector.

The Si detector response was measured at .70 µm and the PbS detector at 1.82 µm.

The responsivity was obtained from:

$$R(\lambda) = \frac{S(43) - S(129)}{L_\lambda(\text{at } 43) - L_\lambda(\text{at } 129)}$$

where 43 and 129 are the values of the terms when the Q-I lamp was at 43 and 129 cm from the Fiberfrax. Note that 129 = 43 x 3 so the intensity at the Fiberfrax surface is reduced by a factor of 9.

The values of spectral radiance responsivity obtained are:

Silica	1° FOV	R (0.70 µm) =	7.5
	15° FOV	R (0.70 µm) =	7.1
PbS	1° FOV	R (1.82 µm) =	102
	15° FOV	R (1.82 µm) =	93

Each R is in units of volt per watt/cm^2-ster-µm.

The incident radiation channel was calibrated by placing the Q-I lamp at 43 and 129 cm from the opal glass diffusing plate. The irradiance responsivity was calculated from:

$$R(\lambda) = \frac{S(43) - S(129)}{E_\lambda(\text{at } 43) - E_\lambda(\text{at } 129)}$$

where the values of E_λ were obtained (upon conversion to units watts/cm^2-μm) at wavelengths of 0.70 and 1.82 μm.

The values obtained were:

Silica $R(0.70) = 0.95$

PbS $R(1.82) = 23.8$

where R is expressed in volts per watt/cm^2-μm.

SUMMARY

The values given by this initial calibration make possible the conversion of voltage signals from the spectroradiometers into meaningful units of energy.

Field operation of the instruments result in a wider range of levels of measurement so that electronic gain settings are used that were not used in the initial calibration. These variations and the complex nature of the spectroradiometers suggest that calibration checks under well controlled conditions should be made periodically.

LITERATURE CITED

Pivovonsky, M., and M. R. Nagel. 1961. Tables of blackbody radiation functions. The MacMillan Co., New York.

TABLE 1

__InSb__   __1°__

· % Ramp = 91.8   λ = 5.23 μm

T_{BB}	T_{Ref}	R	Def'l	ΔS(Rec)	$\Delta V = \Delta S \cdot R$(volts) ($\times 10^{-2}$)	$L_{\lambda BB}$ ($\times 10^{-4}$)	$L_{\lambda Ref}$ ($\times 10^{-4}$)
24	35	.01	-16.3	-1.63	-1.63	2.96	4.10
22	35	.01	-16.5	-1.65	-1.65	2.77	4.10
27	35	.01	-14.5	-1.45	-1.45	3.20	4.10
30	35	.01	-12.7	-1.27	-1.27	3.54	4.10
34	35	.01	- 9.3	-0.93	-0.93	3.90	4.10
40	35	.003	-14.5	-1.45	-0.44	4.72	4.10
46	35	.003	+ 1.8	+0.18	+0.05	5.56	4.10
50	35	.003	+16.4	+1.64	+0.49	6.14	4.10
55	35	.01	+11.8	+1.18	+1.18	7.02	4.10
24	55	.03	-17.2	-1.72	-5.16	2.96	7.02
23.9	50	.03	-13.7	-1.37	-4.11	2.96	6.14
23.9	45	.03	-10.7	-1.07	-3.21	2.96	5.40
23.9	40	.01	-22.5	-2.25	-2.25 23.9C	2.96	4.72
23.8	35	.01	-16.1	-1.61	-1.61	2.96	4.10
23.8	30	.01	- 9.8	-0.98	-0.98	2.96	3.54
23.5	21	.01	- 4.2	-0.42	-0.42	2.96	2.70

__HgCdTe__   __1°__

% Ramp = 19.2   λ = 9.55 μm

T_{BB}	T_{Ref}	R	Def'l	ΔS(Rec)	$\Delta V = \Delta S \cdot R$(volts) ($\times 10^{-2}$)	$L_{\lambda BB}$ ($\times 10^{-4}$)	$L_{\lambda Ref}$ ($\times 10^{-4}$)
24	35	.003	-11.8	-1.18	-3.54	9.53	11.38
22	35	.002	-12.2	-1.22	-3.66	9.20	11.38
27	35	.003	-10.0	-1.00	-3.00	10.00	11.38
30	35	.003	- 8.1	-0.81	-2.43	10.50	11.38
34	35	.003	- 5.0	-0.50	-1.50	11.12	11.38
40	35	.001	- 2.6	-0.26	-0.26	12.38	11.38
46	35	.001	+10.2	+1.02	+1.02	13.55	11.38
50	35	.001	+20.0	+2.00	+2.00	14.30	11.38
55	35	.003	+10.9	+1.09	+3.27	15.35	11.38
24	55	.01	- 9.0	-0.90	-9.00	9.54	15.35
23.9	50	.003	-24.7	-2.47	-7.41	9.54	14.30·
23.9	45	.003	-20.2	-2.02	-6.06	9.54	13.30
23.9	40	.003	-16.0	-1.60	-4.80 23.9C	9.54	12.38
23.8	35	.003	-12.0	-1.20	-3.60	9.54	11.38
23.8	30	.001	-22.7	-2.27	-2.27	9.54	10.50
23.5	21	.001	-12.1	-1.21	-1.21	9.54	9.05

TABLE 2

InSb   15° λ = 5.23 μm

T_{BB}	T_{Ref}	R	Def'l	ΔS(Rec)	$\Delta S \cdot R$(volts) ($\times 10^{-2}$)	$L_{\lambda BB}$ ($\times 10^{-4}$)	$L_{\lambda Ref}$ ($\times 10^{-4}$)
55	35	.01	+20.3	+2.03	+2.03	7.02	4.10
22.5	35	.01	-16.6	-1.66	-1.66	2.80	4.10
50	35	.01	+12.3	+1.23	+1.23	6.14	4.10
22.5	35	.01	-16.5	-1.65	-1.65	2.80	4.10
45	35	.01	+ 5.1	+0.51	+0.51	5.40	4.10
23	35	.01	-16.6	-1.66	-1.66	2.86	4.10
40	35	.003	- 1.0	-0.10	-0.03	4.72	4.10
22.5	35	.01	-16.6	-1.66	-1.66	2.80	4.10
35	35	.003	-19.5	-1.95	-0.59	4.10	4.10
22.5	35	.01	-16.7	-1.67	-1.67	2.80	4.10
30	35	.01	-10.8	-1.08	-1.08	3.54	4.10
22.5	35	.01	-16.8	-1.68	-1.68	2.80	4.10
24.5	35	.01	-14.7	-1.47	-1.47	3.00	4.10
22.5	35	.01	-16.6	-1.66	-1.66	2.80	4.10

Ave. ΔV for 22.5 = -1.66

HgCdTe   15° λ = 9.55 μm

+ 5%
↓

T_{BB}	T_{Ref}	R	Def'l	ΔS(Rec)	$\Delta S \cdot R$(volts) ($\times 10^{-2}$)	$L_{\lambda BB}$ ($\times 10^{-4}$)	$L_{\lambda Ref}$ ($\times 10^{-4}$)
55	35	.003	+18.9	+1.89	+5.95	15.35	11.38
22.5	35	.003	-13.0	-1.30	-4.10	9.25	11.38
50	35	.003	+12.9	+1.29	+4.05	14.30	11.38
22.5	35	.003	-13.0	-1.30	-4.10	9.25	11.38
45	35	.003	+ 7.3	+0.73	+2.30	13.30	11.38
23	35	.003	-13.0	-1.30	-4.10	9.35	11.38
40	35	.001	+ 8.0	+0.80	+0.80	12.38	11.38
22.5	35	.003	-13.2	-1.32	-4.15	9.25	11.38
35	35	.001	- 7.5	-0.75	-0.75	11.38	11.38
22.5	35	.003	-13.0	-1.30	-4.10	9.25	11.38
30	35	.003	- 6.9	-0.69	-2.18	10.50	11.38
22.5	35	.003	-13.0	-1.30	-4.10	9.25	11.38
24.5	35	.003	-11.3	-1.13	-3.56	9.58	11.38
22.5	35	.003	-13.2	-1.32	-4.15	9.25	11.38

Ave. ΔV for 22.5 = -4.10
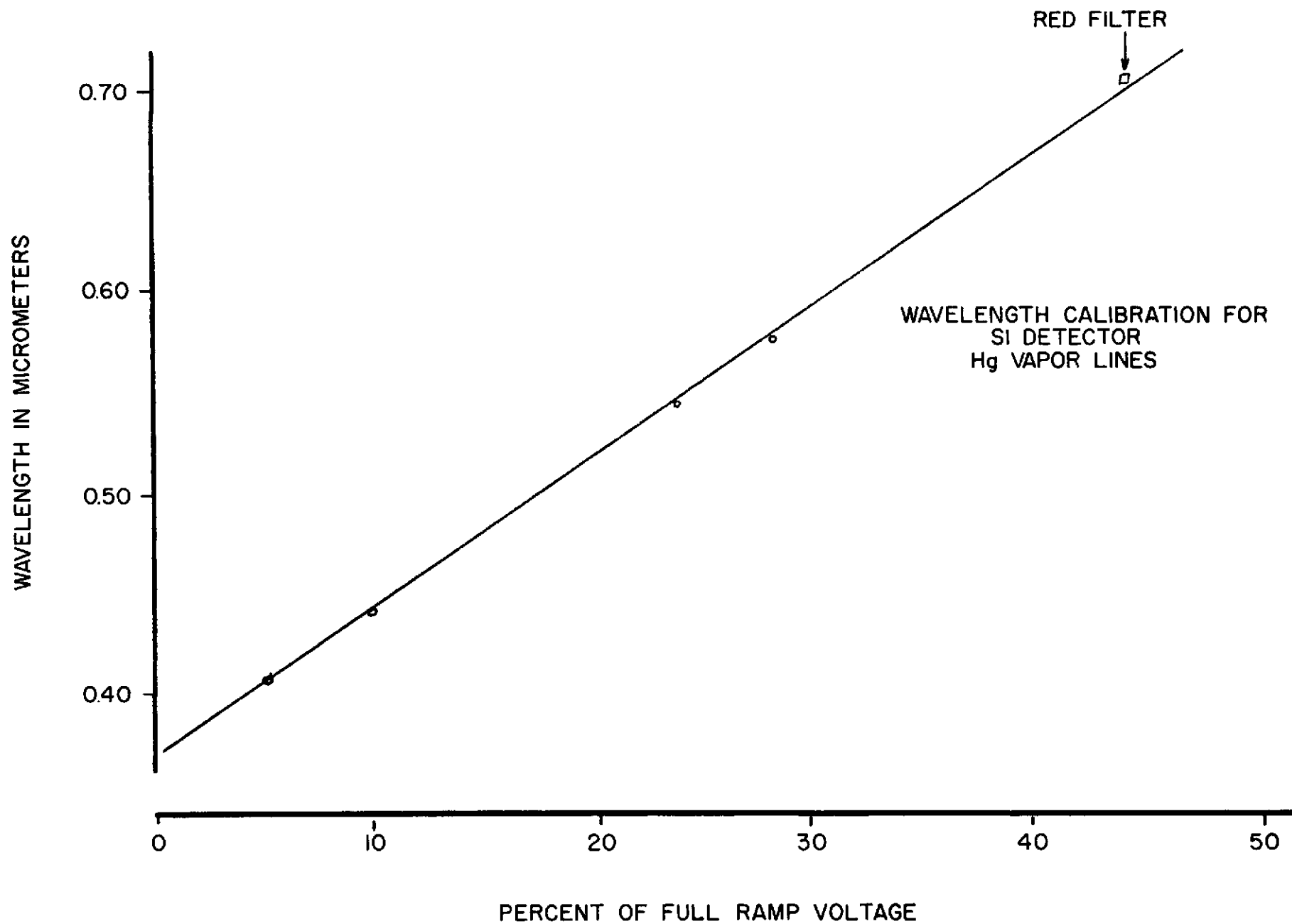
Fig. 1.--Wavelength calibration of Si detector with Hg vapor lamp.
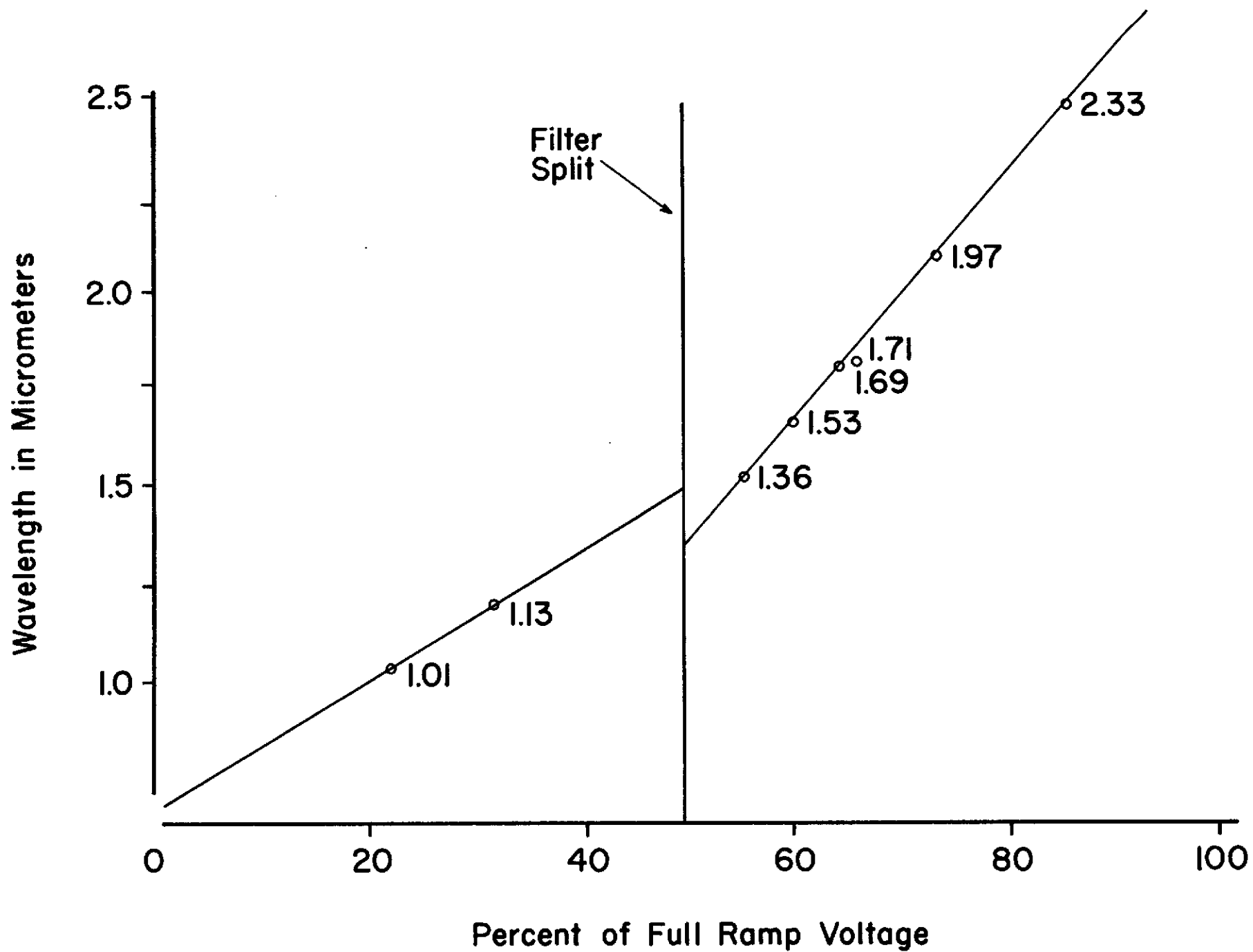
Fig. 2.--Wavelength calibration of PbS detector with Hg vapor lines.
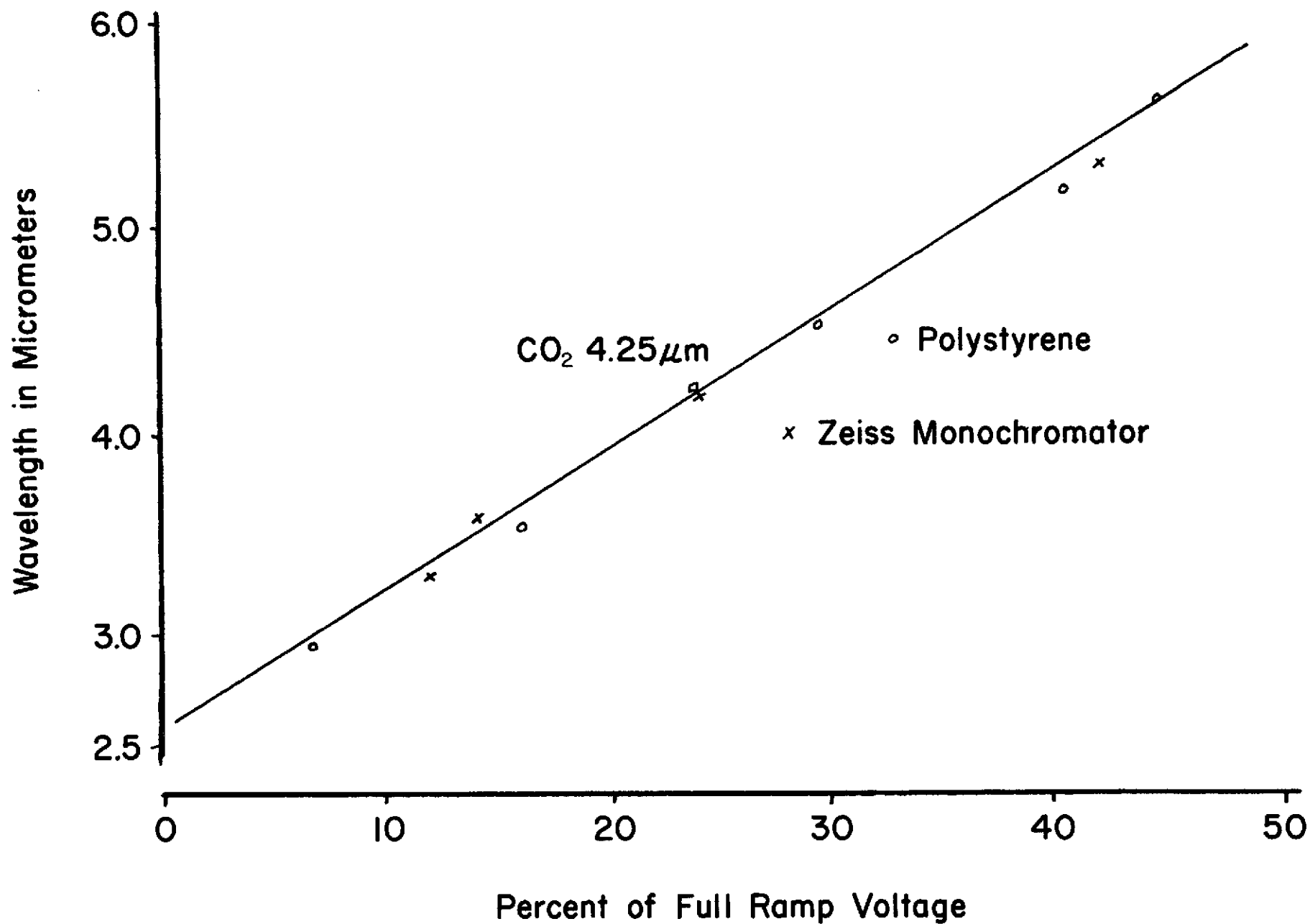
Fig. 3.--Wavelength calibration of InSb detector with polystyrene and Zeiss monochromator.
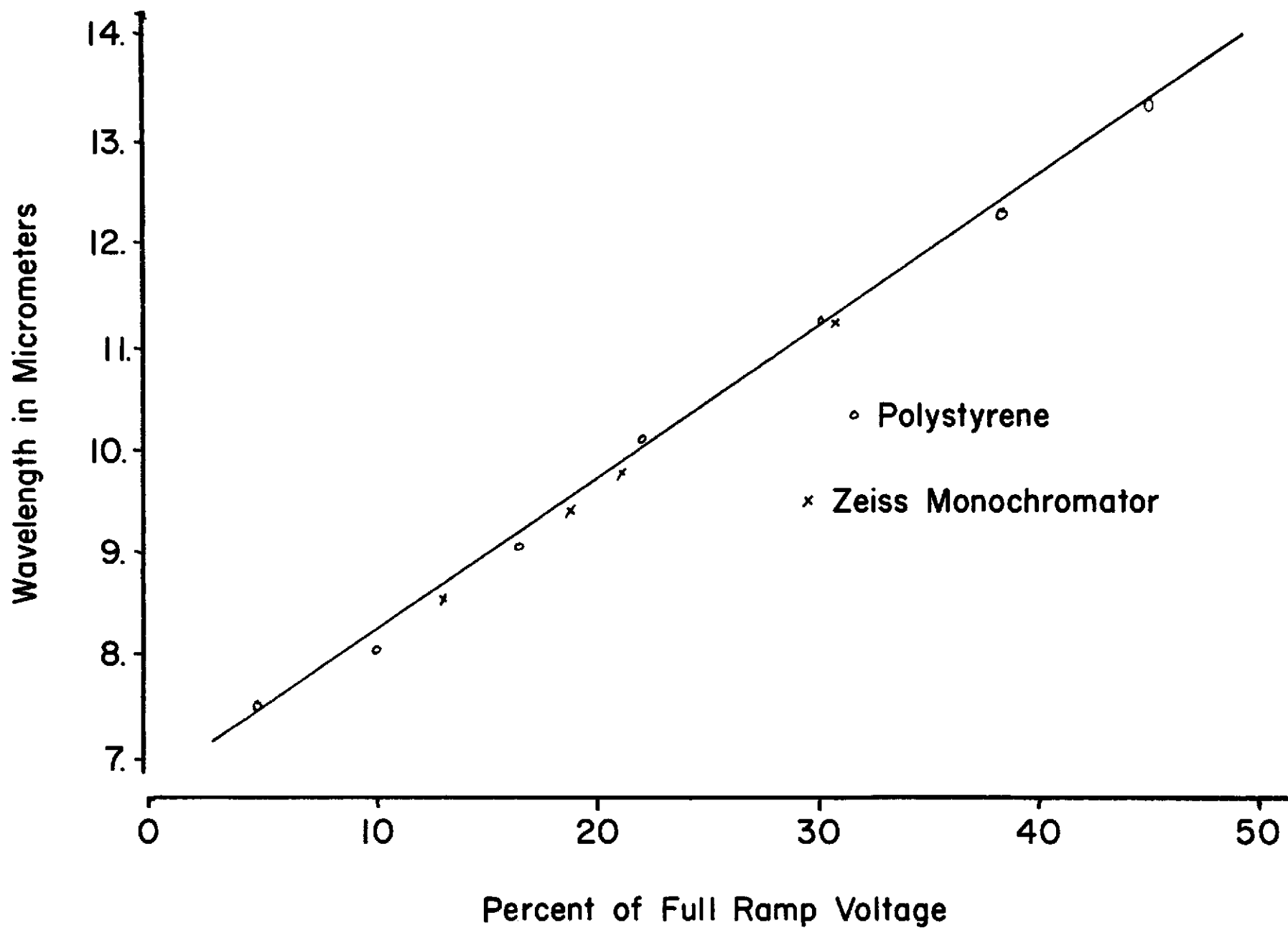
Fig. 4.--Wavelength calibration of HgCdTe detector with polystyrene and Zeiss monochromator.
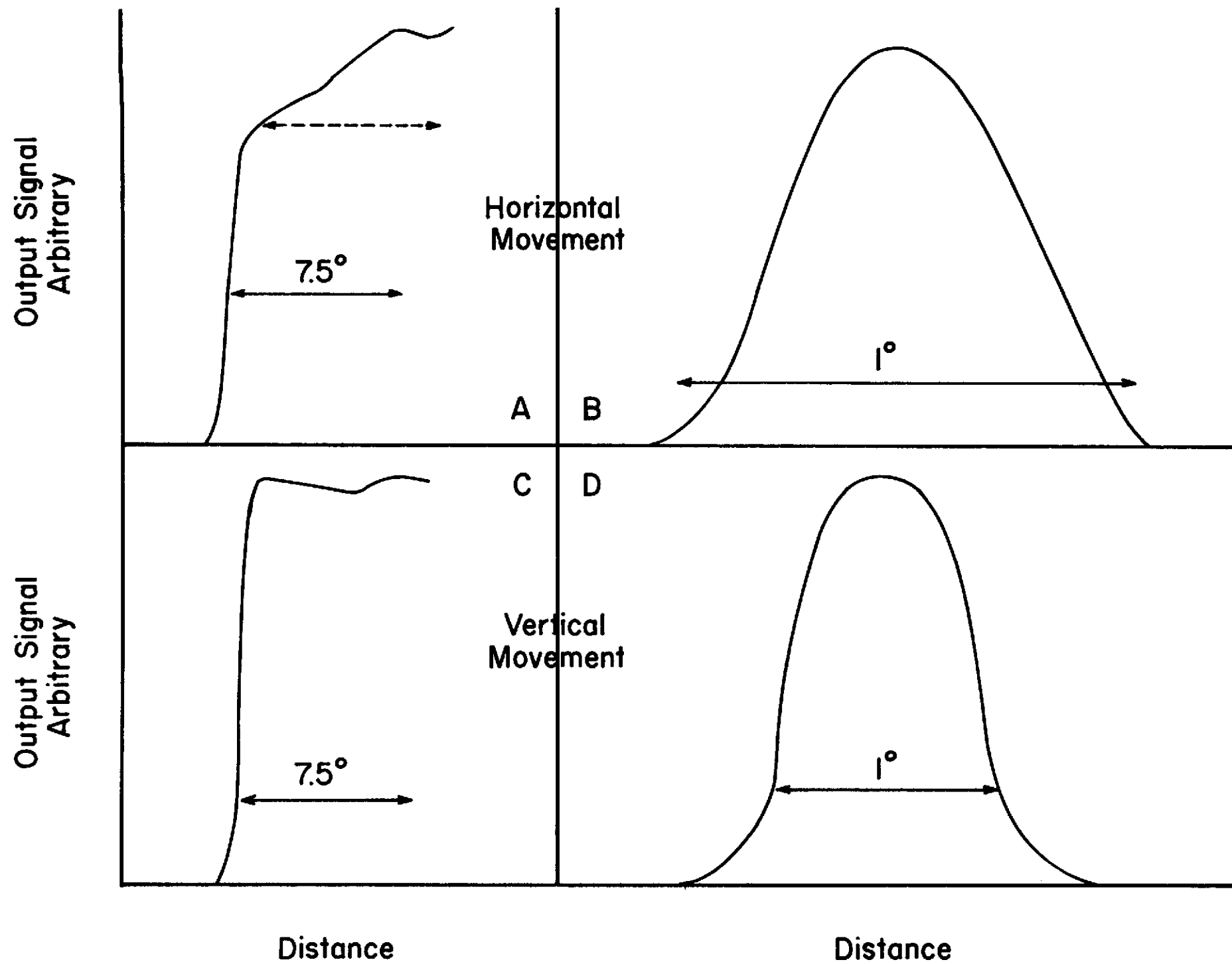
Fig. 5.--Silica detector response to point source light moved across the field of view.
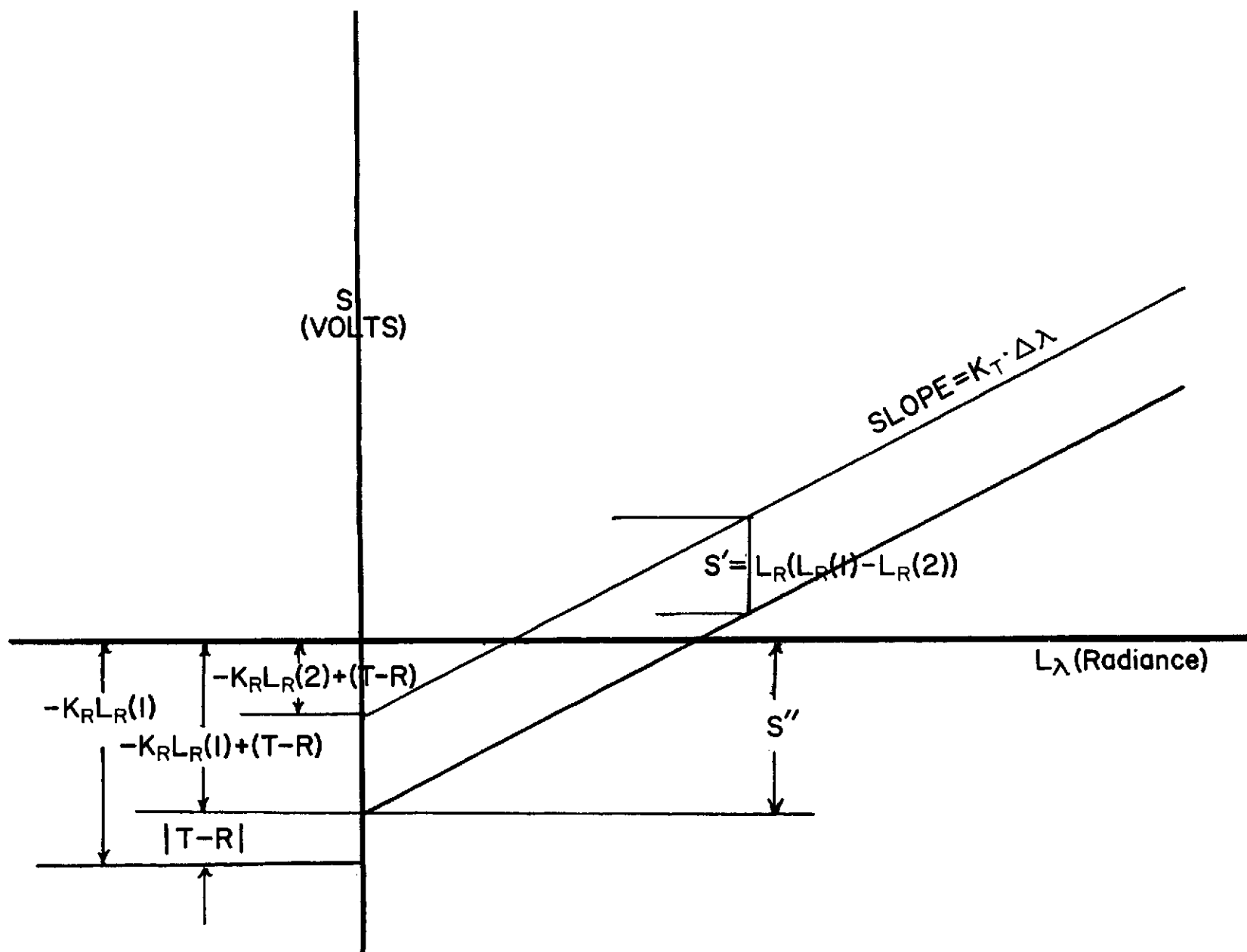
Fig. 6.--Graphic representation of solution of Equation 1 to calculate unknown radiance from signal differences.

A LEAF CROSS SECTION TREATED AS AN OPTICAL SYSTEM

W. A. Allen and A. J. Richardson

INTRODUCTION

The interaction of light with the structure of a dorsiventral leaf was explained by Willstätter and Stoll (W-S) (1913) on the basis of geometrical optics. Figure 1a is a cross section of an albino maple leaf (Acer negundo L.) used by W-S to illustrate their theory. The purpose of this investigation is to determine: first, whether the W-S concept leads to sound predictions and second, whether the W-S idea can be modified to obtain better results. Preliminary results are reported.

Slightly paraphrased, Willstätter and Stoll (W-S) stated:

> "The surfaces of common deciduous leaves are arranged nearly perpendicular to the radiation. The rays enter through the plate-like epidermal cells, pass through the densely-packed palisade cells arranged parallel to the radiation, and then through the groups of mesophyll parenchyma cells in direct contact with the palisade cells. In the absence of absorption, this process occurs with undiminished intensity. The cells located at the upper margin of the spongy mesophyll, and especially those lying deeper in the tissue, change the course of light with their many curved surfaces. The light rays strike the surface between the cell and air at an oblique angle where the greater part is totally internally reflected and scattered. Some light eventually diffuses through the lower epidermis. A particularly important fraction is totally reflected internally and is lost as diffuse radiation through the upper epidermis. A chlorophyll-free leaf reflects light in the same way as a snow surface. A normal leaf, however, is characterized by absorption."

Willstätter and Stoll thus expressed a new idea in a qualitative manner. The broad implications of the W-S concept is that a leaf can be regarded as a complicated optical system consisting of a complex arrangement of upper and lower epidermal cells, and palisade, and spongy parenchyma cells.

Willstätter and Stoll did not generalize their ideas either to light incident at angles other than normal or to leaves other than maple. These generalizations, however, are straightforward. Each different kind of leaf, however, is a new and special problem. While W-S did not specifically discuss the reflectance from the microstructure of the cuticle and the cell walls, these effects are implicit in their concept. Willstätter and Stoll were probably aware of the detailed energy bookkeeping necessary for a strict application of the Snell and Fresnel relations at each interface. Willstätter and Stoll were sufficiently perceptive to isolate the principal causitive agent of leaf reflectance; that is, internal reflectance, without becoming bogged down in a morass of computations associated with ray tracing.

Strictly speaking, the W-S concept is <u>not</u> a theory because the results were obtained by straightforward application of known optical principles expressed by the laws of Fresnel and Snell. If the geometrical, physical, and chemical struc- ture of a leaf is known, the W-S concept implies that reflectance, transmittance, and absorptance can be predicted from ray tracing data and application of the Fresnel relations. Computational difficulties that existed in 1913 forced W-S to be satisfied with a minimum number of rays traced roughly in a plane. A pur- pose of this paper is to quantify the W-S results.

The W-S concepts have been questioned recently by Sinclair (S) (1968) who proposed a diffuse reflectance hypothesis. Mathematical difficulties associated with the diffusion of light have forced theoreticians to take refuge in sim- plified models more amenable to mathematical analysis. A "diffuse hypothesis" is one such simplification. Kubelka and Munk (1931), Melamed (1963), and Allen, et al. (1969) have shown that the actual geometrical structure of a diffusing material such as a leaf can be replaced by simple idealized structures that bear little resemblance to a leaf. The Melamed theory, for example, can be used to replace the cellular structure of a leaf with close-packed, perfectly- diffusing spheres. Allen, et al. (1969) have shown that acceptable results can be obtained when the internal structure of a leaf is simulated by a pile of transparent plates with perfectly-diffusing surfaces. Kubelka and Munk (1931) avoided the geometrical problem entirely by use of differential equations based on perfect diffusion. In each case, however, a "diffuse hypothesis" does not imply that the cellular structure of a leaf cell actually behaves in this manner. In each of the three cases, the diffuse hypothesis was introduced as a convenient mathematical fiction that rendered a hopelessly difficult problem mathematically tractable. In the microscopic world the interaction of light with the internal structure of a leaf is likely to be in accord with the W-S concepts; in the macro- scopic world, the same phenomena can be regarded, for convenience only, as diffuse.

Interaction of light with leaf cellular structure will be investigated in this paper by the ray tracing methods of geometrical optics. A leaf section can be regarded as an unconventional optical system. Each kind of leaf must be investigated separately. Generalizations to new optical systems, based upon previous experience, is dangerous. However, if a sufficient number of leaves, regarded as optical systems, can be tested by ray tracing, a pattern of results may well emerge that can be used as a basis for prediction. Each prediction must be regarded as tentative unless tested by subsequent ray tracing.

The essential difference between the W-S and S approach is the nature of the interaction of a typical ray at an interface. The W-S theory postulates specular interaction, the S theory is based upon diffuse interaction. Both procedures are incorporated in the subsequent analysis.

The problem of ray tracing in conventional optical systems is usually treated in three phases. First, the optical system must be specified. Second, approp- riate equations must be derived to refract and reflect a ray from a spherical interface. Third, suitable equations must be derived to transfer a ray from one interface to another throughout the optical system.

MATERIALS AND METHODS

The Optical System

A conventional optical system is usually centered along a known optical axis. The curvature of each spherical element is specified. The separation of each element along the optical axis is part of the lens prescription. The indices of refraction of all media, usually several, are assumed to be known. The conventional system is finite. Restrictions are usually placed upon the minimum distance that a given ray can approach the rim of a lens. The conventional optical system is normally treated in three dimensions.

The unconventional optical system illustrated in Fig. 1b is simpler in some respects than a conventional system, but in other aspects the system is more complicated. The surfaces consist of a sequence of intersecting circular arcs. The unconventional optical system is not centered and has no optical axis. Two media only are considered, at least initially, and one of these is air with an index of refraction of unity. The geometrical arrangement is specified by the curvature and center of curvature for each interface. The system is considered to be infinite in lateral extent. In order to insure mathematical tractability, the system is assumed to be a periodic structure composed of sequential replications of the fundamental arrangement illustrated in Fig. 1b. The advantage of an assumed periodic representation of leaf structure is that lateral scattering within a leaf can be investigated. A disadvantage is that in the model of Fig. 1b a ray can be oriented in the cuticle such that it would encounter no subsequent refraction regardless of the length of its path. Other rays can be visualized that would proceed laterally great distances by successive interactions with circular interfaces. These contingencies would require calculations based on many additional periods of the fundamental arrangement. The energy bookkeeping would quickly become formidable.

The above difficulties can be neatly avoided, however, if the basic problem is slightly changed. The conceptual problem to this point involves the subsequent history of a single given incident ray. We now assume that each of the periodic arrangements is irradiated simultaneously in the same manner. Every ray that peregrinates from Fig. 1b across the right boundary will be replaced by a ray of the same energy and polarization incident from the left boundary. The new ray will be characterized by the same relative position and direction of the ray that has disappeared. The same method can be used to compensate for a ray that leaves Fig. 1b across the left boundary. The modified model is probably a more nearly accurate representation of reality than the original arrangement. The artifice suggested allows many possible questions to be answered within the framework of the 100 arcs indicated in Fig. 1b.

The system is constrained to two dimensions. Restriction of the problem to two dimensions is desirable because, in general, the internal structure of a typical leaf cannot be accurately represented with spherical surfaces.

The optical system of Fig. 1a is simulated in Fig. 1b by a sequence of 100 intersecting circular arcs each less than π. Each circular arc is determined in a Cartesian coordinate system by three points (x_1, y_1), (x_2, y_2), and (x_3, y_3). [The points (x_2, y_2) are not indicated on the arcs in Fig. 1b]. The center of a typical circle is at the point (a, b) and its radius is designated r. The equation of a typical circle is given by

$$(x-a)^2 + (y-b)^2 = r^2 \qquad . \tag{1}$$

Substitute the three defining points (x_i, y_i) $i = 1, 2, 3$, into Eq. (1) to obtain

$$x_1^2 + y_1^2 + a^2 + b^2 - 2(ax_1 + by_1) = r^2 \qquad ,$$

$$x_2^2 + y_2^2 + a^2 + b^2 - 2(ax_2 + by_2) = r^2 \qquad , \tag{2}$$

$$x_3^2 + y_3^2 + a^2 + b^2 - 2(ax_3 + by_3) = r^2 \qquad .$$

Eliminate r^2 in Eqs. (2) to obtain

$$2(x_1-x_2)a + 2(y_1-y_2)b - x_1^2 - x_2^2 + y_1^2 - y_2^2 \qquad ,$$

$$\tag{3}$$

$$2(x_2-x_3)a + 2(y_2-y_3)b - x_2^2 - x_3^2 + y_2^2 - y_3^2 \qquad .$$

Equations (3) can be readily solved for the unknowns a and b. One of Eqs. (2) can then be used to obtain r.

Figure 1a, and any similar such figure that represents the cross section of a leaf, can always be represented by a sequence of arcs each less than π. (Any arc greater than π can always be subdivided into two arcs each less than π.) We establish the convention that all arcs will be less than π. The test that a point (x, y) lies on the smaller of the two arcs established by the end points (x_1, y_1) and (x_3, y_3) can be expressed by the relation

$$(x-x_1)^2 + (y-y_1)^2 + (x-x_3)^2 + (y-x_3)^2 < (x_3 - x_1)^2 + (y_3-y_1)^2 \qquad . \tag{4}$$

Equation (4) can be derived easily from Fig. 2. The arc BCA in Fig. 2 has been drawn less than π. We have the relation

$$c^2 = a^2 + b^2 - 2ab \cos C \qquad . \tag{5}$$

Since $C > \pi$ by convention, $\cos C < 0$ and the quantity $-ab \cos C > 0$. Therefore

$$c^2 > a^2 + b^2 \quad , \tag{6}$$

and Eq. (4) holds. A point on the dashed arc of Fig. 2 would not satisfy Eq. (4).

There is no difficulty in generalizing the preceding results to the case of four intersecting spheres. Such a generalization, however, is not a good representation of an actual leaf cross section. The palisade cells in Fig. 1a, for example, cannot be simulated by spherical sections. The initial treatment, therefore, will be constrained to two dimensions.

The Refraction and Reflection Relations

Ray tracing through complicated optical systems is not new. Silberstein (1918) introduced the vector method of tracing rays through any system of lenses, prisms, and mirrors. Feder (1951) improved the accuracy of the mathematical relations, extended the treatment to aspheric surfaces, but specialized the results to centered systems. Allen and Snyder (1952) generalized the Feder relations to uncentered optical systems. All three approaches are adapted to a three-dimensional treatment of ray tracing.

The refraction and reflection relations will be derived from fundamentals. The equations will differ from conventional relations because no attempt has been made to achieve maximum accuracy. Conventional ray tracing relations are usually transformed to extract ultimate precision for special cases of small curvatures and other indeterminant situations. Since the optical system in Fig. 1b is merely a rough simulation of Fig. 1a, which is in turn an idealized representation of the real leaf cross section, excessive digital accuracy is not necessary. We shall be able, therefore, to retain simpler forms of the ray tracing equations.

Figure 3 illustrates a unit vector $\underline{n}$ that represents the local normal to the surface separating two homogeneous isotropic media with refractive indices μ and μ'. The direction of the incident ray is given by $\underline{q}$, that of the refracted ray by $\underline{q}'$, and that of the reflected ray by $\underline{q}''$, where all three vectors are unit vectors. The plane $\underline{q} \times \underline{n}$ is the incident plane. The angles of incidence i, of refraction i', and of reflection i'' are given by the relations

$$\sin i = |\, \underline{q} \times \underline{n} \,| \quad , \tag{7}$$

$$\sin i' = |\, \underline{q}' \times \underline{n} \,| \quad , \tag{8}$$

$$\sin i'' = |\, \underline{q}'' \times \underline{n} \,| \quad . \tag{9}$$

The law of reflection can be written

$$\underline{q}'' \times \underline{n} = \underline{q} \times \underline{n} \quad . \tag{10}$$

Operate on both sides of Eq. (10 with $\underline{n}$ x and rearrange to obtain

$$\underline{q}'' = \underline{q} - 2(\underline{n} \cdot \underline{q})\, \underline{n} \quad . \tag{11}$$

The law of refraction (μ' sin i' = μ sin i) where $\underline{q}$, $\underline{n}$, $\underline{q}'$ are coplanar can be written

$$\underline{n} \times \underline{s}' = \underline{n} \times \underline{s} \quad , \tag{12}$$

where $\underline{s} = \mu \underline{q}$ and $\underline{s}' = \mu' \underline{q}'$. Operate on both sides of Eq. (12) with $\underline{n}$ x and rearrange to obtain

$$\underline{s}' = \underline{s} + (\underline{n} \cdot \underline{s}' - \underline{n} \cdot \underline{s})\, \underline{n} \quad . \tag{13}$$

Equation (13) contains the unknown $\underline{s}'$ on both sides of the equation. Since $\underline{s}' \cdot \underline{n} = \mu' \cos i'$ and $\cos i' = \underline{n} \cdot \underline{q}$, we have

$$\sin i' = [1 - (\underline{n} \cdot \underline{q})^2]^{\frac{1}{2}} \quad , \tag{14}$$

$$\sin i' = (\mu/\mu')[1 - (\underline{n} \cdot \underline{q})^2]^{\frac{1}{2}} \quad , \tag{15}$$

$$\cos i' = \{1 - (\mu/\mu')^2[1 - (\underline{n} \cdot \underline{q})^2]\}^{\frac{1}{2}} \quad , \tag{16}$$

$$\underline{s}' \cdot \underline{n} = \mu' \cos i' = \{\mu'^2 - \mu^2 + \mu^2(\underline{n} \cdot \underline{q})^2\}^{\frac{1}{2}} \quad . \tag{17}$$

Equation (13) can now be written in the explicit form

$$\underline{s}' = \underline{s} + \underline{n} \cdot \underline{s} \{[1+(\mu'^2-\mu^2)/(\underline{n} \cdot \underline{s})^2]^{\frac{1}{2}} - 1\}\, \underline{n} \quad . \tag{18}$$

The law of reflection, Eq. (11), can be obtained from the law of refraction, Eq. (18) by the substitution $\mu = \mu' = 1$ and use of the negative root in the radical.

The unit normal vector $\underline{n}$ in Fig. 3 is given by

$$\underline{n} = r^{-1} (\underline{T} + \ell\, \underline{q} - \underline{U}) \quad , \tag{18a}$$

where r is the radius of the circle. If the surface is considered to be diffuse, the unit vector of Eq. (18a) must be replaced with a unit vector with random direction. This artifice will lead to a direct comparison of the W-S and S concepts.

Transfer Equations

A typical circle, Fig. 3, with center specified by $\underline{U}$ and radius r is given by

$$(\underline{R} - \underline{U})^2 = r^2 \quad , \tag{19}$$

where $\underline{R}$ is the radius vector from the origin to a point on the circle. The equation of a typical ray emanating from the point $\underline{T}$ in the direction $\underline{q}$ is given by

$$\underline{R} = \underline{T} + \ell \, \underline{q} \quad , \tag{20}$$

where $\underline{R}$ is the radius vector from the origin to a point on the ray and $\underline{q}$ is a unit vector. Eliminate $\underline{R}$ from Eqs. (19) and (2) to obtain

$$[\ell \, \underline{q} + (\underline{T}-\underline{U})]^2 = r^2 \quad . \tag{21}$$

Expand Eq. (21) to obtain

$$\ell^2 + 2 \, \underline{q} \cdot (\underline{T}-\underline{U}) \, \ell + (\underline{T}-\underline{U})^2 = r^2 \quad . \tag{22}$$

Equation (22) can be expanded into the form

$$\ell^2 + 2B\ell + C = 0 \quad , \tag{23}$$

where

$$B = \underline{q} \cdot (\underline{T}-\underline{U}) = q_x(T_x-a) + q_y(T_y-b) \quad , \tag{24}$$

$$C = (T_x-a)^2 + (T_y-b)^2 - r^2 \quad . \tag{25}$$

Equation (23) has the solution

$$\ell = -B \pm (B^2-C)^{\frac{1}{2}} \quad . \tag{26}$$

Real intersections, in the mathematical sense, occur provided that $B^2>C$. We impose the further restriction that $\ell>0$. A physical intersection occurs when Eq. (4) is satisfied.

The transfer equation in the unconventional optical system of Fig. 1b is expressed by the recursion relation

$$\underline{T}_1 = \underline{T}_0 + \ell\underline{q}_0 \quad . \tag{27}$$

The subscript 1 refers to the situation subsequent to refraction (or reflection) and the subscript 0 pertains to the initial circumstance. Equation (27) is simple because the origin of the coordinate system is not shifted to each successive interface as in conventional ray tracing.

The next interface for a given ray in Fig. 1b is a function of its position and direction. The next interface is obtained by calculating the intersection of a ray with each of the arcs of Fig. 1b. The required solution is that with the smallest optical path length ℓ.

Energy Considerations

Energy considerations seldom arise in conventional ray tracing for three reasons. First, reflectance from air-glass interfaces is normally considered to be a nuisance, and this effect is reduced by anti-reflectance coatings. Second, optical glasses are manufactured as transparent as possible and absorption effects are considered to be negligible. Third, the angle of incidence is usually held relatively small in conventional ray tracing; the difficulties that occur at grazing incidence are, therefore, avoided by the lens designer.

Energy calculations must be a part of the ray tracing in an unconventional system such as Fig. 1b. Angles of incidence will frequently range up to $\pi/2$ in value. Rays will frequently interact with an interface at angles in excess of the critical value. Intense absorption is a fundamental role of chlorophyll. As a consequence, energy bookkeeping must be maintained on each ray at all times. The physical laws that describe the scattering and absorption of energy are due to Fresnel and Lambert.

The portions of the light reflected from the surface of an ordinary dielectric material is given by either

$$R_1 = \sin^2(I-I')\sin^{-2}(I+I') \quad , \tag{28}$$

or

$$R_2 = \tan^2(I-I')\tan^{-2}(I+I') \quad , \tag{29}$$

where I and I' are the angles of incidence and refraction, respectively. The quantity R_1 is the reflection of the light polarized in the plane of incidence, and R_2 is the reflection for the other plane of polarization. In the notation of this paper (Smith, 1966)

$$\cos I = \underline{q} \cdot \underline{n} \quad , \tag{30}$$

$$\cos I' = \underline{q} \cdot \underline{n} \quad . \tag{31}$$

Lambert's law can be written in the form

$$I = I_0 \exp(-k\ell) \quad , \tag{32}$$

where I_0 is the original amplitude of the light, ℓ is the path length through the medium, and k is the absorption coefficient, (Ditchburn, 1963).

RESULTS AND DISCUSSIONS

Ray Tracing Results

Figure 1b illustrates a few preliminary results based upon an assumed medium refractive index n = 1.4. A calculation was performed for the energy distribution at each interface for both states of polarization. A calculation was performed for the amount of energy absorbed along each ray. The initial value of the absorption coefficient was held at an infinitesimally small value in order to investigate the effect of pure scattering. The approximation of slight absorptance approximates the albino maple leaf used by W-S in the example reproduced in Fig. 1a. For illustrative purposes only, each ray was suppressed when its energy fell to less than 1% of the parent ray. The calculation was held to a total of about 100 rays. Table II is a graphical summary of the energy degradation of the initial ray of Fig. 1b for the first five interfaces.

SUMMARY

The Willstätter-Stoll (W-S) theory of light reflectance from a leaf has been verified by extensive ray tracing. The cellular structure of a typical leaf (maple leaf, Acer negundo L.) has been simulated in two dimensions by a chain of intersecting circular arcs that represent the interfaces between plant cells and air. The simulated leaf is treated as a periodic structure of infinite lateral extent based on a fundamental pattern of 100 arcs. The model is characterized by two indices of refraction, typically n_1=1.4 and n_2=1.0 corresponding, respectively, to medium and air. An incident ray of a specified state of polarization divides into a reflected and a refracted component at each interface unless the ray is emerging from the higher index medium at an incident angle in excess of the critical value. In this case reflection is total and there is no refracted ray. The energy of each ray is allocated to its resultant components at each interface by means of the Fresnel relations. Energy is attenuated in the medium by absorption expressed by Lambert's law. The process is continued for a given incident ray until all resultant rays have been absorbed or have emerged as reflectance or transmittance. The problem is tractable in a computer of moderate memory provided that bookkeeping is discontinued for each ray when its energy falls below a prescribed threshold. The calculation results in predicted values of reflectance, transmittance, absorptance, and polarization for each assumed leaf cross section configuration. The technique can be modified to provide predictions based on the assumption that every interface is perfectly diffusive. The results for the perfectly specular and perfectly diffusive cases bracket the experimental values obtained from a real leaf.

The W-S theory of leaf reflectance has been investigated by computer simulation. Preliminary results suggest that the W-S theory yields an acceptable explanation of experimental results. The computer techniques can be generalized to apply to diffuse interfaces. The concepts are also applicable to a simulated plant canopy.

LITERATURE CITED

Allen, W. A., and J. R. Snyder. 1952. Ray tracing through uncentered and aspheric surfaces. J. Opt. Soc. Amer. 42:243-249.

Allen, W. A., H. W. Gausman, A. J. Richardson, and J. R. Thomas. 1969. Interaction of isotropic light with a compact plant leaf. J. Opt. Soc. Amer. 59:1376-1379.

Ditchburn, R. W. 1963. Light (Interscience, John Wiley & Sons, Inc., New York, 1963), 2nd ed. Vol. II, Chap. 15, p. 551.

Feder, D. P. 1951. Optical calculations with automatic computing machinery. J. Opt. Soc. Amer. 41:630-635.

Kubelka, P., and F. Munk. 1931. Ein Beitrag zur Optik der Farbanstriche. Z. Techn. Physik, 12:593-601.

Melamed, N. T. 1963. Optical properties of powders. Part I. Optical absorption coefficients and the absolute value of the diffuse reflectance. Part II. Properties of luminescent powders. J. Appl. Phys. 34:560-570.

Silberstein, L. 1918. Simplified method of tracing rays through any optical system of lenses, prisms, and mirrors (Longmans, Green, and Company, New York, 1918).

Sinclair, T. R. 1968. M. S. Thesis, Purdue University Library, Lafayette, Indiana. p. 126.

Smith, W. J. 1966. Modern optical engineering (McGraw-Hill Book Company, Inc., New York, 1966), 1st ed., Chap. 7, p. 167.

Willstätter, R., and A. Stoll. 1913. Untersuchunger über die assimilation der kohlensaure (Julius Springer-Verlag, Berlin, 1913), p. 122.

Table 1. Energy degradation of an initial ray (unit energy in both vertical and
horizontal polarization) at the first five interfaces indicated in Fig.
1b. (Six generations of rays are listed). The numbers in parentheses
designate the ray. The upper branch of the chart at each interaction
corresponds to the reflected ray; the lower branch pertains to the re-
fracted component. The designation (x) indicates either that the re-
flected component has decreased to less than 1% energy or that total
reflection occurs. The upper and lower number for each ray refers to
vertical and horizontal polarization, respectively. A nominal value has
been assumed for the absorption coefficient.

1	2	3	4	5	6

```
                    (2)
                    0.04396
                    0.00634
                                                        (9)        (14) 0.02199
                                                        0.02269         0.00105
                                            (6)         0.00108    (x)  --
                                            0.46037                     --
                                            0.26338     (10)       (15) 0.01376
                              (4)                        0.43005        0.00319
                              0.46671                    0.25793    (16) 0.41628
   (1)                        0.26700                                    0.25473
   1.00000
   1.00000
                                            (x)
                                            --
                                            --

                    (3)
                    0.95603
                    0.99365
                                                        (x)
                                                        0.00029
                                            (7)         0.00022
                                            0.01312
                                            0.01138     (11)       (x)  0.00034
                                                        0.01283         0.00017
                              (5)                       0.01115    (17) 0.01231
                              0.48345                                   0.01083
                              0.72054     (12)          (18) 0.03428
                                                        0.03439         0.00015
                                            (8)         0.00016    (x)  --
                                            0.47032                     --
                                            0.70916     (13)       (19) 0.01383
                                                        0.43496         0.00886
                                                        0.70754    (20) 0.42113
                                                                       0.69868
```

Fig. 1a.--Cross section of maple leaf (Acer negundo L.) used by Willstätter and Stoll to illustrate their theory of leaf reflectance.
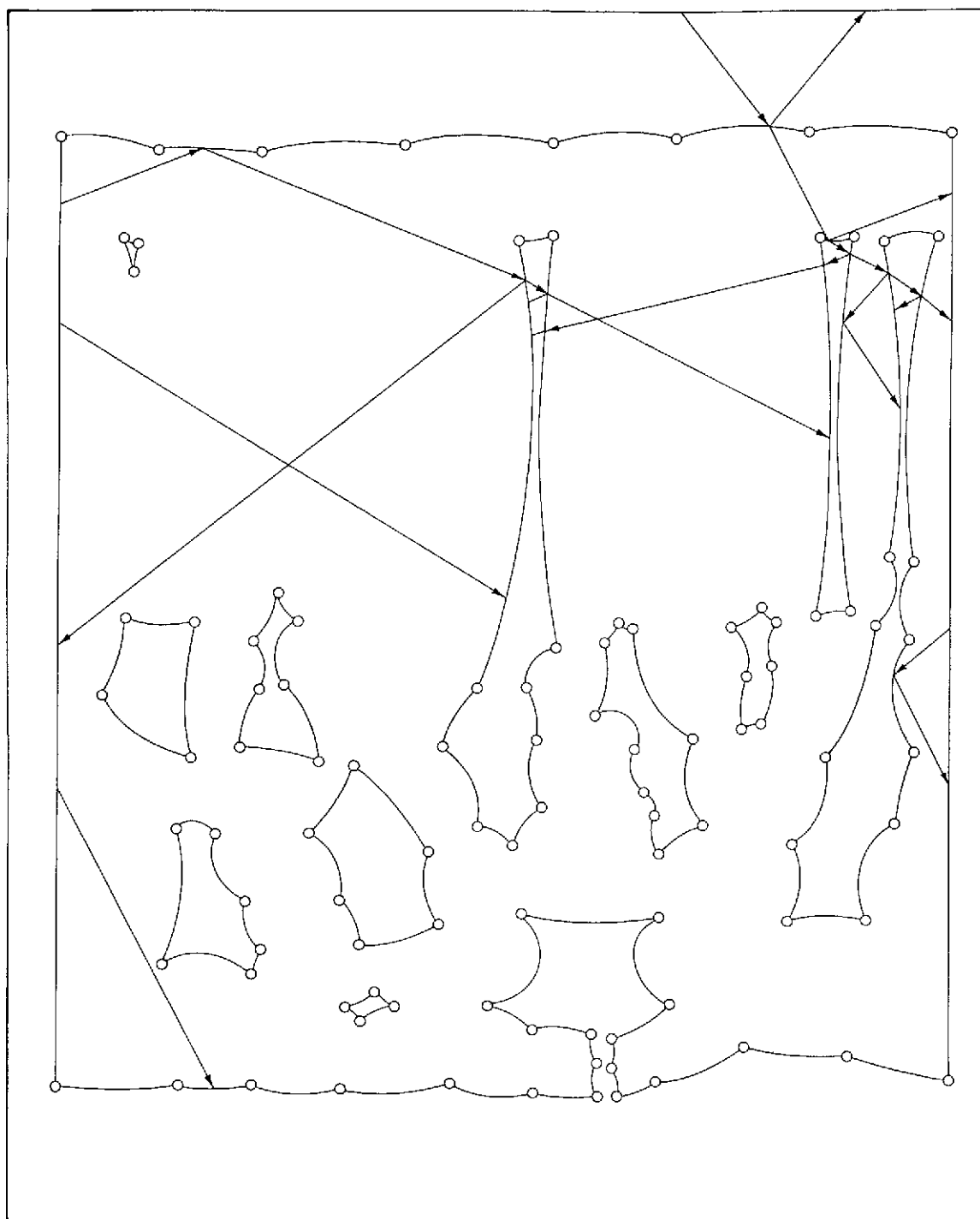
Fig. 1b.--Simulation of (a) by means of a sequence of 100 intersecting circular arcs each less than 180 deg. The indicated rays originate from a single parent ray that impinges on the upper epidermis. Note that each ray leaving the right-hand edge is replaced by another ray that enters the left-hand edge. The indicated six generations of rays correspond to Table 1.
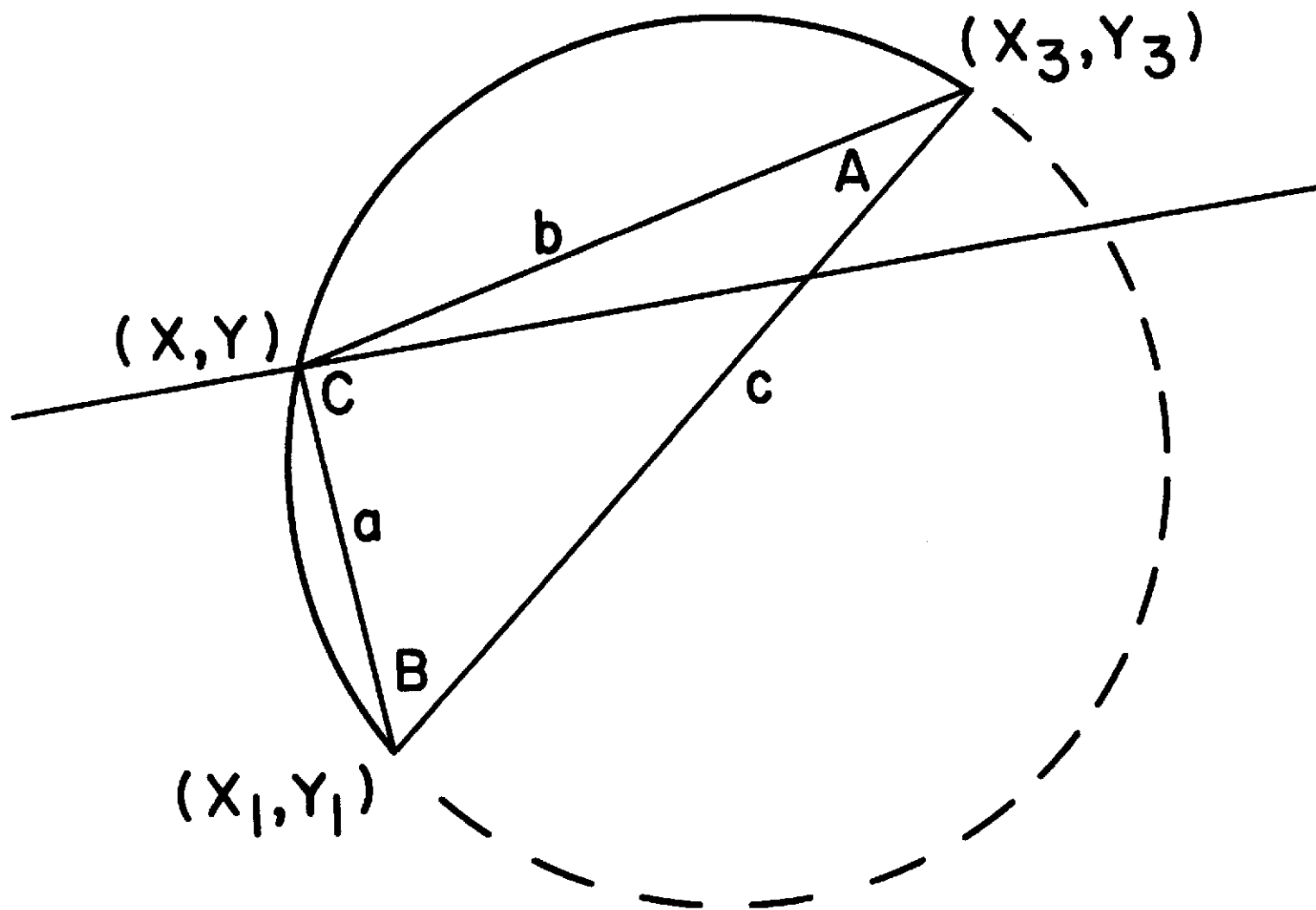
Fig. 2.--Sketch of a typical arc (solid curve) used to simulate cell wall. A ray (straight line) intersects the circle typically in two points. The indicated intersection (x, y) on the solid arc is by convention the only meaningful solution between the line and circle.
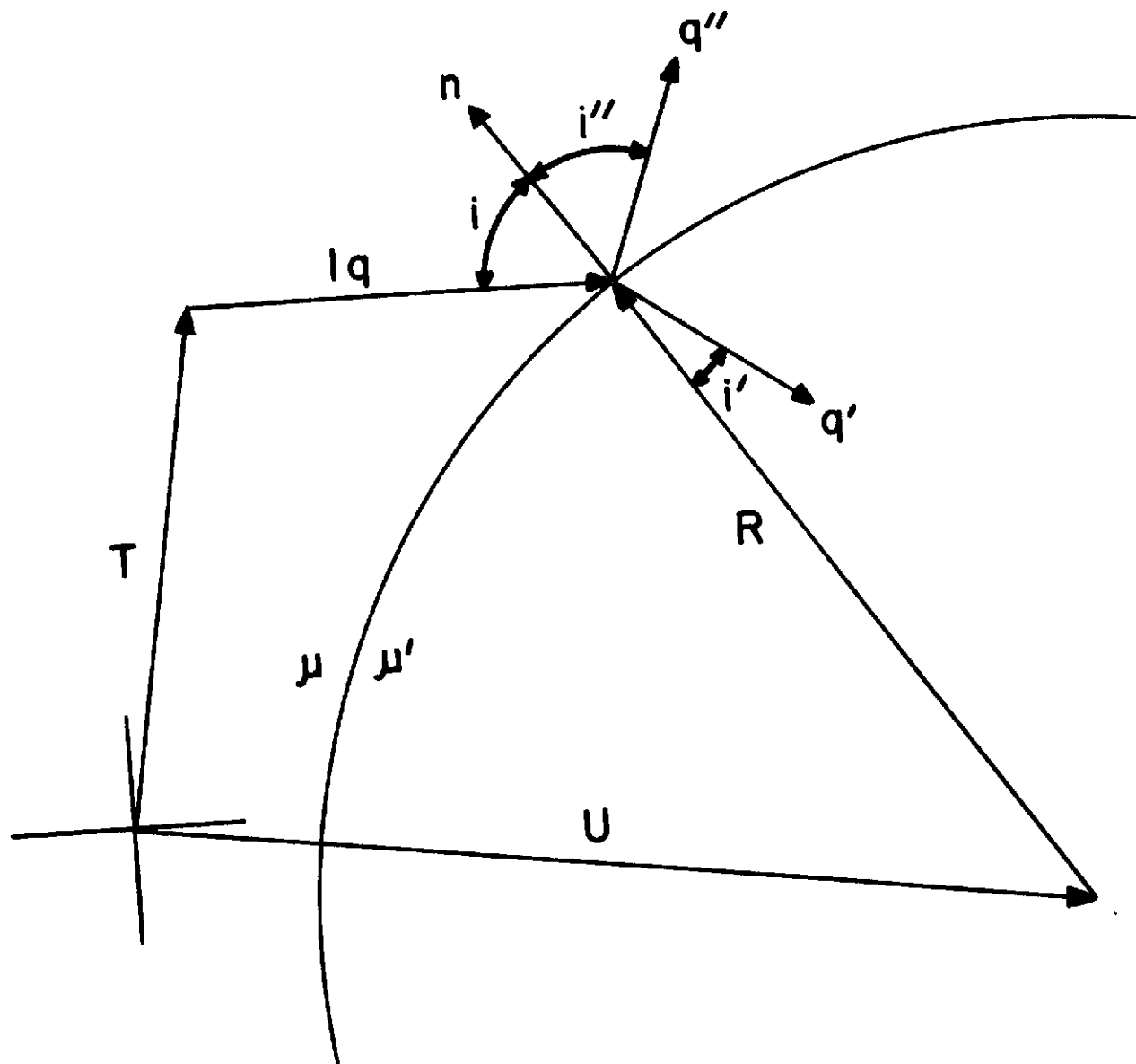
Fig. 3.—The nature of reflection and refraction produced by a spherical dielectric interface specified by the refractive indices µ and µ'.

DISCRIMINATION AMONG DIFFERENT KINDS OF PLANT LEAVES

BY SPECTRAL REFLECTANCE IN THE NEAR INFRARED

W. A. Allen, H. W. Gausman, and A. J. Richardson

The following information is from a
manuscript prepared for publication
in the Journal of Remote Sensing of
Environment. These results were pro-
duced under Research Outline 67,
"Effective Optical Constants of Single
Leaves and Plant Canopies."

INTRODUCTION

A flat plate model, with diffusing external and internal surfaces, has been
introduced previously (Allen et al., 1969) to explain the spectral reflectance of
a corn leaf over the wavelength range 0.5 to 2.5 μm. A corn leaf was chosen
because it is relatively compact. The flat plate model was generalized later to
the noncompact case (Allen et al., 1970; Gausman et al., 1970). The terms
compact and noncompact refer, respectively, to leaves that have relatively few
and to leaves that have many intercullular air spaces in the mesophyll.

Measurements on many kinds of leaves indicate that a typical noncompact leaf
can be regarded as a pile of N identical elementary compact layers separated by
air spaces. The absorption of a typical leaf over the spectral range 1.4 to 2.5
μm can be regarded as equivalent to a pile of N water layers of total thickness D.
The geometrical configuration of the flat plate model can be specified by the
numbers N and D. The quantity N-1 [the void area index (VAI)] is the assumed
number of air layers in the leaf model. The VAI is zero for a compact leaf.

Absorption of light by a leaf is caused largely by a superposition of two
effects: absorption attributable to leaf pigments, and absorption caused by
liquid water (Allen et al., 1969). Absorption by chlorophylls and carotenoids
occurs principally in the visible region of the spectrum, and absorption by water
occurs largely in the 1.4 to 2.5 μm region. Light scattering is produced by
Fresnel reflections from the surfaces of the assumed compact layers of the leaf.
If the leaf is compact, the reflections are produced at the exterior leaf surface.
A noncompact leaf is characterized by extensive internal reflections at inter-
cellular air interfaces.

Both geometrical and physical characteristics of a typical leaf can be
specified with considerable accuracy by means of the following four entities: an
effective index of refraction n, an effective absorption coefficient k, an
equivalent water thickness D, and the assumed number of compact layers N (Allen
et al., 1969; Allen et al., 1970; Gausman et al., 1970). The first two parameters
are optical constants that vary with wavelength, and the second two constants are
geometrical quantities that specify the internal structure of the leaf.

If the diffuse reflectance and transmittance of a single leaf is known, the effective optical constants can be calculated, and the reflectance of stacked leaves, or leaves arranged in their natural state in a plant canopy, can be predicted (Allen and Richardson, 1968). The principal advantage obtained by the transformation of spectrophotometric measurements into optical constants is that predictions are facilitated for leaf arrangements such as those that occur in a natural plant canopy located at a remote distance.

Leaf reflectance is analogous to that of a powder superimposed upon a background of known reflectance R_g. If the powder depth is too shallow, the reflectance has R_g characteristics. As the powder depth increases, a depth is finally reached when the powder reflectance predominates over R_g. The limiting reflectance value R_∞, approached asymptotically with powder depth, is an intrinsic property of the powder and is, therefore, independent of R_g. The limiting reflectance R_∞ is obtained practically, both with powders and stacked leaves, at a thickness of a few millimeters (Wendlandt and Hecht, 1966). Reflectance R_∞ can be obtained directly in the laboratory by measuring the reflectance of leaves stacked sufficiently deep[1]

The reflectance R_∞ is also an important attribute of a thick plant canopy. Important information can be inferred from a measurement of plant-canopy reflectance even if little else is known about the canopy except that it is thick. A value R_∞ can be otained for a thick canopy by a remote sensor, provided that it is measured in spectral regions of atmospheric transparency. In the case of a powder, the value R_∞ can be used to infer the average particle size (Kortüm et al., 1963). The principal information from leaves, inferred from R_∞ measured in the 1.4 to 2.5 μm range, is also a characteristic linear quantity. This characteristic length correlates with leaf thickness and number of intercellular air spaces (Gausman et al., 1970).

SUMMARY

Spectral reflectance measurements centered at 1.25, 1.65, and 2.20 μm were investigated for discriminating among 24 different kinds of leaves. These three channels are located at the peaks of atmospheric windows III, IV, and V[2]. In accordance with a flat plate model introduced previously, a leaf can be regarded as a pile of N identical elementary compact layers separated by air spaces. The reflectance R_∞ of an infinite thickness of such leaves is a function of the calculated thickness D/N for a typical assumed elementary compact layer. The quantity D is the thickness of water with average absorptance, over the spectral range 1.4 to 2.5 μm, equivalent to that of the leaf.

---

[1] The term sufficiently deep applied to leaves over the spectral region 0.5 to 2.5 μm amounts at most to a stack of 8 leaves. In the visible and in the water absorption regions, a stable value of reflectance is attained when leaves are stacked to a depth of only on or two.

[2] Atmospheric windows I, II, III, IV, and V are located at the following respective spectral bands: 0.73 - 0.94, 0.94 - 1.13, 1.13 - 1.38, 1.38 - 1.90, and 1.90 - 2.70 μm (Plass, 1965).

Figure 1 displays R_∞ at the 1.65 µm wavelength as a function of N and D. The assumed functional relationship is specified by

$$R_\infty = 1 + \Sigma a_i (D/N)^i \qquad ,$$

where the coefficients a_i, (i=1, 2, ..., 5), are determined constants. The parameter N is the calculated number of identical elementary compact layers in the leaf and D is the thickness of water with absorptance equivalent to the leaf (equivalent water thickness). The curved surface of Fig. 1 is bounded by the planes R_∞= 5-, R_∞= 20, N = 1.0, N = 2.5, and D = 600 µm. The straight lines on the curved surface that pass through the reflectance axis are reflectance contours; the curved surface is developable. The reflectance surface of Fig. 1 can be visualized as a portion of a spiral ramp of increasing pitch centered around the reflectance axis. Such a surface exists for each wavelength. Reflectance diminishes as D increases when N is held constant. This limiting value of reflectance with increasing D is the component produced by the upper epicuticular surface of the leaf. Reflectances for virtually all 24 kinds of leaves discussed fall within plotting error on the curved surface in Fig. 1. Reflectance has meaning neither for N < 1 (VAI < 0), nor for D < 0. Reflectance for D = 0 is taken conventionally as unity.

The standard error of estimate is about 1% at 1.65 µm between observations and computed values. Similar values at 1.25 and 2.20 µm are not as promising; the standard errors of estimate are about 4% at these wavelengths. The quantities R_∞ and D can be regarded as abservables. The parameter N, a measure of the intercellular air spaces in the leaf, is more difficult to determine experimentally. Leaf reflectance R_∞ over the range 1.0 to 2.5 µm is a function of leaf water content and intercellular air space.

A surprisingly high reflectance was obtained for leaves around 1.00 µm but has no special value for the purpose of discriminating among different kinds of leaves. At 1.00 µm, many different kinds of leaves appear equally reflective. This ambiguity of information is a result of the high transparency of water in the 1.00 µm region of the spectrum. At 1.65 µm, however, water has appreciable absorption but the reflectance signal is still sufficiently high to be useful. Reflectance at 2.20 µm is characterized by relatively high liquid water absorption.

LITERATURE CITED

Allen, W. A., and A. J. Richardson. 1968. Interaction of light with a plant canopy, J. Opt. Soc. Amer. 58:1023-1028.

Allen, W. A., H. W. Gausman, A. J. Richardson, and J. R. Thomas. 1969. Interaction of isotropic light with a compact plant leaf. J. Opt. Soc. Amer. 59:1376-1379.

Allen, W. A., H. W. Gausman, and A. J. Richardson. 1970. Mean effective optical constants of cotton leaves. J. Opt. Soc. Amer. 60:542-547.

Gausman, H. W., W. A. Allen, R. Cardenas, and A. J. Richardson. 1970. Relation of light reflectance to histological and physical evaluations of cotton leaf maturity. Appl. Opt. 9:545-552.

Kortüm, G., W. Brown, and G. Herzog. 1963. Principles and techniques of diffuse reflectance spectroscopy. Angewandte Chemic. 2:333-404.

Plass, G. N. 1965. Atmospheric Phenomena, in: Handbook of Military Infrared Technology (W. L. Wolfe, Ed.) U.S. Govern. Printing Office, Washington, D.C. p. 177-279.

Wendlandt, W. W., and H. G. Hecht. 1966. Reflectance Spectroscopy, Interscience Publ., John Wiley & Sons, Inc., New York. p. 62.
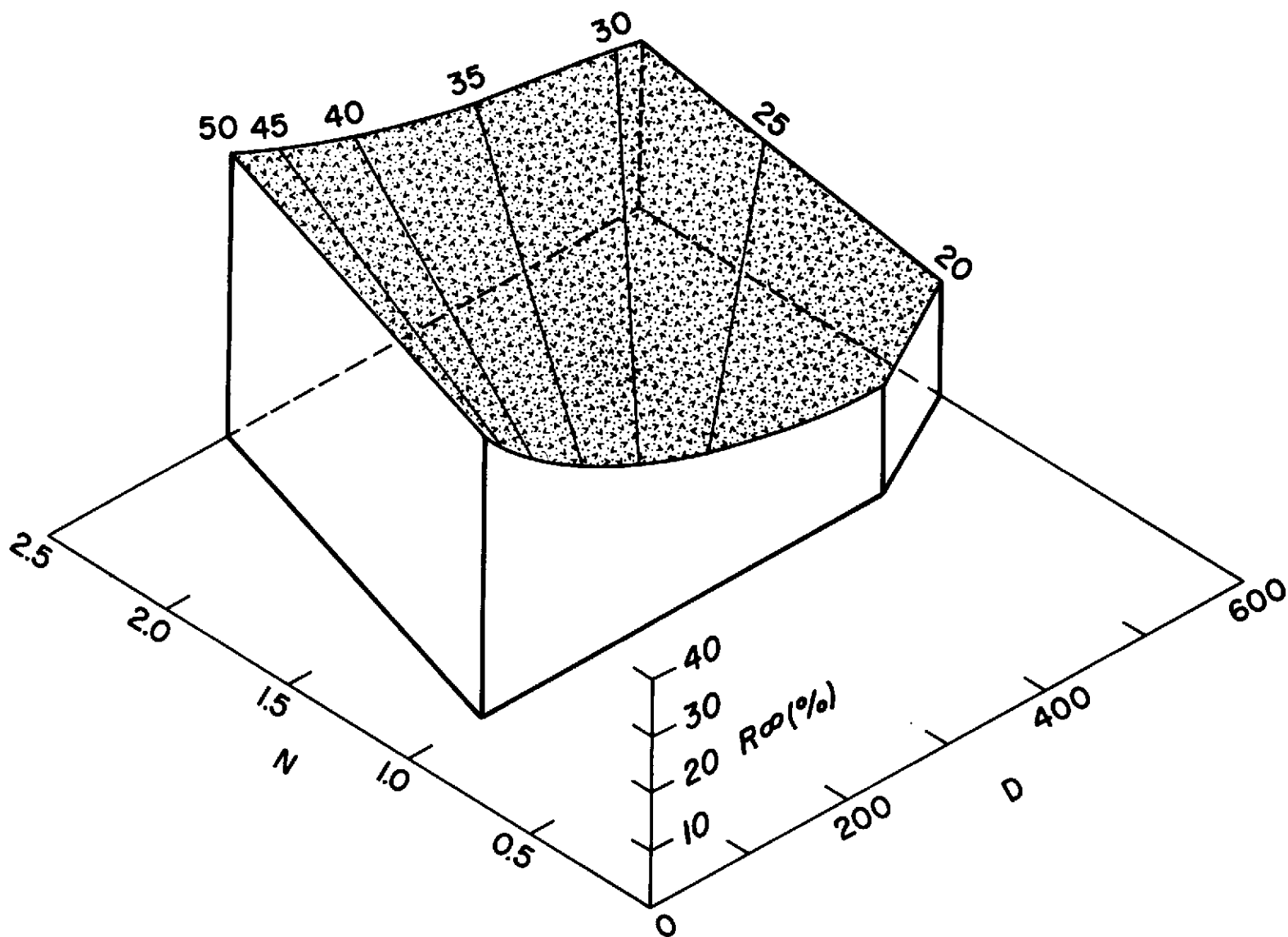
Fig. 1.--Infinite reflectance R∞ at the 1.65 μm wavelength plotted as a function of N and D for 24 different kinds of leaves. The parameter N is the calculated number of identical elementary compact layers in the leaf, and D is the water thickness with light absorptance equivalent to that of the leaf. The straight lines on the curved surface are reflectance contours.

THE LEAF MESOPHYLLS OF TWENTY CROPS, THEIR LIGHT SPECTRA,

AND OPTICAL AND GEOMETRICAL PARAMETERS

H. W. Gausman, W. A. Allen, C. L. Wiegand, D. E. Escobar,

R. R. Rodriguez, and A. J. Richardson

The following information is from SWC Research Report 423
(multilithed locally) of the same title, June 1971. 88 p.
These results were produced under Research Outline 57,
"Physiological and Histological Factors Affecting
the Spectra of Leaves."

INTRODUCTION

To interpret remote sensing data acquired from aircraft and spacecraft, the
reflectance produced by features on the earth's surface must be understood. The
specific problem in agriculture is the interpretation of reflectance produced by
vegetation, usually superimposed upon a soil background. Plant leaves yield
most of the signal measured by remote sensors in aircraft and spacecraft. There-
fore, their interaction with electromagnetic radiation must be understood.

The literature dealing with the interaction of light with plant leaves and
leaf mesophyll structure is reviewed in a Technical Monograph (Gausman et al.,
1970b) and is not repeated here. Attention is directed, however, to the research
of Aboukhaled (1966) who related the optical properties of leaves to their energy-
balance, photosynthesis, and water use efficiency.

Leaf mesophylls among 20 agricultural crops were compared with:
(1) spectrophotometrically measured percent reflectances and transmittances, and
calculated absorptances of the leaves over the 500- to 2500-nanometer (nm)[1] wave-
length interval (WLI), (2) percent leaf water (H_2O) contents, (3) leaf thickness
measurements, and (4) optical and geometrical leaf parameters.

MATERIALS AND METHODS

Twenty plant genera were selected that are presently economically important or
have the potential of becoming valuable in the Texas Lower Rio Grande Valley's
agricultural enterprise. Pigweed was included because it is used by some farmers
as a plow-under or green manure crop. Hence, it will be considered here as a
crop rather than a weed. The leaves of the selected genera varied in their leaf
mesophyll arrangements, leaf thicknesses and H_2O contents, and other structural
differences such as palisade layer arrangement. Leaf characteristics of the
20 crops and the families they represent are indicated in Table 1, and typical
photomicrographs of leaf transections are depicted in Fig. 1.

---

[1] Both nanometer (nm) and micrometer (μm) are used herein to denote spectral
wavelengths. A nm is 10^{-3} μm; a nm is comparable to a millimicron (mμ), and
a μm is equivalent to a micron (μ).

All plants were field grown in the summer of 1970 except that lettuce and onions were purchased in a fresh condition at a local market, soybeans and beans were grown in a greenhouse, and wheat was grown during the 1969 season.

Ten mature and healthy-appearing leaves were sampled from each of the 20 plant genera. Immediately after excision, leaves were wrapped in Saran or Glad-Wrap to minimize dehydration. Leaves were wiped with a slightly dampened cloth preceding spectrophotometric measurements to remove surface contaminants. Only one-half (split longitudinally) of the tubular onion leaf was used for spectrophotometric measurements.

A Beckman Model DK-2A spectrophotometer equipped with a reflectance attachment was used to measure spectral diffuse reflectance and transmittance on adaxial (top) surfaces of single leaves over the 500- to 2500-nm wavelength interval (WLI). Data have been corrected for decay of the MgO standard (Sanders and Middleton, 1953) to give absolute radiometric data. Absorptance was calculated from the absolute values as: Absorptance = 100 - (percent reflectance + percent transmittance).

Leaf thickness and diffuse reflectance and transmittance measurements and tissue fixation processing were completed within 6 hours after leaves were harvested or obtained for each genus.

Leaf thickness was measured with a linear displacement transducer and digital voltmeter (Heilman et al., 1968). Leaf area was determined with a planimeter, with the exceptions that areas per leaf of corn, sorghum, and sugarcane were calculated by the method of Slickter, Wearden, and Pauli (1961); area per leaf of cotton was calculated by Johnson's method (1967). Percent leaf H_2O content was determined on an oven-dry weight basis by drying at 68C for 72 hours and cooling in a desiccator before final weighing. Leaf thickness and H_2O content determinations were not made on wheat leaves.

Tissue pieces, taken near the center of leaves approximately one-half inch on either side of the midrib, were fixed in formalin-acetic acid-alcohol (FAA), dehydrated with a tertiary butanol series, embedded in paraffin, stained with either the safranin-fast green or the safranin-fast green-orange G combinations (Jensen, 1962), and transversally microtomed at 12 or 14 μ thicknesses. The relatively thick transverse sections were used to accentuate intercellular spaces, and thus enhance differences in mesophyll arrangements among the crops. Photomicrographs were obtained with a Zeiss Standard Universal Photomicroscope.

Spectrophotometrically measured reflectance and transmittance, and calculated absorptance of seven WL (550, 800, 1000, 1450, 1650, 1950, and 2200 nm) were analyzed for variance (Steel and Torrie, 1960); Duncan's Multiple Range Test (Duncan, 1955) was used to test differences among means of the seven WL at the 5% probability level. Standard deviation was calculated to compare the leaf reflectance, transmittance, and absorptance of the crops at the 550- and 1000-nm WL. Coefficients were calculated to evaluate the correlation of leaf thickness with leaf H_2O content. Coefficients were also obtained for correlations of reflectance, transmittance, and absorptance with g of H_2O/cm^3 of leaf tissue, leaf H_2O content on an oven-dry weight basis, and leaf thickness. Correlation coefficients of ± 0.775 were chosen as levels of significance because they account for 60% of the variation (r^2 x 100) between two series of variates. This is often referred to as the biological level of significance.

RESULTS AND DISCUSSION

H_2O content. Thick, succulent lettuce leaves had the highest H_2O content (97.0%), and dorsiventral avocado, orange, and peach, and compact sugarcane leaves had the lowest H_2O contents (range 60.6 to 72.4%). Compact corn, sorghum, and sugarcane leaves within the family Gramineae, and dorsiventral cotton and okra leaves within the family Malvaceae had similar H_2O contents.

Leaf thickness. Soybean, peach, pumpkin, and pigweed leaves were thinnest (range .140 to .170 mm) and sunflower, cantaloupe, lettuce, and onion leaves were thickest (range .407 to .978 mm). Within the families Malvaceae and Gramineae, cotton and okra, and sugarcane and sorghum were alike in leaf thickness.

Leaf thickness was poorly correlated with H_2O content. Highest coefficients accounted for only 31 to 34% (r^2 x 100) of the variation between leaf thicknesses and H_2O contents.

Reflectance, transmittance, and absorptance. The data (average of 10 replications) for the reflectance, transmittance, and absorptance of leaves for each crop at each of 41 wavelengths (50 nm increments over the 500- to 2500-nm WLI are given in Tables 2, 3, and 4, respectively.

Mean reflectances, transmittances, and absorptances for the 550-, 800-, 1000-, 1450-, 1650-, 1950-, and 2200-nm wavelengths (WL) were compared using Duncan's Multiple Range Test. Onion and bean leaves had the lowest (18.1%) and highest (31.6%) reflectances, respectively. Orange leaves had the lowest transmittance (20.4%) and soybean leaves had the highest transmittance (34.9%). Among the 20 crops, onion leaves had the highest absorptance of 57.4%, and sorghum and soybean leaves as a group had the lowest absorptances (36.7 to 36.9%).

Intensive study was given to the 550- and 1000-nm WL representing the visible (400 to 750 nm) and near-infrared (750 to 1350 nm) spectral regions, respectively. Data for lettuce leaves were omitted because the leaves sampled from the head of lettuce were immature.

550 nm. The mean reflectance of the crop leaves at the 550-nm WL was 13.3% ± 2.8% (one standard deviation). The majority of crops fell within the 13.3% ± 2.8% range except avocado and orange (8.9 and 10.2%, respectively), and corn, pepper, sorghum, bean, and sugarcane leaves (16.2 to 18.6%). High reflectances are indicative of low chlorophyll contents, and conversely low reflectances are indicative of high chlorophyll contents.

At the 550-nm WL, transmittances of orange, tomato, and avocado (1.9 to 5.5%) and okra, soybean, onion (14.8 to 18.8%) fell outside the 9.8% ± 4.2% range. In general, the spectral transmittance curves for all mature and healthy leaves were similar to their spectral reflectance curves over the 500- to 2500-nm WLI, but slightly lower in magnitude.

The mean absorptance for the crops at 550-nm WL was 76.9% ± 5.8%. Thirteen crops fell within the 76.9% ± 5.8% range. Sugarcane, onion, bean, and pepper leaves with low absorptance (69.2 to 70.6%) and peach, tomato, avocado, and orange leaves with high absorptance (82.9 to 87.9%) fell outside the 76.9% ± 5.8% range. The leaves with high absorptance had well-differentiated dorsiventral mesophylls with many chloroplasts in their palisade cells. Leaves with low absorptance had poorly differentiated mesophylls--less distinction between pali-sade and spongy parenchyma cells.

1000 nm. The 1000-nm WL can be used to evaluate the influence of leaf meso-phyll arrangement on near-infrared (750 to 1350 nm) light reflectance. The mean reflectance of the crop leaves at the 1000-nm WL was 48.0% ± 3.9%. The reflec-tance of onion (38.5%) and orange and bean (55.6 and 56.2%, respectively) fell outside the 48.0% ± 3.9% range. However, only one-half of the tubular onion leaf (split longitudinally) was used for spectrophotometric measurements. Thus, dis-counting onion as an unusual leaf, compact pigweed, corn, sugarcane, and soybean leaves had the lowest reflectances (45.1 to 46.0%), and dorsiventral bean, orange, and pepper leaves with very porous mesophylls had the highest reflectances (51.0 to 56.2%). A leaf with a compact mesophyll has lower light reflectance (fewer cell wall-air space interfaces for light refraction) and concomitantly higher transmittance than a leaf with a porous mesophyll.

At the 1000-nm WL, the mean transmittance of all crop leaves was 47.9% ± 3.7%. All crops fell within this range except orange and bean (38.9 and 42.0%, respec-tively) and soybean, pigweed, and onion (52.2 to 54.0%).

The mean absorptance of all crop leaves at the 1000-nm WL was 4.0% ± 1.7%. Soybean and bean leaves (1.8%) and sugarcane, tomato, and onion leaves (6.7 to 7.5%) fell outside the 4.0% ± 1.7% range. Soybean and bean leaves with low absorptance of near-infrared light have very porous mesophylls.

Correlations. Correlation coefficients equal to or larger than ± 0.775 are considered that accounted for at least 60% of the variation (0.775^2 x 100) between leaf thickness and reflectance; leaf thickness and absorptance; leaf H_2O content and reflectance, and leaf H_2O content and absorptance. Negative coefficients exceeding -0.775 were obtained for correlations between light reflectance and percent leaf H_2O content for sugarcane at 1450-, 1650-, and 2200-nm; for corn at 550- and 1450-nm; for pigweed at 1450-nm; and for tomato at 1450- and 2200-nm WL. Soybean was the only crop that had positive coefficients exceeding 0.775 for the correlation between reflectance and leaf thickness at the 550-, 800-, and 1000-nm WL, and a negative coefficient that exceeded -0.775 for the correlation between transmittance and leaf thickness at the 1000-nm WL. Soybean leaves also had large negative coefficients for the correlation between reflectance and leaf thickness at the 1450-, 1950-, and 2200-nm WL, and for the correlation between transmittance and leaf thickness at the 1450-, 1650-, 1950-, and 2200-nm WL. Peach, pigweed, tomato, bean, and onion crops also had high negative coefficients for the correlation between transmittance and leaf thickness at two or more of the 1450-, 1650-, 1950-, and 2200-nm WL. High positive coefficients were obtained for the correlation between leaf thickness and percent light absorptance for the soybean, peach, pigweed, bean, and onion crops at three or more of the 1450-, 1650-, 1950-, and 2200-nm WL.

It was thought that the amount of H_2O in the leaf tissue that was placed over the port of the spectrophotometer might have influenced the spectral energy measurements. Accordingly, g of H_2O/cm^3 of leaf tissue was calculated for each crop leaf used in this study except for wheat. Coefficients for the correlations of g of H_2O/cm^3 of leaf tissue with reflectance, transmittance, and absorptance are given in Table 7. There was no correlation between reflectance and g of H_2O/cm^3 of leaf tissue. With transmittance, coefficients above 0.775 occurred with only okra leaves at 1000-, 1450-, 1650-, 1950-, and 2200-nm WL. The correlation between absorptance and g of H_2O/cm^3 of leaf tissue gave high positive coefficients for okra leaves at 1450-, 1650-, and 2200-nm. Variability in g of H_2O/cm^3 among okra leaves had an important influence on their light absorptance and transmittance compared with the variability among leaves of the other crops.

Optical and Geometrical Leaf Parameters

The flat-plate model (Allen et al., 1969) for calculation of effective optical constants of leaves has been applied to leaves of the 20 crops. All available values of reflectance and transmittance for the leaves of 20 crops were reduced to average values $\bar{a}$, $\bar{b}$ at the 41 WL 0.50, 0.55, ..., 2.50 µm. Optical parameters a, b are defined elsewhere (Allen and Richardson, 1968). Thirteen data points in the vicinity of plant pigment and H_2O absorption bands were deleted in advance (WL 0.50, 0.55, 0.60, 0.65, 0.70, 1.40, 1.45, 1.50, 1.90, 1.95, 2.00, 2.45, and 2.50 µm) from calculations of refractive indices, n. Such editing is justified because determination of the index of refraction n is weak in the vicinity of absorption bands.

Figures 2a, 2b, ..., 2t display the 95% confidence bands of the dispersion curves. Computational and statistical procedures used have appeared elsewhere (Allen et al., 1970 a, b; Freeze, 1964). Statistically, 95% of experimental points fall within the confidence limits. The dispersion curves of Figs. 2a, 2b, ..., 2t assumed to be cubics in wavelength λ, are expressed by the relation

$$n = \Sigma \ a_i \lambda^i \ , \tag{1}$$

where the coefficients a_0, ..., a_3 were determined by regression. Table 5 contains the coefficients of Eq. (1) for all data discussed.

The dispersion curves of most of the leaves illustrated in Fig. 2 are remarkably similar. With the exceptions of onion (H), pigweed (J), and lettuce (S), the dispersion curves are characterized by similar shapes and relatively close confidence bands. The exceptions mentioned are cases where the flat-plate model appears not to apply. However, the onion, pigweed, and lettuce leaves indicated as exceptions were different from the other crop leaves--only one-half of the tubular onion leaves was used, lettuce leaves were immature, and veins of pigweed leaves (Fig. 1) are surrounded by large, cubical, parenchymatous cells.

Table 6 includes the leaf parameters that relate to the amount of H_2O and air in the leaf. The quantity D in the flat-plate model is the equivalent thickness of pure liquid H_2O necessary to produce the observed leaf absorption. The quantity N in the model is the number of compact layers into which D must be subdivided in order to achieve the observed partition of energy between reflectance and transmittance. The infinite reflectance R_∞ at 1.65 μm, produced by leaves piled sufficiently deep, is listed in column 5 of Table 6. The quantity R_∞ can be measured directly; the number listed in Table 6, however, is a calculated value obtained by techniques previously described (Allen and Richardson, 1968). The entries of Table 6 were obtained by adjusting the quantity D, over the spectral range 1.4 to 2.5 μm, to achieve the best fit of the leaf absorption k to the absorption k_o for pure liquid H_2O. Column 6 of Table 6 is the standard error (S.E.) calculated from the relation

$$S.E. = \{\Sigma[\log (k/k_o)]^2/[n(n-1)]\}^{\frac{1}{2}} \tag{2}$$

The summation in Eq. (2) includes the 23 values at 0.05-μm intervals over the range 1.4 to 2.5 μm. This quantity S.E. (standard error) can be considered a figure of merit because S.E. would vanish entirely if the model was exact and the material was H_2O. The quantities D and S.E. in Table 6 are positively correlated (r = 0.728).

The quantities D/N and R_∞ are strongly correlated. Figure 3 indicates the relationship. The quantity D and the leaf thickness are also correlated with R_∞. The thinner the leaf, the greater will be reflectance produced by a pile of such leaves. This fact has important implications in the interpretation of remote sensing data.

Table 7 is a compilation of the mean absorption spectra in cm^{-1} units over the range 1.4 to 2.5 μm for the leaves of 20 crops. These values correlate (r = 0.998) with those previously obtained (Allen et al., 1970 b) on other leaves of agricultural interest. The published values for pure liquid H_2O are also presented in Table 10 for comparative purposes. Figures 4 and 4a are comparisons of experimental and computed values of leaf H_2O thickness obtained by procedures previously discussed (Gausman et al., 1970 a). The shaded portions on the bar graphs represent plus or minus one standard deviation. All data are plotted for the laboratory H_2O determinations that were made on entire leaves. Sugarcane, corn, sorghum, and wheat leaves are not included in Fig. 4 and 4a. Their thickness and H_2O content determinations in the laboratory were made on sections of entire leaves. With the exception of pumpkin, avocado, okra, tomato, cantaloupe, and lettuce, there is no statistically significant difference between H_2O obtained experimentally and H_2O determined theoretically. However, none of the six exceptions exhibit a highly statistically significant difference (unpaired t test) between observed and computed values for leaf H_2O.

Table 8 includes the absorption spectra, over the 0.5- to 1.3-μm range, for 11 kinds of plant leaves (first 11 entries) reported in an earlier paper (Gausman et al., 1970 b) plus the 20 (last 20 entries) crop leaves introduced in the present paper. Note that corn appears twice--once in the earlier work and then in the 20 leaves reported in this paper.

SUMMARY

Thick, succulent lettuce leaves had the highest H_2O content (97.0%), and dorsiventral avocado, orange, and peach, and compact sugarcane leaves had the lowest H_2O contents (60.6 to 72.4%).

Soybean, peach, pumpkin, and pigweed leaves were thinnest (.140 to .170 mm) and sunflower, lettuce, and onion leaves were thickest (.407 to .978 mm).

The mean reflectances of most crops at 550 nm fell within the 13.3 ± 2.8% (standard deviation) range except avocado and orange (8.9 and 10.2%, respectively), and corn, pepper, sorghum, bean, and sugarcane leaves (16.2 to 18.6%). The spectral transmittance curves were similar to their spectral reflectance curves, but slightly lower in magnitude. Leaves with high absorptance had well-differentiated dorsiventral mesophylls with many chloroplasts in their palisade cells. Leaves with low absorptance had poorly differentiated mesophylls.

At the 1000-nm wavelength, pigweed, corn, sugarcane (compact mesophylls), and soybean leaves had the lowest reflectances (45.1 to 46.0%) and dorsiventral bean, orange, and pepper leaves with very porous mesophylls had the highest reflectances (51.0 to 56.2%). Relative to absorptance, values for soybean and bean leaves (1.8%) and sugarcane, tomato, and onion leaves (6.7 to 7.5%) fell outside of the 4.0% (mean) ± 1.7% (standard deviation) range.

Effective optical constants were calculated. The dispersion curves of most of the crop leaves were similar. Sixteen crops were analyzed to obtain geometrical parameters that specify the amount of H_2O and air in the leaf. Statistically, there was no highly significant difference between H_2O obtained experimentally and water determined theoretically.

LITERATURE CITED

Aboukhaled, A. 1966. Optical properties of leaves in relation to their energy-balance, photosynthesis, and water use efficiency. Ph.D. Thesis, University of California Library, Davis. 139 p.

Allen, W. A., H. W. Gausman, and A. J. Richardson. 1970 a. Mean effective optical constants of cotton leaves. J. Opt. Soc. Amer. 60:542-547.

Allen, W. A., H. W. Gausman, A. J. Richardson, and J. R. Thomas. 1969. Interaction of isotropic light with a compact leaf. J. Opt. Soc. Amer. 59:1376-1379.

Allen, W. A., H. W. Gausman, A. J. Richardson, and C. L. Wiegand. 1970 b. Mean effective optical constants of thirteen kinds of plant leaves. Appl. Opt. 9:2573-2577.

Allen, W. A., and A. J. Richardson. 1968. Interaction of light with a plant canopy. J. Opt. Soc. Amer. 58:1023-1028.

Curcio, J. A., and C. C. Petty. 1951. The near infrared absorption spectrum of liquid water. J. Opt. Soc. Amer. 41:302-304.

Duncan, D. B. 1955. Multiple range and multiple F tests. Biometrics 11:1-42.

Freeze, F. 1964. Linear regression methods for forest research. Forest Products Lab., Madison, Wisc. p. 81.

Gausman, H. W., W. A. Allen, R. Cardenas, and A. J. Richardson. 1970 a. Relation of light reflectance to histological and physical evaluations of cotton leaf maturity. Appl. Opt. 9:545-552.

Gausman, H. W., W. A. Allen, Marcia Schupp, C. L. Wiegand, D. E. Escobar, and R. R. Rodriguez. 1970 b. Reflectance, transmittance, and absorptance of light of leaves for eleven plant genera with different leaf mesophyll arrangements. Texas A&M Technical Monograph No. 7. 38 p.

Heilman, M. D., C. L. Gonzalez, W. A. Swanson, and W. J. Rippert. 1968. Adaptation of a linear transducer for measuring leaf thickness. Agron. J. 60:578-579.

Jensen, W. A. 1962. Botanical histochemistry. W. H. Freeman & Co., San Francisco, Calif. 408 p.

Johnson, R. E. 1967. Comparison of methods for estimating cotton leaf areas. Agron. J. 59:493-494.

Sanders, C. L., and E. E. K. Middleton. 1953. The absolute spectral diffuse reflectance of magnesium oxide in the near infrared. J. Opt. Soc. Amer. 43:58.

Slickter, F. C., S. Wearden, and A. W. Pauli. 1961. Leaf area determination in grain sorghum. Agron. J. 53:187-188.

Steel, R. G. D., and J. H. Torrie. 1960. Principles and procedures of statistics. McGraw-Hill, New York. 481 p.

Table 1. Common, scientific, and family names; leaf mesophyll arrangements; and structural characteristics of plant leaves used in this study. Common names are used in the text.

Common name[1]	Scientific name[2]	Family name	Mesophyll arrangement[3]	Additional structural characteristics
Avocado	Persea americana Mill.	Lauraceae	Dorsiventral	Thick cuticle, multiple palisade layers, long and narrow palisade cells.
Bean	Phaseolus vulgaris L.	Leguminosae	Dorsiventral	Very porous mesophyll
Cantaloupe	Cucumis melo L. var. cantalupensis Naud.	Cucurbitaceae	Dorsiventral	Multiple palisade layers, hairs lower epidermis.
Corn	Zea mays L.	Gramineae	Compact	Bulliform cells, hairs upper epidermis
Cotton	Gossypium hirsutum L.	Malvaceae	Dorsiventral	Glandular hairs, nectaries, lysigenous glands.
Lettuce	Lactuca sativa L.	Compositae	Compact	Large cells, porous mesophyll.
Okra	Hibiscus esculentus L.	Malvaceae	Dorsiventral	Well differentiated, porous mesophyll.
Onion	Allium cepa L.	Amaryllidaceae	Dorsiventral	Tubular leaves.
Orange	Citrus sinensis (L.) Osbeck	Rutaceae	Dorsiventral	Thick cuticle with wax layers, multiple palisade layers, lysigenous cavities.
Peach	Prunus persica (L.) Batsch	Rosaceae	Dorsiventral	Multiple palisade layers, porous mesophyll
Pepper	Capsicum annuum L. and other spp.	Solanaceae	Dorsiventral	Druse crystals
Pigweed	Amaranthus retroflexus L.	Amaranthaceae	Compact	Druse crystals, veins surrounded by large, cubical, parenchymatous cells

VI.9

Table 1. (Continued)

Common name[1]	Scientific name[2]	Family name	Mesophyll arrangement[3]	Additional structural characteristics
Pumpkin	Cucurbita pepo L.	Cucurbitaceae	Dorsiventral	Multiple palisade layers, hairs upper, and lower epidermis
Sorghum	Sorghum bicolor (L.) Moench	Gramineae	Compact	Bulliform cells
Soybean	Glycine max (L.) Merr.	Leguminosae	Dorsiventral	Porous mesophyll
Sugarcane	Saccharum officinarum L.	Gramineae	Compact	Bulliform cells
Sunflower	Helianthus annuus L.	Compositae	Isolateral	Hairs upper and lower epidermis
Tomato	Lycopersicon esculentum Mill.	Solanaceae	Dorsiventral	Hairs upper and lower epidermis, glandular hairs lower surface
Watermelon	Citrullus lanatus (Thunb.) Mansf.	Cucurbitaceae	Dorsiventral	Multiple palisade layers, glandular hairs lower surface
Wheat	Triticum aestivum L.	Gramineae	Compact	Bulliform cells

[1]   Generic names used as common names are not italicized or capitalized in the text.

[2]   Names are those used by New Crops Research Branch (Dr. Edward E. Terrell), ARS, USDA, Beltsville, Maryland.

[3]   Arbitrary definitions of mesophyll arrangements used herein are: dorsiventral, a usually porous (many intercellular air spaces) mesophyll with palisade parenchyma cells in its upper and spongy parenchyma cells in its lower part; compact mesophyll with little intercellular air space and no differentiation into palisade and spongy parenchyma cells; isolateral, tending to have long narrow cells throughout a porous mesophyll.

Table 2. Average percent reflectances of top leaf surfaces of 10 leaves for each of 20 crops for 41 WL (nm) over the 500- to 2500-nm WLI.

Crop	500	550	600	650	700	750	800	850	900	950	1000	1050	1100	1150
Avocado	8.2	8.9	6.8	7.2	26.6	47.9	50.4	50.3	50.1	49.4	49.7	49.7	49.3	47.1
Bean	15.2	18.5	12.0	10.7	37.3	55.7	56.9	56.9	56.5	55.8	56.2	56.6	56.0	53.6
Cantaloupe	11.6	12.7	10.0	9.9	28.6	46.1	47.7	47.7	47.5	46.8	47.3	47.6	47.0	44.6
Corn	12.7	16.2	12.0	9.3	24.8	45.4	46.3	46.4	46.2	45.5	45.7	46.0	45.5	43.3
Cotton	9.8	11.8	8.0	7.7	28.6	45.8	47.2	47.2	46.9	46.2	46.6	47.0	46.4	44.2
Lettuce	27.6	30.3	26.8	23.6	33.7	37.6	37.6	37.5	36.7	34.6	35.3	36.3	35.0	30.3
Okra	10.8	12.9	9.5	9.2	29.0	47.2	49.0	49.2	49.0	48.4	48.7	49.0	48.5	46.6
Onion	10.1	11.6	8.5	8.1	25.0	39.4	40.5	40.4	39.6	37.7	38.5	39.4	38.2	33.3
Orange	8.9	10.2	7.2	7.1	28.9	53.2	55.8	55.9	55.7	55.2	55.6	55.7	55.4	53.1
Peach	9.6	10.9	8.3	8.6	29.1	47.7	49.5	49.5	49.3	49.0	49.3	49.4	49.1	47.7
Pepper	12.8	16.8	11.0	9.3	32.8	50.5	51.6	51.6	51.4	50.7	51.0	51.4	40.8	48.5
Pigweed	10.9	12.4	9.3	9.0	26.6	43.9	45.7	45.5	45.4	44.8	45.1	45.1	44.6	42.8
Pumpkin	10.2	11.8	8.9	10.6	29.1	44.9	46.4	46.3	46.2	45.8	46.7	46.2	45.7	44.2
Sorghum	15.0	17.2	13.3	11.3	28.2	45.8	47.3	47.4	47.3	46.9	47.0	47.0	46.8	45.5
Soybean	10.9	13.1	8.7	7.9	28.8	45.6	46.6	46.5	46.3	45.9	46.0	46.2	45.8	44.5
Sugarcane	15.9	18.6	13.4	11.4	29.9	45.8	46.9	46.8	46.4	45.6	45.7	46.0	45.4	42.9
Sunflower	9.6	11.0	8.4	8.5	27.5	45.4	47.3	47.3	47.1	46.5	46.9	47.2	46.6	44.1
Tomato	10.0	11.1	8.6	8.6	25.9	46.6	48.4	48.6	48.5	47.8	48.3	48.6	48.0	45.4
Watermelon	11.9	14.4	10.7	9.9	30.4	45.6	46.8	47.0	47.0	46.3	46.8	47.2	46.6	44.5
Wheat	10.3	13.4	9.6	7.7	27.3	50.2	51.5	51.7	51.4	51.0	51.2	51.5	51.0	48.9

Table 2. Continued.

Crop	1200	1250	1300	1350	1400	1450	1500	1550	1600	1650	1700	1750	1800	1850
Avocado	46.8	47.1	45.2	41.0	26.3	19.2	23.1	29.0	32.5	34.1	33.2	31.2	30.3	23.1
Bean	53.5	53.6	50.8	44.9	25.6	18.5	24.6	33.1	38.4	40.9	40.6	37.5	35.2	24.2
Cantaloupe	44.3	44.5	41.9	36.7	20.6	14.8	19.1	25.5	29.9	32.0	31.5	28.9	27.4	19.4
Corn	43.2	43.5	41.8	38.3	23.4	16.8	21.0	27.1	31.0	32.9	32.6	30.1	28.8	23.1
Cotton	44.0	44.2	42.0	37.5	21.7	15.2	19.6	26.2	30.4	32.3	31.9	29.4	27.9	19.9
Lettuce	29.6	29.8	26.4	21.4	11.8	9.1	10.4	13.0	15.4	16.8	16.8	15.0	13.8	10.6
Okra	46.2	46.4	44.5	40.4	25.6	18.1	22.3	28.8	33.0	35.0	34.5	32.3	30.8	23.0
Onion	32.5	32.9	29.0	23.0	10.3	6.8	8.4	12.0	15.1	17.2	17.0	14.6	13.1	9.4
Orange	52.8	53.0	51.2	47.1	31.2	22.3	26.6	33.3	37.6	39.8	39.0	36.6	35.4	27.8
Peach	47.7	47.8	46.5	43.0	30.3	24.3	28.8	34.3	37.5	38.9	38.0	36.4	35.6	27.4
Pepper	48.4	48.6	46.4	41.7	25.0	17.6	22.6	30.0	34.7	36.9	36.6	33.9	32.2	23.4
Pigweed	42.5	42.6	40.6	36.2	21.5	15.6	19.9	26.1	30.0	31.8	31.3	29.1	27.6	19.5
Pumpkin	44.0	44.0	42.1	37.4	24.6	19.0	23.6	29.2	32.6	34.6	33.1	31.3	29.5	21.6
Sorghum	45.3	45.4	44.3	41.7	30.9	24.7	28.2	33.2	36.1	37.4	36.9	35.3	34.2	28.2
Soybean	44.5	44.4	43.1	40.1	27.7	21.8	26.1	31.9	35.2	36.6	36.3	34.5	33.3	25.5
Sugarcane	42.6	42.7	40.5	35.9	20.7	14.4	18.3	24.2	28.0	30.4	30.0	27.5	25.9	18.8
Sunflower	44.0	44.2	41.7	36.4	20.4	14.3	18.4	24.9	29.3	31.3	30.5	28.1	26.6	18.9
Tomato	45.2	45.4	42.7	37.3	20.5	14.4	18.9	25.6	30.0	32.1	31.7	28.9	27.3	19.1
Watermelon	44.4	44.5	42.2	37.5	22.0	16.6	21.2	27.4	31.2	33.0	32.4	29.9	28.7	20.5
Wheat	48.8	49.2	47.2	43.5	27.7	21.7	26.5	32.7	36.4	38.2	37.4	35.2	34.3	27.3

Table 2. Continued.

Crop	1900	1950	2000	2050	2100	2150	2200	2250	2300	2350	2400	2450	2500
Avocado	9.7	7.5	10.2	13.2	15.7	18.1	19.5	17.4	14.2	11.6	9.5	7.8	7.0
Bean	8.0	6.0	9.4	14.1	18.9	22.6	24.0	21.5	17.2	12.8	9.5	7.2	5.9
Cantaloupe	8.1	6.9	8.6	11.1	14.2	16.5	17.5	15.7	12.6	9.9	8.0	6.6	6.0
Corn	7.9	7.2	9.7	12.6	15.8	18.3	19.8	17.6	14.4	11.6	9.3	7.5	6.7
Cotton	7.6	6.0	7.9	10.8	14.1	16.7	16.8	15.8	12.5	9.8	7.5	6.0	5.3
Lettuce	6.2	5.6	6.4	7.4	8.4	9.2	9.4	8.8	7.7	6.6	5.8	5.2	4.9
Okra	9.4	7.0	9.4	12.8	16.3	19.0	20.2	18.3	14.9	11.8	9.3	7.3	6.5
Onion	4.9	4.4	4.9	5.6	6.6	7.6	8.0	7.4	6.3	5.4	4.8	4.6	4.5
Orange	11.4	8.6	12.0	15.8	19.2	22.1	23.6	21.2	17.4	14.1	11.1	9.0	7.8
Peach	12.5	10.5	14.4	18.3	21.6	24.3	25.7	23.1	19.3	16.0	13.2	10.7	9.5
Pepper	8.5	6.6	9.4	13.2	17.1	20.2	21.5	19.3	15.4	11.7	8.9	6.8	5.7
Pigweed	7.7	5.8	8.0	11.0	14.3	16.8	17.8	15.9	12.9	9.9	7.6	5.9	5.1
Pumpkin	9.0	7.1	10.6	14.0	17.2	19.5	20.9	18.2	14.9	12.1	9.6	7.6	7.0
Sorghum	14.1	12.0	15.6	19.1	22.1	24.5	25.8	23.7	20.4	17.4	14.7	12.4	11.3
Soybean	10.2	8.1	12.1	16.6	20.6	23.5	24.8	22.7	19.1	15.4	12.1	9.5	8.2
Sugarcane	7.6	6.2	8.2	10.5	13.1	15.5	16.4	14.5	11.8	9.5	7.8	6.5	6.0
Sunflower	8.0	6.5	8.1	10.4	13.2	15.4	16.2	14.4	11.6	9.3	7.6	6.5	6.0
Tomato	7.3	6.0	7.9	10.7	13.7	16.3	17.3	15.3	12.2	9.5	7.4	6.0	5.4
Watermelon	8.0	6.9	9.1	12.1	15.3	17.7	18.8	16.8	13.5	10.8	8.5	6.9	6.2
Wheat	9.7	9.0	12.8	16.6	20.2	22.6	24.4	21.7	18.2	15.0	12.2	9.7	8.5

Table 3. Average percent transmittances of top leaf surfaces of 10 leaves for each of 20 crops for 41 WL (nm) over the 500- to 2500-nm WLI.

Crop	500	550	600	650	700	750	800	850	900	950	1000	1050	1100	1150
Avocado	2.3	4.1	1.4	3.1	24.9	42.4	44.8	45.4	45.5	45.5	46.1	46.6	46.3	45.0
Bean	6.9	10.9	5.5	3.6	26.6	40.9	42.0	42.2	42.0	41.5	42.2	42.4	41.9	39.9
Cantaloupe	4.9	8.7	3.9	2.4	27.5	46.3	48.1	48.6	48.6	48.0	48.8	49.5	49.0	46.5
Corn	3.7	9.8	3.7	0.7	22.6	48.9	50.5	50.9	51.1	50.7	51.2	51.7	51.6	49.7
Cotton	8.1	13.1	7.0	4.2	30.6	47.8	49.1	49.4	49.3	39.0	49.4	49.9	49.6	47.8
Lettuce	38.4	44.3	39.5	34.0	49.5	55.3	55.6	55.5	54.8	52.6	53.7	54.9	53.7	48.2
Okra	5.9	14.8	5.8	4.1	27.1	44.6	46.4	46.7	46.9	46.7	47.3	47.8	47.6	46.0
Onion	11.7	18.8	10.8	6.6	35.8	54.3	55.7	55.7	55.0	52.9	54.0	55.4	54.1	48.2
Orange	0.7	1.9	0.5	0.5	17.6	36.0	38.2	38.6	38.6	38.4	38.9	39.5	39.3	37.7
Peach	3.5	6.2	2.6	2.8	27.1	45.5	47.3	47.6	47.7	47.6	47.9	48.3	48.1	47.1
Pepper	6.9	12.6	6.4	3.1	28.4	44.8	46.2	46.5	46.4	46.0	46.5	47.0	46.7	44.9
Pigweed	5.4	9.5	3.7	2.7	28.6	49.2	51.6	52.0	52.0	51.9	52.4	52.9	52.6	51.0
Pumpkin	5.6	8.8	4.3	5.6	30.0	47.1	48.9	49.4	49.6	49.5	50.1	50.6	50.4	49.1
Sorghum	5.0	9.0	4.2	2.1	24.4	46.7	49.1	49.6	49.8	49.9	50.3	50.8	50.7	49.8
Soybean	10.0	15.6	8.7	5.4	32.5	50.0	51.4	51.8	51.9	51.8	52.2	52.6	52.4	51.4
Sugarcane	7.5	12.2	6.9	4.1	26.7	45.0	46.9	47.2	47.3	46.9	47.6	48.1	47.9	46.0
Sunflower	6.3	9.1	5.7	5.1	27.8	46.4	48.4	48.8	48.8	48.4	49.1	49.7	49.2	46.8
Tomato	2.6	5.5	1.5	0.9	23.6	41.9	43.8	44.3	44.4	44.0	44.7	45.3	44.9	42.6
Watermelon	5.2	9.6	4.3	2.0	28.7	45.2	46.6	47.1	47.4	47.2	47.9	48.5	48.2	46.3
Wheat	1.9	5.8	2.1	0.7	20.3	41.8	43.4	43.9	44.1	43.9	44.6	45.2	45.1	43.4

Table 3. Continued.

Crop	1200	1250	1300	1350	1400	1450	1500	1550	1600	1650	1700	1750	1800	1850
Avocado	45.1	45.6	44.0	39.4	26.1	20.5	25.6	32.0	35.8	37.6	37.0	35.4	34.1	25.1
Bean	40.0	40.2	38.1	33.5	17.3	11.8	17.3	24.9	29.6	32.2	32.2	29.5	27.9	18.5
Cantaloupe	46.6	47.0	44.5	39.2	20.6	14.6	19.7	28.2	33.7	36.6	36.5	33.6	32.0	21.8
Corn	49.8	50.5	49.0	45.9	28.8	20.5	26.8	35.1	40.2	43.0	43.1	40.6	39.6	32.0
Cotton	47.9	48.3	46.6	42.7	26.7	19.6	25.4	33.2	38.0	40.4	40.3	38.1	37.0	27.1
Lettuce	47.4	48.0	43.7	35.9	14.6	6.2	11.1	19.9	26.6	30.5	31.0	27.0	24.4	15.2
Okra	46.1	46.5	45.0	41.5	26.8	19.3	24.5	32.0	36.6	39.2	39.1	37.0	35.9	27.3
Onion	47.4	48.1	43.4	35.1	12.5	4.1	8.7	17.5	24.3	28.4	28.8	24.7	22.0	13.1
Orange	37.6	38.2	36.9	33.7	20.1	13.0	17.2	23.5	27.6	30.0	29.6	27.6	26.9	20.2
Peach	47.3	47.7	46.7	43.9	31.5	26.2	31.3	37.4	40.9	42.8	42.3	40.9	40.6	31.7
Pepper	45.0	45.4	43.7	39.8	23.9	16.9	22.7	30.4	35.3	37.8	37.8	35.4	34.0	25.0
Pigweed	51.2	51.6	49.9	45.8	29.9	23.1	29.1	37.1	41.9	44.5	44.4	42.2	41.0	30.3
Pumpkin	49.3	49.7	48.2	43.7	29.5	23.8	29.7	36.8	41.2	43.5	43.1	41.1	39.5	29.2
Sorghum	50.0	50.4	49.6	47.3	35.1	28.2	33.2	39.9	44.0	46.2	46.3	44.8	44.1	36.6
Soybean	51.6	51.9	50.8	48.0	34.9	28.7	34.3	41.3	45.3	47.4	47.5	45.8	44.8	35.5
Sugarcane	46.0	46.5	44.9	40.8	24.6	17.3	23.0	30.7	35.7	38.5	38.4	36.0	34.8	25.1
Sunflower	46.8	47.3	45.1	40.0	22.2	15.0	21.0	29.1	34.4	37.0	36.6	34.0	32.7	22.5
Tomato	42.6	43.0	40.7	35.9	18.6	12.3	17.9	25.7	30.8	33.4	33.3	30.5	29.1	19.6
Watermelon	46.5	47.0	45.0	40.7	24.1	18.3	24.3	31.8	36.5	38.8	38.6	36.2	35.3	25.3
Wheat	43.6	44.2	42.8	39.7	24.3	18.5	23.9	30.7	34.7	36.8	36.3	34.3	33.7	26.7

Table 3. Continued.

Crop	1900	1950	2000	2050	2100	2150	2200	2250	2300	2350	2400	2450	2500
Avocado	8.8	6.7	12.3	17.3	21.2	24.0	25.2	23.3	19.8	16.2	12.1	9.8	6.9
Bean	3.7	1.9	5.4	10.3	15.3	18.6	19.7	18.4	15.2	11.3	7.8	4.9	3.5
Cantaloupe	4.2	2.1	6.0	11.5	16.9	20.5	21.8	20.1	16.4	12.1	8.1	5.0	3.4
Corn	6.5	5.0	11.8	18.6	24.6	28.5	30.3	28.3	24.4	19.9	14.8	9.7	7.0
Cotton	7.4	4.5	10.2	16.8	22.6	26.2	27.7	26.1	22.5	17.9	12.9	8.8	6.6
Lettuce	2.1	0.5	1.7	4.5	8.8	12.2	13.5	12.2	9.0	5.6	2.9	1.4	0.8
Okra	8.6	5.2	10.7	16.8	22.2	25.7	27.1	25.7	22.2	18.1	13.6	9.7	7.5
Onion	1.2	0.5	0.6	2.5	6.0	9.0	10.2	8.8	6.0	3.1	1.2	0.5	0.5
Orange	5.3	2.6	6.2	10.3	14.1	16.8	18.1	16.5	13.6	10.7	7.8	5.1	3.8
Peach	12.6	10.4	17.3	23.4	28.1	31.2	32.5	30.6	27.2	23.6	19.1	14.7	12.2
Pepper	6.3	3.8	8.9	15.0	20.5	24.2	25.6	24.2	20.8	16.4	11.9	8.1	6.0
Pigweed	9.9	6.9	13.5	20.7	26.8	30.7	32.2	30.6	26.9	22.2	17.0	12.4	9.6
Pumpkin	10.2	8.3	14.9	21.4	26.8	30.1	31.3	29.4	25.8	21.5	16.7	11.9	10.2
Sorghum	15.4	12.2	19.9	26.7	31.9	35.3	36.9	35.4	32.1	28.2	23.6	18.4	15.6
Soybean	14.6	11.7	19.3	26.7	32.7	36.3	37.7	36.3	33.0	28.6	23.5	18.5	15.8
Sugarcane	6.7	4.0	9.3	15.1	20.0	23.7	25.0	23.0	19.3	15.1	10.8	7.0	4.9
Sunflower	6.0	2.3	6.5	11.9	17.1	20.5	21.6	19.7	16.1	12.1	8.2	5.0	3.3
Tomato	3.7	1.8	5.4	10.2	15.2	18.6	19.8	18.2	14.8	10.8	7.2	4.3	3.0
Watermelon	6.1	4.6	10.1	16.1	21.3	24.7	26.1	24.4	20.7	16.6	12.2	8.2	6.3
Wheat	6.0	5.2	10.7	15.9	20.4	23.3	24.7	22.8	19.6	16.2	12.3	8.6	6.5

Table 4. Average percent absorptances for top leaf surfaces of 10 leaves for each of 20 crops for 41 WL (nm) over the 500- to 2500-nm WLI.

Crop	500	550	600	650	700	750	800	850	900	950	1000	1050	1100	1150
Avocado	89.5	87.0	91.8	89.1	48.5	9.6	4.7	4.2	4.3	5.0	4.2	3.6	4.4	7.9
Bean	77.9	70.6	82.4	85.7	36.1	3.4	1.2	1.0	11.5	2.7	1.8	1.0	2.1	6.5
Cantaloupe	83.5	78.6	86.0	87.7	43.8	7.6	4.2	3.7	3.9	5.2	3.9	2.9	4.0	9.0
Corn	83.6	74.0	84.3	90.0	52.6	5.7	3.2	2.7	2.7	3.9	3.2	2.3	2.8	7.0
Cotton	82.1	75.1	85.0	88.1	40.8	6.4	3.7	3.4	3.8	4.8	4.0	3.2	4.1	7.9
Lettuce	34.0	25.4	33.8	42.4	16.8	7.1	6.8	7.0	8.5	12.8	11.0	8.8	11.3	21.5
Okra	83.3	72.2	84.7	86.7	43.8	8.2	4.5	4.1	4.1	4.9	4.0	3.2	4.0	7.4
Onion	78.2	69.7	80.7	85.3	39.3	6.2	3.8	4.0	5.4	9.4	7.5	5.2	7.7	18.4
Orange	90.4	87.9	92.3	92.4	53.5	10.8	6.0	5.6	5.7	6.4	5.5	4.8	5.3	9.2
Peach	86.8	82.9	89.1	88.5	43.8	6.8	3.2	2.9	3.0	3.4	2.8	2.3	2.8	5.2
Pepper	80.3	70.6	82.6	87.5	38.8	4.7	2.2	1.9	2.2	3.3	2.4	1.6	2.5	6.5
Pigweed	83.7	78.2	87.0	88.3	44.9	6.9	2.7	2.5	2.6	3.4	2.5	2.0	2.7	6.2
Pumpkin	84.2	79.5	86.8	83.8	40.9	8.0	4.7	4.3	4.2	4.6	3.2	3.1	4.0	6.8
Sorghum	80.1	73.8	82.6	86.6	47.4	7.5	3.6	3.0	2.8	3.3	2.7	2.2	2.5	4.7
Soybean	79.1	71.3	82.7	86.6	38.7	4.4	2.0	1.8	1.8	2.3	1.8	1.2	1.8	4.1
Sugarcane	76.6	69.2	79.7	84.5	43.4	9.2	6.2	6.0	6.3	7.5	6.7	5.9	6.7	11.1
Sunflower	84.1	79.9	85.9	86.4	44.8	8.2	4.3	3.8	4.1	5.1	4.1	3.2	4.3	9.1
Tomato	87.4	83.6	90.0	90.4	50.6	11.5	7.8	7.1	7.1	8.2	7.0	6.0	7.0	12.1
Watermelon	82.9	75.9	85.0	88.1	40.9	9.2	6.5	5.9	5.7	6.5	5.3	4.4	5.3	9.2
Wheat	87.8	80.7	88.3	91.6	52.5	8.0	5.1	4.4	4.4	5.1	4.2	3.3	3.8	7.7

Table 4. Continued.

Crop	1200	1250	1300	1350	1400	1450	1500	1550	1600	1650	1700	1750	1800	1850
Avocado	8.1	7.3	10.8	19.5	47.6	60.4	51.3	39.0	31.7	28.3	29.7	33.4	35.6	51.8
Bean	6.5	6.2	11.1	21.6	57.2	69.8	58.1	42.1	32.0	26.9	27.3	33.0	36.8	57.3
Cantaloupe	9.1	8.5	13.5	24.1	58.8	70.6	61.3	46.3	36.4	31.4	35.0	37.6	40.6	58.8
Corn	7.1	6.0	9.3	15.8	47.8	62.7	52.3	37.7	28.8	24.1	24.4	29.4	31.6	44.9
Cotton	8.0	7.5	11.4	19.9	51.6	65.1	55.0	40.6	31.7	27.2	27.8	32.5	35.1	52.9
Lettuce	23.0	22.2	30.0	42.7	73.6	84.7	78.5	67.1	58.1	52.7	52.2	58.0	61.8	74.2
Okra	7.7	7.0	10.5	18.1	47.6	62.6	53.2	39.2	30.4	25.8	26.5	30.7	33.2	49.7
Onion	20.0	19.0	27.6	41.9	77.2	89.1	82.9	70.5	60.6	54.4	54.2	60.7	64.9	77.5
Orange	9.6	8.8	11.9	19.2	48.6	64.6	56.2	43.2	34.8	30.2	31.4	35.9	17.7	51.9
Peach	5.0	4.5	6.8	13.1	38.3	49.5	39.9	28.1	21.6	18.3	19.6	22.6	25.8	40.9
Pepper	6.6	6.0	10.0	18.5	51.1	65.4	54.7	39.5	30.1	25.3	25.6	30.8	33.8	51.6
Pigweed	6.3	5.8	9.5	18.0	48.6	61.3	51.0	36.8	28.1	23.7	24.3	28.8	31.4	50.1
Pumpkin	6.7	6.4	9.8	18.8	45.9	57.2	46.8	33.9	26.1	22.0	23.8	27.6	31.0	49.2
Sorghum	4.8	4.2	6.2	11.0	33.9	47.1	38.6	26.9	19.9	16.4	16.8	20.0	21.6	35.1
Soybean	4.0	3.7	6.1	11.9	37.4	49.5	39.7	26.9	19.5	15.9	16.2	19.8	21.8	38.9
Sugarcane	11.4	10.7	14.6	23.3	54.7	68.2	58.8	45.0	36.0	31.1	31.5	36.5	39.3	55.6
Sunflower	9.2	8.6	13.3	23.6	57.3	70.7	60.6	46.0	36.4	31.7	32.9	37.9	40.7	58.6
Tomato	12.1	11.5	16.6	26.9	60.9	73.3	63.2	48.7	39.2	34.5	35.1	40.6	43.6	61.3
Watermelon	9.2	8.6	12.8	21.8	54.0	65.1	54.5	40.8	32.3	28.2	29.1	33.9	36.0	54.2
Wheat	7.6	6.6	10.0	16.8	48.0	59.7	49.6	36.7	29.0	25.1	26.3	30.6	32.0	45.8

Table 4. Continued.

Crop	1900	1950	2000	2050	2100	2150	2200	2250	2300	2350	2400	2450	2500
Avocado	81.5	85.7	77.5	69.4	63.1	57.9	55.4	59.3	66.0	72.2	78.4	82.3	86.1
Beans	88.3	92.1	85.2	75.5	65.7	58.8	56.3	60.1	67.6	75.9	82.8	89.0	90.6
Cantaloupe	87.8	91.1	85.4	77.4	68.9	63.0	60.7	64.2	71.0	78.0	83.9	88.4	90.6
Corn	85.6	87.8	78.5	68.8	59.6	53.2	50.0	54.1	61.2	68.6	75.9	82.8	86.3
Cotton	85.0	89.5	82.0	72.4	63.3	57.1	63.3	42.0	65.0	72.3	79.6	85.2	88.1
Lettuce	91.7	93.9	91.9	88.1	82.9	78.6	77.1	79.1	83.3	87.8	91.3	93.4	94.3
Okra	82.1	87.8	79.9	70.4	61.5	55.3	52.6	56.0	62.8	70.1	77.2	83.0	86.0
Onion	93.9	95.1	94.5	91.9	87.4	83.3	81.8	83.8	87.7	91.5	94.1	94.9	95.0
Orange	83.3	88.8	81.8	73.9	66.8	61.0	58.3	62.3	69.0	75.2	81.2	85.9	88.4
Peach	74.9	79.2	68.4	58.3	50.3	44.5	41.9	46.4	53.5	60.4	67.8	74.6	78.3
Pepper	85.1	89.5	81.7	71.8	62.4	55.6	52.9	56.5	63.8	71.8	79.2	85.0	88.2
Pigweed	82.4	87.4	78.6	68.3	58.9	52.5	50.1	53.5	60.2	67.9	75.4	81.7	85.3
Pumpkin	80.8	84.0	74.5	64.5	56.0	50.4	47.9	52.4	59.3	66.4	73.6	80.5	82.7
Sorghum	70.5	75.9	64.5	54.2	46.0	40.2	37.4	41.0	47.5	54.4	61.8	69.2	73.2
Soybean	75.3	80.2	68.6	56.7	46.7	40.2	37.6	41.0	47.9	56.0	64.4	72.0	76.1
Sugarcane	85.7	89.8	82.5	74.3	66.9	60.8	58.6	62.3	68.9	75.4	81.4	86.5	89.1
Sunflower	87.1	91.2	85.4	77.6	69.7	64.1	62.2	65.9	72.3	78.6	83.6	88.5	90.7
Tomato	89.0	92.2	86.7	79.1	71.1	65.2	63.0	66.4	73.0	79.7	85.4	89.6	91.6
Watermelon	85.9	88.5	80.8	71.8	63.4	57.6	55.1	58.9	65.8	72.6	79.3	84.9	87.5
Wheat	84.2	85.8	76.5	67.5	59.4	54.1	50.9	55.5	62.8	68.8	75.5	81.7	85.0

Table 5. Coefficients of dispersion curve $n = \Sigma\ a_i\lambda^i$ for leaves of 20 crops where λ is expressed in micrometers.

Crop	a_0	a_1	a_2	a_3
Corn	1.403	0.017	-0.065	0.011
Watermelon	1.377	0.076	-0.098	0.016
Orange	1.390	0.037	-0.071	0.010
Sunflower	1.355	0.110	-0.116	0.020
Peach	1.347	0.117	-0.115	0.018
Pumpkin	1.406	0.011	-0.058	0.007
Sugarcane	1.402	0.079	-0.145	0.032
Pigweed	1.721	-0.626	0.334	-0.071
Avocado	1.398	0.063	-0.120	0.025
Onion	1.481	-0.217	0.156	-0.044
Okra	1.347	0.134	-0.134	0.022
Cotton	1.320	0.196	-0.177	0.030
Tomato	1.379	0.062	-0.078	0.010
Cantaloupe	1.425	-0.062	0.013	-0.008
Bean	1.365	0.059	-0.067	0.006
Sorghum	1.408	0.004	-0.055	0.009
Pepper	1.393	0.005	-0.031	-0.003
Soybean	1.394	0.003	-0.033	0.127
Lettuce	1.792	-0.878	0.587	-0.127
Wheat	1.487	-0.185	0.085	-0.021

Table 6. Parameters that specify amount of H_2O and intercellular air
space in leaves of 20 crops. Table headings are defined
elsewhere[a].

Crop	D(μm)	N	D/N	R_∞[b](%)	S.E.
Corn	173	1.44	119.6	41.8 ± 0.8	.013
Watermelon	203	1.59	127.8	39.9 ± 0.9	.018
Orange	209	2.27	91.9	44.7 ± 0.5	.019
Sunflower	242	1.54	157.1	36.9 ± 0.5	.017
Peach	119	1.65	72.0	50.3 ± 0.5	.019
Pumpkin	152	1.48	102.3	44.0 ± 0.5	.017
Sugarcane	224	1.55	144.1	36.4 ± 0.5	.022
Pigweed	173	1.43	121.1	41.0 ± 0.4	.017
Avocado	190	1.73	109.3	40.8 ± 0.7	.022
Onion	606	1.13	533.6	18.5 ± 0.6	.094
Okra	181	1.65	109.5	42.6 ± 0.7	.017
Cotton	199	1.52	130.8	39.7 ± 0.4	.016
Tomato	260	1.70	152.7	36.6 ± 0.8	.019
Cantaloupe	239	1.56	152.8	37.6 ± 0.5	.016
Bean	219	2.20	99.5	46.9 ± 0.5	.015
Sorghum	101	1.51	67.0	50.7 ± 0.7	.018
Pepper	189	1.76	107.3	44.4 ± 0.6	.015
Soybean	111	1.45	76.8	50.8 ± 1.0	.015
Lettuce	524	1.05	499.7	17.6 ± 1.5	.018
Wheat	169	1.82	92.4	45.6 ± 0.8	.017

[a] Allen, Gausman, and Richardson (1970).

[b] At 1.65 μm WL.

Table 7. Mean[a] absorption spectra in cm^{-1} units over the 1.4- to 2.5-μm range of the leaves of 20 crops compared with published values for pure liquid H_2O[b].

Wavelength (μm)	Leaf	Water
1.40	14.3 ± 1.0	12.5
1.45	24.6 ± 2.0	25.8
1.50	16.5 ± 1.5	18.5
1.55	9.9 ± 0.3	9.8
1.60	6.8 ± 0.3	6.5
1.65	5.6 ± 0.3	5.1
1.70	5.8 ± 0.4	5.2
1.75	7.2 ± 0.4	6.0
1.80	8.1 ± 0.3	8.1
1.85	15.5 ± 1.0	9.8
1.90	58.7 ± 6.4	81.0
1.95	77.9 ± 18.7	106.0
2.00	49.5 ± 3.2	68.0
2.05	33.7 ± 1.9	43.0
2.10	24.2 ± 0.6	26.0
2.15	19.3 ± 0.7	19.0
2.20	17.6 ± 0.6	16.0
2.25	20.3 ± 0.8	18.0
2.30	26.4 ± 1.0	22.0
2.35	34.8 ± 0.7	31.0
2.40	46.3 ± 1.9	43.0
2.45	59.8 ± 1.9	60.0
2.50	70.0 ± 4.2	83.0

[a] Each kind of leaf was assigned a statistical weight of unity.

[b] Curcio and Petty (1951).

Table 8. Absorption spectra in cm^{-1} units over the 0.5- to 1.3-μm range for 31 kinds of plant leaves. The first 11 entries have been reported previously (Gausman et al., 1970b).

Plant leaf	Wavelength (μm)								
	0.5	0.6	0.7	0.8	0.9	1.0	1.1	1.2	1.3
Eucalyptus	56.3	61.0	9.7	0.7	0.6	0.6	0.5	1.2	1.6
Banana	55.2	60.2	9.7	0.4	0.4	0.5	0.5	1.2	1.7
Rose	108.1	128.8	18.9	0.6	0.5	0.5	0.5	1.0	1.5
Ligustrum	44.9	48.7	5.7	0.3	0.3	0.4	0.4	1.1	1.5
Ficus	45.5	48.1	5.9	0.3	0.3	0.4	0.4	1.1	1.6
Oleander	54.7	57.6	9.7	0.8	0.7	0.8	0.7	1.4	1.7
Crinum	29.5	29.5	4.6	0.3	0.3	0.5	0.4	1.2	1.7
Begonia	21.6	19.3	3.0	0.2	0.2	0.3	0.3	1.0	1.6
Hyacinth	42.7	47.3	7.7	0.4	0.3	0.4	0.3	1.0	1.6
Corn	76.2	81.7	15.7	0.7	0.6	0.6	0.5	1.2	1.7
Sedum	10.4	10.2	2.0	0.1	0.1	0.3	0.2	1.0	1.5
Corn	70.2	79.1	15.0	0.5	0.4	0.5	0.5	1.2	1.7
Watermelon	52.0	62.0	8.7	0.9	0.8	0.7	0.7	1.4	2.0
Orange	103.6	121.3	14.4	0.8	0.8	0.7	0.7	1.4	1.8
Sunflower	45.0	50.6	8.6	0.5	0.5	0.5	0.5	1.1	1.7
Peach	112.1	137.1	17.0	0.7	0.7	0.6	0.6	1.2	1.7
Pumpkin	74.2	84.7	13.4	0.9	0.7	0.7	0.6	1.3	1.8
Sugarcane	30.2	37.0	8.4	0.8	0.8	0.9	0.9	1.6	2.1
Pigweed	54.7	78.3	13.5	0.4	0.4	0.4	0.4	1.1	1.7
Avocado	98.0	121.8	13.7	0.7	0.6	0.6	0.6	1.3	1.7
Onion	13.4	15.6	2.8	0.2	0.2	0.4	0.4	1.1	1.7
Okra	54.7	61.8	11.2	0.7	0.6	0.6	0.6	1.3	1.8
Cotton	48.6	58.0	9.2	0.5	0.5	0.6	0.6	1.2	1.8
Tomato	59.2	82.0	9.2	0.9	0.8	0.8	0.8	1.4	2.1
Cantaloupe	44.4	54.3	8.3	0.5	0.4	0.4	0.5	1.1	1.8
Bean	36.2	46.2	7.1	0.1	0.2	0.2	0.2	0.9	1.6
Sorghum	82.6	102.1	20.8	0.9	0.7	0.7	0.6	1.3	1.8
Pepper	46.3	53.5	8.8	0.3	0.3	0.3	0.3	1.0	1.6
Soybean	74.5	91.4	15.0	0.5	0.4	0.4	0.4	1.1	1.6
Lettuce	2.6	2.7	1.0	0.4	0.5	0.6	0.6	1.6	2.3
Wheat	105.7	108.3	16.3	0.8	0.7	0.7	0.6	1.3	1.8
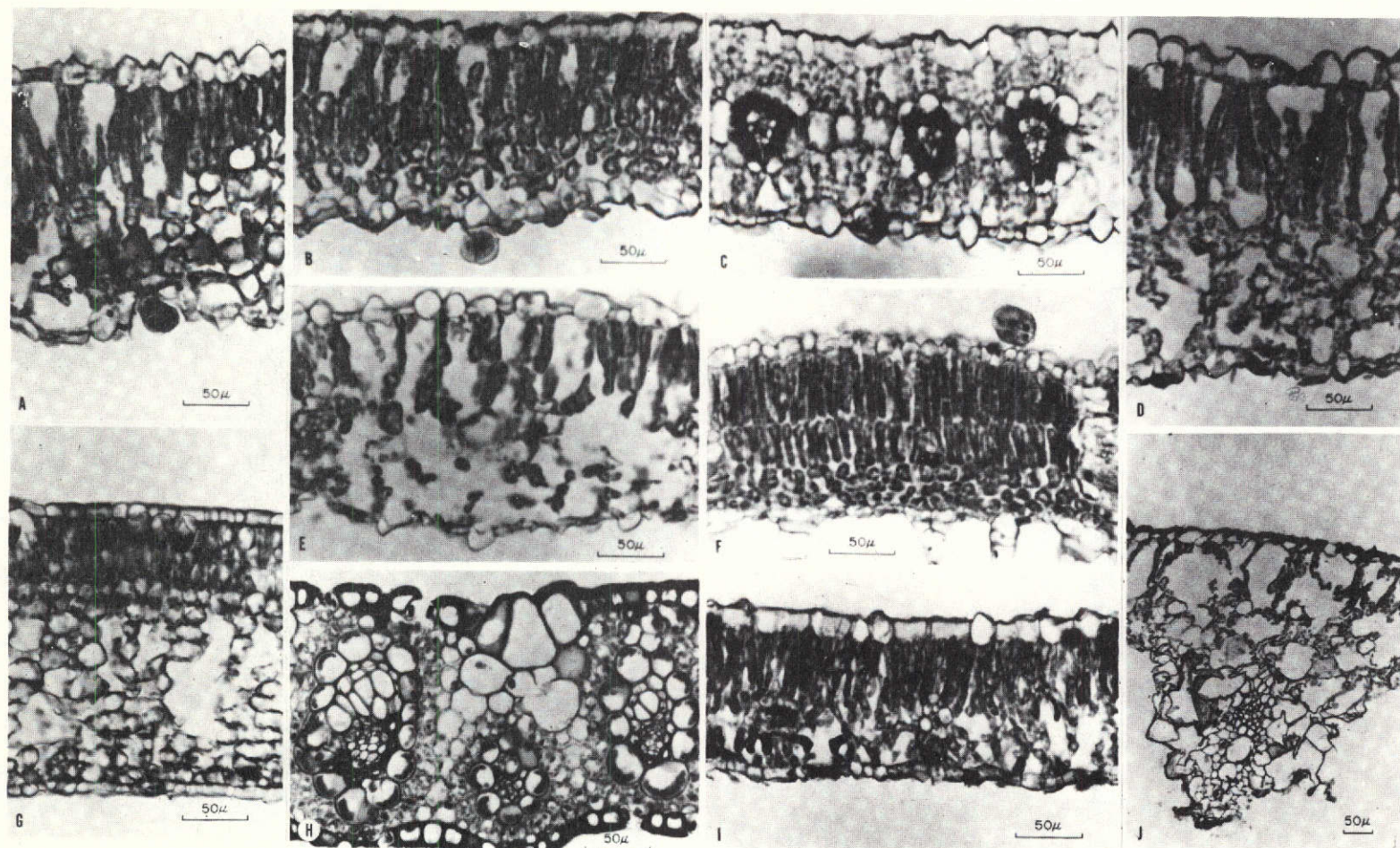
Fig. 1.--Photomicrographs of leaf transections of 20 plant genera differing in leaf thicknesses, mesophyll arrangements, and other gross structural characteristics. All photomicrographs are 200 X except that onion is 80 X. A = cotton, B = watermelon, C = pigweed, D = tomato, E = soybean, F = pumpkin, G = orange, H = sugarcane, I = peach, J = onion, K = corn, L = pepper, M = cantaloupe, N = lettuce, O = okra, P = avocado, Q = bean, R = sunflower, S = wheat, T = sorghum.
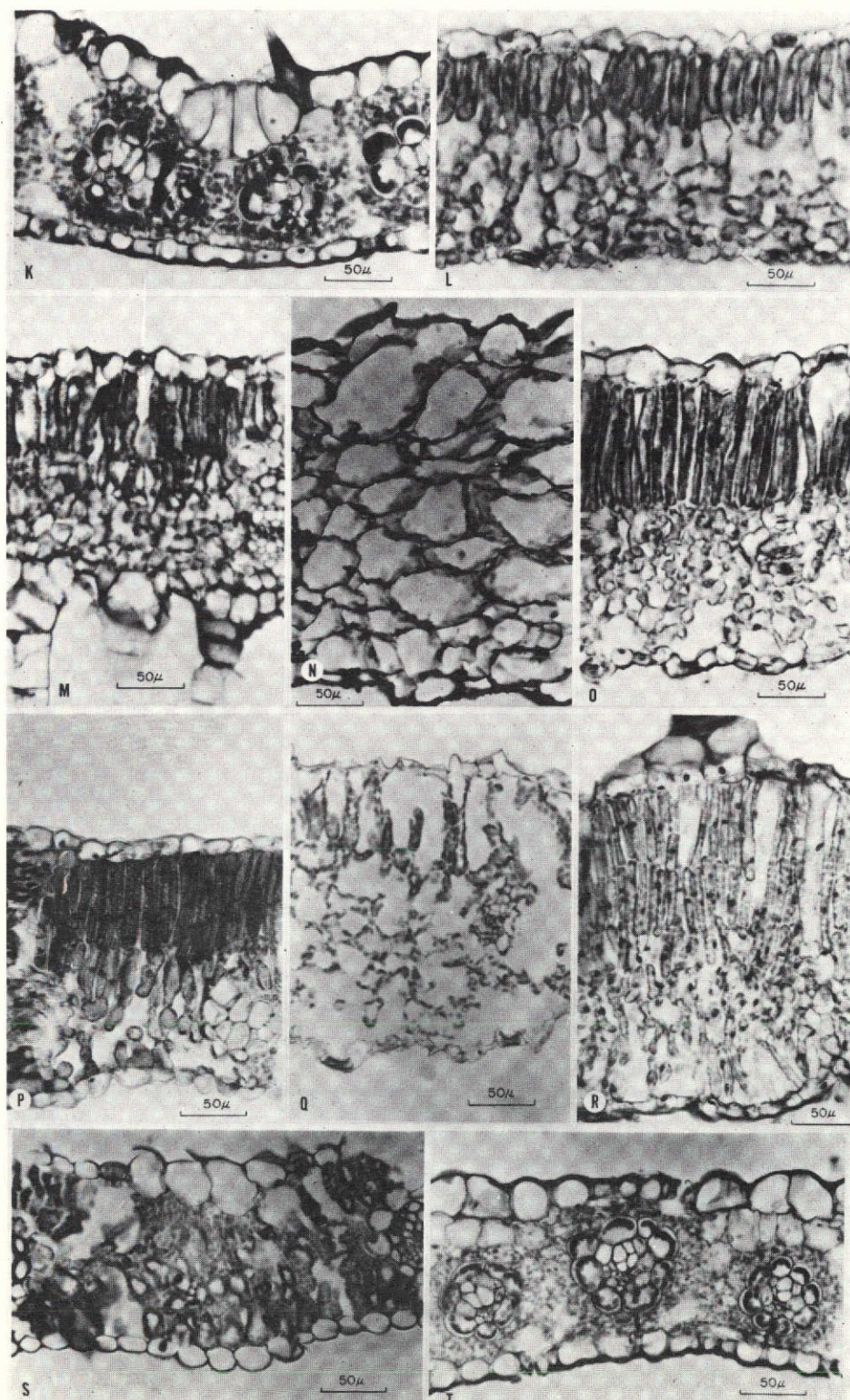
Fig. 1.--Continued.
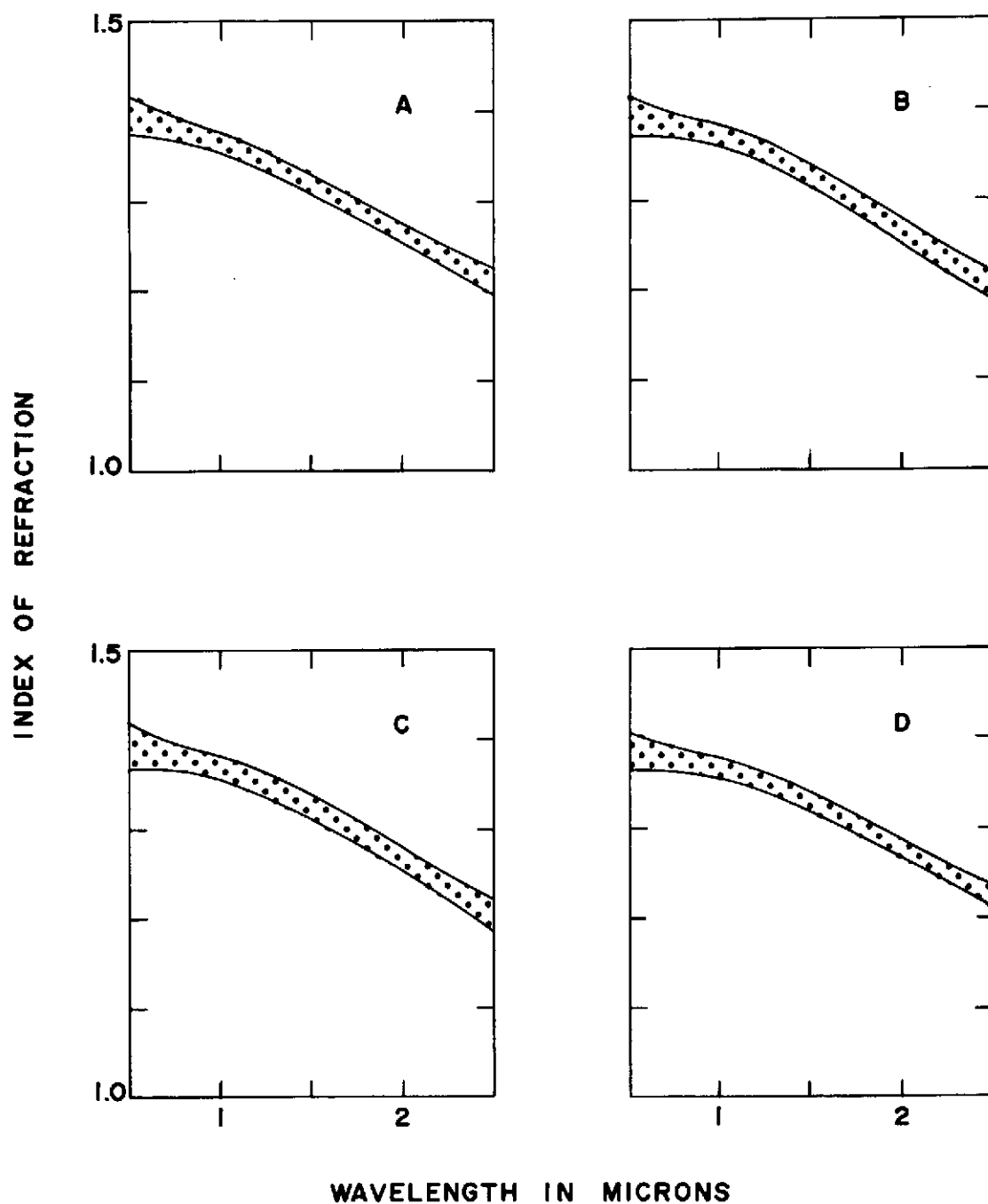
Fig. 2.--Dispersion curves for (A) corn; (B) watermelon; (C) orange;
(D) sunflower; (E) peach; (F) cotton; (G) orka; (H) onion; (I) avocado;
(J) pigweed; (K) sugarcane; (L) pumpkin; (M) tomato; (N) cantaloupe;
(O) bean; (P) sorghum; (Q) pepper; (R) soybean; (S) lettuce; and
(T) wheat.
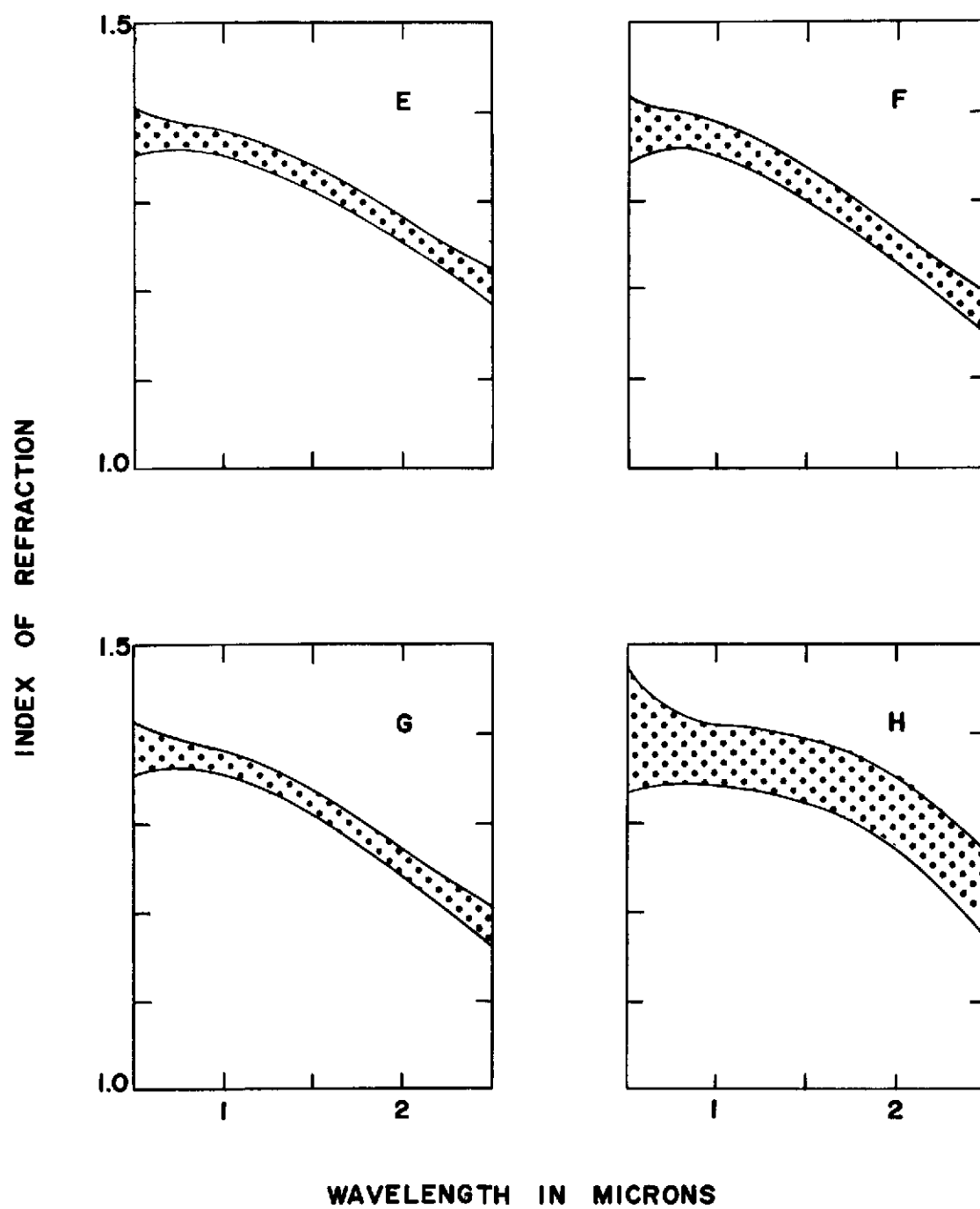
Fig. 2.--Continued
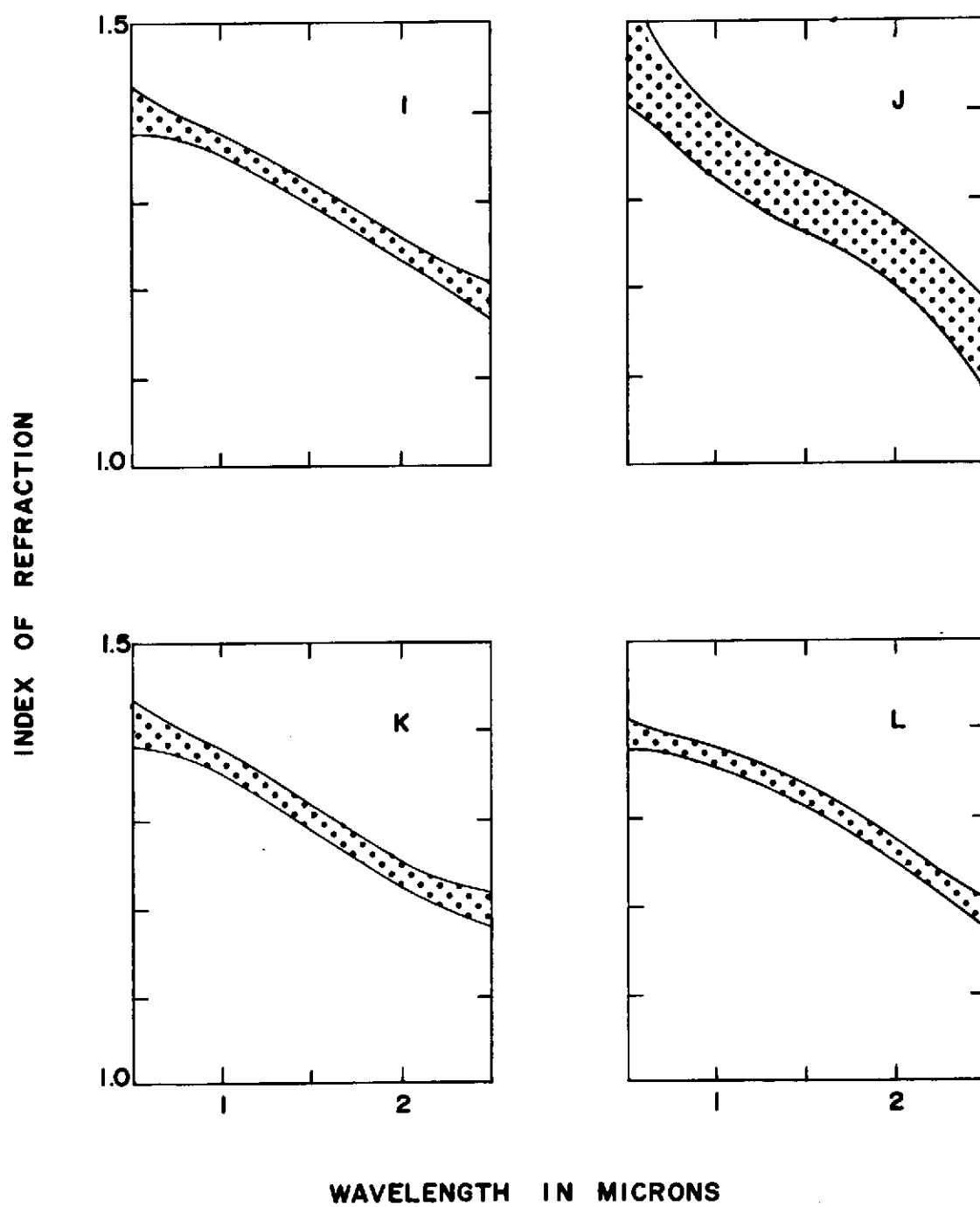
Fig. 2.--Continued
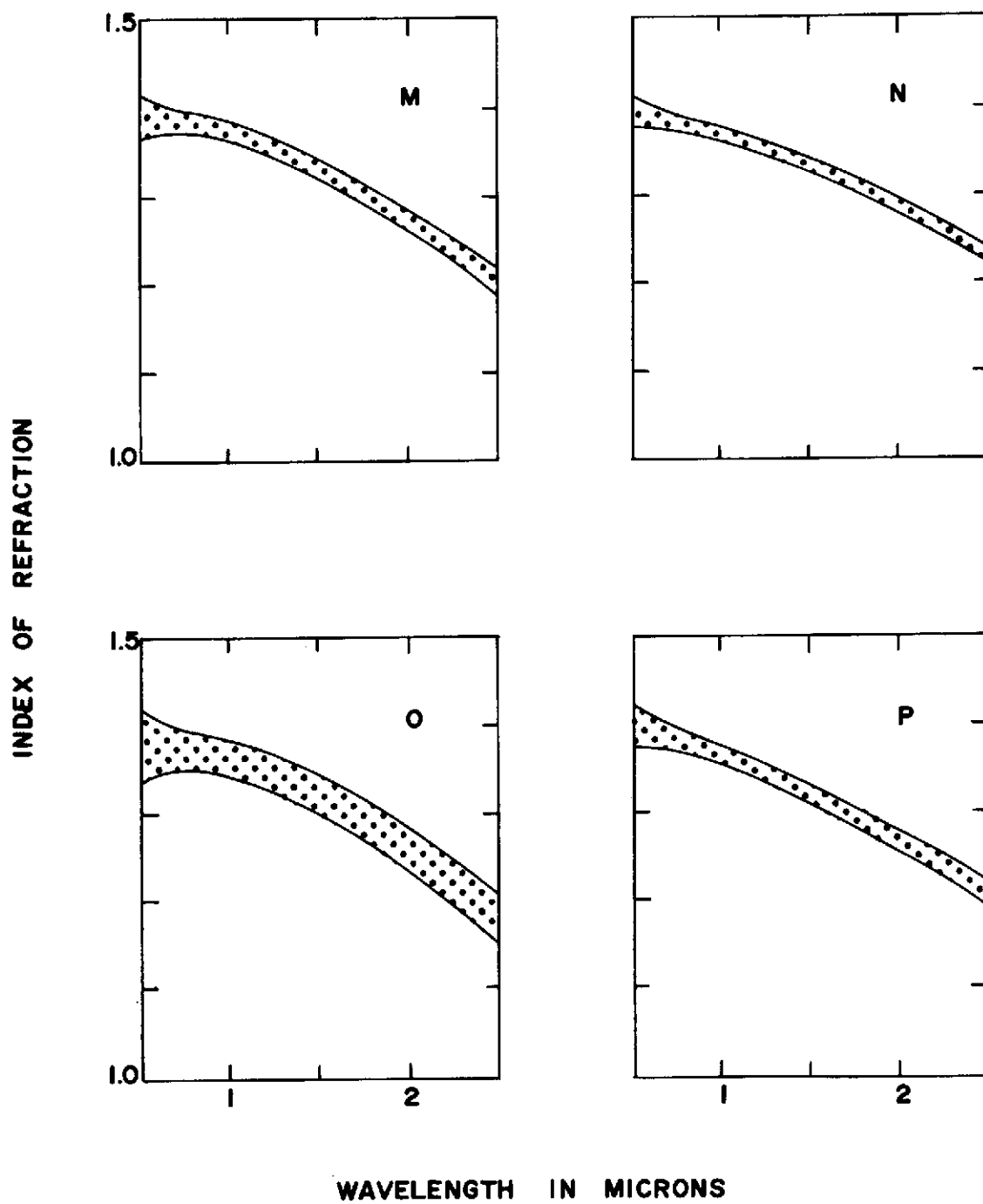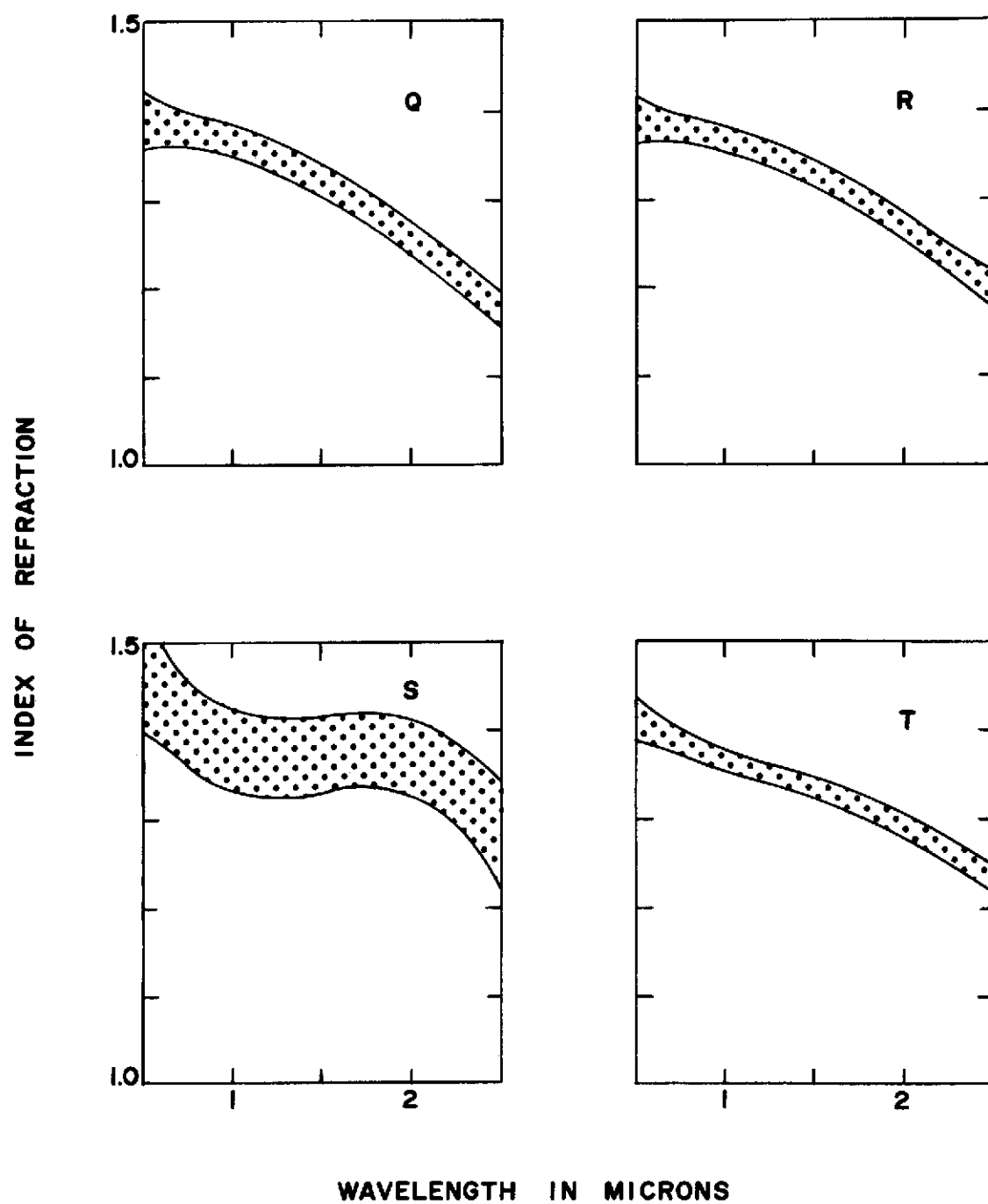
Fig. 2.--Continued

Fig. 2.--Continued
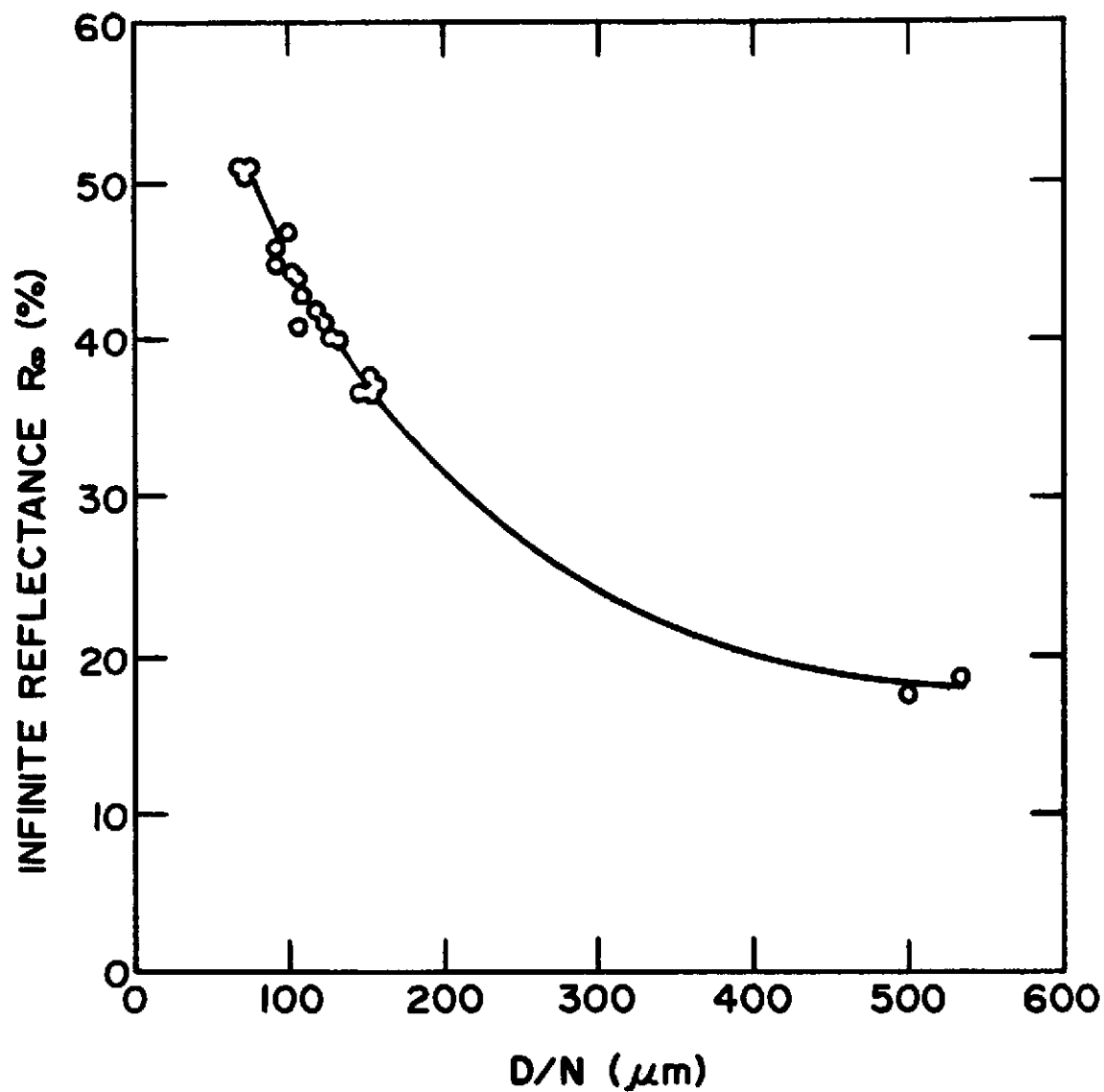
Fig. 3.--Infinite reflectance R∞ at 1.65 μm for 20 genera of plant leaves plotted as function of characteristic linear dimension D/N.
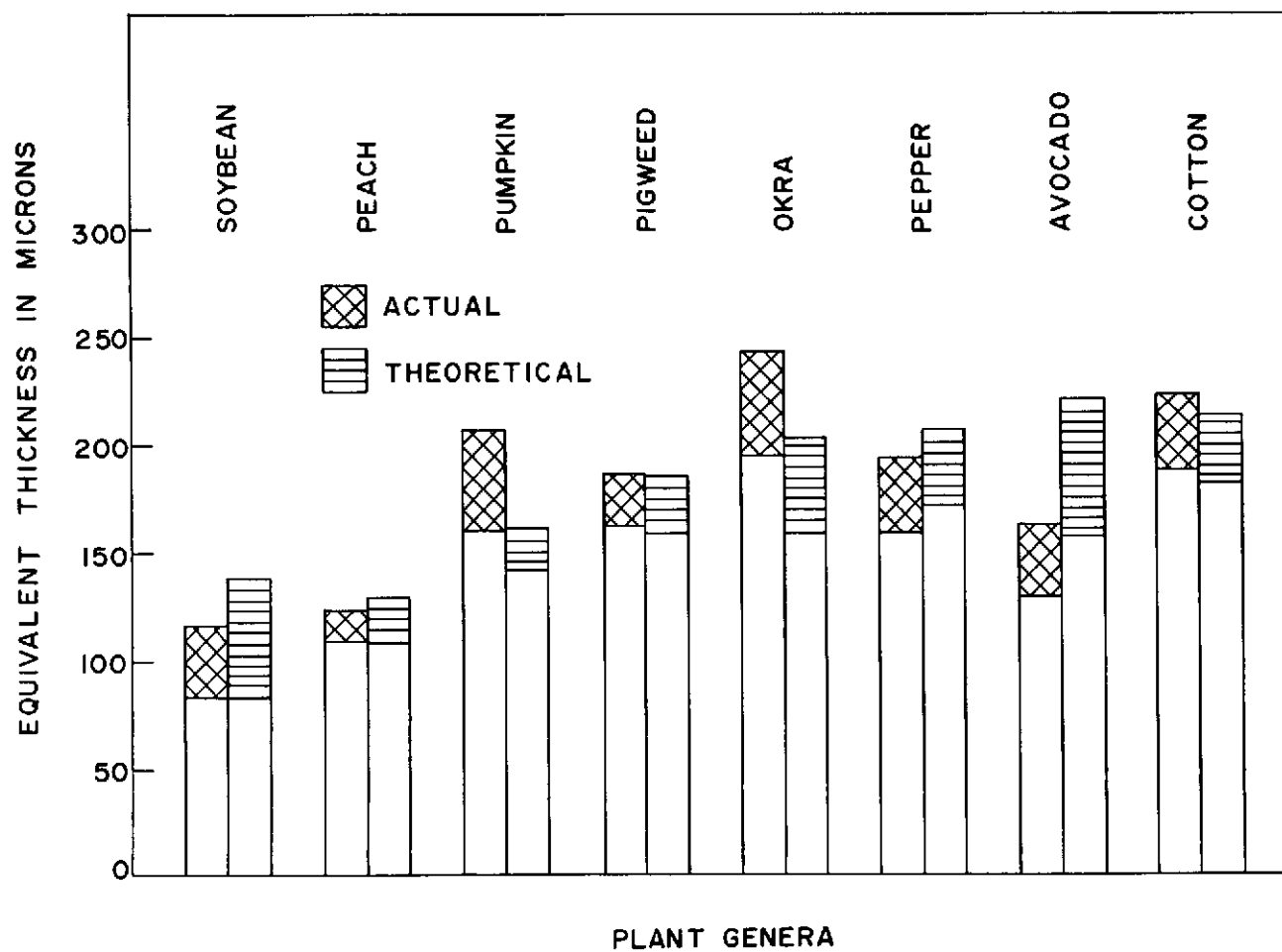
Fig. 4.--Comparison of observed and computed values of effective H_2O thickness of leaves. The shaded areas represent a variation of one standard deviation.
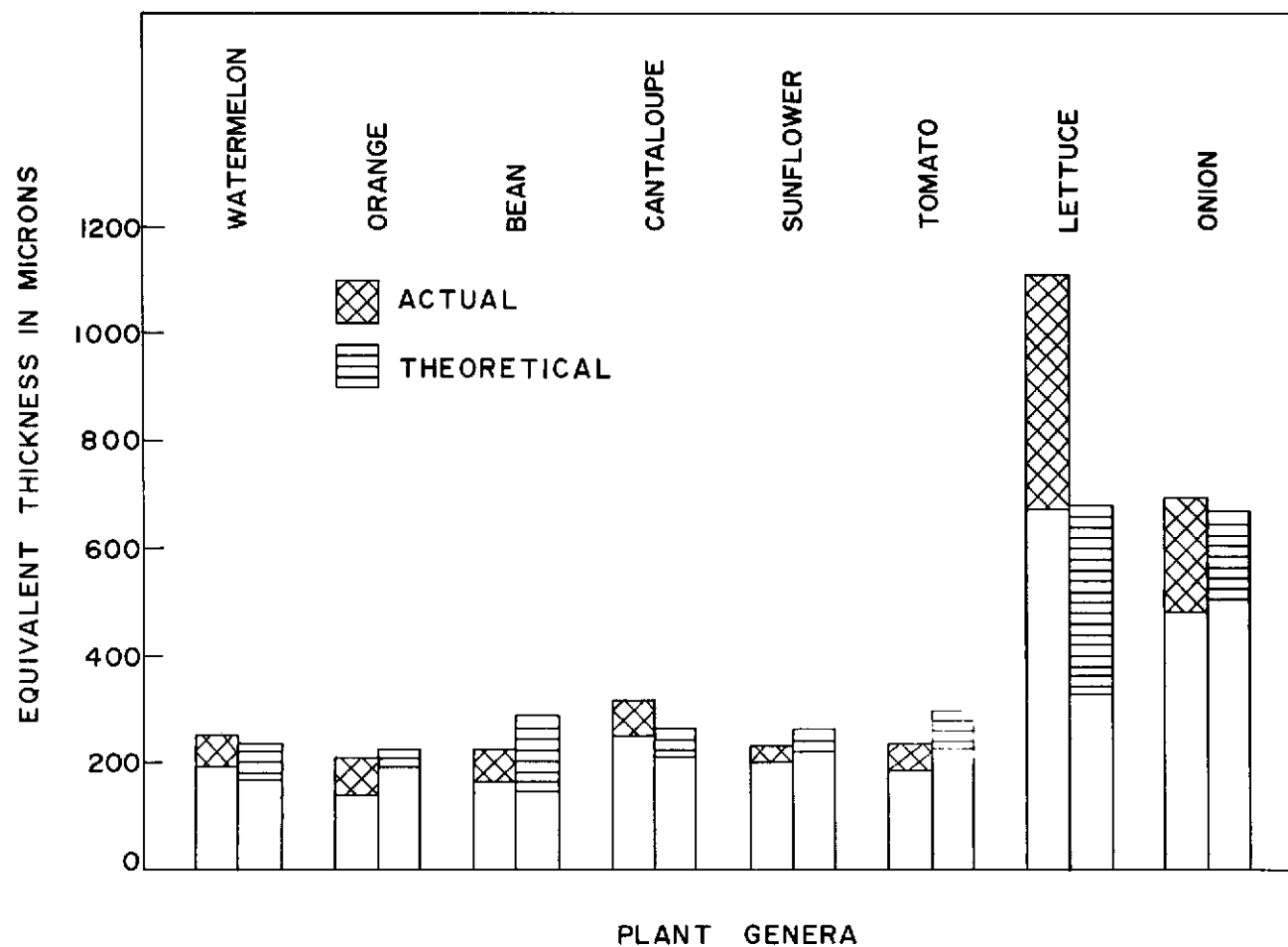
Fig. 4a.--Comparison of observed and computed values of effective H_2O thickness of leaves. The shaded areas represent a variation of one standard deviation.

EFFECTS OF LEAF AGE FOR FOUR GROWTH STAGES OF COTTON AND CORN

PLANTS ON LEAF REFLECTANCE, STRUCTURE, THICKNESS, WATER AND

CHLOROPHYLL CONCENTRATIONS AND SELECTION OF WAVELENGTHS

FOR CROP DISCRIMINATION

H. W. Gausman, W. A. Allen, R. Cardenas, and A. J. Richardson

SUMMARY

The stage of plant development (growth stage) when overflights are made is important in remote sensing applications. Results are summarized on effects of leaf age within growth stages of cotton (Gossypium hirsutum L.) and corn (Zea mays L.) plants on leaf light reflectance. Thickness, structure, water (H_2O), and chlorophyll (CHL) concentrations of leaves are considered because they influence reflectance; and therefore, they affect the selection of optimum spectral channels for the discrimination of vegetation.

The symbols S_1, S_2, S_3, and S_4 (S = stage) will represent the seedling, pre-bloom, boll, and mature (10% of bolls open) growth stages for cotton plants, and the seedling, pre-tassel, tassel and silk, and mature (from S_3 until the milk stage of corn kernels) growth stages for corn, respectively.

Average cotton leaf thicknesses for S_1, S_2, S_3, and S_4 were .197, .261, .235, and .254 mm, respectively. Generally, leaf thickness increased with leaf age within all growth stages except S_1.

Water contents of cotton leaves were relatively constant among growth stages (74.9 to 79.0%). Within S_1 and S_2, youngest leaves, compared with older leaves, had the lowest H_2O contents (77.0 and 74.0%, respectively); and for S_3 and S_4, leaves second to the youngest had the lowest H_2O content. The highest H_2O content obtained was 83.1% for the first true leaves sampled within S_1.

Average corn leaf thicknesses for S_1, S_2, S_3, and S_4 were .201, .246, .235, and .264 mm, respectively. Within each growth stage, youngest leaves were thinner (.173 to .225 mm) than older leaves (.218 to .279 mm).

Average corn leaf H_2O contents for S_1, S_2, S_3, and S_4 were 84.0, 84.0, 78.6, and 74.1%, respectively. Youngest leaves, compared with older leaves, had the lowest H_2O contents within S_1 and S_2. For S_3 and S_4, there was generally a progressive increase in H_2O content with leaf maturation (76.4 to 81.4%).

The youngest cotton leaves within all growth stages had less light reflectance over the 750- to 2500-nm wavelength interval (WLI) than older leaves. In the 500- to 750-nm visible WLI, young leaves had equal or less reflectance than older leaves at S_1, S_2, and S_4, but at S_3 reflectance was second to the highest. In the 750- to 1350-nm WLI, reflectance increased with leaf age. At the 1000-nm wavelength (WL) reflectances were 29.1, 43.2, 45.4, 48.8, and 51.7% for leaves from nodes 5 (youngest), 4, 3, 2, and 1, respectively. With S_2, S_3, and S_4, age of leaves had little influence on reflectance beyond leaves second to the youngest.

Young corn leaves had less reflectance at S_1 over the 750- to 1350-nm WLI than older leaves. Reflectances at the 1000-nm WL were 36.8, 39.4, 40.0, 41.0, and 40.6% for nodes 8 (youngest), 7, 6, 5, and 4, respectively. The most important results occurred at S_2 over the 500- to 750-nm WLI. Reflectances at the 550-nm WL decreased as age of leaves increased; values from youngest to oldest leaves were 27.6, 20.1, 16.9, 13.4, and 12.1%. Apparently a redistribution of metabolites at S_2 curtailed chlorophyll production in young leaves.

The correlation of reflectance with CHL concentration for all growth stages of corn gave a highly significant coefficient (p = 0.01) of -0.75 at the 550-nm WL, and a significant coefficient (p = 0.05) of -0.50 at the 650-nm WL. The correlation of reflectance with CHL concentration for all growth stages of cotton was not significant at the 550-nm WL, but highly significant (r = -0.71) at the 650-nm WL.

Corn leaf maturation within growth stages increased near-infrared light (750- to 1350-nm WLI) reflectance very little because mesophylls remained relatively compact. Cotton leaf mesophylls become "spongy" with maturation, and mature leaves had much higher near-infrared light reflectance than young leaves.

A correlation analysis showed that channels 680, 850, 1650, and 2200 nm are optimum channels for the discrimination of vegetation.

LIGHT REFLECTANCES, CHLOROPHYLL ASSAYS,

AND PHOTOGRAPHIC FILM DENSITIES OF

ISOGENIC BARLEY LINES

R. Cardenas and H. W. Gausman

This information is from a paper prepared
for publication in the Agronomy Journal.
These results were produced under Research
Outline 57, "Physiological and Histological
Factors Affecting the Reflectance of
Leaves."

INTRODUCTION

Isogenic lines have a gene absent that is necessary for chlorophyll (CHL) synthesis in leaves. They are useful for evaluating the contribution of CHL to photosynthate production (Brown et al., 1971). The CHL of green leaves usually absorbs 70 to 90% of the light in the blue (about 450 nm) or red part (about 675 nm) of the spectrum (Horwitz, 1965). Absorptance is smallest in the wavelength (WL) region around 550 nm, where a reflection peak of usually less than 20% occurs from top leaf surfaces. Low pigment content results often in high reflectances (Benedict and Swidler, 1961; Birth and McVey, 1968; Clayton, 1965; Kleshnin and Shul'gin, 1959; Myers et al., 1963; Rabideau, 1946). For example, light green leaves of cabbage and lettuce had 8 to 28% higher reflectance than the average of 6 darker green species (Myers et al., 1963).

This paper presents results of research that compared spectrophotometrically measured light reflectance of 6 isogenic barley lines over the 350- to 700-nm wavelength interval (WLI) with chlorophyll assays and with responses of Kodak Ektachrome MS Aerographic film 2448 (CC) and Kodak Aerochrome Infrared film 2443 (AIR).

MATERIALS AND METHODS

Six isogenic barley lines (seed was obtained through the courtesy of Donald W. Fryrear, USDA-ARS-SWC, Big Spring, Texas 79720) (Betzes, Pale Green Betzes, Compana, Golden Compana, Liberty, Golden Liberty) were planted in unreplicated plots four beds wide (3 ft spacing among beds) and 12 ft long. Two rows were seeded on each bed. The seeding rate was 20 seeds per 1 ft of row length; seeding depth was approximately 1 in.

Leaves obtained for spectrophotometric measurements and CHL assays were randomly selected and detached from the fourth node from the plant base of each isogenic line. Reflectances of top (adaxial) surfaces of 5 leaves from each isogenic line were measured over the 350- to 700-nm WLI with a Beckman Model DK-2A ratio-recording spectrophotometer equipped with a reflectance attachment. Since

single leaves were too narrow to cover the 2-cm diameter port of the spectrophotom-
eter, edges of two leaves were slightly overlapped. The overlapped area was
placed over the spectrophotometer's port off-center so that the beam of light from
the instrument impinged on one leaf thickness, excluding the leaf mid-rib.

Total CHL, CHL a, and CHL b were determined according to standard procedures
(Benedict and Swidler, 1961). Chlorophyll concentrations are given in milligrams
per gram (Mg/g) of dry weight of plant tissue. Percent water content was deter-
mined on one row of plants from each of the 6 isogenic lines by oven drying at
68C for 48 hrs.

Photographs with 70-mm CC and AIR film were taken from the bucket of a Truco
aerial lift ("cherry picker") with two Hasselblad cameras with 50-mm focal length
lens. A Tiffen yellow filter was used on the camera with AIR film. Photographs
were taken at a height of 50 ft above plants.

Optical count readings were made on CC and AIR transparencies with a Joyce,
Loebl recording microdensitometer using no filter (white light), red (Wratten 92),
green (Wratten 93), and blue (Wratten 94) bandpass filters in the densitometer's
light beam. The microdensitometer output is in optical counts that are punched
onto paper tape. The paper tape output consists of a base line count corresponding
to the standard optical densities of the first step of the calibrated step wedge
in use, plus added counts that depend on the particular step on the wedge that
balances the light transmission by the film being analyzed in the second light
beam. The distance the uniformly graduated step wedge travels to balance the trans-
mission by the film determines the count registered by the encoder. One of the
double rows from each isogenic line was selected for optical count readings. One
scan line was run for each isogenic line for each of the two filters. Fifty
readings (data bits) were taken on each scan line. The same rows were used for all
filters and films.

RESULTS AND DISCUSSION

Visually, Betzes, Liberty, Compana, Pale Green Betzes, Golden Compana, and
Golden Liberty appeared very dark green, dark green, green, light green, yellow,
and whitish yellow in color, respectively. Figure 1 presents spectrophotometric
reflectance measurements and total CHL assays for the six isogenic lines of barley.
The correlation of reflectance at the 550 WL with total CHL was statistically
significant ($r = -0.87$, $p = 0.05$). Golden Liberty with the lowest total CHL con-
centration (1.80 mg/g ± 0.03--one standard error) had the highest reflectance at
the green peak of the 550-nm WL compared with the other isogenic lines. At the
550-nm WL, Liberty and Betzes (CHL concentrations of 6.70 ± 0.07 and 5.65 ± 0.12
mg/g, respectively) had lower reflectances (17.8 and 17.9%, respectively) than the
other isogenic lines. However, Compana with the highest CHL concentration of 6.73
± 0.07 mg/g did not have the lowest reflectance. In general, however, low CHL
concentration was associated with high reflectance at the 550-nm WL.

Chlorophyll a and b concentrations ranged in the same order as total CHL among
the six isogenic lines. The ratio of CHL a to b was essentially alike for all
lines (a:b = 0.68 to 0.71) except Betzes (a:b = 0.79) and Golden Liberty (a:b =
0.58). The decreased concentration of CHL b relative to a for Golden Liberty is

apparent in Fig. 1. The curve for Golden Liberty is less symmetrical about the vertical dashed line drawn above the 550-nm WL than the curves for the other isogenic lines. Chlorophyll a and b have absorption maxima in vivo at about 675 and 650 nm, respectively (Clayton, 1965).

Best discrimination among isogenic lines was achieved with white light and a green filter (data for red and blue filters not shown) for both CC and AIR films. The widest range in optical counts, however, was obtained for the AIR film compared with the CC film. Hence, the AIR film, compared with the CC film, with either white light or the green filter appears best for discrimination among the isogenic lines. With the AIR film, highest readings of 97.0 (white light) and 98.7 (green filter) were obtained with Compana, and lowest readings of 47.1 (white light) and 46.6 (green filter) were obtained with Golden Liberty.

Reference to Fig. 1 shows that Compana had the highest and Golden Liberty the lowest CHL content. The correlations of optical count readings (Table 1) with total CHL content (Fig. 1) were significant, p = 0.05. Coefficients were -0.88, -0.86, -0.94, and -0.94 for CC film + white light, CC film + green filter, AIR film + white light, and AIR film + green filter, respectively.

In conclusion, CHL concentrations of the isogenic lines were negatively correlated with spectrophotometrically measured reflectances. Golden Liberty and Betzes, however, had a decreased concentration of CHL b relative to CHL a compared with the other isogenic lines. Optical count readings made on the CC and AIR films with a densitometer were negatively correlated with CHL concentrations. Discrimination among the isogenic lines appears best with AIR compared with CC film.

LITERATURE CITED

Benedict, H. M., and R. Swidler. 1961. Nondestructive method for estimating chlorophyll content of leaves. Science 133:2015-2016.

Birth, G. S., and G. R. McVey. 1968. Measuring the color of turf with a reflectance spectrophotometer. Agron. J. 60:640-643.

Brown, J. H., R. F. Eslick, and A. H. Ferguson. 1971. Studies with barley isogenic lines: II. The influence of leaf color on plant growth. Agron. Abs. p. 31.

Clayton, R. C. 1965. Molecular physics in photosynthesis. Blaisdell Pub. Co., New York. 205 p.

Carter, D. L., and V. I. Myers. 1963. Light reflectance and chlorophyll and carotene contents of grapefruit leaves as affected by Na_2SO_4, NaCl and $CaCl_2$. Proc. Amer. Soc. Hort. Sci. 82:217-221.

Horwitz, W., editor. 1965. Official methods of analysis, 10th ed. Association of Official Agricultural Chemists, Wash., D. C. 957 p.

Kleshnin, A. F., and I. A. Shul'gin. 1959. The optical properties of plant leaves. Dokl. Akademii Nauk SSSR, v. 125, p. 1158. Translation: A.I.B.S. Doklady 125:108-110.

Myers, V. I., L. R. Ussery, and W. J. Rippert. 1963. Photogrammetry for detailed detection of drainage and salinity problems. Trans. ASAE 6:322-324.

Rabideau, G. S., C. S. French, and A. S. Holt. 1946. The absorption and reflection spectra of leaves, chloroplast suspensions and chloroplast fragments as measured in an Ulbricht sphere. Amer. J. Bot. 33:769-777.

Thomas, J. R., and G. F. Oerther. 1971. Estimating leaf nitrogen content by reflectance measurements. Agron. J.

Table

Table 1. Optical count readings obtained for the isogenic lines with no
filter (white light) and a green filter for CC and AIR films.

Isogenic line	Film type			
	CC		AIR	
	White light	Green filter	White light	Green filter
Betzes	64.3	56.1	84.6	90.9
Compana	62.3	54.8	97.0	98.7
Liberty	60.9	51.5	85.2	91.5
Pale Green Betzes	57.4	45.5	75.6	81.8
Golden Compana	57.8	48.2	66.4	71.5
Golden Liberty	53.8	43.5	47.1	46.6
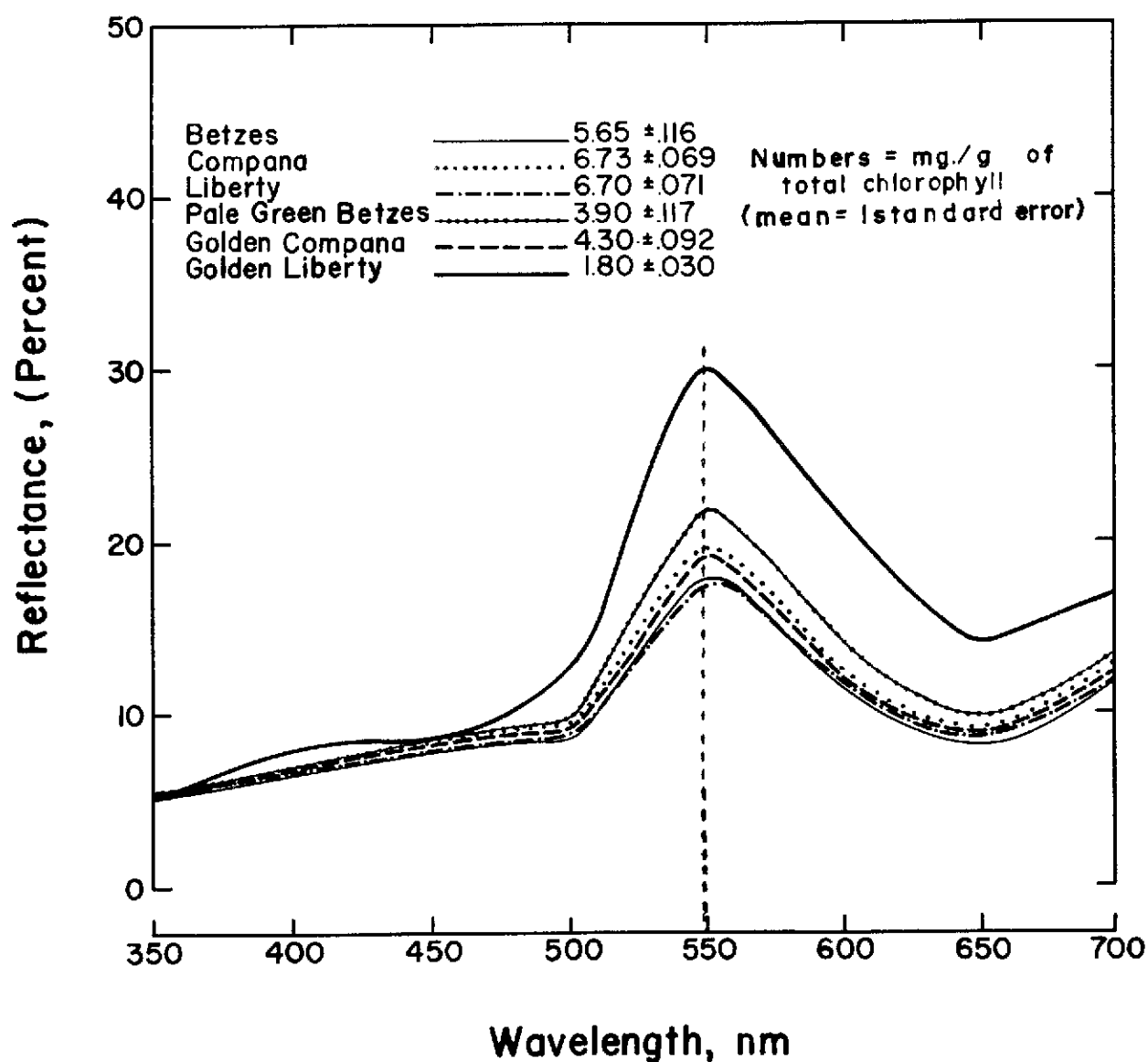
Fig. 1.--Spectrophotometric reflectance measurements over the 350- to 700-nm wavelength interval and total chlorophyll concentrations of six isogenic barley lines. Each spectrum is an average of six leaves.

LIGHT REFLECTANCE, TRANSMITTANCE, AND ABSORPTANCE OF NUTRIENT

SUFFICIENT AND DEFICIENT SQUASH LEAVES

D. E. Escobar, R. R. Rodriguez, and H. W. Gausman

These results were produced unter Re-
search Outline 57, "Physiological and
Histological Factors Affecting the
Spectra of Leaves."

INTRODUCTION

The objective of research summarized here was to study the effects of mineral element deficiencies on the spectral properties of Mexican squash (Cucurbita L.) leaves. The interaction of nutrient-deficient leaves with light must be understood to interpret imagery obtained from aircraft and spacecraft mounted sensors.

MATERIALS AND METHODS

Mexican squash plants were grown hydroponically in eight nutrient solutions-- one control (complete set of nutrients) and seven nutrient-deficient sets (-Ca, -Fe, -K, -Mg, -N, -P, -S). A growth chamber environment was used.

First true leaves of the same chronological age were detached from two replications of the plants, except deceased calcium deficient plants, 18 days after planting for spectrophotometric measurements. A Beckman Model DK-2A ratio recording spectroreflectometer was used to measure the spectral diffuse reflectance and transmittance of top (adaxial) surfaces of single leaves over the 500- to 2500-nm wavelength interval (WLI). Data have been corrected for the decay of the $BaSO_4$ standard to give absolute radiometric data (W. A. Allen's method, Weslaco, Texas). Absorptance was calculated as: 100 - [percent reflectance + percent transmittance].

Data of nine wavelengths (WL)--500, 550, 600, 650, 700, 750, 800, 850, and 900 nm--were analyzed for variance (Steel and Torrie, 1960) for reflectance, transmittance, and absorptance; Duncan's multiple range test (Duncan, 1955) was applied to means of the nine WL.

RESULTS AND DISCUSSION

Most attention was given to the 500- to 900-nm WLI, representing the visible (500 to 750 nm) and the beginning portion of the near-infrared (750 to 900 nm) spectral regions, because these regions affect the response of photographic film. Figure 1 portrays the diffuse reflectance spectra over the 500- to 900-nm WLI. In the visible region, leaves had a variable effect on reflectance because of pigment concentration differences. Average percent reflectances at the 550-nm WL were 8.9, 10.7, 12.1, 19.1, 22.3, 26.4, and 30.2% for -P, control, -S, -N, -K, -Fe, and -Mg leaves, respectively.

At the 900-nm WL (near-infrared region), mean reflectances in ascending order were 45.7, 46.4, 47.0, 48.1, 48.2, 49.2, and 50.7% for -Fe, control, -S, -P, -K, -Mg, and -N leaves, respectively. The near-infrared spectral region is primarily affected by leaf structure.

Statistically, -Fe and -Mg leaves had the highest (p = 0.05) average reflectance of 33.5 to 36.3% for the nine WL compared with the control and -P and -S leaves had lowest reflectances ranging from 26.2 to 27.2%.

Percent transmittance (Fig. 2) varied among leaves in the visible region. Average values obtained at the 550-nm WL for -P, -N, control, -S, -K, -Mg, and -Fe leaves were 13.6, 16.0, 18.3, 20.2, 24.9, 29.5, and 33.9%, respectively. In the near-infrared region (900-nm WL), transmittance values were 45.1, 49.6, 50.0, 52.8, 53.8, 54.0, and 54.6% for -N, -K, -Mg, -P, control, -S, and -Fe leaves, respectively.

According to Duncan's test, -N, -P, control, -S, and -K leaves were alike (p = 0.05) with transmittances ranging from 26.9 to 32.9%; -Mg and -Fe leaves were alike with transmittances of 36.0 and 40.3%, respectively.

Figure 3 shows that -Fe leaves had the lowest and -P leaves had the highest absorptances in the visible region. Mean absorptances at the 550-nm WL were 39.7, 40.3, 52.8, 64.7, 67.7, 71.0, and 77.5% for -Fe, -Mg, -K, -N, -S, control, and -P leaves, respectively. Mean absorptances at the 900-nm WL were -1.0, -1.0, -0.2, -0.2, 0.7, 2.2, and 4.2% for -P, -S, control, -Fe, -Mg, -K, and -N leaves, respectively.

Duncan's test showed that -Fe and -Mg leaves had the lowest statistically alike absorptances of 26.2 and 27.7%, respectively, compared with the highest statistically alike absorptances ranging from 41.4 to 44.3% for -N, control, and -P leaves.

SUMMARY

Nutrient deficiencies, with the exception of -P, increased the visible light reflectance of Mexican squash leaves as much as 20% at the 550-nm WL compared with leaves of nutrient-sufficient plants. Near-infrared light reflectance was affected to a much lesser extent. In the visible region, -Mg leaves had the highest and -P leaves had the lowest reflectance. In the near-infrared region, -N leaves had the highest and -Fe leaves had the lowest reflectance. Effects of nutrient levels on transmittance and absorptance are discussed.

LITERATURE CITED

Duncan, D. G. 1955. Multiple range and multiple f tests. Biometrics 11:1-42.
Steel, R. G. D., and J. H. Torrie. 1960. Principles and Procedures of Statistics. McGraw-Hill, New York. 481 p.
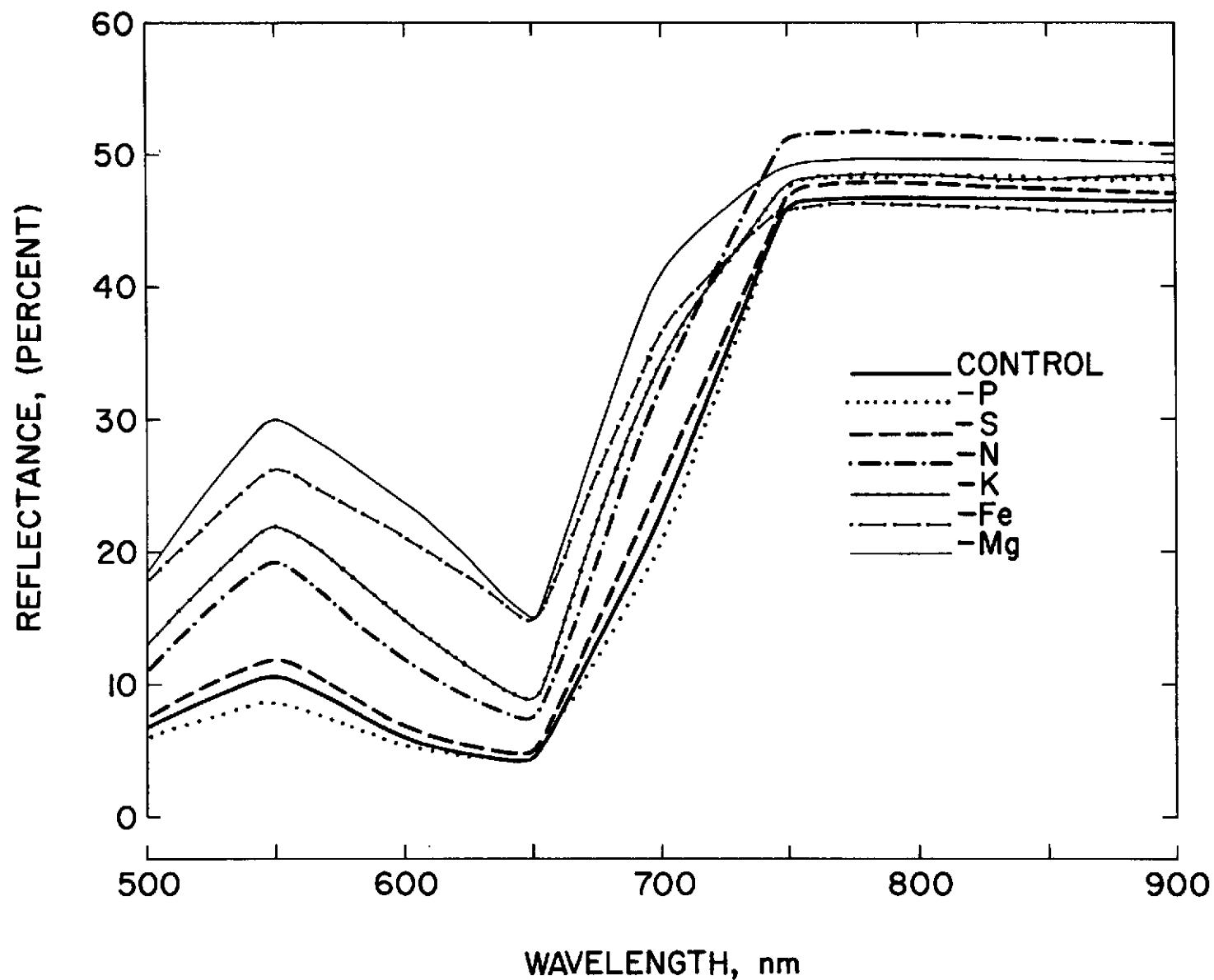
Fig. 1.--Light reflectance of top (adaxial) surfaces of nutrient sufficient (control) and deficient (-P, -S, -N, -K, -Fe, -Mg) mexican squash leaves over the 500- to 900-nm wavelength interval. Each spectrum is an average of two leaves.
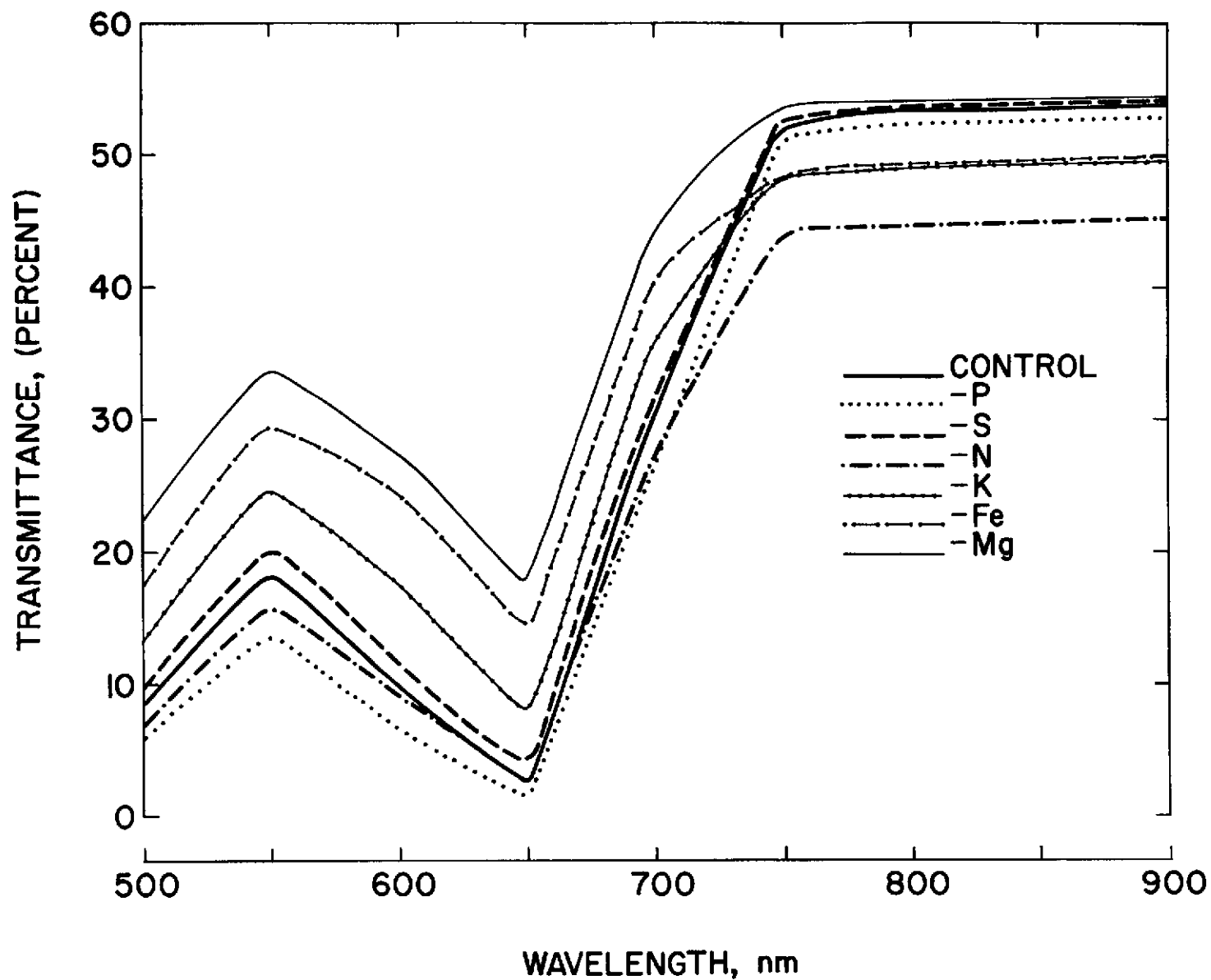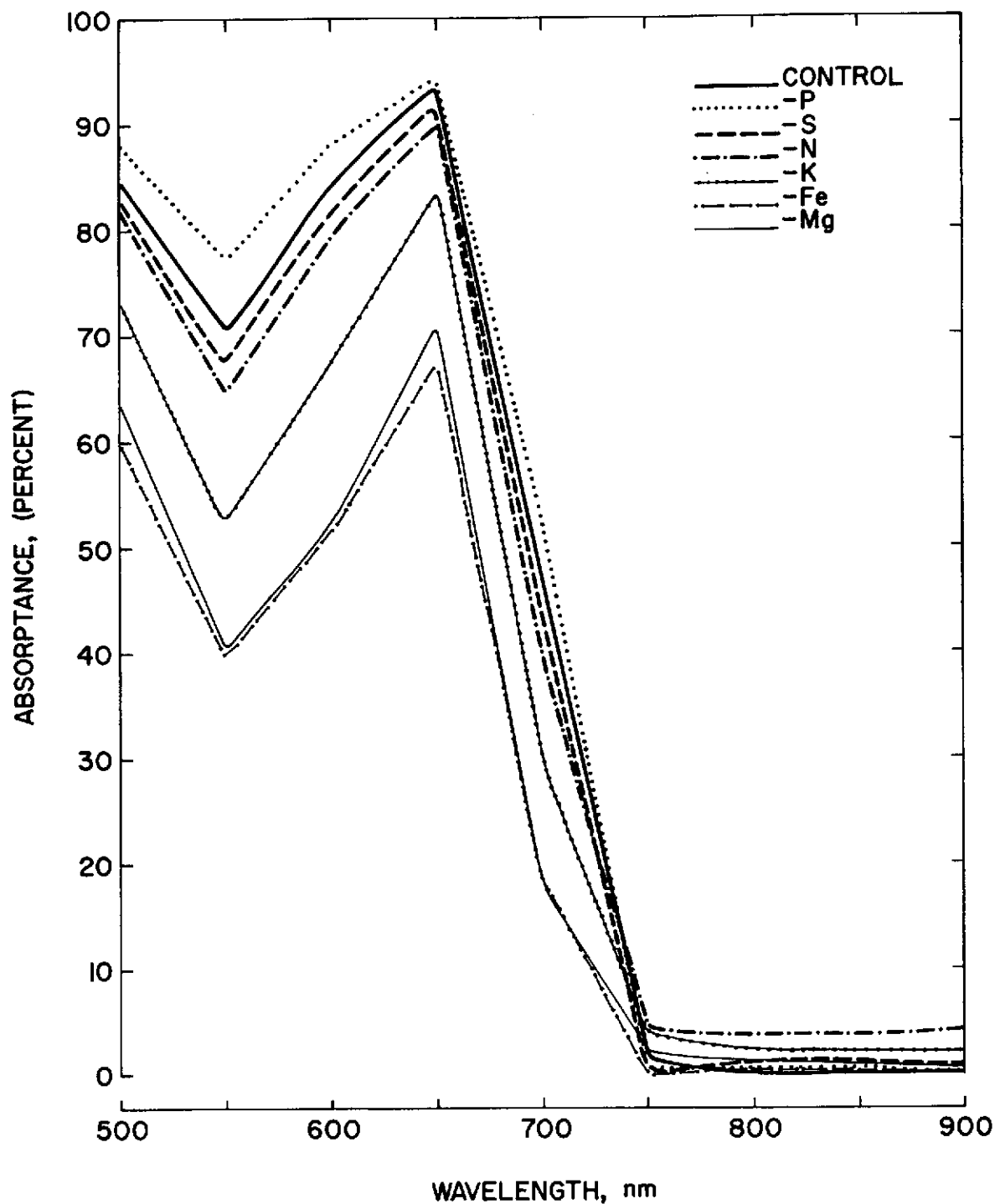
Fig. 2.--Light transmittance of top (adaxial) surfaces of nutrient sufficient (control) and deficient (-P, -S, -N, -K, -Fe, -Mg) mexican squash leaves over the 500- to 900-nm wavelength interval. Each spectrum is an average of two leaves.

Fig. 3.--Light absorptance of top (adaxial) surfaces of nutrient sufficient (control) and deficient (-P, -S, -N, -K, -Fe, -Mg) mexican squash leaves over the 500- to 900-nm wavelength interval. Each spectrum is an average of two leaves.

PHOTOMICROGRAPHIC RECORD OF LIGHT REFLECTED

AT 850 NANOMETERS BY CELLULAR CONSTITUENTS

OF Zebrina pendula LEAF EPIDERMIS

H. W. Gausman

The following manuscript has been sub-
mitted for publication in Letters to
NATURE. These results were produced
under Research Outline 61, "Microspectro-
photometric Study of Light Absorptance
by Plant Cells."

INTRODUCTION

The study reported here is based on light reflected at the 850-nm near-
infrared wavelength by cellular constituents of the lower leaf epidermis of
Zebrina pendula, Schnizl. (Wandering Jew). Results show that Zebrina cellular
membranes reflect more near-infrared light than the surrounding protoplasm, and
that the middle lamella reflects more near-infrared light than the cell walls.
The evidence indicates that refractive index discontinuities other than cell
wall-air interfaces are responsible for a part of the near-infrared light reflec-
tance by plant leaves.

The interaction of light with plant leaves is being investigated at the Rio
Grande Soil and Water Research Center at Weslaco, Texas. Spectrophotometrical
and histological measurements in the laboratory are used to explain differences
in reflectances of leaves from "healthy" and "stressed" plants. The information
facilities predicting reflectances of plant canopies in the field that may be
detected by sensors in air or spacecraft (Wiegand et al., 1969).

Willstätter and Stoll (1913) explained reflectance and transmittance of a
plant leaf on the basis of critical reflection of visible light at the cell wall-
air interface of spongy mesophyll tissue. Near-infrared light (750 to 1350 nm)
reflectance has been mathematically related to numbers of intercullular air
spaces (lacunae) in leaf mesophylls (Allen et al., 1969; Gausman et al., 1970).
An increase in air spaces increases reflectance, because diffused light passes
more often from a high (hydrated cell walls, 1.33) to a low (intercellular air,
1.0) refractive index. However, a hypothesis was advanced that leaf reflectance
derives from the diffuse characteristics of plant cell walls (Sinclair, 1968).
This stimulated us to investigate the interaction of leaf cells and their con-
stituents with near-infrared light.

SUMMARY

Light reflected from living Zebrina specimens was recorded on Kodak high speed black-and-white infrared film on dimensionally stable .01-cm Estar Base (Eastman Kodak Co., 1971) in a camera mounted on the monocular observation tube of the microscope—a component of a Leitz microspectrophotometer assembly. For a reflectance measurement, collimated light at the 850-nm wavelength, 80-nm in-line mirror monochromator spectral slit width (Leitz technical description, Pamphlet 52-13/Engl.), was transmitted through a fixed field diaphragm and objective into an illuminator mounted on the microscope tube. Light was supplied by a high-pressure Xenon lamp with maximum output at the 800-nm wavelength. A 25/0.65 achromatic oil or water immersion objective (oil was used in this study) transmitted reflected light from the object of the specimen upward in the monocular microscope tube with a 15 X eyepiece at its apex. The resolving power of the objective at the 850-nm wavelength was 0.8 microns (the size of the smallest distance between two points that can be differentiated) (Richard and Klein, 1970).

The sequence of phases from the glass slide on which the plant tissue was mounted to the objective was: plant tissue—tap water—No. 1 cover slip—immersion oil (refractive index 1.1515). A 15% reflectance standard was also exposed to light at the 850-nm wavelength for comparative purposes, and for an evaluation of variability among like exposures on different films. The sequence of phases from the surface of the reflectance standard to the objective was: immersion oil—glass slide—tap water—No. 1 cover slip—immersion oil. Oil and glass have essentially the same refractive indices. The surface of the reflectance standard and the plant tissue were the same distance from the objective. Film density measurements indicated that the repeatability of exposures among films was excellent. Films were developed with a Nikor tank and reel at 29.4C for 8 min. with Kodak D-76 developer, fixer, and hypo clearing agent.

Research was conducted in an air-conditioned room (about 22C) with subdued light intensity near the microspectrophotometer. All tissue was viable as evidenced by protoplasmic streaming. Photographic tests indicated that results were unaffected by extraneous light or by internal reflecting and stray light centers in the objective.

Preliminary photomicrographic results indicate that cellular membranes reflect near-infrared light more strongly than the surrounding protoplasm (Fig. 1). This is evident with the membranes of the cytoplasm (plasma-lemma), nucleus (nuclear membrane), and chloroplasts (chloroplast envelope). The vacuolate membrane (tonoplast is not apparent in Fig. 1.

Figure 1 also shows that the middle lamella (C) reflects near-infrared light more strongly than the cell walls (B). The cell walls are composed primarily of cellulose, and calcium pectate (a cementing material) is very abundant in the middle lamella. All cellular membranes are composed of lipids and proteins (Bonner and Varner, 1965). It is apparent that cellular membranes composed of lipids and proteins differentially reflect light compared with cell walls and other cellular constituents.

When a light beam passes from one medium into another in which its velocity is different, as from water into air, its direction of propagation changes if the light strikes the interface at angles other than 90 degrees. This directional change of a light beam because of different velocities is known as refraction. In plant leaves, for example, near-infrared light beams pass from hydrated cell walls (refractive index 1.33) into intercellular air spaces or lacunae (refractive index 1.0) in the leaf mesophyll. As a leaf mesophyll becomes more porous (an increase in intercellular air spaces), reflectance of near-infrared light increases compared with a leaf with a nonporous mesophyll (Gausman et al., 1970).

The refractive indices of lipids exceed 1.4 for the sodium D-line at temperatures of 35.0 to 85.6C (Handbook of Chemistry, 1968). For comparative purposes, a 19% sucrose solution (sucrose is contained in the sap in cell vacuoles) has a refractive index of 1.36217 at 20C (Methods of Analysis, 1965). Thus, the velocity of light would be less in lipids than in the sucrose solution. Undoubtedly, there is also a difference among the refractive indices of the cellulosic components of the cell wall and the pectic material in the middle lamella.

The results obtained by photographically recording the reflectance of light -: the 850-nm wavelength are analogous to the principle of a phase microscope that allows visualization of different parts of a cell without staining. Light passing through a specimen is refracted as a function of refractive indices of cells and their constituents (Richard and Klein, 1970). Direct rays pass through an objective plate and are retarded (wavelength shift), but diffracted light passes through the plate and the wavelength is not shifted. Phase differences among tissues or cell organelles are perceived as various shades of gray.

Black-and-white infrared photography of reflected light at the 850-nm wavelength appeared to enhance the differentiation of tissues of organelles within the resolving power of the objective. However, the time of exposure of the film to near-infrared light is extremely critical, and it is very difficult to obtain a desirable perceptivity. The resolving power of a film is controlled largely by the contract of the emulsion, and its turbidity (turbidity (density) depends on light absorptance of the emulsion and its scattering power) (Harrison et al., 1949). Resolving power depends mainly on the density an image attains and is greatest for intermediate densities.

One of the primary difficulties of this study was the inability to focus the object of a specimen in the near-infrared at the 850-nm wavelength. Blue light permits more critical focusing than green or red light because of increased resolving power, but the object may be more difficult to see. In this study the specimens were focused at 550 nm, since the human eye is most sensitive to the green wavelengths with a peak at about 550 nm.

In 1842 Dutrochet (Gabriel and Fogel, 1965) realized that a plant cell was a polyhedron (now thought to be a tetrakaidecahedron, 14-sided) and that it caused various refractions of visible light rays. Evidence here indicates that a cell and its constituents affect the reflectance of near-infrared light at the 850-nm wavelength, and undoubtedly absorptance and transmittance, too. This agrees with a recent conclusion (Woolley, 1971) that refractive index discontinuities other than air-cell interfaces are responsible for a part of near-infrared light reflectance by leaves.

The study summarized here will be extended using the scanning capabilities of the microspectrophotometer assembly. Wavelengths will be scanned across specimens, and data will be logged on paper tape for computer input for data reduction and statistical studies. For photographic work, a second camera will be used to take black-and-white panchromatic photographs of the same specimen object at the 550-nm wavelength that was subjected to black-and-white near-infrared photography.

LITERATURE CITED

Allen, W. A., H. W. Gausman, A. J. Richardson, and J. R. Thomas. 1969. Interaction of isotropic light with a compact plant leaf. J. Opt. Soc. Amer. 59:1376-1379.

Bonner, J., and J. E. Varner. 1965. Plant biochemistry. Academic Press, New York. p. 64-87, 151-186.

Gabriel, M. L., and S. Fogel. 1965. Great experiments in biology. Prentice-Hall, Englewood Cliffs, New Jersey. p. 7.

Gausman, H. W., W. A. Allen, R. Cardenas, and A. J. Richardson. 1970. Relation of light reflectance to histological and physiological evaluations of cotton leaf maturity (Gossypium hirsutum L.) Appl. Opt. 9:545-552.

Handbook of biochemistry. 1968. (edit. by Sober, H. A., and R. A. Harte). E-11 The Chemical Rubber Co.,Cleveland, Ohio.

Harrison, G. R., R. C. Lord and J. R. Loofbourow. 1949. Practical spectroscopy. Prentice-Hall, New York. p. 148.

Kodak technical information sheet. 1971. Eastman Kodak Company, Rochester, New York.

Methods of analysis. 1965. (edit. by Horwitz, W.) A.O.A.C., Washington. p. 831.

Richard, M., and Klein, D. T. 1970. Research methods in plant science. The Natural History Press, Garden City, New York. p. 95, 97.

Sinclair, T. R. 1968. Pathway of solar radiation through leaves. M. S. Thesis, Purdue Univ., Lafayette, Indiana. 179 p.

Wiegand, C. L., H. W. Gausman, W. A. Allen, and R. W. Leamer. 1969. Interaction of electromagnetic energy with agricultural crops. Proc. 2nd Ann. Earth Resources Aircraft Program Review, Vol. II, Sec. 22, 1-14 (NASA, Houston, Texas)

Willstätter, R., and A. Stoll. 1913. Untersuchungen über die Assimilation der Kohlensäure (Springer, Berlin). p. 122-127.

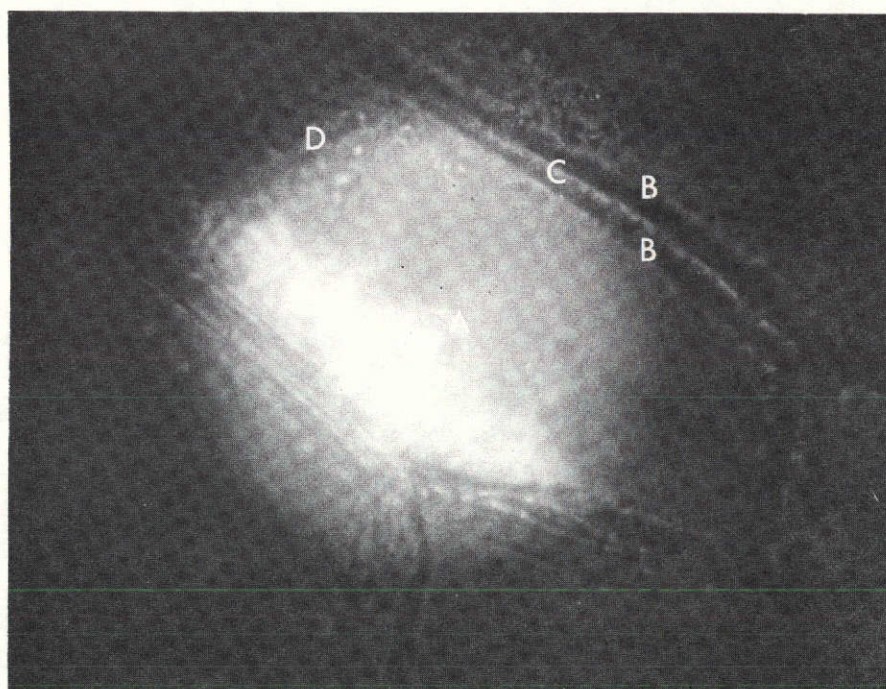Woolley, J. T. 1971. Reflectance and transmittance of light by leaves. Plant Physiol. 47:656-662.

Fig. 1.--Photomicrograph (three second exposure) of a portion
of the lower epidermal cell of a leaf of Zebrina pendula,
Schnizl. (Wandering Jew), about 2500 X, specifically focused
to perceive the nucleus. White and dark areas denote high
and lower light reflectance at a wavelength of 850 nm,
respectively. Strongly reflected light is apparent for the
nuclear membrane (A), plasmalemmas (B), middle lamella (C),
and chloroplast envelope (D) compared with adjacent, darker
areas.

THE EFFECTS OF CITRUS BLACKFLY FEEDING - INJURY ON LEAF STRUCTURE
AND ITS INFLUENCE ON THE REFLECTANCE CHARACTERISTICS OF CITRUS FOLIAGE

W. G. Hart, H. W. Gausman, and R. R. Rodriguez

These results were produced under
Research Outline 57, "Physiological
and Histological Factors Affecting
the Spectra of Leaves."

INTRODUCTION

Damage to citrus foliage caused by the citrus blackfly, Aleurocanthus woglumi Ashley, is of two types -- feeding-injury and physiological damage caused by a sooty-mold fungus (Capnodium citri) which develops on honeydew excreted by the developing insect. When sooty-mold deposits become heavy, they reduce the photosynthesis of the affected plant. The extent of the damage caused by the feeding injury to foliage is more difficult to determine, but it is considered to be significant. Color infrared aerial photography with Kodak Ektachrome Infrared Aero 8443 and Aerochrome 2443 has been used to detect the presence of sooty-mold deposits caused by insect activity on citrus foliage (Hart and Myers, 1968; Hart et al., 1972). The nature of the blackfly feeding-injury and its effects on the spectral properties of citrus foliage has not been investigated. This paper reports results obtained in studies to determine the effects of blackfly feeding-injury on leaf structure, and the influence of the leaf damage on the reflectance characteristics of citrus foliage.

MATERIALS AND METHODS

Ten orange leaves were randomly selected. Five of these leaves were blackfly damaged and five were normal in appearance. Leaves of approximately the same chronological age were selected because a young leaf has less light reflectance than a mature leaf (Gausman et al., 1969). The leaves were wrapped in Glad Wrap to limit dehydration immediately after they were detached from the trees. Before spectrophotometric measurements were made, the leaves were wiped with dampened paper towels to remove surface contamination.

A Beckman Model DK-2A ratio-recording spectroreflectometer was used to measure diffuse reflectance and transmittance over the 500- to 2500-nm wavelength (WLI) of top (adaxial) and bottom (abaxial) leaf surfaces.

Data have been corrected for decay of the $BaSO_4$ standard to give absolute radiometric data (W. A. Allen's method, Weslaco, Texas). Absorptance was calculated as: 100 - [percent reflectance + percent transmittance].

Leaf thickness was measured with a linear displacement transducer and digital voltmeter (Heilman et al., 1968). Leaf area was determined with a planimeter.

Percent leaf water content was determined on an oven-dry weight basis by drying at 68C for 72 hours and cooling in a desiccator before final weighing.

Analyses of variance (Steel and Torrie, 1960) and Duncan's multiple range test (Duncan, 1955) were used in the statistical analyses of the data. Standard errors were calculated for means of leaf thickness and water content data.

To study effects of blackfly damage on leaf structure, tissue pieces were taken near the center of leaves, approximately 1 cm from the midrib. Samples were fixed in formalin-acetic acid-alcohol (FAA), dehydrated with tertiary butanol, embedded in paraffin, stained with safranin-fast green (Jensen, 1962), microtomed at a thickness of 10 μ, and photographed with a Zeiss Standard Universal Photomicroscope.

RESULTS AND DISCUSSION

Figure 1 shows photomicrographs of transections of unaffected (upper photomicrograph) and blackfly-damaged (lower photomicrograph) orange leaves. The transection of the damaged leaf shows that damaged cells occur near the lower epidermis. Many cells appear empty, and the cell walls are greatly thickened. Damaged areas remained heavily stained in the histological process. The damaged leaf areas were chlorotic on the blackfly-damaged leaves.

The reflectance and transmittance spectra for top and bottom surfaces of blackfly-damaged and unaffected orange leaves showed that the main effect of blackfly damage was in the visible region (500 to 750 nm) of the 500- to 2500-nm WLI. Hence, statistical analyses were conducted on measurements made over the 500- to 750-nm WLI. Wavelengths used were 500, 550, 600, 650, 700, and 750 nm.

Damaged leaves had significantly higher (p = 0.05) reflectance and transmittance (average of all wavelengths) from top leaf surfaces than unaffected leaves, Table 1. Reflectances were 20.8 and 18.9%, and transmittances were 12.8 and 12.0% for damaged and unaffected leaves, respectively. Absorptance was significantly higher for unaffected leaves (69.1%) than for damaged leaves (66.3%).

Table 1 statistically compares (Duncan's test, p = 0.05) means of wavelengths for reflectance, transmittance, and absorptance for top leaf surfaces. All mean comparisons were significant for reflectance. For transmittance and absorptance, means were statistically alike for the 500- and 600-nm wavelengths, all other mean comparisons were different.

For bottom leaf surfaces, damaged leaves had significantly higher (p = 0.05) reflectance and transmittance (average of all wavelengths) than unaffected leaves, Table 2. Reflectances were 26.0 and 24.1%, and transmittances were 13.6 and 12.4% for damaged and unaffected leaves, respectively. Absorptance was significantly higher for unaffected leaves (63.5%) than for damaged leaves (60.5%).

Table 2 statistically compares (Duncan's test, p = 0.05) means of wavelengths for reflectance, transmittance, and absorptance for bottom leaf surfaces. All means were statistically different except means were alike for the 500- and 600-nm wavelengths.

Table 3 presents the leaf thicknesses and percent water contents of damaged and unaffected orange leaves. Mean leaf thicknesses of the damaged and unaffected leaves were 0.181 ± .003 mm (standard error) and 0.186 ± .006 mm, respectively. Damaged and unaffected leaves had average water contents of 54.7 ± 1.6% and 54.5 ± 2.1%, respectively. It is evident that blackfly damage had little effect on the thicknesses and water contents of orange leaves compared with unaffected leaves.

SUMMARY

Studies were conducted to determine effects of blackfly feeding-injury on leaf structure and reflectance characteristics of citrus foliage. Blackfly damaged leaves had more visible light reflectance and transmittance (1 to 2% range) at the 550-nm wavelength than unaffected leaves. It made little difference if measurements were made on the bottom or the top of leaf surfaces.

Blackfly damage of citrus leaves had little effect on near-infrared light reflectance, leaf thickness, and leaf water content compared with unaffected leaves.

LITERATURE CITED

Duncan, D. B. 1955. Multiple range and multiple f tests. Biometrics 11:1-42.

Gausman, H. W., W. A. Allen, V. I. Myers, and R. Cardenas. 1969. Reflectance and internal structure of cotton leaves (Gossypium hirsutum L.). Agron. J. 61:374-376.

Hart, W. G., and V. I. Myers. 1968. Infrared aerial color photography for detection of populations of brown soft scale in citrus groves. J. Econ. Entomol. 61:617-624.

Hart, W. G., S. J. Ingle, M. R. Davis, and C. Mangum. [Probably 1972]. Aerial infrared color photography as a survey method for citrus blackfly. Manuscript prepared for publication in J. Econ. Entomol.

Heilman, M. D., C. L. Gonzalez, W. A. Swanson, and W. J. Rippert. 1968. Adaptation of a linear transducer for measuring leaf thickness. Agron. J. 60:578-579.

Jensen, W. A. 1962. Botanical histochemistry. W. H. Freeman and Co., San Francisco, Calif. 408 p.

Steel, R. G. D., and J. H. Torrie. 1960. Principles and procedures of statistics. McGraw-Hill, New York. 481 p.

Table 1. Average reflectance, transmittance, and absorptance values of top leaf surfaces of five black-fly-damaged (D) and five unaffected (U) orange leaves.

Wave-length	Reflectance			Transmittance			Absorptance		
	D	U	Mean*	D	U	Mean*	D	U	Mean*
nm	%	%	%	%	%	%	%	%	%
500	9.5	8.0	8.8 a	2.8	2.0	2.4 a	87.7	90.0	88.9 a
550	13.5	10.8	12.2 b	7.0	5.6	6.3 b	79.5	83.6	81.6 b
600	8.7	6.9	7.8 c	2.8	1.7	2.3 a	88.5	91.4	90.0 a
650	6.2	5.4	5.8 d	.7	.5	.6 c	92.6	94.0	93.3 c
700	31.3	27.3	29.3 e	22.3	20.2	21.3 d	46.4	52.6	49.5 d
750	55.5	55.1	55.3 f	41.5	41.8	41.7 e	3.0	3.1	3.1 e
Mean	20.8 a	18.9 b		12.8 a	12.0 b		66.3 a	69.1 b	

* Means followed by common letters are alike, p = 0.05.

Table 2. Average reflectance, transmittance, and absorptance values of bottom leaf surfaces of five blackfly-damaged (D) and five unaffected (U) orange leaves.

Wave-length	Reflectance			Transmittance			Absorptance		
	D	U	Mean*	D	U	Mean*	D	U	Mean*
nm	%	%	%	%	%	%	%	%	%
500	16.3	14.5	15.4 a	2.9	2.1	2.5 a	80.7	83.4	82.1 a
550	22.4	20.2	21.3 b	7.4	5.9	6.7 b	70.2	73.8	72.0 b
600	16.9	14.0	15.4 a	3.0	2.0	2.5 a	80.1	84.0	82.1 a
650	11.1	8.8	10.0 c	.6	.6	.6 c	88.2	90.6	89.4 c
700	36.6	33.8	35.2 d	23.4	20.7	22.1 d	40.0	45.5	42.8 d
750	52.5	53.5	53.0 e	44.0	43.1	43.6 e	3.5	3.4	3.5 e
Mean	26.0 a	24.1 b		13.6 a	12.4 b		60.5 a	63.5 b	

* Means followed by common letters are alike, p = 0.05.

Table 3.   Leaf thicknesses and percent water contents of blackfly-
           damaged and unaffected orange leaves.

| Leaf | Leaf thickness | | Water content | |
No.	Damaged	Unaffected	Damaged	Unaffected
	mm	mm	%	%
1	.176	.185	52.2	52.5
2	.183	.174	59.2	59.2
3	.189	.208	51.4	51.9
4	.171	.178	57.6	59.6
5	.186	.186	52.7	49.1
Mean	.181	.186	54.7	54.5
Standard error	.003	.006	1.6	2.1

SPONGY PARENCHYMA CELL

AIR SPACE
(INTERCELLULAR LACUNA)

STOMA

LOWER EPIDERMAL CELL

SPONGY PARENCHYMA CELL

AIR SPACE
(INTERCELLULAR LACUNA)

LOWER EPIDERMAL CELL

INSECT DAMAGED AREA
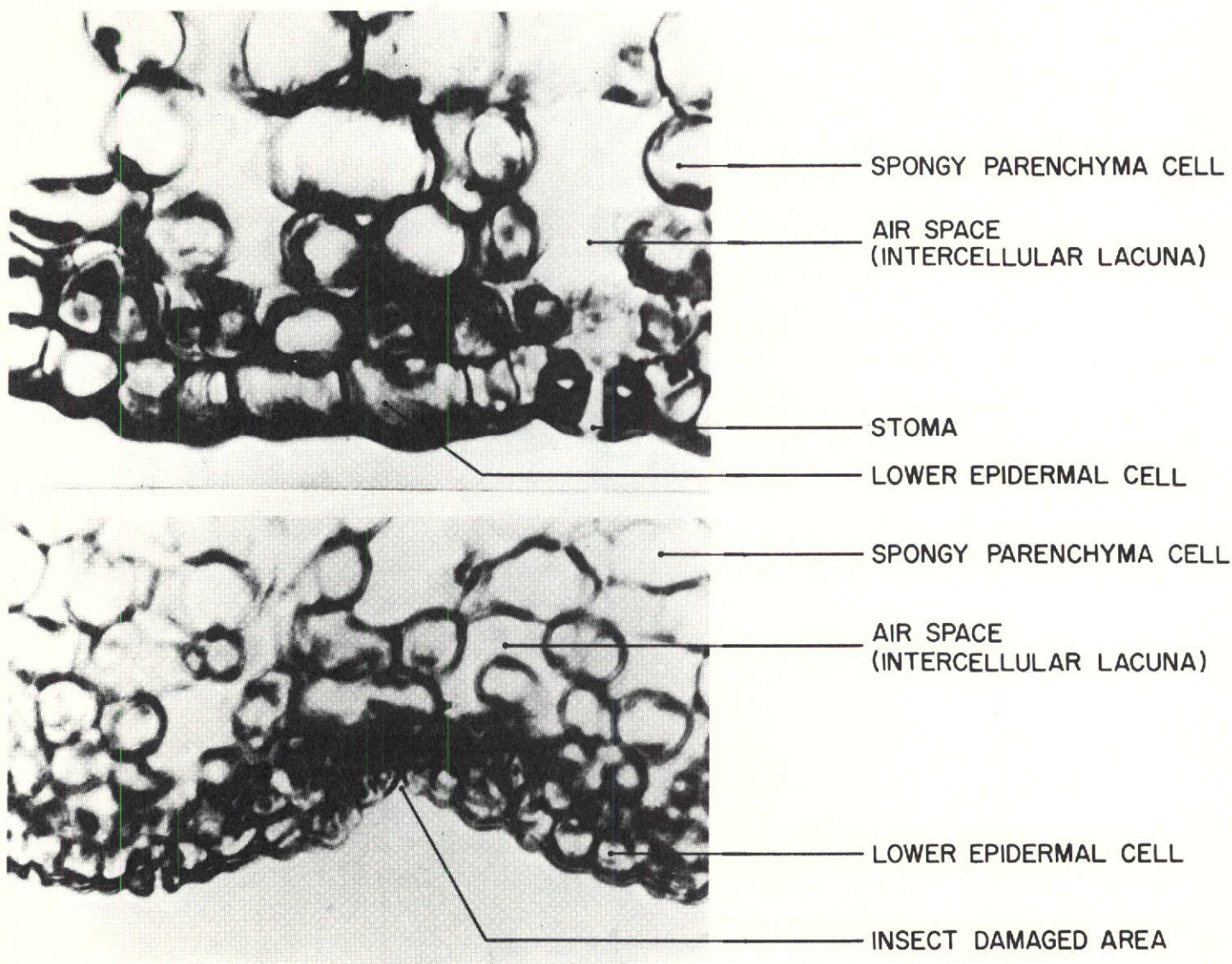
Fig. 1.--Photomicrographs (940X) of transections of orange leaves illustrating portions of unaffected (upper) and blackfly-damaged (lower) leaves.

CALIBRATION OF A LABORATORY SPECTROPHOTOMETER

FOR SPECULAR LIGHT BY MEANS OF STACKED GLASS PLATES

W. A. Allen and A. J. Richardson

The following information is from a
manuscript prepared for publication in
the Review of Scientific Instruments.
These results were produced under Re-
search Outline 67, "Effective Optical
Constants of Single Leaves and Plant
Canopies."

INTRODUCTION

This paper deals with calibration of a laboratory spectrophotometer (Beck-
man DK-2A with a reflectance attachment). The DK-2A originally employed mag-
nesium oxide (MgO) as reflecting surfaces and has been calibrated in that con-
figuration (Richardson et al., 1969). Subsequent to the recent introduction of
barium sulfate ($BaSO_4$) reflectance paint by Eastman Kodak (Grum and Luckey,
1968), our DK-2A was modified to utilize $BaSO_4$ paint[1] both as reflectance stan-
dards and as a coating for the integrating sphere. In view of this drastic
modification, a new calibration of the DK-2A was considered necessary.

The DK-2A utilizes a single beam of light that is chopped into a sample and
reference beam to provide a double-beam system within the sample compartment.
Both sample and reference beams have common detection and amplification compo-
nents. Ratio recording eliminates inaccuracies that result from such effects as
source fluctuations, changes in amplifier gains, sensitivity or spectral response
of the detector, and the presence of common absorbing gases in the sample and
reference paths. Systematic errors, however, still exist in the instrument.
These discrepancies arise from variation in the reflectance paint, and from an
accumulation of small undetermined errors.

Calibration of the DK-2A involves the solution of two separate problems.
First, the absolute optical properties of the reflectance standards must be
obtained. Second, systematic residuals between observed and calculated values of
reflectance and transmittance are approximated and largely removed by means of a
computer. This procedure effectively eliminates the systematic portion of the
error; the irreducible part that remains is accepted as random error.

---

[1] Commercial paint is available from Distillation Products Industries
under the name Eastman White Reflectance paint.

MATERIALS AND METHODS

Reflectance standards are not issued by the National Bureau of Standards for the spectral range 0.5 - 2.5 μm (John C. Schleter, private communication dated 12 February 1968). A new standard was adopted, therefore, that consisted of a pile of No. 1, 22 x 50 mm Corning cover glasses. Such glass plates have been used previously as reflectometer standards (Benford, 1923)[2]. The advantage of glass plates as a standard is that their reflectance can be predicted from electromagnetic theory provided that the complex index of refraction is known for the glass.

Cover glasses were used as taken directly from the carton. No additional cleaning was attempted; however, precautions were taken to avoid additional contamination such as fingerprints. All plates were placed in a desiccator for 24 hours before use to remove most of the moisture adhering to the glass surfaces. The No. 1 cover glasses have a nominal thickness between 0.13 and 0.16 mm and are composed of stirred glass. Measured indices of refraction at the wavelengths 0.4861, 0.5893, and 0.6563 μm were 1.5324, 1.5260, and 1.5231, respectively (Elmer L. Jolley, private communication dated 23 June 1967). These refractive indices are consistent with published values for crown glass (Smith, 1966). Figure 1 is a plausible dispersion curve for crown glass based upon available data.

The glass plates were divided into 9 piles. The 9 piles consisted, respectively, of 1, 3, 5, 7, 11, 15, 22, 36, and 90 plates. The total reflectance and transmittance of each pile was measured over the spectral range 0.5 - 2.5 μm. The number of plates in the piles was selected to correspond roughly to the relative reflectance values 10, 20, 30, ..., 90%. Figures 2a and 2b are plots of relative reflectance and transmittance for the indicated number of plates. Figure 2 is presented for pictorial effect only; the actual data, sampled at discrete wavelengths 0.50, 0.55, ..., 2.50 μm, were recorded on paper tape by a Datex SDS-1 Spectrophotometer Data Recording System. The undulating character of some of the traces in Fig. 2 are interference effects induced at glass surfaces in near contact. This phenomenon could have been reduced by canting each plate at a slight angle to its neighbor. The interference effects in the data of Fig. 2 increase the random error of the instrument, but do not contribute to the systematic error.

Six standards, composed of BaSO4 paint deposited on aluminum plates, were supplied by Beckman. No significant differences were found among the reflectances of these 6 standards when the standards were differentially examined with the DK-2A. A standard was arbitrarily selected and positioned in one port of the DK-2A while the remaining standards, treated as unknown specimens, were placed in the other port. Both the 100% and zero lines were checked with procedures recommended by the manufacturer and were found to be well within acceptable tolerances.

---

[2] Product Engineering Laboratory Products Department, Corning Glass Works.

Absolute Reflectance of BaSO4 Paint Standards

The first task was to determine the absolute reflectance of the BaSO4 paint standards over the spectral range 0.5 - 2.5 μm based upon the adoption of the dispersion curve of Fig. 1 as a primary standard. The initial mathematical analysis following was performed with the data of Fig. 2 based upon the known reflectance of MgO (Sanders and Middleton, 1953).

At a given wavelength, the specular reflectance R and transmittance T of a pile of N glass plates is given by the relation

$$(a-a^{-1})/T = (b^N-b^{-N})/R = ab^N-a^{-1}b^{-N} \qquad , \qquad (1)$$

where a and b are numbers determined by experiment (Stokes, 1862). The reflectance r and transmittance t of a single plate is expressed by

$$(a-a^{-1})/t = (b-b^{-1})/r = ab-a^{-1}b^{-1} \qquad , \qquad (2)$$

where Eq. (2) was obtained from Eq. (1) by setting $N = 1$.

Equations (1) have been fitted to experimental data of the form illustrated in Fig. 2 (Allen and Richardson, 1968). These procedures were applied to the data of Fig. 2 in order to obtain the parameters a and b. The analysis was performed at 0.50, 0.55, ..., 2.50 μm wavelengths. Typical residuals between observed and calculated values for reflectance and transmittance are displayed in Fig. 3. Since the reflectance of BaSO4 was not known at this point, the reflectance of MgO was used in the calculations.

The reflectance r and transmittance t of a single cover glass can be calculated with considerable precision by means of Eq. (2) after a and b have been determined. The following relations have been derived (Allen et al., 1969):

$$r = R_{12} + (T_{12}\tau^2 R_{12}T_{21})/(1=\tau^2 R_{23}R_{21}) \qquad , \qquad (3)$$

$$T = T_{12}\tau T_{23}/(1-\tau^2 R_{23}R_{21}) \qquad ; \qquad (4)$$

where τ is the transmissivity of a single cover glass. The subscript notation in Eqs. (3) and (4) indicates reflectivity R_{ij}, or transmissivity T_{ij}, for light interacting with contiguous media ($i=j\pm1$). In the present application, media 1 and 3 are air and medium 2 is crown glass. In the case of smooth surfaces $R_{12} = R_{21} = R_{23}$ and $T_{12} = T_{23} = 1-R_{12}$. Equations (3) and (4), therefore, can be simplified to the forms

$$r = R + \tau^2[(1-R)^2 R]/(1-\tau^2 R^2) \qquad , \qquad (5)$$

$$t = \tau(1-R)^2/(1-\tau^2 R^2) \qquad , \qquad (6)$$

where $R = R_{12}$ should not be confused with the same symbol that appears in Eq. (1). Eliminate τ between Eqs. (5) and (6) and solve for R to obtain the relation

$$R = \{1+2r-r^2+t^2-[(1+2r-r^2+t^2)^2-4r(2-r)]^{\frac{1}{2}}\}/[2(2-r)] \qquad . \qquad (7)$$

Solve Eq. (5) for τ^2

$$\tau^2 = (r-R)/[1-2R+rR)] \qquad . \qquad (8)$$

[A relation equivalent to Eq. (8), expressed in terms of transmittance instead of reflectance, can be obtained by solving Eq. (6) for τ.] Reflectance r and transmittance t of a single plate are known from Eqs. (2). Equation (7) can be used to calculate R with considerable precision.

Reflectance R from the front surface of a glass plate of relative index of refraction n is given for a dielectric medium by the Fresnel relations (Smith, 1966).

$$R = \tfrac{1}{2}[\sin^2(I-I')\sin^{-2}(I+I') + \tan^2(I-I')\tan^{-2}(I+I')] \qquad , \qquad (9)$$

where I and I', the respective angles of incidence and refraction, are related by Snell's law

$$n \sin I = n' \sin I' \qquad . \qquad (10)$$

The data of Fig. 2 were obtained with an arrangement of the DK-2A in which light was incident upon the plates at an angle 5 deg from normal. Reflectance from crown glass at 5 deg incidence can be calculated from Eq. (9) where I = 5 deg and n = 1.523. Experience has shown, however, that under these conditions Eq. (9) can be approximated, within experimental uncertainty, by the relation

$$R = [(n-1)/(n+1)]^2 \qquad . \qquad (11)$$

Solve Eq. (11) for n to obtain

$$n = (1+R + 2R^{\frac{1}{2}})/(1-R) \qquad . \qquad (12)$$

The data of Fig. 2 were introduced into the sequence of Eqs. (1), (2), (5), (6), (7), (9), (10), and (12) to obtain the dispersion curve of crown glass based upon the trial assumption that the reflectance of the $BaSO_4$ is the same as MgO. Since the assumption is admittedly an approximation, the resultant dispersion curve deviated somewhat from that of Fig. 1. Iteration continued until a reflectance curve was obtained that led to a dispersion curve coincident (within experimental uncertainty) with Fig. 1. Careful interpolations and extrapolations from the successive trial results considerably reduced the amount of calculation necessary. The reflectance curve obtained, illustrated in Fig. 4, was adopted as the reflectance curve of the $BaSO_4$ paint standard. The smooth curve in Fig. 4 is a cubic equation $R = \Sigma\ a_i \lambda^i$ fitted in the sense of least squares to the data; the coefficients a_i are listed in Table 1. Within experimental uncertainty, the mathematical relation is equivalent to the experimental results.

The coefficient of absorption k of the glass plates was not used in the calculation. This value was calculated in the regular analysis, however, and is plotted in Fig. 5. The slight detail that appears at wavelengths 1.40 and 1.95 μm is associated with water that still adheres to the surfaces of the plates. The detail at 2.2 μm is caused by the silica in the glass. Otherwise the curve is uninteresting and plausible.

Determination of Non-Linear Corrections

Figure 3 indicates the existence of a systematic error of the order of several percent between observed and computed values of reflectance and transmittance. The computed values were based upon the reflectance of MgO. The shape of the sketched curves suggests that the respective reflectance and transmittance residuals can be well approximated by the following cubic functions:

$$R_o - R_c = a_o + a_1\lambda + a_2\lambda^2 + a_3\lambda^3$$
$$+ b_1R + b_2R^2 + b_3R^3$$
$$+ c_2\lambda R + c_3\lambda R^2$$
$$+ d_3\lambda^2 R \quad , \tag{13}$$

and by a similar expression obtained when T is substituted for R in Eq. (13). Another analysis was then performed, using the reflectance of the actual BaSO$_4$ standards (Fig. 4), to obtain improved residuals appropriate to the actual problem. The results were not significantly different from those of Fig. 3 except that the experimental transmittance values in the vicinity of the origin became more compatible with the assumed cubic correction equations.

The observed value of reflectance on a record such as Fig. 2a is designated A while the computed value is termed R. The residuals between observed and computed quantities vanish when the following relation holds:

$$\lambda(A + \delta) - R = 0 \quad . \tag{14}$$

The quantity δ in Eq. (14) is the systematic correction that must be applied to the recorded reflectance value A; the quantity λ is the reflectance of the BaSO$_4$ paint standard. Solve Eq. (14) for δ

$$\delta = \lambda^{-1} (R - \lambda A) \quad . \tag{15}$$

The quantity R − λA is a calculated value that appears in the computer analysis. Equation (15) applies to reflectance; a similar relation, where T is substituted for R, must be used in order to correct systematic errors in transmittance. Reflectance residuals $\delta = R_o - R_c$, using Eq. (13) were fitted by regression to obtain optimum values for the 10 coefficients. A similar procedure was followed to obtain corrected values of transmittance. The 20 corrections were generated and applied automatically to values of reflectance and transmittance measured with the DK-2A.

Decay of the BaSO$_4$ Paint Standard With Time

When MgO was used as a reflectance standard, the decrease of its reflectance with time was recognized as a problem (Sanders and Middleton, 1953). If a secondary standard such as Vitrolite[3] is compared at regular time intervals with the MgO standard, the Vitrolite will appear to become more highly reflecting with time. When it was advantageous to preserve a MgO reflectance standard for a long period of time, the ratio V_i/V_f was applied to all measured values of reflectance. The quantity V_i is the initial reflectance of the Vitrolite at a given wavelength, and V_j is the actual measured value of the Vitrolite at a later time when a measurement was taken. This procedure has also been adopted in the case of the BaSO$_4$ painted standards. The extent to which the BaSO$_4$ standards will degrade with time is not known, but the contingency has been provided for.

RESULTS AND DISCUSSION

Two analyses were performed to test the results of the calibration. The first analysis was based upon the same glass plates used in the calibration. The standard deviation (σ) between observed and computed quantities, illustrated in Fig. 2, was 1.27%. Corrections calculated for the reflectance of BaSO$_4$ and corrections for the systematic errors, when applied to Fig. 2, reduced σ to 0.41%. Figure 6 is a plot of Fig. 3 after the systematic errors have been removed. The reduction in σ is ascribed to successful calibration.

The second analysis was based upon glass cover plates acquired from another vendor[4]. An almost equally good fit ($\sigma = 0.48\%$) was obtained in this case also. Optical parameters determined for the new glass were slightly different from those used in the calibration, but the discrepancies were well within those expected for crown glass.

The implication of the results is that the instrument in its original configuration was afflicted with experimental error--68% systematic and 32% random. The calibration removed the systematic component. The random error that remained is well within instrumental tolerances.

A precautionary note should be added. Calibration as described in this paper is based on the interaction of specular light with flat surfaces. There is no assurance that calibration achieved in the specular mode will also apply when the instrument is used to measure diffuse light. Nevertheless, this assumption has been tacitly made.

---

[3] Vitrolite is a ceramic tile supplied by the U. S. National Bureau of Standards as a reflectance surface.

[4] Diamond Brand Cover Glass, No. 1, 22 x 60 mm, Robox Surgical Instrument Co., Inc., 810 18th Street, N. W., Washington, D. C. 20006.

SUMMARY

Stacked glass plates have been used to calibrate a laboratory spectrophotometer, over the spectral range 0.5 - 2.5 μm, for specular light. The uncalibrated instrument was characterized by systematic errors when used to measure the reflectance and transmittance of stacked glass plates. Calibration included: first, a determination of the reflectance of a standard composed of $BaSO_4$ paint deposited on an aluminum plate; second, the approximation of the reflectance and transmittance residuals between observed and computed values by means of cubic equations; and finally, the removal of the systematic errors by a computer. The instrument, after calibration, was accurate to one percent when used to measure the reflectance and transmittance of stacked glass plates.

LITERATURE CITED

Allen, W. A., and A. J. Richardson. 1968. Interaction of light with a plant canopy. J. Opt. Soc. Amer. 58:1023.

Allen, W. A., H. W. Gausman, A. J. Richardson, and J. R. Thomas. 1969. Interaction of isotropic light with a compact plant leaf. J. Opt. Soc. Amer. 59:1376.

Benford, F. A. 1923. Reflection and transmission by parallel plates. J. Opt. Soc. Amer. and Rev. Sci. Instru. 7:1017-1025.

Grum, F., and G. W. Luckey. 1968. Optical sphere point and a working standard of reflectance. Appl. Opt. 7:2289.

Richardson, A. J., W. A. Allen, and J. R. Thomas. 1969. Discrimination of vegetation by multispectral reflectance measurements. Proceedings of the Sixth International Symposium on Remote Sensing of Environment, Univ. of Michigan Press, Ann Arbor. p. 1143-1156.

Sanders, C. L., and E. E. K. Middleton. 1953. The absolute spectral diffuse reflectance of magnesium oxide in the near infrared. J. Opt. Soc. Amer. 43:58.

Smith, W. J. 1966. Optical materials and coatings. Modern optical engineering, McGraw-Hill Book Company, New York, 1st ed., Chap. 7, p. 152.

Smith, W. J. 1966. Optical materials and coatings. Modern optical engineering, McGraw-Hill Book Company, New York, 1st ed., Chap. 7, p. 167.

Stokes, G. G. 1862. On the intensity of the light reflected from or transmitted through a pile of plates. Proc. Roy. Soc. London 11:545-556.

Table 1. Coefficients a_i for use in the cubic equation $R = \Sigma a_i \lambda^i$ plotted in Fig. 4.

i	a_i
0	0.97942
1	-0.08367
2	+0.02264
3	-0.00133

Table 2. Coefficients for terms of cubic equations (Eq. 13) used
to remove systematic errors.

Coefficient	Reflectance	Transmittance
a_o	-0.00146	+0.02288
a_1	+0.00271	-0.01087
a_2	-0.00268	+0.00204
a_3	+0.00085	-0.00039
b_1	+0.00332	-0.29070
b_2	+0.00993	+0.72314
b_3	+0.01179	-0.44473
c_2	-0.07676	+0.00236
c_3	+0.08079	-0.01178
d_3	+0.00997	+0.00510
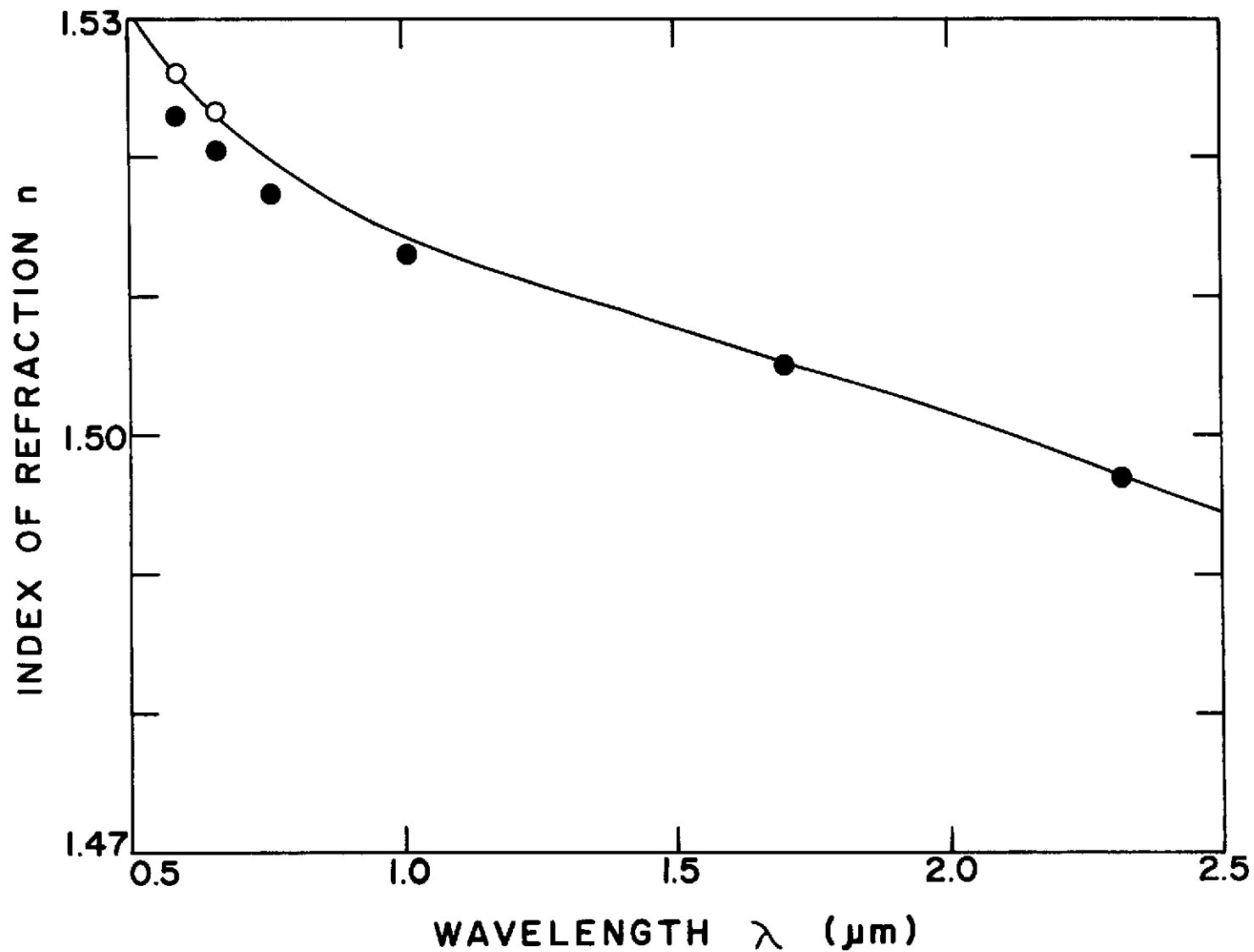
Fig. 1.--Dispersion curve for cover glasses. Points O, for stirred glass, were measured by Corning Glass Works. Points ●, for crown glass, were taken from Smith (1966). The curve was sketched to favor the experimental values in the region where both experimental and handbook data existed.
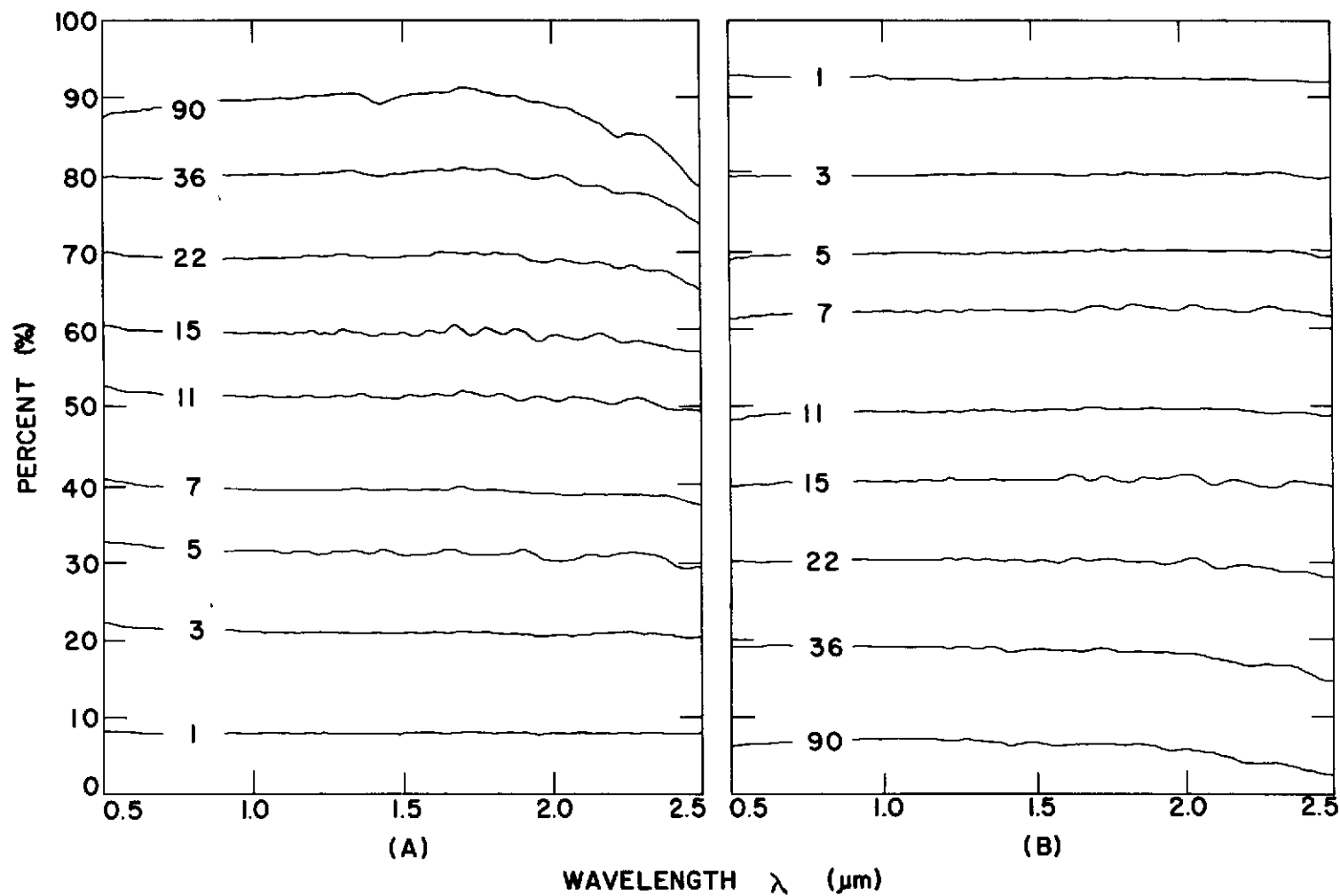
Fig. 2.--Relative reflectance (A) and transmittance (B) of the indicated number of glass plates arranged in nine separate piles with respect to a BaSO₄ paint standard.
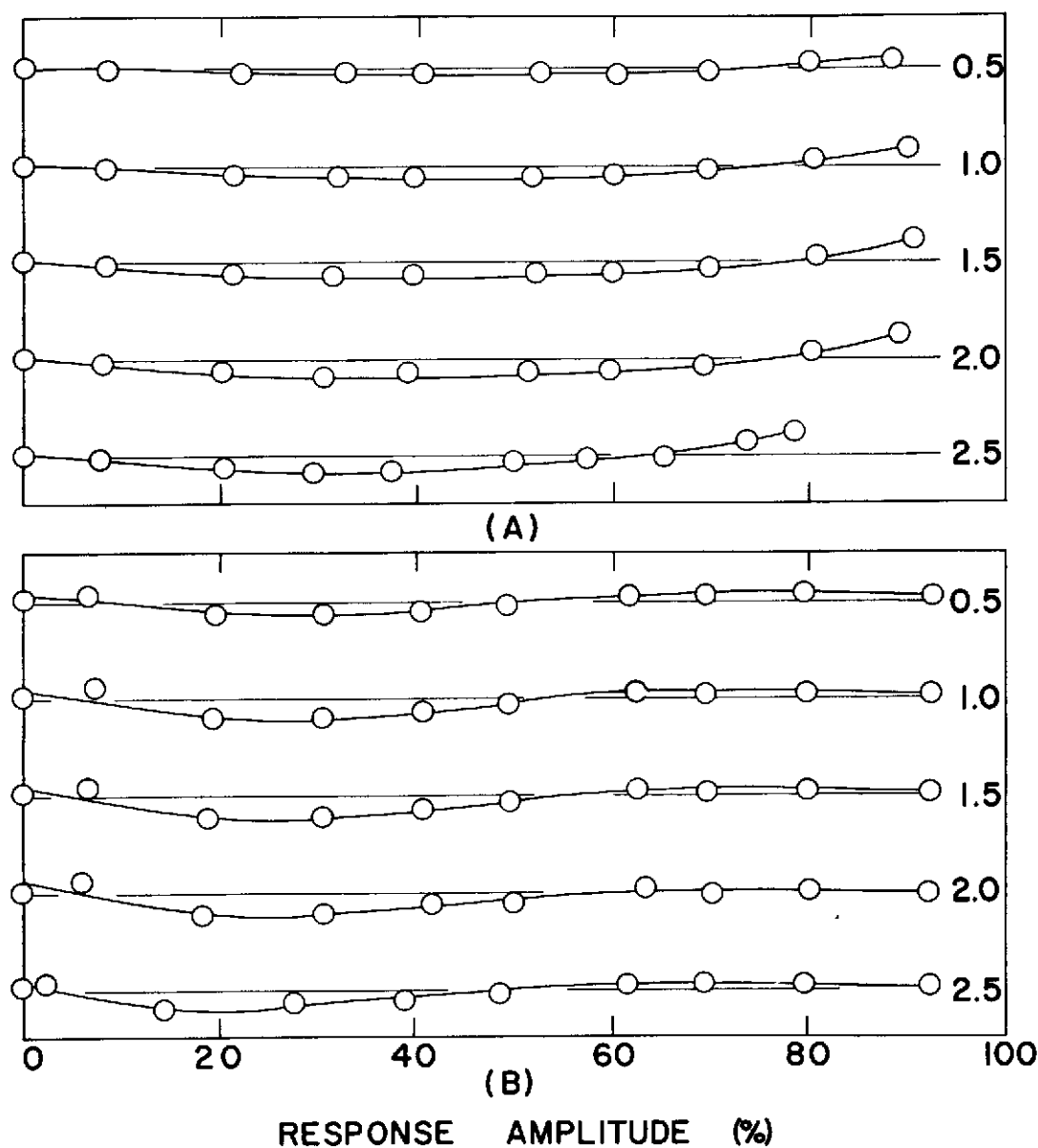
Fig. 3.--Typical residuals for glass plates at wavelengths 0.5, 1.0, ..., 2.5 μm. (A) Reflectance and (B) Transmittance. Individual curves are separated by 10%. Calculated values are based upon MgO as a reflectance standard. The standard deviation between observed and computed quantities is 1.27%.
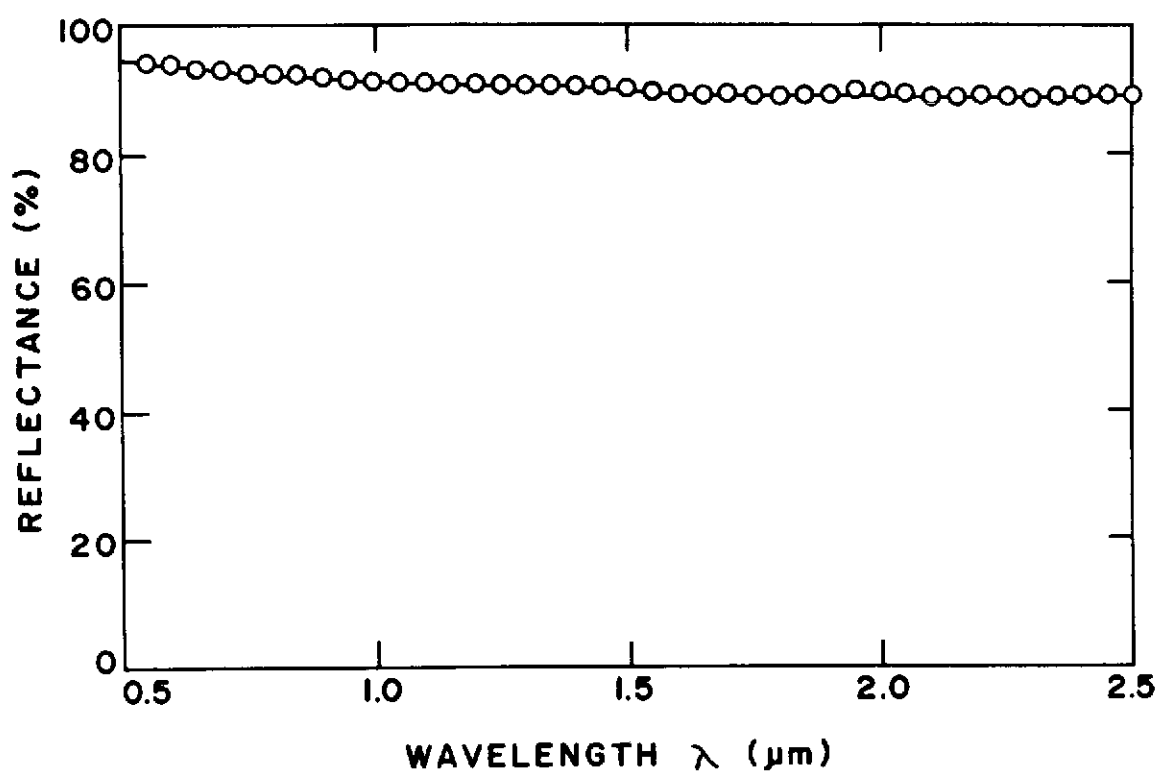
Fig. 4.--Absolute reflectance of BaSO$_4$ paint standard determined by
the method introduced in this paper. The data can be approximated
with adequate precision by the cubic R = $\Sigma a_i \lambda^i$ where the coefficients
a$_i$ (i = 0, 1, 2, 3) are listed in Table 1.
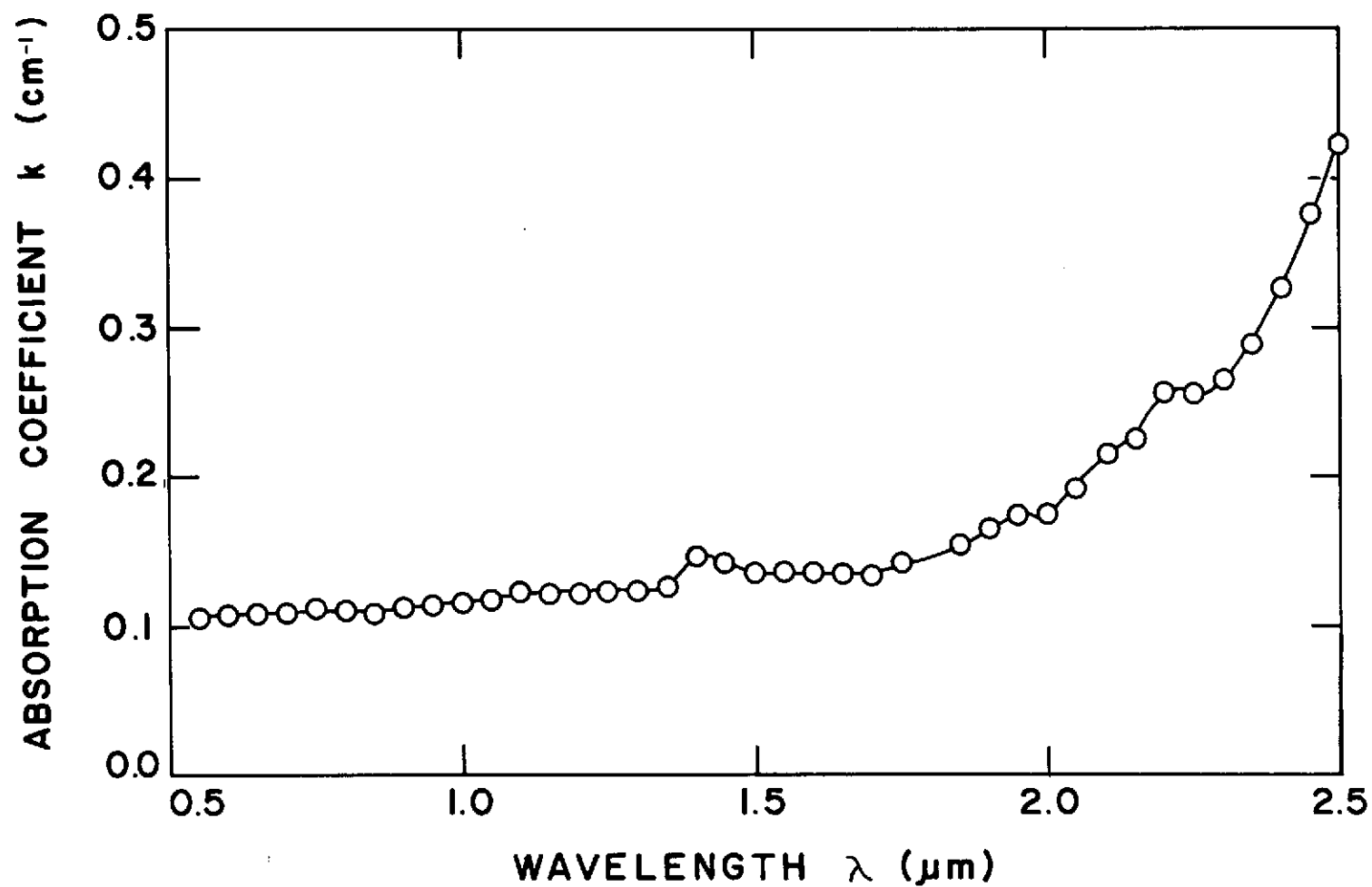
Fig. 5.--Absorption coefficient k for crown glass obtained by the method introduced in this paper. The detail that appears at 1.40 and 1.95 μm results from liquid water that adheres to the surfaces of the glasses. The detail at 2.2 μm is associated with the silica in the glass.
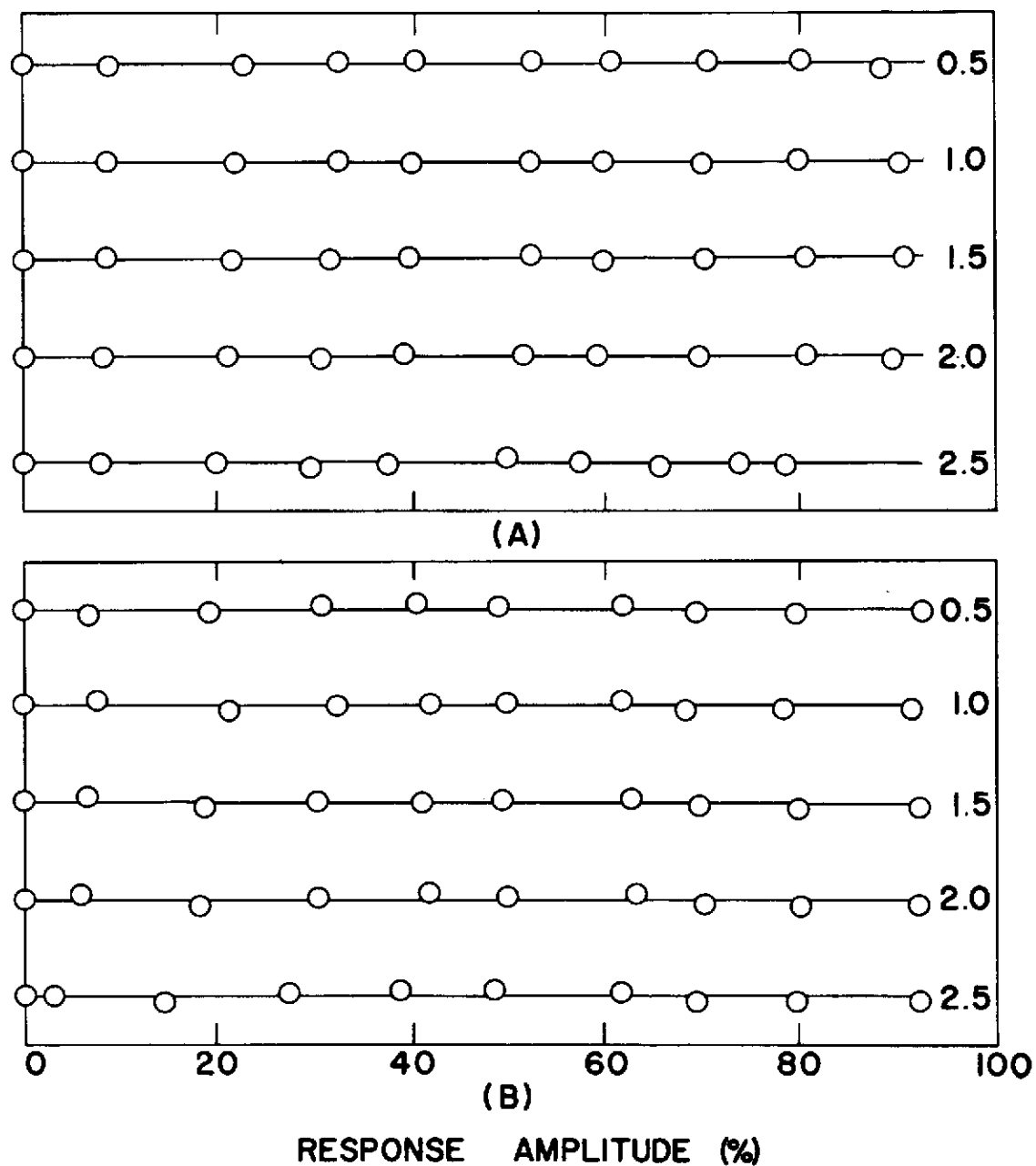
Fig. 6.--Typical residuals for glass plates at wavelengths 0.5, 1.0, ..., 2.5 μm. (A) Reflectance and (B) Transmittance. Successive curves are plotted 10% apart. The standard deviation between observed and computed quantities is 0.41%.

A SPECTRORADIOMETER FOR FIELD USE

R. W. Leamer

INTRODUCTION

This report describes the configuration and operation of a field spectro-radiometer (Exotech Model 20 Spectroradiometer) that measures the intensity of incident and reflected radiation from .37 to 2.52 μm and emitted radiation from 2.76 to 13.88 μm. The instrument was built by Exotech Incorporated from specifications and plans furnished by the USDA. Exotech contributed many engineering concepts based on knowledge of the theory involved.

The instrument consists of two systems with each system made up of an optical unit and a control unit. One system covers the spectral range 0.37 to 2.52 μm; the other system covers the spectral range of 2.76 to 13.88 μm. The optical units of the two systems mount side by side on a tiltable base mounted on an aerial lift truck. Separation between the objective lenses is less than 12 inches to minimize parallax.

The control units are mounted in a camper-type equipment van, and they are connected to the optical units through 200 feet of cable. Preamplifiers and auxiliary electronics in the optical units are designed to operate without picking up interferences over this length of cable. The entire system is designed to operate over the range of temperatures encountered outdoors.

MATERIALS AND METHODS

Circular Variable Filters

Spectral scans are made by rotating circular variable filters (CVF) through the optical path in front of detectors. A CVF consists of a multilayer, dielectric coating deposited on a rigid, circular substrate so that coating thickness varies linearly with angle of rotation while remaining constant along a radius. The spectral characteristics of these filters allows them to act as narrow band-pass interference filters at any point around the circumference of the filter. As the filter is rotated through a beam of incident radiation, the center frequency of the radiation passing through the filter changes. The filters have a band width of 1 to 2% of the center wavelength (WL).

Present methods of making CVFs limit each segment to one octave; the longest WL is no more than two times as long as the shortest WL. The instantaneous band-pass width depends upon the angular-slit width of the optical system and the solid angle of radiation incident on the filter.

This type of CVFs provides two important advantages for a field instrument. First, there are no stringent alignment requirements, and second, a simple shaft angle encoder can give a reading related to WL.

Optical System

Each CVF must have an optical system to collect radiation and direct its path through the CVF onto a detector. Refracting optics are used to allow the optical head to be sealed against dust and humidity in a field environment. Figure 1 shows the optical layout of the instrument. Fused silica lenses are used in the short WL unit because of its good mechanical properties. KRS 5 lenses, coated for maximum transmission at 3 μm, are used in the long WL unit. KRS 5 has relatively high optical transmission through the long WLs extending into the visible. Transmission in the visible WLs simplifies optical alignment and permits rapid field checking for maladjustments.

A mirror assembly which deflects the main beam through a right angle is inserted between the primary lens and the chopper blade.

The primary lenses may be removed to enlarge the field of view from 1° (lenses in) to 15° (lenses removed).

A beam chopper is included as part of the optical system to give an alternating signal from the detectors. The chopper blade is highly reflective on both surfaces and is located so that the beam falling on each CVF comes alternately from the blackbody reference or through the primary optics.

Spectral qualities of incident radiation must also be measured to give additional information about reflective properties of a target. The short WL unit has a reference surface of Coors alumina exposed to incident radiation. The reference surface is held in an adjustable mount so that the angle of incidence on the reference plate can be maintained equal to that on target surface. Radiation passing through the Coors alumina is diffused in an almost ideal Lambertian pattern. The diffused radiation passing through the reference plate can be directed into the main optical path by a remote-controlled mirror. Consequently, in the short WL unit, spectral scans may be made of the incident radiation or the radiation reflected from a target by activating a solenoid that controls the mirror.

Detectors

Silicon (Si) and cooled lead sulfide (PbS) detectors are used in the short WL unit while InSb and HgCdTe detectors are used to measure the long WL radiation.

The Si detector measures the radiation in the 0.35 μm to 0.74 μm range. This detector operates in the photovoltaic mode so that the short circuit current is proportional to the radiation incident on the Si detector. The short circuit current is easily measured through a low impedance amplifier which eliminates the cell capacitance making the detector response relatively independent of chopping frequency. The silicon detector operates at ambient temperature.

Radiation over the 0.65- to 2.80 μm spectral region is measured with a PbS detector. PbS detectors operate over a wide temperature range, but the output from any given radiation level is highly temperature dependent. The PbS detector in this instrument is cooled to 77K to eliminate the temperature sensitivity. PbS detectors decrease in responsivity with chopping frequencies faster than 100 cps;

however, the basic noise level of the detector also falls with increasing chopping frequency. The chopping frequency for both short WL detectors is consequently not critical and can thus be matched to that of the long WL detectors.

The spectral intensity in the 2.8 to 5.6 µm range is measured by an Indium Antimonide (InSb) detector in the long WL unit. Cooling to 77K is necessary to get spectral coverage to 5.6 µm. This detector also operates in the unbiased photovoltaic mode where the preamplifier circuit measures the short circuit current that is a linear function of radiation incident on the detector. Operating in this mode requires no bias supply on the preamplifier.

A HgCdTe detector is used to measure the 7.04- to 13.88 µm spectral range. Satisfactory operating characteristics are obtained by cooling this detector to 77K. A transformer coupled preamplifier is required for the HgCdTe detector because it operates in the photoconductive mode that requires a bias supply that must be applied with a low detector impedance of several hundred ohms.

Chopping frequency is more critical in the long WL unit than in the short WL unit. Both long WL detectors operate more effectively at chopping frequencies above 1,000 cps. Both detectors operate at the same chopping frequency because a single chopper is used in each WL unit. Chopping rate used is 1,200 cps for all four detectors.

Detector Cooling

Joule-Thompson coolers are used for each of the three cooled detectors. Identical coolers are fitted inside glass Dewars that have the detectors sealed in the end exposed to the three optical paths. Commercial high-purity, extra dry nitrogen gas is fed at 1,200 to 1,500 pounds/in^2 through a pressure regulator, a molecular sieve filter, and a solenoid control valve into the cryostat assembly.

The adiabatic cooling allows the Dewars to be operated in any position so the instrument may be aimed in any direction desired.

Reference Blackbodies

Two blackbody references are used. In the short WL system, the temperature of the blackbody is unimportant because at normal operating temperatures around 300K its radiance will be three or four orders of magnitude below that of a target illuminated by sunlight. The blackbody in the short WL unit is a block of copper, faced with a series of shallow V grooves whose surfaces have been oxidized to produce a high emissivity and very low reflection.

The temperature of the reference blackbody in the long WL unit must be known. The blackbody used is a temperature controlled block of copper surrounded by an insulated enclosure. A resistive heater and a temperature sensing element are also in the insulated enclosure. The operating temperature is chosen by setting a dial on the electronic control unit; the temperature is then maintained at the desired level through a proportional dc controller attached to the temperature sensor and the resistive heater. The blackbody temperature control circuit will maintain the blackbody at any temperature from ambient to 100C.

Electronics

All power for the spectroradiometer is derived from 60 cycle, 110 volt primary circuit. All ac and dc at other voltages and frequencies used are derived internally in the instrument. The CVFs and the chopper wheels are driven with 110 volt, 60 cycle motors. The blackbody heater in the long WL unit is powered by a 28 VCD source controlled by a thermistor temperature sensor located in the blackbody assembly.

Signal processing amplifiers and circuits are powered with 15 VCD supply from a transformer-rectifier-regulator off of the primary power circuit. The bias voltage for the trimetal detector is also furnished from this unit.

The operating controls, indicators, and power supplies are in the control units in the mobile van. Input signals from the detector preamplifiers pass through an adjustable attenuator to a synchronous demodulator. The demodulator is a solid state, full-wave type using field-effect-transistors as the synchronous switches. An input buffer amplifier in a voltage-follower connection provides high input impedance and additional signal gain as required. The inverter amplifier, operating at unit gain, provides the inversion of the input signal necessary for the full wave operation. This operation improves output signal to noise ratio by doubling the output ripple frequency that eases subsequent filtering. The output amplifier has a very low output impedance, and it provides additional filtering through a time constant which can be adjusted to match various spectrum scan rates.

The demodulator sync signal for both detectors in each optical unit is picked off the single chopper blade. A mechanical adjustment is provided for the sync pickoff detector but, because two detectors with different time constants share each chopper, sync adjustment for each detector is required. The phase shifter of each detector is followed by a squaring amplifier to provide square wave driving signals to the demodulating FET switches.

The design of the preamplifier is critical in an instrument of this kind. At low frequency, Johnson noise from the feedback resistor is proportional to the square root of the resistor temperature and inversely proportional to the square root of the resistance. In the high frequency portion of the band-pass, input-voltage noise from the operational amplifier dominates. The high frequency portion tends to be the more important when integrated over the total bandwidth.

Operation

The spectroradiometer set up for field use has the optical units mounted on the bucket of an aerial lift truck and the control units in a mobile laboratory. Power for the instrument may come from a regular 110 volt, 60 cycle system or from a portable generator in more remote locations. The spectroradiometer is not seriously handicapped by the normal variations in voltage and cycle rate from a portable generator.

The optical units are connected to the control units by a 200 foot cable for each of the long and the short wavelength systems. All control functions, other than aiming the optical units, are performed from the control units in the camper.

Each optical unit has a 1X-power telescope mounted parallel to the optical path from the instrument to the target. Crosshairs in the telescope can be adjusted to coincide with the center of field of view at any distance. A camera with a remote controlled electrical film advance and shutter-cocking mechanism is mounted to look through one telescope. The other telescope may be used by an operator in the bucket to aim the instrument at the desired target. Aiming may also be done by moving the bucket of the aerial lift to the desired location.

This instrument is designed to allow mounting in an aircraft. Shorter cables are provided to connect the optical units and control units for this type of installation. Scanning rates are rapid enough (two complete scans per second) to measure spectra from moderate sized fields. The rapid scanning rates require more elaborate recording equipment than do the slower rates.

Each detector puts out a signal varying from 0 to 5 volts dc, depending on the amount of energy falling on the detector. A filter wheel position signal is developed by each WL system. This position signal is a 1,000 step staircase ramp from 0 to 5 volts that is reset to zero at the beginning of each revolution of the filter wheel. Each control setting on the control unit, such as scanning speed (6 position), amplifier gain (7 position), blackbody temperature (linear 10 turn pot), incident/target control (3 position), has an analog output signal that varies with setting. Recording these signals gives all the information needed to measure the distribution of energy through the spectrum incident on or reflected from a target.

Detector signal strength at any WL may be converted to energy units by multiplying by a calibration factor for that WL (taking into account the amplifier gain, etc.).

Output

Determining the units of radiant energy falling on the detector at each WL gives a curve representing the spectrum of the incident or reflected energy. Comparing the reflected spectrum to the spectrum of incident energy allows the percent reflection at each WL to be calculated. The incident energy in the long WL band is such a small proportion of the emitted energy that the incident is not measured. Each target gives a typical blackbody emittance curve. This emittance curve is compared to the emittance of the temperature of the internal reference blackbody. Thus, the equivalent blackbody temperature of each target can be calculated. In cases where the actual surface temperature of the target is known, the emissivity of the target can be calculated.
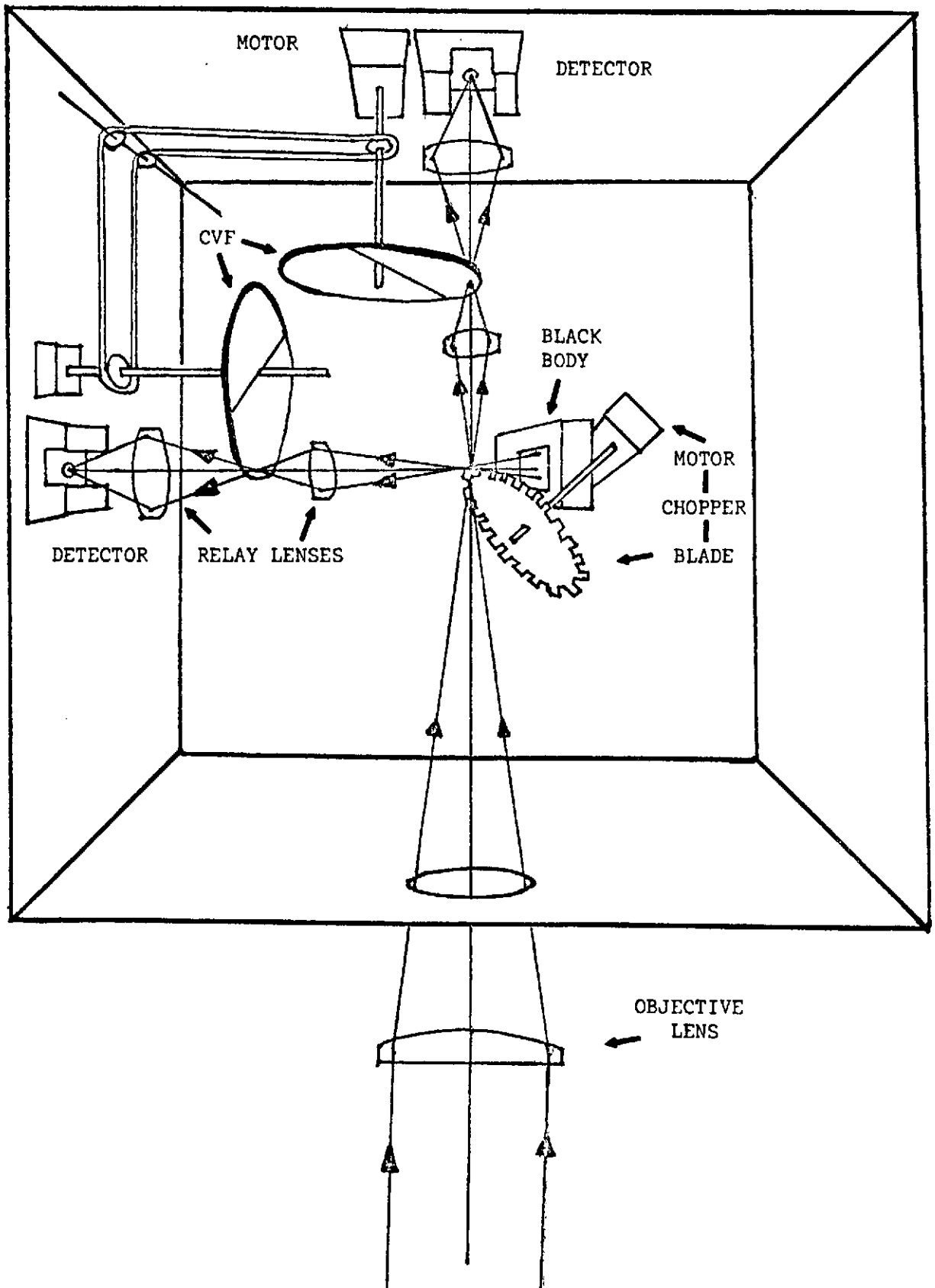
Fig. 1.--Optical layout of field spectroradiometer.

COMPUTER FACILITIES AT WESLACO

R. J. Torline

INTRODUCTION

When last year's annual report was prepared, specifications for an on-site computer had been submitted to GSA for approval. In December 1970, an IBM 1800 Processor Controller was acquired through intra-government transfer.

The 1800 system was configured on delivery as shown in Fig. 1. It was a one-disk, two-tape drive system with a Card Reader/Punch and a Printer.

A basic operating system was generated under IBM's Multiprogramming Executive (MPX) Version 3 Modification 0. This system permitted a temporary platform for the conversion of programs that had previously been used on timesharing and the development of a new system of programs to perform statistical analyses required for data reduction. In April 1971, the basic design of the system was changed to satisfy current needs and projected growth (Fig. 2), requiring a new system generation under the Executive of MPX Version 3 Modification 1.

PRESENT SYSTEM

The present system consists of an IBM 1800 Processor Controller with 32K core storage with one each of the following:

1443	Printer w/144 print positions
1442	Card Reader/Punch
1816	Keyboard-Printer
1826	Data adapter with process interrupt, one group of digital input, and one group of digital output
1054	Paper Tape Reader
1055	Paper Tape Punch

This system is capable of processing and analyzing all data recorded on paper tape from laboratory and field instruments. Because of the nature and volume of these data, however, it was evident that the processing of paper tapes would occupy 80% of CPU prime time. It was also noted that the capability of processing analog information had not been achieved. The processing of analog information through the 1826 Data Adapter was feasible, but its cost was prohibitive.

The solution was to interface the 1800 to an existing mini-computer, with a high speed Optical Paper Tape Reader and analog to digital conversion capabilities. The mini-computer is a Hewlett-Packard (H-P) 2114B, with 8K core storage, equipped with a Model 33 Teletype, a Photo-electric Paper Tape Reader, a Medium Speed Paper Tape Punch, and an Optical Marked Card Reader. The H-P also has interfaced equipment consisting of a Digital Volt Meter (DVM), a 200-Channel Crossbar Scanner, a Digital to Analog Converter, and a Time Base Generator. The two interfaced computers, capable of operating independently, allow researchers at Weslaco to perform most data handling and processing requirements necessary in agricultural research.

Data recorded on marked cards, such as ground truth observations, can be processed on the H-P and stored, or the data can be further processed with more complex statistical programs on the IBM 1800. The H-P is capable of constantly monitoring and sampling data from field located instruments. Analog data obtained from multispectral scanners, mounted in aircraft or spacecraft, can be processed and analyzed; pattern recognition techniques can be applied to these data. Multi-channel, analog data recorded on magnetic tape can be digitized at a rate of nearly 30 channels/sec. Data recorded on paper tape from various instruments can be processed at 20 times the previous input rates. This allows more CPU time for ground, aircraft, or spacecraft digital information.

FUTURE PLANS

Provisions are being made for future growth. Proposed additions to the IBM 1800 include increased memory, another magnetic tape drive comparable to the existing drive, and an image display device. The latter two additions will allow researchers to display digital magnetic tape produced from data generated by multispectral scanners mounted in aircraft or spacecraft. This instrumentation would greatly decrease the man-hour and computer time ordinarily required to analyze such vast amounts of data.

The present computer system and planned growth would allow researchers at Weslaco to process and analyze remotely sensed data for applications to larger geographical areas.
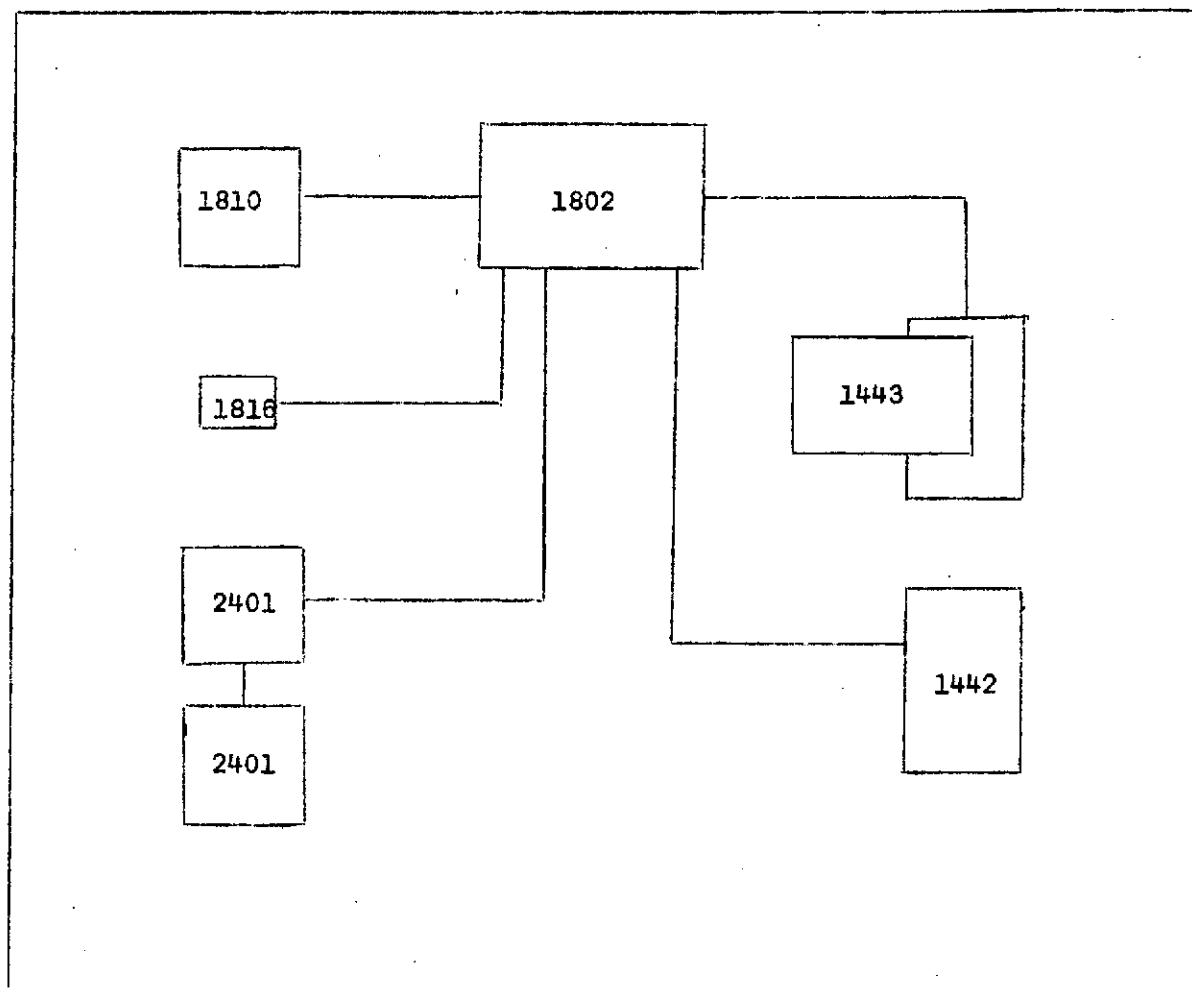
Figure 1.   IBM 1800 system at USDA Weslaco, Texas from Dec. 1970 to Mar. 1971.

1802--32K Process Controller
1810--1 Drive Disk Storage
1816--Keyboard-Printer
2401--7- and 9-track Magnetic Tape units
1443--Printer
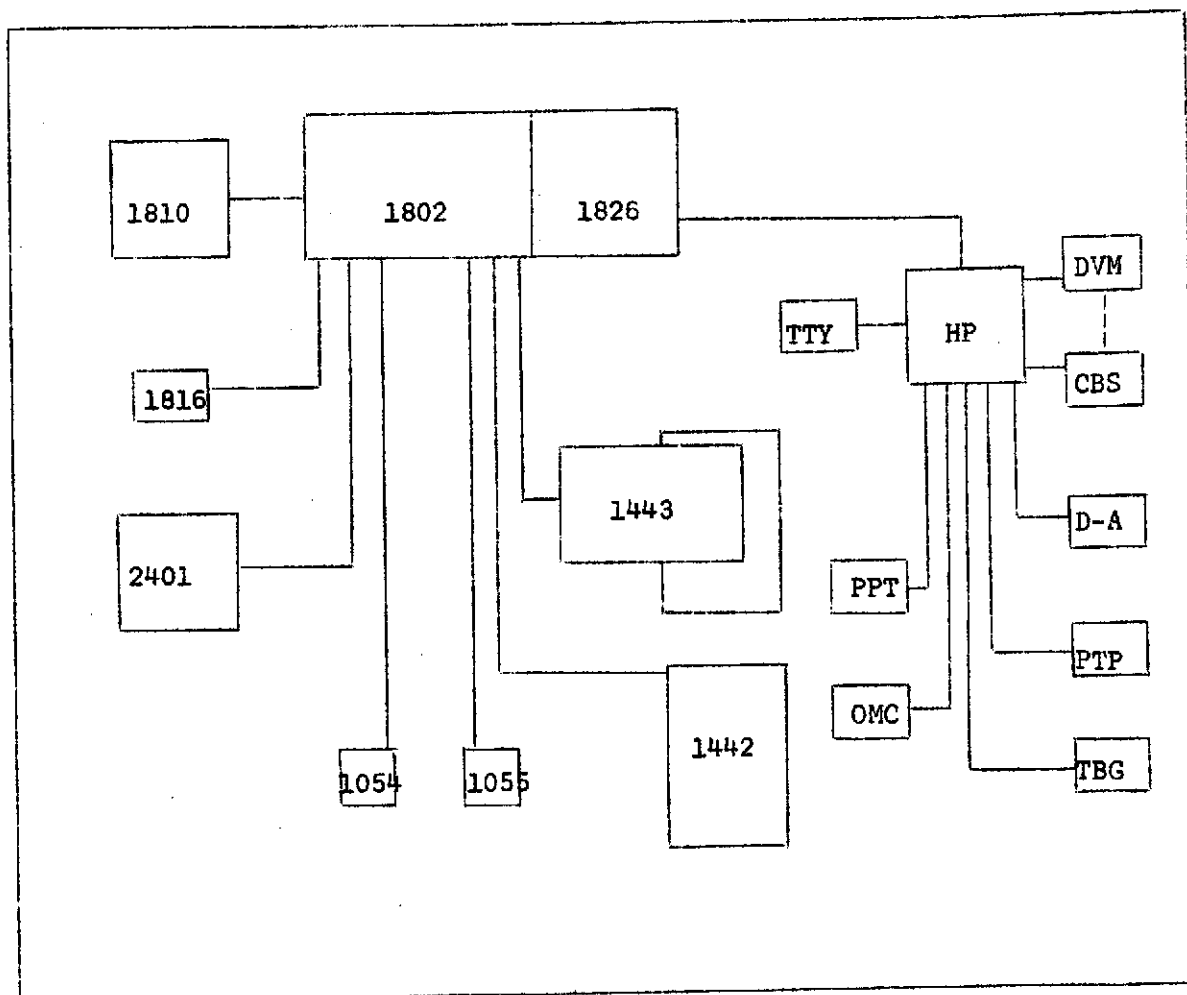1442--Card Reader/Punch

Figure 2. IBM 1800 system at USDA Weslaco, Texas from Apr. 1971 to Dec. 1971, including interfaced Hewlett-Packard mini-computer and peripherals.

1802--Processor Controller
1810--2 Drive Disk Storage
1816--Keyboard-Printer
2401--9-track Magnetic Tape
1443--Printer
1442--Card Reader/Punch
1826--Data Adapter
1054--Paper Tape Reader
1055--Paper Tape Punch
 HP--Hewlett-Packard 2114B, 8K Computer System
TTY--Model 33 Teletype
PTP--60 character/sec Paper Tape Punch
DVM--Digital Voltmeter with analog to digital
        conversion capabilities
CBS--200 Channel Cross-Bar Scanner can be used in
        conjunction with the DVM
PPT--Photoelectric Paper Tape Reader
OMC--Optical Marked Card Reader
D-A--Digital to analog conversion capabilities
TBG--Time Base Generator

A VISUAL DISPLAY TO AID ANALYSIS OF DIGITAL DATA

R. J. Torline

INTRODUCTION

The use of multispectral sensors in airborne and space vehicles permits wide areal coverage. The data collected can be analyzed for information about the static or dynamic state of our natural resources. The U. S. Department of Agriculture at Weslaco, Texas is interested specifically in the soil and water conditions that affect plant growth.

The coverage capability of airborne or space vehicles results in a vast amount of analog and digital magnetic tape to process and analyze. Information in nonphotographic wavelengths must be converted to a form that personnel skilled in agricultural, geographical, and geological disciplines can use. The human mind cannot relate to digital magnetic tape. A data display allows the investigator to study the data in real time to determine what ground area a given portion of the magnetic tape data represents, and to locate areas for more detailed study with the digital computer.

The line printer of a computer system can generate gray-scale maps of the area covered by the digital magnetic tape. However, the investigator must single out from these voluminous printouts, the fields or areas of special interest to him. The full time use of one or more magnetic tape drives as well as the line printer for this purpose would also prohibit others from using these peripherals. Thus it becomes necessary to provide some other means of data display.

MATERIALS AND METHODS

The USDA at Weslaco proposes to use a Cathode Ray Tube (CRT) type of display system with at least 50 intensity levels to simulate gray-scale mapping, and a cursor. This system would allow the investigator to review the digital information while batch processing jobs are being handled in a background mode on a multiprogramming system.

Digital image processing can be performed on multispectral information to suppress undesired data and noise, to enhance features of interest, and to permit quantitative measurements or comparisons to be made on the image information. Well-known photographic and electronic filtering techniques are available in software algorithms for noise removal, selective filtering, edge enhancement, thresholding, and subtraction. The extraction of quantitative information from digital images is greatly aided by such techniques as edge detection, contour tracing, shape determination, and area calculations.

The interpretation of multispectral data by the image analyst is a subjective adventure. Vital information is often masked by undesirable distortions or distractions. The speed and accuracy of digital processing equipment can be applied to produce an image of higher quality, and to remove a substantial amount of subjectivity from human image analysis efforts. Judgments by the analyst become more credible and thus more useful.

A CRT display system at Weslaco would alter the present computer system to the configuration of Fig. 1. The additional 2401 Magnetic Tape unit used in conjunction with the image display would allow investigators to select areas of interest from the original digitized magnetic tape and record these data on the second magnetic tape unit. It would also allow greater flexibility in other related and nonrelated data handling programs.

SUMMARY

With the volume of multispectral data available, a CRT image display system would provide a powerful tool for use in solving many agricultural, environmental, and sociological problems. The use of a CRT display on multispectral scanner data, from such sources as the NASA 24-channel and University of Michigan 19-channel scanners, as well as digitized data from ERTS-A (Earth Resources Technology Satellite) and Skylab's EREP (Earth Resources Experimental Package) would allow Weslaco's researchers to develop a better understanding of the interaction of electromagnetic energy with the agricultural environment.
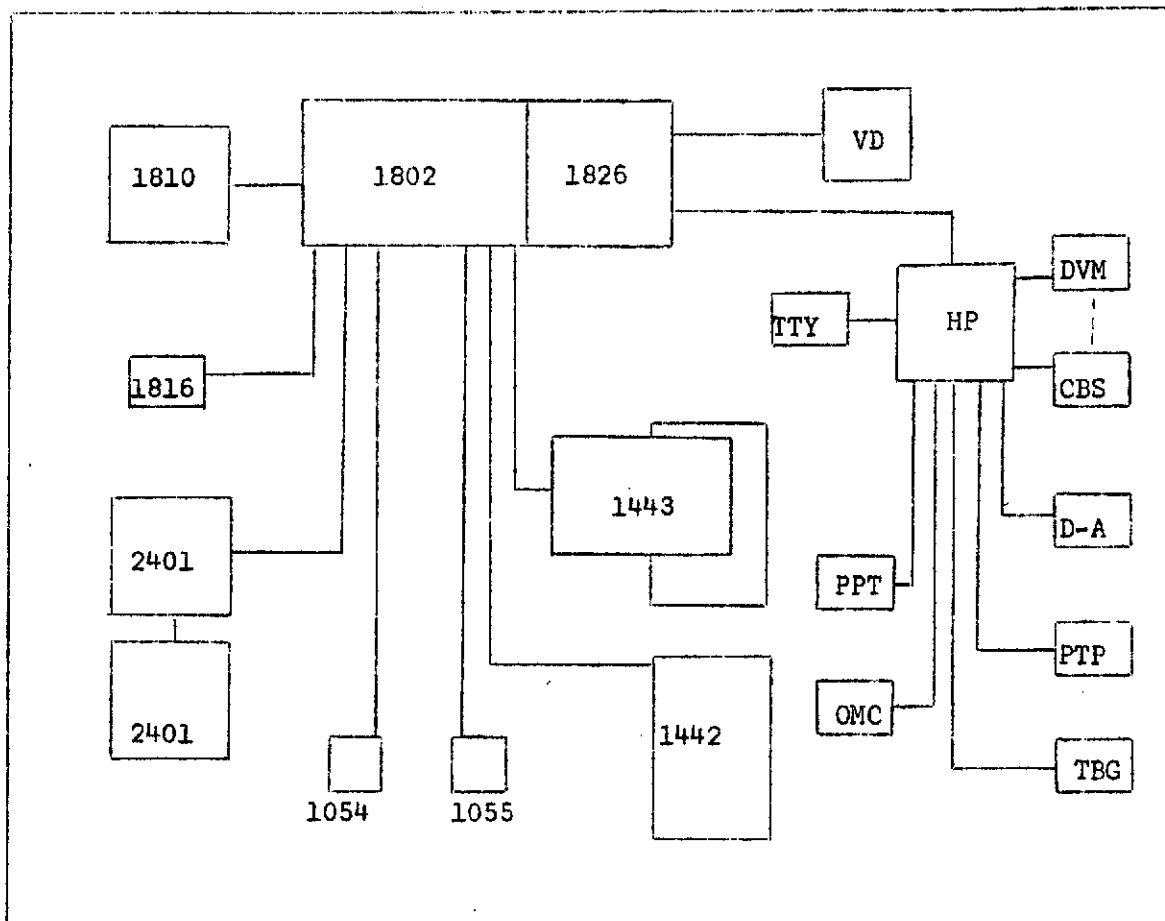
Fig. 1.--Proposed changes to IBM 1800 system at USDA, Weslaco, Texas including
interfaced Hewlett-Packard mini-computer and peripherals.

     1802--Processor Controller
     1810--2 Drive Disk Storage
     1816--Keyboard-Printer
     2401--9-track Magnetic Tape
     1443--Printer
     1442--Card Reader/Punch
     1826--Data Adapter
     1054--Paper Tape Reader
     1055--Paper Tape Punch
      HP--Hewlett-Packard 2114B, 8K Computer System
     TTY--Model 33 Teletype
     PTP--60 character/sec. Paper Tape Punch
     DVM--Digital Voltmeter with analog to digital
           conversion capabilities
     CBS--200 Channel Cross-bar Scanner can be used in
           conjunction with the DVM
     PPT--Photoelectric Paper Tape Reader
     OMC--Optical Marked Card Reader
     D-A--Digital to analog conversion capabilities
     TBG--Time Base Generator
      VD--Visual Display System to include additional
           2401 magnetic tape unit

FIELD SPECTRORADIOMETER DIGITAL LOGGER

R. W. Leamer

SUMMARY

The field spectroradiometer owned by the USDA, Weslaco is designated by Exotech, Inc. (the builder) as a Model 20 Rapid Scan Spectroradiometer. It is designed to measure the spectral radiometric properties of agricultural cover, natural terrain, and soils from either ground based platforms or from aircraft. The spectroradiometer rotates circular variable filters (CVF) through the optical path in front of detectors to obtain the spectral distribution information. Four filter wheels, each with its own detector, are used to cover the .37- to 13.88-μm spectral range. Spectra are scanned at six possible speeds from two scans/sec to two scans/min.

An analog voltage signal proportional to the radiometric energy passing through the filter is generated by each detector. A 1000 pulse per revolution (rev) signal indicates the wavelength of the energy passing through the CVF. Four radiometric signals and two pulse train signals are produced simultaneously. All these are analog (A) voltage signals that must be converted to digital (D) values.

Ten bit digital words are required to record the maximum accuracy of the spectroradiometer. At the maximum scan rate, the intensity measurements alone produce 8000 ten-bit words/sec (4 CVF x 2 rev/sec x 1000 samples/rev). The wavelength dependent signal gives forth 4000 words/sec (2 pulse trains x 1000 pulses per rev x 2 rev/sec).

Thus, a data logger suitable for this spectroradiometer would have to make 12,000 A to D conversions/sec and record all D values. The fact that all signals are being generated simultaneously adds to the complexity of the data logging problem.

The spectroradiometer has a number of controls that affect the conversion of output signals to radiometric values. Besides the scanning speed control (6 positions), each detector has a separate electronic amplifier with a gain control (7 positions); the reference blackbody for the long wavelength detectors has an adjustable temperature control (10-turn pot); and the short wavelength detectors have a scanning mode control (3 positions): one, incident; two, reflected; or three, alternate incident and reflected. All these controls produce A signals related to their settings that must be recorded along with the radiometric data. The recording of other housekeeping information such as date, time, target identification, temperature, humidity, etc., is necessary for adequate interpretation of radiometric data.

Initial steps have been taken to get a data logging system for the Exotech spectroradiometer. A two-step procedure is being used: first, formal proposals are being requested (RFP) from several companies to whom the logging requirements for the spectroradiometer are being sent; and second, the proposals resulting from these requests will be evaluated, balanced against available funds, and final specifications of a data logger will be written.

MINI-MAXI COMPUTER INTERFACE

R. J. Torline and R. E. Smithey

INTRODUCTION

The U. S. Department of Agriculture at Weslaco has five paper tape data collecting systems and several analog outputting and recording devices. The paper tape output devices are: (1) a 200-channel data logger used in a micrometeorological program, (2) a 20-channel data logger that punches 10 reading averages for each channel along with date and time information, (3) a Beckman DK-2A Spectrophotometer used for measurements of light reflectance and transmittance over the 0.35 to 2.50 μm wavelength range, (4) a Leitz microspectrophotometer used for measuring reflectance from microscopic samples over the 0.3 to 1.0 μm wavelength range, and (5) a Joyce-Loebl microdensitometer used to measure optical densities of photographic transparencies. In addition, outputs from various devices such as a Barnes Model T5 infrared camera, a field spectroradiometer and sensitive anemometers are recorded on 2 Ampex 7-track analog recorders. With the volume of output data generated, it becomes necessary to optimize reduction of the information to analyze the data.

The 2 μsec cycle time of the Hewlett-Packard (HP) 2114B minicomputer (owned by the USDA), with its high speed optical paper tape reader (OPTR), looked promising. Data from the various paper tape devices could be summarized to eliminate much of the volume. Data from the analog (A) recorders could also be digitized by a digital (D) voltmeter (DVM) and read by the HP. The major problem, however, was the storage of these intermediate data.

The HP is an 8K (K = 1024 computer words) memory machine with only two output devices--a Teletype 33 and a medium speed paper tape punch. It would be too costly in many cases to read and reduce voluminous data and then restore the data on paper tape.

On the other hand, the use of the IBM (International Business Machine) 1800 at USDA, Weslaco would provide several means of intermediate data storage (listings, paper tape, cards, magnetic tape, or disk). The IBM 1800, a 4 μsec 32K machine, would read, process, and store large volumes of both paper tape and A data (the IBM 1800 is not yet equipped with A to D conversion capabilities). Such a system provides the researcher with a means of handling data from various sources. However, the slow speed of the paper tape reader (14.8 characters/sec) and the cost of A to D conversion prohibit optimum use of this computer.

The ideal solution then appeared to be the interfacing of the high speed of the HP system to the greater storage capabilities of the IBM 1800 system. Such an interface offers many advantages over two independent computer systems.

MATERIALS AND METHODS

Hardware- and software-oriented problems are involved in interfacing computers. The hardware poses the problem of interfacing two systems that differ in logic levels. With the IBM 1800 posing DTL (diode transistor logic) and the HP posing TTL (transistor-transistor logic), it became necessary to provide one computer system with the means of recognizing the logic of the other. Since a major percentage of the computer industry has adopted TTL, it was necessary to convert the IBM 1800 to recognize this logic.

To determine what circuitry would be required by both computers for the interface, it was necessary to determine the characteristic input and output (I/O) (levels, voltages, potential drops, resistances) features of each computer.

The 1800 I/O logic levels are:

Type	Logic	Range (Volts)
Digital (D) I/O	0	-6 to -30
(individual bit levels)	1	-1 to +30
D I/O sync	0	-6 to -18
	1	-0.5 to +0.5
D I/O ready	0	-12(through a 1000Ω resistance)
	1	0 to -0.5

The HP I/O logic levels are:

Type	Logic	Range (Volts)
D I/O	0	+2.4 to +5.0
	1	0.0 to 0.5
ENCODE-FLAG	0	+2.4 to +5.0
(equivalent to sync and ready)	1	0.0 to +0.5

Interfacing "adaptors," known as RPQ's, are supplied by IBM for various interfacing applications. The RPQ's required in this particular situation were found to be C08240 for the D input, C08241 for the D output, and C08296 for the I/O Sync. The IBM 1800 has separate ready and sync commands for D input and D output.

Because the HP is limited to 7 I/O slots in its main frame, it was determined that to obtain optimum use of the HP's I/O capabilities a duplex interface card, HP 12566A-M2 microcircuit, should be used rather than two individual microcircuit cards for I/O. Two cards for I/O would diminish I/O capabilities on the HP. The duplex card permits the bidirectional transfer of data between the HP computer and I/O devices. This card has but one set of commands for I/O operations called flag and encode, and they correspond to the IBM 1800's DI ready and sync and DO ready and sync. Therefore, the IBM 1800's ready lines were tied parallel to the HP's flag and the sync lines were tied parallel to the HP's encode.

During the interfacing procedures, it was discovered that the lack of separate I/O control lines from the HP prevents conversational computers. A temporary solution was the installation of a single pole (double throw switch) to switch from an input to an output operation and vice versa. A future solution is the acquisition of an I/O extender (14 I/O slots) for the HP, along with separate I/O microcircuit cards. These features would give the desired results and also useful additional I/O slots in the HP.

Although both the IBM 1800 and HP are 16-bit word machines, the notation or numerical ordering of each bit is different. The 16 bits of the HP are numbered from left to right; whereas, they are numbered right to left on the IBM 1800. Since bit 0 on the HP and bit 15 of the IBM 1800 are the sign bits, the physical wiring was opposite that of the bit pattern notation.

Programming the IBM 1800 to accept D data from the HP was not difficult. Once the D input channel (64) on the 1826 Data Adapter was tested to insure proper transfer to bit patterns from the HP to the IBM 1800, only one routine was required in the HP to send data and one routine was needed for the IBM 1800 to accept data. However, it was still necessary to let each machine know how many words were being sent or received; the first word sent or received was a word count of how many subsequent data words were to follow. The IBM 1800 Multi-programming Executive (MPX) provides D input and output routines for the computer user.

Programming the HP required that an I/O routine be written in HP Assembler language to output information to the IBM 1800. Present programming allows only interger values to be sent or received. Fractional data will require transformations (bit manipulation) before transfer can be accomplished. For some unknown reason, data words (bit patterns) sent by the IBM 1800 arrived in HP memory as the complement of the correct bit pattern. This programming problem was solved by first complementing the bit patterns in the IBM 1800 before transmission to the HP.

SUMMARY

Disregarding current input and output (I/O) problems, it is generally believed that the HP (Hewlett-Packard 2114B mini-computer)--IBM (International Business Machine) 1800 computer (maxi-computer) interface has given a tremendous gain in computing power, and the mini-maxi computer interface has greatly extended I/O capabilities. Transfer rates of paper tape characters read on the HP-OPTR (optical paper tape reader) and sent to the IBM 1800 range from 138.9 to 541.9 characters/sec, while the transfer rate of 16-bit computer words from memory to memory is greater than 7000 words/sec.

Current uses of the interface include the processing of paper tape data collected from various instruments, the processing of neutron probe readings (used to determine soil moisture in field experiments) that are recorded in the field on marked sense cards and read by the optical mark card reader on the HP, and the processing of single channel analog (A) tape.

Additional uses involve the processing of A tape generated from such devices as hot wire anemometers, the Barnes Model T5 infrared camera, and many varied optical mechanical scanners. Another planned use of the interface is the loading of core image programs from the IBM 1800 disk into HP memory. This feature alone will give a tremendous amount of flexability allowing HP core image programs currently stored on paper tape to be loaded into HP memory from the 1800 disk as required. The loading time of core image programs would be greatly reduced for large programs.

The mini-maxi computer interface has made current data processing at USDA faster and more efficient. This interface will provide new applications to problem solving as future experiments are conducted.

PUBLICATIONS

Published During This Reporting Period

1. Allen, W. A., H. W. Gausman, A. J. Richardson, and C. L. Wiegand. 1970. Mean effective optical constants of thirteen kinds of plant leaves. Appl. Opt. 9:2573-2577.

2. Richardson, A. J., R. J. Torline, D. A. Weber, R. W. Leamer, and C. L. Wiegand. 1970. Comparison of computer discrimination procedures using film optical densities. SWC Res. Rep. 422, Mimeo., 85 p.

3. Baumgardner, F. J. (ed.), R. W. Leamer, and J. R. Shay. 1970. Remote sensing techniques used in agriculture today. Aerial Space Science and Agricultural Develop., Amer. Soc. Agron. Spec. Pub. No. 18. p. 9-26.

4. Wiegand, C. L., and J. F. Bartholic. 1970. Remote sensing in evapotranspiration research on the Great Plains. Proc. Great Plains Agricultural Council Evapotranspiration Seminar, Research Committee. Kansas State Univ., Manhattan. Pub. No. 50. p. 137-180.

5. Gausman, H. W., W. A. Allen, R. Cardenas, and R. L. Bowen. 1970. Detection of foot rot disease of grapefruit trees with infrared color film. J. Rio Grande Valley Hort. Soc. 24:36-42.

6. Gausman, H. W., W. A. Allen, M. L. Schupp, C. L. Wiegand, D. E. Escobar, and R. R. Rodriguez. 1970. Reflectance, transmittance and absorptance of electromagnetic radiation of leaves of eleven plant genera with different leaf mesophyll arrangements. Texas A&M Univ., Tech. Monogr. 7. 38 p.

7. Allen, W. A., H. W. Gausman, and C. L. Wiegand. 1970. Spectral reflectance from plant canopies and optimum spectral channels in the near infrared. Proc. 3rd Ann. Earth Resources Aircraft Program Status Review, NASA-MSC, Houston. II:23:1-15.

8. Gausman, H. W., R. Cardenas, and W. G. Hart. 1970. Aerial photography for sensing plant anomalies. Proc. 3rd Ann. Earth Resources Aircraft Program Status Review, NASA-MSC, Houston. II:24:1-15.

9. Bartholic, J. F., C. L. Wiegand, R. W. Leamer, and L. N. Namken. 1970. Thermal scanner data for studying freeze conditions and for aiding irrigation scheduling. Proc. 3rd Ann. Earth Resources Aircraft Program Status Review, NASA-MSC, Houston. II:27:1-23.

10. Richardson, A. J., R. J. Torline, and W. A. Allen. 1970. Computer discrimination procedures applicable to aerial, space, and ERTS multispectral data. Proc. 3rd Ann. Earth Resources Aircraft Program Status Review, NASA-MSC, Houston. II:28:1-24.

11. Gausman, H. W. 1971. Photographic remote sensing of "sick" citrus trees. Proc. Intl. Wksp. on Earth Resources Survey Systems, Univ. of Mich., Ann Arbor. May 3-14. 2:15-30.

12. Wiegand, C. L. 1971. Agricultural applications and requirements for thermal infrared scanners. Proc. Intl. Wksp. on Earth Resources Survey Systems, Univ. of Mich., Ann Arbor. May 3-14. 2:66-81.

13. Wiegand, C. L., R. W. Leamer, D. A. Weber, and A. H. Gerbermann. 1971. Multibase and multiemulsion space photos for crops and soils. Photogram. Eng. 37:147-156.

14. Gerbermann, A. H., H. W. Gausman, and C. L. Wiegand. 1971. Color and color-IR films for soil identification. Photogram. Eng. 37:359-364.

15. Gausman, H. W., W. A. Allen, R. Cardenas, and A. J. Richardson. 1971. Effects of leaf nodal position on absorption and scattering coefficients and infinite reflectance of cotton leaves, Gossypium hirsutum L. Agron. J. 63:87-91.

16. Allen, W. A., H. W. Gausman, A. J. Richardson, and R. Cardenas. 1971. Water and air changes in grapefruit, corn, and cotton leaves with maturation. Agron. J. 63:392-394.

17. Gausman, H. W., W. A. Allen, D. E. Escobar, R. R. Rodriguez, and R. Cardenas. 1971. Age effects of cotton leaves on light reflectance, transmittance, and absorptance and on water content and thickness. Agron. J. 63:465-469.

18. Gausman, H. W., and M. L. Schupp. 1971. Rapid transectioning of plant leaves. Agron. J. 63:515-516.

19. Thomas, J. R., L. N. Namken, G. F. Oerther, and R. G. Brown. 1971. Estimating leaf water content by reflectance measurements. Agron. J. 63:845-847.

20. Gausman, H. W., W. A. Allen, C. L. Wiegand, D. E. Escobar, R. R. Rodriguez, and A. J. Richardson. 1971. The leaf mesophylls of twenty crops, their light spectra, and optical and geometrical parameters. SWC Res. Rep. 423, Mimeo., 88 p.

21. Richardson, A. J., R. J. Torline, and W. A. Allen. 1971. Computer identification of ground patterns from aerial photographs. Proc. 7th Intl. Symp. Remote Sens. of Environ., Univ. of Mich., Ann Arbor. III:1357-1375.

22. Gausman, H. W., W. A. Allen, C. L. Wiegand, D. E. Escobar, and R. R. Rodriguez. 1971. Leaf light reflectance, transmittance, absorptance, and optical and geometrical parameters for eleven plant genera with different leaf mesophyll arrangements. Proc. 7th Intl. Symp. Remote Sens. of Environ., Univ. of Mich., Ann Arbor. III:1599-1626.

23. Cardenas, R., H. W. Gausman, and A. Peynado. 1971. Detection of boron and chloride toxicities by aerial photography. Proc. 3rd Bien. Wksp. on Aerial Color Photogr. in the Plant Sci., Gainesville, Fla., Mar. 2-4. p. 267-288.

In Press:

1. Allen, W. A., and A. J. Richardson. Calibration of a laboratory spectro-
   photometer for specular light by means of stacked glass plates.
   Rev. Sci. Instruments.

2. Cardenas, R., A. Peynado, H. W. Gausman, A. H. Gerbermann, and R. L.
   Bowen. Photographic sensing of boron and chloride toxicities of citrus
   trees. J. Rio Grande Valley Hort. Soc.

3. Gausman, H. W., P. S. Baur, Jr., M. P. Porterfield, and R. Cardenas.
   Effects of salt treatments of cotton plants (Gossypium hirsutum L.) on
   leaf mesophyll cell microstructure. Agron. J.

4. Wiegand, C. L., and L. J. Bartelli. Remote sensing for conservation and
   environmental planning. Proc. Soil Cons. Soc. Amer., 1971 Ann. Meeting,
   Columbus, Ohio.

In Preparation:

1. Allen, W. A., H. W. Gausman, and A. J. Richardson. Discrimination among different kinds of plant leaves by spectral reflectance in the near infrared. J. Remote Sens. Environ.

2. Allen, W. A., H. W. Gausman, and C. L. Wiegand. Spectral reflectance produced by plant canopies. ASP Manual of Remote Sens.

3. Allen, W. A., and A. J. Richardson. A leaf cross section treated as an optical system. Proc. 4th Ann. Earth Resources Aircraft Program Status Review.

4. Bartholic, J. F., L. N. Namken, and C. L. Wiegand. Aerial thermal scanner to determine temperature of soil and of crop canopies differing in water conditions. Agron. J.

5. Bartholic, J. F., and L. N. Namken. Canopy temperature as an indicator of plant water stress. J. Appl. Meteorol.

6. Cardenas, R., C. E. Thomas, and H. W. Gausman. Photographic pre-visual detection of watermelon mosaic virus in cucumber. J. Amer. Phytopathol. Soc.

7. Cardenas, R., and H. W. Gausman. A comparison of the light reflectance among isogenic barley lines with their chlorophyll assays and photographic film densities. Agron. J.

8. Cooper, G. R., R. L. Bowen, and H. W. Gausman. The use of Kodak Aerochrome infrared color film, type 2443, as a remote sensing tool. Proc. 4th Ann. Earth Resources Aircraft Program Status Review, or Proc. 8th Intl. Symp. on Remote Sens. of Environ.

9. Gausman, H. W., W. A. Allen, R. Cardenas, and A. J. Richardson. Age effects of leaves within four growth stages of cotton and corn plants on reflectance, water and chlorophyll, and wavelength reflection for crop discrimination. Agron. J.

10. Gausman, H. W. Photomicrographic record of light reflected at 850 nanometers by cellular constituents of Zebrina pendula leaf epidermis. Letters for Nature.

11. Gausman, H. W. Physiological factors influencing electromagnetic radiation. ASP Manual of Remote Sens.

12. Gausman, H. W., W. A. Allen, R. Cardenas, and A. J. Richardson. Effects of leaf age for four stages of cotton and corn plants on leaf reflectance, structure, thickness, water and chlorophyll concentrations and selection of wavelengths for crop discrimination. Proc. 4th Ann. Earth Resources Aircraft Program Status Review, and Proc. 8th Intl. Symp. on Remote Sens. of Environ.

13. Richardson, A. J., J. R. Thomas, and R. J. Torline. Preprocessing methods for plant genera discrimination using reflected light. Photogram. Eng.

14. Richardson, A. J., C. L. Wiegand, R. W. Leamer, A. H. Gerbermann, and R. J. Torline. Discriminant analyses of Bendix scanner data. Proc. 4th Ann. Earth Resources Aircraft Program Status Review.